2020

DEVELOPMENT OF FORECASTING AND SCHEDULING METHODS AND DATA ANALYTICS BASED CONTROLS FOR SMART LOADS IN RESIDENTIAL BUILDINGS.

S M MAHFUZ ALAM

DEVELOPMENT OF FORECASTING AND SCHEDULING METHODS AND DATA ANALYTICS BASED CONTROLS FOR SMART LOADS IN RESIDENTIAL BUILDINGS.

By

S. M. Mahfuz Alam

A Dissertation

Submitted in Partial Fulfillment of the

Requirements for the Degree of

Doctor of Philosophy

Major: Electrical and Computer Engineering

The University of Memphis

December 2020

DEDICATION

This PhD dissertation is dedicated to my son Abdullah Bin Mahfuz Nahiyan, my family members for their everlasting encouragement and sacrifice towards my success.

ACKNOLEDGEMENT

First of all, I would like to sincerely thank the Almighty Allah, the creator of the heavens and earths for his bounty less mercy, guidance on everything towards achieving my degree. Then I would love to express my sincere gratitude to my dissertation supervisor Dr. Mohd. Hasan Ali for his encouragement, guidance, support throughout my study at the University of Memphis. His encouragement has greatly motivated me doing research on smart buildings and his coursework helped me build a solid foundation in power systems and related topics and paved the way for finding new topics related to my research on smart buildings. I would love to express my sincere gratitude to all my course teachers who helped me develop knowledge and skills in diverse areas. I want to sincerely thank all of PhD dissertation committee members, Dr. Eddie Jacobs, Dr. Muhammad Shah Jahan and Dr. John Hochstein, for their consent to be part of the committee, their valuable time, precious comments and advices.

I am very grateful to all my past and present members of the Electric Power and Energy Systems (EPES) lab for their encouragement, support and friendship throughout my research time in the lab.

Finally, I am ever grateful to my parents, my lovely wife, all other family members, friends and colleagues at DUET for their continuous help and encouragement for completing my studies and thesis and being strong during adverse conditions.

PREFACE

The contents of this dissertation are obtained from six papers that are the outcome of this Ph.D. research. The contents in chapters 1, 2, 3, 4, 5, and 6 are published in Journal of Energies. Two conference papers are presented at the IEEE PES Innovative Smart Grid Technologies (ISGT) Conference 2020 and IEEE PES Transmission & Distribution (T&D) Conference and Exposition 2020. Three papers are currently under review at the International Journal of Electrical Power and Energy Systems, IEEE Systems Journal, and Journal of Modern Power Systems and Clean Energy. The articles that have been used as chapters in this Ph.D. dissertation are summarized below:

Chapters 1, 2, 3 and 6: S. M. M. Alam and M. H. Ali, "Equation Based New Methods for Residential Load Forecasting", *Journal of Energies*, 13(23), 6378, 2020.

Chapters 1, 2, 3 and 6: S. M. M. Alam and M. H. Ali, "A New Fuzzy Logic Based Method for Residential Loads Forecasting," Paper ID: 2020TD0342, *Proceedings of the IEEE Power & Energy Society (PES) Transmission & Distribution (T&D) Conference & Exposition*, Chicago, IL, USA, October 12-15, 2020.

Chapters 1, 2, 3 and 6: S. M. M. Alam and M. H. Ali, "A New Subtractive Clustering Based ANFIS System for Residential Load Forecasting," *Proceedings of the IEEE PES Innovative Smart Grid Technologies (ISGT) Conference*, Washington DC, USA, pp. 1-5, February 17-20, 2020.

Chapters 1, 2, 5 and 6: S. M. M. Alam and M. H. Ali, "Analysis of COVID-19 Effect on Residential Loads and Distribution Transformers", revised and resubmitted to *International Journal of Electrical Power and Energy System*.

Chapters 1, 2, 5 and 6: S. M. M. Alam and M. H. Ali, "Real Time Determination and Visualization of Health Conditions of Smart Loads in Residential Buildings", Submitted to *IEEE Systems Journal*.

Chapters 1, 2, 4 and 6: S. M. M. Alam and M. H. Ali, “Load Scheduling of Smart Residential Building Based on Levelized Cost of Renewable sources, Battery, Day-type and Incentives and COVID-19 Situation”, revised and resubmitted to *Journal of Modern Power Systems and Clean Energy*.

ABSTRACT

A smart building is the one that is equipped with automated systems such as lighting, shading, heating, ventilation, and air-conditioning (HVAC), etc., for fulfilling consumers' demand. An efficient load forecasting system helps the building energy management system (BEMS) schedule the loads, operate the energy sources and energy storage systems effectively during peak hours to reduce the cost of energy and remove the burden on the grids. Furthermore, load scheduling is a key element for demand side management (DSM) system to actively participate in the demand response program. Researchers have been investigating on improved and effective load forecasting and load scheduling methods over the last decade. The conventional method such as the artificial neural network (ANN) technique needs a lot of previous or historical data for training and learning. Moreover, the correlation between the inputs and output is very crucial for the better performance of the ANN methods. Similarly, other conventional methods such as random forest, LSBoosting and long short-term memory (LSTM) have their own drawbacks.

In order to overcome the drawbacks and limitations of conventional methods, this dissertation proposes new methods for load forecasting and scheduling. An effective real-time health monitoring system with a view to checking the health condition of all loads and getting a pre-alert before the advent of a disaster or faults is proposed. In addition, a web-based application to be accessed by any smart device such as smart television, mobile phone, etc., is suggested. Moreover, the impact of increased energy consumption during office hours due to the COVID-19 pandemic on the local distribution transformer is analyzed. Also, the behind-the-meter (BTM) sources to mitigate the adverse effect of increased load on distribution transformer is proposed.

Simulation results performed by MATLAB/Simulink software indicate that the proposed load forecasting and scheduling methods perform better than conventional methods. The proposed

health monitoring system is effective and can provide both normal operating and alert messages based on operating conditions. Moreover, it is found that the load consumption has increased due to COVID-19 lockdown situations. Finally, the proposed BTM solution can mitigate the adverse effect of increased loads and reduces the transformer loss.

TABLE OF CONTENTS

LIST OF TABLES

LIST OF FIGURES

Figure Page

I. INTRODUCTION

A. Background

The energy consumption in residential and commercial buildings all over the USA is almost 40% of overall electrical energy production. With the increase of comfort demand of residents, the energy consumption is ever-increasing [1]-[2]. Therefore, providing the required power by the grid is a hard task especially during peak hours of the days. However, this problem can be solved in two ways. Firstly, by proper planning and allocation of energy resources by the grid, adequate power can be supplied to the consumers. Secondly, by implementing effective demand-side energy management system in the smart building that is capable of scheduling the load efficiently, the total cost of energy can be reduced by utilizing less loads that are operated by the grid power during the peak hours without affecting the consumers' comfort demands [3]-[4]. An efficient load forecasting system helps the buildings' energy management system schedule the loads, operate the energy sources and energy storage systems effectively during peak hours to reduce cost of energy and remove burden on the grids [5]-[7]. It also creates the possibility for the smart building to sell energy to the grid during peak hours [8]. Moreover, with the knowledge of load forecasting, the grid can allocate resources ahead of time and efficiently to meet up the load demands [9]-[10]. Therefore, researchers have been investigating on improved and effective load forecasting over the last two decades. Based on the forecast horizon or time scale, the load forecasting is classified generally into three categories. The first type of load forecasting is known as short-term load forecasting (STLF) when the forecasting is done from one hour to maximum one week. It is normally used for adjusting the grid generation or rescheduling the demand for smart buildings [11]. When the forecasting ranges from one week to maximum one month, then that forecasting is called medium-term load forecasting (MTLF). The final one is known as long

term load forecasting (LTLF) when forecasting ranges from one month to year. Both the MTLF and LTLF are very useful for planning asset utilities [12].

Moreover, load scheduling is a key element for demand side management (DSM) system to actively participate in the demand response program. It also ensures the effective utilization of residential load to increase the efficiency of the system, minimization of the energy cost while maintaining the consumers' comfort demand to the utmost levels. It also helps the grid provide power with minimum energy source utilization during the peak power demand [13]. Fig. 1 shows the components of building's demand side management system. Moreover, efficient loads can be scheduled based on smart forecasting or smart meter data [14]. Nowadays the scheduling based on smart meter data has been gaining research popularity. In most of the research, the effective scheduling is done by shifting the schedulable/shifting load to a time slot where electricity price is lower or total electric charges get smaller. Various constraints, such as users' comfort, power generation, electricity price, energy storage operation and its state of charge, etc. can be considered.

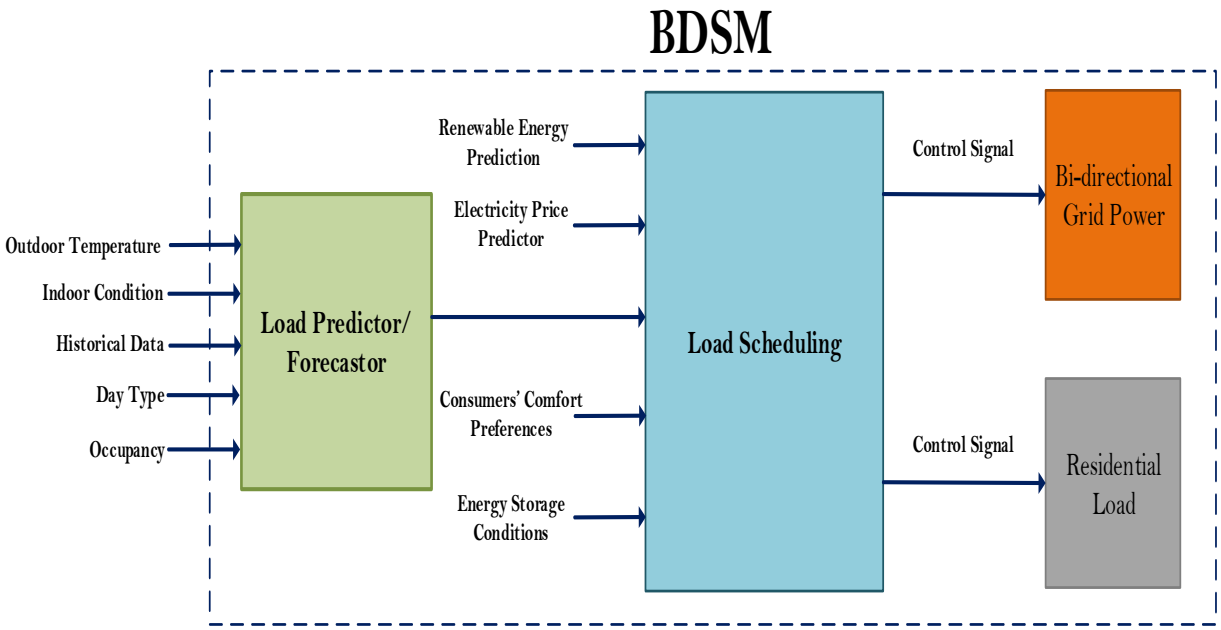

Fig. 1. The components of buildings' demand side management system.

Building Energy Management System (BEMS) is the centralized control system that controls automated systems such as heating, ventilation and air-conditioning (HVAC), lighting, etc., energy resources, and energy storage. Along with scheduling of loads based on the predictions, another purpose of the BEMS is to ensure the optimized and efficient coordination among the loads, energy sources and energy storage so that the inhabitants' can have their desired level of comfort by minimum consumption and reduced cost of electrical energy [15]-[16]. The components of BEMS are:

- Automated systems for providing inhabitants' demand.
- Energy sources for providing power to automated systems and even to grid if possible.
- Energy storage to keep a balance between production and demand power.

Researchers have been trying to improve the performance of the lighting, heating and HVAC systems in smart buildings. Some of them mainly have focused on the effective use of these systems so that the cost of energy can be reduced. Others have proposed efficient controllers that can optimize the system performance and improve the efficacy of the system by machine learning methods or internet of things (IoT) technology [17]-[18]. Moreover, there has been some research on smart load that can be controlled from the BEMS system or personally from outside according to conditions and demands [19]-[20].

Moreover, with technological advancement, all loads are being manufactured with features such as remote controllability, remote monitoring, energy efficient operation, etc. A smart home with a centralized controller, that can control the loads based on the demand or power availability, is very common nowadays. The centralized controller can even be utilized for load monitoring or fault analysis of the loads with the available data. Therefore, researchers are giving much

importance and priority to fault analysis and performance degradation study of residential loads. However, all the previous works found in the literature deal mostly with the diagnosis and detection of faults for the HVAC system only. But other loads such as water heater, refrigerator, etc., can also have their health issues. Therefore, it is important to know and visualize the health status of all the smart loads in residential buildings in real-time. A concept of the monitoring system that receives real-time operating data of all the loads and analyzes these data, based on the safe operational conditions, is needed.

The novel Coronavirus (COVID-19) has impacted every aspect of human life not only in the USA but also all over the world. The number of deaths due to COVID-19 has been piling up each day. Fig. 2. shows the COVID-19 statistics for the last eight months (March 2020 to October 2020) in Shelby County, Memphis, Tennessee, USA [21]. Many states in the USA have declared an emergency and imposed orders to be in partial/fully lockdown conditions. In order to remain safe, people were forced to stay at home, work from home wherever possible and the educational institution, public places were closed in Memphis from March 24th, 2020. Because of people's staying at home, the energy consumption patterns of residential buildings have changed. Specially, during the office hours, the load consumptions in buildings have increased dramatically.

It is noteworthy that the increased load consumptions at houses due to the COVID-19 situation will impact the residential distribution transformers. In particular, load patterns of distribution transformers will change. Even the distribution transformers may be overloaded. The safe operation of residential transformers depends on various factors such as temperature, loads, fault, etc. The hottest winding temperature of the transformer, top oil temperature, and loss of life due to insulation aging are important features that indicate the safe operational range and life span of residential distribution transformers [22]-[23].

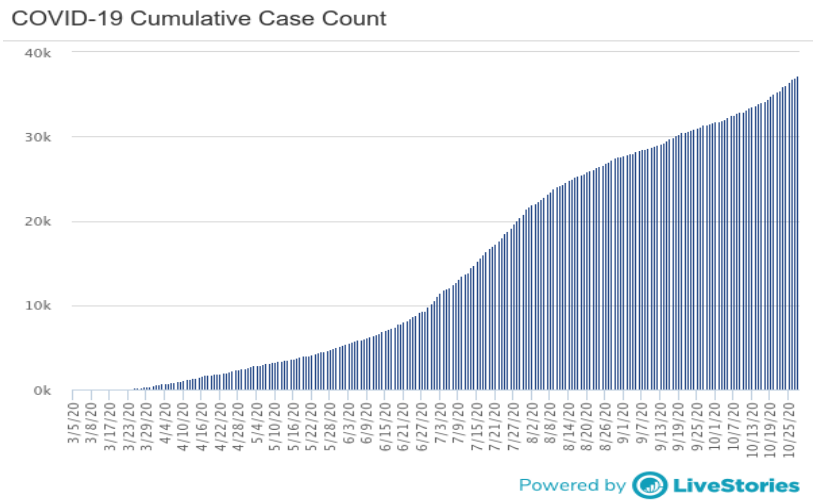

Fig. 2. COVID-19 statistics in Shelby county, Memphis, TN, USA [21].

Due to overloading, the distribution transformers may get damaged. Moreover, along with load magnitude, the harmonic contents in load current have severe effects on transformers' hottest temperature rise, top oil temperature rise, loss of life and transformer failure. Therefore, the operation of distribution transformer due to change in load patterns at residential buildings needs attention and should be investigated. If the lockdown situation due to this COVID-19 continues for a long time, the local distribution transformers will have much chance of getting overloaded. Therefore, it is important to analyze the potential impact of increased residential energy consumptions during office hours on distribution transformers and explore appropriate solutions to mitigate the adverse impacts.

Therefore, based on the above discussion, the drawbacks of the existing methods of load forecasting, load scheduling, health monitoring systems and impact on the distribution transformer during COVID-19 pandemic situations can be summarized as:

- The conventional load forecasting methods such as artificial neural network (ANN), support vector regression (SVR) method, adaptive neuro fuzzy inference system (ANFIS) system require lots of features and data during

training to effectively predict the loads. However, lots of data and other information are not always available for all the buildings. Therefore, new forecasting methods are still required that can predict the systems' outcome with a moderate amount of data and less input/features. Moreover, forecasting methods should be practically and easily implementable.

- The load scheduling found in the literature are based on assumptions of features of all the components. However, load scheduling in a smart building needs to be realistic and should be implemented in real practice. Therefore, real features of all components such as renewable energy sources, grid power, battery energy storage system along with actual demand response programs, that are available in practice, should be considered for implementing realistic load scheduling.
- No work has been found on the health status monitoring of all the loads in a smart building, although it will be a crucial element in future smart homes.
- No work has been found on the impact of the COVID-19 pandemic situation on the consumers' load pattern change or the overloading conditions of residential distribution transformers.

To overcome the limitations and drawbacks of all the previous works, this dissertation:

- Proposes prediction methods for residential loads forecasting that are not only efficient in prediction but also practically implementable and feasible.
- Proposes multi-objective load scheduling for smart residential loads that can be effective in normal operating conditions.

- Proposes real time heath condition monitoring system of all the smart loads of a smart building that will be the pivotal features of smart homes in the near future.
- Analyses the effect of COVID-19 situation on the energy consumption in residential buildings and the effect of increased loads on local distribution transformer. In addition, to mitigate the adverse effect of increased loads on distribution transformer, few solutions such as the behind-the-meter (BTM) sources implementation, load scheduling, and less utilization of loads having high harmonic distortion are proposed.

B. Motivation

The motivations behind this research are proposing implementable load forecasting techniques, scheduling methods, real time health monitoring system for all loads and impact analysis of load consumption due to COVID-19 pandemic situation on distribution transformers. These points are described below:

- Energy consumption of the automated system is ever increasing. Therefore, feasible and practically implementable load prediction/ forecasting system is crucial element for demand side management system to facilitate effective loads' scheduling ahead of time to cope with the increasing demands with the resources available and consumers' comfort demand requirements. Without effective load forecasting, the demand side management system will not be effective with proper allocation of resources and management of loads which may reduce the efficiency of the building's

management system or even endanger power system stability in the buildings.

- The efficient scheduling methods should consider electricity price, levelized cost of energy sources, energy storage, the consumers' preference and day type while scheduling. Therefore, the scheduling based on predicted load is crucial to remove huge energy demand on the grid. The smart building should be capable of responding to the grid demands to enjoy incentive and low energy cost because of buildings' participation in the demand response. All the features of components such as grid power, renewable energy sources, energy storage, even the demand response program, while considering scheduling, should be realistic and practically implementable. Without proper load scheduling, the consumers' comfort desire cannot be fulfilled to the maximum with available resources and low cost of energy.
- The real-time health status monitoring system will be a very essential element in future smart homes to be aware of the health condition of all loads and take preventive measures before any fault happening and reduce the damages to the loads. Moreover, this health monitoring system should be accessible through any smart device to see and take actions remotely or in presence in the buildings. Without the real-time health monitoring system, the consumer will be unaware of the performance degradation of loads before it gets too late to recover.

- The impact of COVID-19 situation has impact on energy consumption pattern change of the consumers, as consumers are forced to stay at home leaving their daily activities. Therefore, investigations are required on the effects of energy consumption pattern change on residential distribution transformer so that preventive measures can be taken in case of overloading conditions. Moreover, the safe operating range of energy consumption should also be investigated to prevent the shortening of transformers' operating lifespan. Without the analysis of the increased load on the distribution transformer, the consumer will be unaware of the consequence of energy consumption which may cause transformer failure.

C. Objectives

The main objectives of this dissertation are:

- Developing effective prediction systems with improved efficacy over the conventional methods, such as artificial neural network, support vector machines, random forest, gradient boosting, long short term memory (LSTM), based on the new input features and that are easily and practically implementable.
- Implementing new scheduling methods on net-zero smart building with a view to fulfilling its being net-zero building with added features like consideration of indoor conditions, number of occupants with their comfort preferences, limitation of total harmonic distortion and power loss to the

minimum while ensuring the occupant's comfort to the maximum. In addition, all the costs of renewable and battery energy storage should be calculated in terms of the levelized cost of energy to make the scheduling realistic.

- Proposing new real-time web-based health status monitoring system of smart loads available in the smart building that will be the key feature of future smart buildings.
- Analysis of the COVID-19 effect on energy consumption in residential buildings and the adverse effect of increased consumption on residential distribution transformer, and consequently exploration of appropriate mitigation solutions that are practically feasible and implementable.

D. Novelty of the Proposed Work

The novelties of this proposed work are:

- Developing both linear and non-linear equation-based prediction systems based on the heating degree days (HDD), cooling degree days (CDD), number of occupants and the day type (i.e normal working days, weekend, special days) that are easily and practically implementable. The equation-based prediction systems perform better than that of PSO tuned fuzzy and ANFIS systems.
- Developing new fuzzy and ANFIS systems that take only temperature and newly developed variable from the number of occupants and day types. The calculations required for both methods are less than the conventional systems and the parameters are tuned by particle swarm optimization (PSO)

technique. Both systems perform better than the conventional ANN system, random forest, gradient boosting and LSTM methods.

- Developing an efficient Scheduling of loads based on an objective function that considers minimizing weighted some of the energy cost, consumers discomfort, total harmonic distortion and power loss while providing power to the loads. The inclusion of the levelized cost of the renewable energy sources, incentive and levelized cost of battery while considering energy cost as well as considering both thermal and scheduling discomfort equation modification for consumers discomfort based on indoor conditions, number of occupants, occupants' preferences and the day type.
- Proposing a real-time health status monitoring system that can alert the consumers ahead of time about the fault or anomaly behavior that can lead to a probable failure or can be damaging for the smart loads. Moreover, a real-time web-based monitoring system is proposed for all the loads that can be easily visualized in smart television, smart mobile phones, smartwatches, etc.
- Analyzing the energy pattern changes of residential loads, especially during the office hours (9.0 am to 6.00 pm) and their impacts on the residential transformers in terms of hottest winding temperature, top oil temperature, and percentage loss of life (%LOL). Mathematical modeling of the hottest winding temperature of the transformer, top oil temperature, and loss of life are utilized to conduct the proposed analysis. Moreover, to mitigate the adverse effects of increased energy consumptions at houses on distribution

transformers, the operation of the BTM sources such as the photovoltaic (PV) power, battery energy storage, and electric vehicle during office hours, load scheduling, and less utilization of loads having high harmonic distortion while scheduling, are proposed as solutions.

E. Organization of this Dissertation

This dissertation is organized in the following way:

In chapter 2, a detailed literature review on load forecasting, load scheduling, smart loads' control, faults' analysis of residential loads, etc., is presented. Chapter 3 and Chapter 4 discuss the load forecasting and load scheduling methods for smart residential buildings, respectively. In chapter 5, the smart loads' control mechanism is presented. Finally, chapter 6 concludes the contents and contributions of this dissertation with the recommendation for the scope of future work.

II. LITERATURE REVIEW

In this chapter, a detailed literature review on the load forecasting approaches, load scheduling methods, fault diagnosis and health monitoring system of smart loads, and harmonic effect on the transformer loss is provided with a view to investigating the performance of conventional methods and finding any drawbacks that can be further improved.

As discussed in the introduction section, based on the forecast horizon or time scale, the load forecasting can be classified generally into three categories, namely short-term load forecasting (STLF), medium-term load forecasting (MTLF) and long-term load forecasting (LTLF) [11]-[12]. Moreover, among various types of methods that are found in the literature, the most common is either time series or regression model type. The performance of time series models such as exponential smoothing, autoregressive integrated moving average (ARIMA) model, etc., depends upon the correlation between the loads and their previous values and very large data set [11], [24]-[26]. Other popular conventional methods that are found in the literature are regression trees [27]-[28]. The random forest is a homogeneous ensemble approach having the combination of many decision trees without dependency on each other [29]. The drawback of the random forest method is its inability to extrapolate meaning that its prediction range is confined by the range in the training data as it takes the average value of all the trees. Moreover, it can be overfitted if the data set is large or noisy. Gradient boosting tree is another ensemble method that has been used for prediction [30]-[31]. The contrast between gradient boosting tree and the random forest is that it utilizes one tree for error minimization based on the experience of the previous tree. However, the gradient boosting tree method is more vulnerable and can be overfitted in the presence of noise during data training and also more parameters are needed to be tuned as compared to random forest. However, once it is properly tuned, it performs better than the random

forest approach. Moreover, multiple linear regression-based forecasting methods perform well for linear systems only, whereas the buildings' loads are mostly non-linear in nature and the power consumption is non-linear as well [32]-[33]. Therefore, researchers have been focusing more on artificial intelligent based prediction system because of its ability to predict non-linear load well based on different indoor and outdoor conditions [34].

The artificial intelligence-based method includes Fuzzy logic (FL), adaptive neuro fuzzy inference system (ANFIS), artificial neural network (ANN), support vector Machine (SVM), etc. Among the artificial intelligence systems, the ANN method has been found to be popular for load forecasting [35]-[39]. A multi block neural network, with a view to predicting price and load, has been proposed in a recent work [40]. Moreover, the Ridgelet and Elman neural networks-based load forecasting has been described in another work [41]. However, the ANN method requires a lot of historical data during the training and validation stage for future data prediction [11]. Moreover, the performance of the ANN depends upon several factors such as the correlation between the inputs and output, the proper and efficient tuning of weight and bias of the hidden and output layer [35].

Therefore, in order to get better prediction method, the authors in [42] proposed a new two input fuzzy logic system for residential load forecasting that performs better than the ANN system. Between the two inputs of the fuzzy system, one is the temperature and the other is a variable that is calculated from the occupancy number and day type. In another work, a fuzzy based peak energy management system is proposed for industrial consumers [43]. Moreover, a new subtractive clustering based ANFIS system is proposed by authors [44], where the temperature and another variable calculated from occupancy and day type, are considered as inputs, and the proposed ANFIS system performed better than the conventional ANN system. It is to note here that fuzzy

logic is a non-linear system that operates on IF-THEN logic [45]. In addition, a fuzzy system is a slow system as it operates on the fuzzy rules that are dependent on the number of inputs, the membership function for each input. If each input has m membership functions and there are n inputs in the fuzzy system, then m^n rules need to be evaluated for each iteration of the fuzzy system, and therefore it is practically not suitable for implementation especially if the number of inputs exceeds two as the system becomes slower. Moreover, the ANFIS system is a combination of both neural network and fuzzy systems. Therefore, the ANFIS system requires a lot of data for the training and validation of the system. In addition, like the fuzzy system, the ANFIS system is slower system to implement practically for prediction if the number of inputs exceeds two.

Moreover, in recent times, the upgraded version recurrent neural network named long short term memory model has been popular for forecasting [46]-[48]. The LSTM operates well where conventional recurrent network fails with large scale of sequential input data. However, the LSTM is more complicated than conventional neural networks and it is a black box lacking interpretability. Moreover, it doesn't perform well if input data set is small and if the parameters are not properly tuned or input data are not sequential.

In addition, stochastic optimization-based prediction systems have been gaining popularity for forecasting. They are utilized in case of uncertainty in the system. The bidding strategies and demand uncertainties of large consumers are proposed by hybrid stochastic approach in a work [49]. Similarly, stochastic optimizations have been proposed for dealing uncertainties in cooling demand and risk assessment of large consumers respectively [50]-[51].

Load scheduling is a pivotal component in smart buildings that enables them to actively schedules loads effectively based on demand response requirements. It strikes balance between the consumers' comfort demand and cost of electricity ensuring efficient use of resources and keeping

the highest possible efficiency of the system. It also helps the grid operate with minimum energy sources to meet the demands during the peak hour [52]. Therefore, different scheduling schemes have been proposed in the literature. Among them, the load scheduling with a view to reducing the energy cost has been most popular.

The load scheduling methods with a view to reducing or controlling the cost of energy, which are found in the literature, have three energy source conditions. The first one is load scheduling with a view to reducing the cost of grid power. In this case, the grid power availability and the cost of it are mainly considered for load scheduling. The costs of grid power that are mainly considered are real-time price or time of use (TOU) price [53]-[58]. In these works, the real-time or TOU price are mainly assumed and no real data that are offered by the utility service providers have not been considered. In most cases, it is assumed that the consumers are getting power through the smart meter by which they know the real-time price. Although this has been a common mode of analysis, still the scheduling based on realistic time of use price and incentives that are offered by the utility service provider in the USA, need further investigations.

The second type of scheduling for residential building that is found in the literature is facilitated with both grid power and battery energy storage [59]-[61]. In this case, a hybrid electric vehicle can be considered as a battery storage system. The battery energy storage is operated in such a way that it charges during the off-peak hour when the electricity price is low and try to give power to the load whenever possible or mostly in peak hours when the electricity price is high. In [60], although the battery operating cost is claimed to be assumed, the levelized cost of battery energy storage, which represents the cost of battery operation in terms of kWh, has not been considered, and therefore it needs to be considered as the battery has operating life and degradations.

The last type of load scheduling is for the buildings that are facilitated with renewable energy sources such as solar, wind power, etc., and grid power with or without battery energy storage [8], [62]-[68]. In this case, load scheduling is mainly done with available renewable energy without taking grid power or taking minimum grid power. And a battery acts as a secondary device. In most of the research ([63]-[66]), the grid power is minimized to reduce the cost of energy without considering the levelized cost of renewable energy and battery energy storage. In some work [62], PV and Wind cost is taken from online, that is not realistic in terms of the annual cost. In [8], the cost of renewable energy is simply assumed. The authors in [67] have considered the cost of PV energy. However, it is never mentioned how the cost is obtained and no such value is found. The cost of PV energy is again assumed in [68]. Moreover, the renewable energy cost should be presented in terms of levelized cost of energy as it takes into account the installation cost, bank loan, operation and maintenance cost and productivity during the lifespan of the energy sources. That is the reason why the DoE and national research laboratories in USA always express the renewable energy expenses in terms of levelized cost of energy as it is realistic. The costs of renewable energy that are found in the above-mentioned literature are either assumed or the data are obtained online that are not levelized cost of energy as well. Therefore, the cost of renewable energy and battery energy storage should be expressed in levelized cost of energy for cost calculation with a view to reducing the cost of energy while scheduling to be realistic.

Moreover, the energy consumption or load pattern of a residential building depends on the normal working days, weekends and special days [42], [44]. The special day is a day when the energy consumptions will be much higher than that of working days or weekends although it can be working days or weekends. It varies from family to family based on their culture, habits, etc. Therefore, while load scheduling the strategy should be different for normal working days,

weekends and special days. The load scheduling, based on the three different days mentioned above, has not been considered in the literature for residential buildings to the best of our knowledge.

Furthermore, one energy scheduling is found in the literature considering the total harmonic distortion as constrain [69] with a view to reducing the voltage, frequency deviation of medium sized commercial building. Similarly, another work [70] proposed energy scheduling considering total harmonic distortion as constrains to investigate the effect of total harmonic distortion on microgrid economics. However, the total harmonic distortion, along with power loss associate with it, should be considered as a percentage of the total power provided to the loads while scheduling.

Another objective of load scheduling is to maximize the comfort demand of the consumers based on their preference while keeping the cost of energy as low as possible. Therefore, the load scheduling based on thermal discomfort, visual discomfort, etc., has been found in the literature [71]-[74]. In [75], the percentage of discomfort, that a member of a large group of people is likely to feel, is proposed based on temperature, relative humidity and cloth types of occupants. However, it does not mention how it varies with the number of people or how large the group should be. The humidity, number of occupants, and the inside temperature of the building for HVAC settings, to control the thermal comfort/discomfort of the occupants, should be considered. In addition, no work has considered humidity inside the building as a comfort feature to the best of our knowledge although humidifier in the building is available that can be tuned based on the dry bulb temperature, number of occupants and other features. That is also true for indoor luminance for visual comfort. Therefore, these three terms combinedly can be considered as indoor discomfort features that need to be minimized.

Moreover, as the technology is getting more advanced, the operating data of all smart loads can be easily accessed or even monitored. However, very few research works have considered the fault analysis and performance degradation study of residential loads. A review was conducted on all the data mining technologies applied to the HVAC and water heater system for fault detection and diagnosis with their pros and cons [76]. The main concentration of that work was on the fault detection methods rather than the fault type of HVAC or water heater system. In another review paper, a detailed analysis of fault detection and diagnosis methods of HVAC loads with comparative analysis of pros and cons of each method, is proposed in [77]. Another work reviewed all the methods applied for HVAC and lighting system with a view to finding the current challenges and looking for proposing solutions based on current technologies [78]. A review work summarized the data mining and classification techniques that are used for the fault diagnosis of the HVAC loads [79]. Moreover, the challenges of diagnosis for HVAC fault are proposed and the comparisons among the various promising methods are also provided for the office building in a work [80].

The abnormal fault analysis, based on the deep neural network, is proposed in a work where previous load data are utilized as references for the fault detection [81]. The detailed analysis of known and unknown faults on the air handling component is proposed in another work with the hidden Markov model for failure mode identification and a new statistical model for new fault identification [82]. A health monitoring system is proposed with the combination of fuzzy system and neural network for the HVAC system for fault classification, trends and detection [83]. Moreover, the system is claimed to be effective in providing pre-alert to the user for an upcoming fault resulting in higher energy usage and operational cost. A bimodal parameter estimator is proposed with the capability to detect and diagnose of faults in condensing boiler of HVAC system

with limited amount of data [84]. A deep neural network-based fault detection system for the cooling system is proposed that can detect the new or unknown type of fault. A Monte Carlo (MC) dropout system is proposed as an assistive system with the deep neural system mentioned above for fault detection [85].

A lab setup is proposed in a research work for the HVAC system with a view to detecting and diagnosis fault [86]. In another work, a combination of Dempster Shafer (DS) evidence theory and support vector machine-based fault detection model is proposed and experimented with a real setup for the solar water heater fault detection and diagnosis [87]. A complete data set for fault detection of the air handling system in HVAC system, based on the simulation and experimental results, are developed with a view to facilitating fault diagnosis in residential building [88]. A convolution neural network is proposed in another work for detecting and diagnosing faults in the heat source of the HVAC system [89]. However, the convolution network in the above work is reported to be unable to determine the impact of the fault. A virtual temperature sensor concept is proposed for ventilation unit fault detection and diagnosis, analyzed by both linear & non-linear regression methods and statistical methods [90]. Three classifiers, based on supervised learning, is proposed for air handling system with a view to evaluating both the influence of different faults on the co-efficient of performance (COP) and the efficacy of the proposed classifier in classifying the faults [91].

In a research work, the authors proposed a web-based framework for fault management system having the capability of detecting fault of HVAC system for commercial building [92]. That work is practically implemented by the data driven approach for a commercial building in San Diego, USA. In another work, a machine learning-driven MATLAB/SIMULINK model is proposed for HVAC fault detection and diagnosis for office buildings [93]. Moreover, a multi-

level machine learning method is proposed for the HVAC fan coil for fault diagnosis in a work for smart residential building [94]. The authors, in a work, examine the vibration of a normal washing machine and a washing machine without and with faulty rotor of the same company by discrete wavelet method [95]. Durability aspects associated with the use of washing machines and existing testing methods are reviewed and a testing procedure, for assessing and verifying the durability of washing machines, is further developed in another work [96]. The failure mode and durability of washing machine and dishwasher, with analysis on the importance of components that need to be repaired along with the time duration of repairment, are discussed in another work [97].

Moreover, no work is found in the literature to investigate the impact of the COVID-19 pandemic situation on energy consumption pattern change or the impact of energy consumption change on residential distribution transformers. However, the effects of overloading on the distribution transformers are analyzed in [98]-[100]. Moreover, transformers' hottest temperature rise, top oil temperature rise, loss of life and transformer failure are influenced by the harmonic contents present in load currents [101]-[102]. Based on this knowledge, the effect of the increased load because of the lockdown condition can be further investigated.

A. Conclusion of the Chapter:

In this chapter, the detailed literature review is done on several topics related to smart buildings such as load forecasting, load scheduling, real-time health monitoring and fault diagnosis system of smart loads and contributing factors for the increased loss on distribution transformer with a view to gaining knowledge on the state of art. Moreover, the drawbacks of conventional methods are mentioned in order to propose new methods to improve performance.

III. LOAD FORECASTING

In a smart building, load forecasting is an essential element to help the demand side management manage loads effectively and efficiently ahead of time. Therefore, it is an indispensable prerequisite for an efficient load scheduling system. Many research works have been ongoing on load forecasting over the last two decades. However, in smart buildings, all the components in the centralized controller or demand-side management system such as load forecasting, load scheduling are real-time applications. Therefore, the load forecasting methods should be efficient, real-time applicable and faster in calculations. Considering the above features, this work proposes forecasting methods that have the following characteristics:

- They are practically implementable and feasible.
- The important features that play vital roles in energy consumption in the buildings are considered as inputs of the proposed load forecasting systems to predict the load consumption effectively and efficiently.
- It performs well with lesser number of inputs which makes systems faster and requires less time, calculations for prediction. Moreover, it requires less amount of smart meter data for the training of the parameters.

In this chapter, the general descriptions of the proposed methods of load forecasting are discussed first and followed by contemporary popular methods in the literature. Finally, the performance comparisons among the proposed methods and conventional methods, in terms of simulation results and performance indices such as absolute mean average error, root mean square error, absolute mean average percentage error, are presented to validate the efficacy of the proposed systems for residential load forecasting. In this work, the predicted data for all methods are simulated in MATLAB software.

A. Proposed Methodologies

1. Equation Based Prediction System

This method considers two non-linear equation-based systems and one linear equation-based system for residential load forecasting based on heating degree days, cooling degree days, occupancy and day type which are applicable to any residential buildings having small sets of smart meter data. The co-efficients of the proposed nonlinear equations and linear equation are tuned by particle swarm optimization (PSO) and multiple linear regression method, respectively.

The load consumption of a building depends highly on temperature. The increase in temperature increases the load consumption if the temperature is above a certain temperature, in general 65°F in USA, due to higher cooling requirement. In addition, if the temperature goes below the same temperature, the load consumption increases due to the higher requirement of heating. Therefore, the energy consumption of a residential building is dependent upon HDD and CDD that represent the temperature below or above the 65ºF. Based on this fact, energy consumption, e, can be expressed as the following:

$$e \propto HDD$$

$$e \propto CDD$$

Moreover, for the same temperature, HDD, CDD, the energy consumption increases with an increase in number of occupants and decreases with a decrease in occupants in the same apartment. Therefore,

$$e \propto Occupant$$

In addition, the energy consumption pattern of a building changes with any special day or special occasion. The special day depends on the family living in a building when there may have

some religious festival celebrations, some family events happening, or more than usual family members staying in the building for some reasons. Also, it can be a normal working day or weekend or even holiday. Therefore,

$$e \propto Day\ type$$

Therefore, based on the above discussion, three types of equations, as shown from (1) to (3) below, have been developed for load predictions in this work. The first equation is linear in nature as variable HDCC, occupant number (O) and day type (D) values are linearly multiplied with the co-efficients to predict the total energy consumption of the day. Moreover, the other two equations are non-linear in nature as some power values of HDCC, O are multiplied with the co-efficients whereas D is used as power for equations (2) and (3). The exponential component is used in (2) whereas the variable is a constant whose values are determined by the optimization algorithm for (3).

$$e = C_1 HDCC + C_2 O + C_3 D + C_4 \quad (1)$$

$$e = C_5 HDCC^m + C_6 O^n + C_7 exp^D + C_8 \quad (2)$$

$$e = C_9 HDCC^p + C_{10} O^q + C_{11} a^D + C_{12} \quad (3)$$

where, e and O represent the total load consumptions in kWh in a day and the number of occupants present on that day, respectively. HDCC represents the HDD values which is the difference between the average day's temperature and 65°F if the temperature is below or equal to 65°F. Moreover, HDCC represents the CDD values which is the difference between 65°F and the day's average temperature values if the temperature is above 65°F. The co-efficients C_1, C_5, and C_9 depend on HDD or CDD values for (1) to (3), respectively. C_2, C_6, C_{10} are the co-efficients for number of occupants. The co-efficients C_3, C_7, and C_{11} vary with the day type. The co-efficients

C_4, C_8, and C_{12} are considered to be off-sets that are dependent on HDD, CDD, occupancy and the day-type. The values for D for normal working days, weekend and special days are considered to be 0, 1, and 2, respectively, for this work. The equations proposed in (1) and from (2) to (3) are linear and non-linear in nature, respectively, and their performances certainly depend on the properly tuned values of the co-efficients with the varying HDD, CDD values, occupancy or the type of the days. Therefore, multiple linear regression method and PSO algorithm have been utilized to obtain the co-efficients of the linear equation in (1) and non-linear equations proposed in (2)-(3), respectively, in order to predict the optimal total energy consumption of the day.

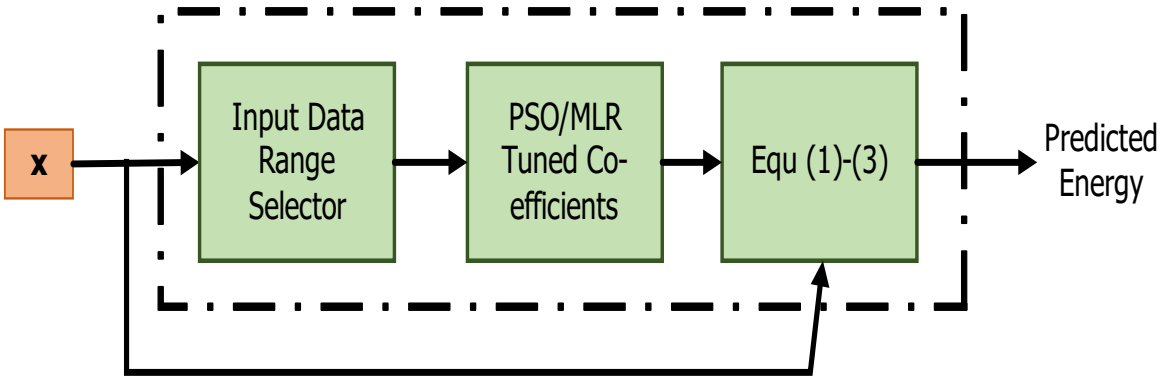

Fig. 3. Block diagram of equation-based prediction system.

The working principle of the equations for residential load predictions, which consider the HDD, CDD, occupancy and the values of D, based on normal working days, weekends or special days, as inputs (x) are shown in Fig. 3. In this work, generalized equations are formulated based on the inputs. The dotted line, as shown in Fig. 3., represents the equation-based prediction systems. At first, the inputs (x) are fed into the equation-based prediction system so that the ranges of the input variables are selected. Once the ranges of the variables are selected, the MLR/PSO tuned co-efficient values are sent to the main equation block where the equations from (1) to (3) are utilized to predict the energy consumption based on the inputs and the co-efficients. Then, multiple linear regression method or PSO provide the optimized co-efficient ($C_1 \ldots C_4$ /

$C_5 \ldots C_8/C_9 \ldots C_{12}$) values for the proposed equations from (1)-(3) based on the range of inputs (i.e HDD, CDD, O, D) which are summarized in Table 1, Table 2 and Table 3 later. Finally, the predicted total energy consumption per day is calculated with the corresponding equations and selected coefficients, constants and inputs (i.e., HDD, CDD, number of occupants, etc.), that are provided to both PSO and Equation, as shown in Fig. 3.

i. Parameter Tuning by Multiple Linear Regression (MLR) Algorithm

In MATLAB, the command, regress is used for calculating the co-efficients of the linear model that has the following format:

$$y = Cx \tag{4}$$

subject to

$$\sum (y - e)^2 = minimum$$

Where the input matrix, x= [HCDD; O; D; U], C= [C_1 C_2 C_3 C_4] and y represent the anticipated output obtained from the smart meter. U is a unity vector of length of HDCC vector to determine the values of C_4 by the multiple linear regression algorithm and introduced in the x matrix as dummy as for each set of data, the columns number of C matrix should be equal to the rows number of x matrix. By matrix multiplication of C and x matrix, the predicted output (e) is calculated and put to the condition shown above until the co-efficient values (C_1,….C_4) for which, the summation of square of the difference between the anticipated output (y) and predicted output (e), gets minimum.

ii. Parameter Tuning by Particle Swarm Optimization (PSO) Algorithm

As already mentioned, in this work the PSO method has been used for parameters tuning of non-linear equations shown in (2) and (3). It has been applied in wide applications such as

energy management [103]-[104], load predictions [105]-[107], etc. It is very easy to implement and has faster convergence speed and effective over other optimization algorithms such as the Genetic algorithm [104].

In PSO, a random number of particles are chosen for search space and the objective function is defined. Based on the cost function at any current location, the optimal position and cost are determined and updated among the particles. Each particle then finds its new position based on its current position, previous velocity and global optimal location among the particles. After updating their positions and velocity vectors, again the best position and cost among the particles are circulated and updated. Therefore, by updating the situations (position and velocity vectors) and collaborating the information of optimal best location and optimal cost, the swarm as a group reaches its optimal goal.

The PSO algorithm is characterized by the two-model equations of velocity and position vector in an N-dimensional solution space as shown below:

$$v_i^{k+1} = wv_i^k + c_1 r_1 \left(p_i^k - x_i^k\right) + c_2 r_2 \left(p_g^k - x_i^k\right) \tag{5}$$

$$x_i^{k+1} = x_i^k + v_i^{k+1} \tag{6}$$

where v_i^{k+1} represents i^{th} particle velocity of $(k+1)^{th}$ iteration of N-dimensional search space. Similarly, x_i^k corresponds to i^{th} particle velocity of k^{th} iteration. p_i^k and p_g^k correspond to the individual best position of ith particle and global best position of the swarm, respectively. Moreover, r_1 and r_2 are randomly chosen numbers which are uniformly distributed between 0 and 1 and c_1, c_2 are known as learning factors that control the significance of the best solution. The values for both learning factors are chosen to be 2. The value for the inertia co-efficient, w for each iteration number is calculated using the following equation:

$$w = w_{max} - \frac{t(w_{max} - w_{min})}{MaxI} \tag{7}$$

where, w_{max} and w_{min} represent the upper and lower value of w and t, $MaxI$ correspond to the current iteration number and maximum iteration number respectively.

The objective function for the current work is considered as follows:

$$f_{obj} = y - e \tag{8}$$

subject to

$$|y - e| = minimum$$

The procedure of the PSO algorithm is described as follows:

Part I: Initialization

1. Load the input (x) and anticipated output (y) value based on the smart meter data.

2. Set the parameters of the PSO obtained from several trials which gave the optimal output.

   Search space dimension = 1

   Population size = 30

   Maximum number of iterations = 150

   w_{max} = 0.9 and w_{min} = 0.2

   Penalty factor = 500

Part II: Iteration

1. Randomly generation of velocity and position vectors which is done by PSO.

2. Evaluate the cost function based on (5) to measure the fitness values for the corresponding inputs.

3. Start the iteration

   Run the algorithm 150 times.

   Based on (5) and (6), update the velocity and position vectors.

   Determine the predicted energy (e) for the predicted horizon. If the constraint is violated, then add the penalty factor.

   Determine the cost function.

   Update the individual best and global best values based on the cost function.

   Update the inertia weight.

   Repeat step 3 until the maximum number of iterations is reached.

After the optimal co-efficients are obtained from the MLR and PSO, the co-efficients are put into (1) to (3) to get the predicted outputs. The co-efficients, based on different HDD, CDD, occupancy and day type condition, as determined by the MLR and PSO methods, are shown in Table 1, Table 2 and Table 3 for equations (1) to (3) respectively.

Interpretability is the main advantage of this proposed method. The model explains the energy consumption based on the heating degree days (HDD), cooling degree days (CDD), occupancy and the day type. Moreover, it requires moderate amount of data (energy consumption, HDD, CDD, occupancy, day type) for parameter co-efficient tuning by MLR and PSO.

Table 1: Co-efficients of Equation 1 Determined by MLR Method

Condition	C_1	C_2	C_3	C_4
$CDD \geq 17°F, O \geq 0, D \geq 0$	0.882	1.499	10.260	0.00
$0 < CDD < 17°F, O \geq 0, D \geq 0$	1.857	23.054	2.920	-38.64
$HDD \geq 20°F, O \geq 0, D \geq 0$	-0.247	10.583	-0.676	6.48
$0.1 \leq HDD < 20°F, O \geq 0, D \geq 0$	1.825	5.195	4.092	-19.57

Table 2: Co-efficients of Equations 2 Determined by PSO

Conditions	Equation (2)					
	m	N	C_5	C_6	C_7	C_8
$CDD \geq 17$ $O \geq 2$ $D \geq 1$	0.642	0.906	1.662	6.779	8.723	-4.370
$CDD \geq 17$ $O \geq 2$ $D = 0$	0.462	0.389	14.455	11.955	5.289	-1.656
$10 \leq CDD \leq 16$ $O \leq 1$ $D \leq 1$	0.001	1.356	8.487	10.121	2.624	-8.716
$3 \leq CDD \leq 9$ $O \geq 3$ $D = 2$	0.001	0.695	0.010	9.275	3.164	0.645
$0 \leq CDD < 3$ $O \leq 2$ $D \leq 2$	0.368	0.974	2.964	6.079	2.269	-9.368
$HDD \geq 30$ $O \geq 0$ $D \geq 0$	0.253	0.852	8.723	14.206	0.010	-18.75
$20 \leq HDD < 30$ $O \geq 0$ $D \geq 0$	1.043	1.155	1.649	3.158	1.195	-17.32
$10 \leq HDD < 20$ $O \geq 0$ $D \geq 0$	0.534	1.262	1.059	17.918	0.010	1.127
$0.1 \leq HDD < 10$ $O \geq 0$ $D \geq 0$	0.0291	1.2687	0.0100	3.8381	0.0100	3.0354

Table 3: Co-efficients of Equations 3 Determined by PSO

Conditions	Equation (3)						
	p	q	A	C_9	C_{10}	C_{11}	C_{12}
$CDD \geq 17$ $O \geq 2$ $D \geq 1$	0.952	1.056	-6.80	3.070	13.146	-3.545	-6.80
$CDD \geq 17$ $O \geq 2$ $D = 0$	0.125	0.992	-10.9	12.784	4.393	-17.94	-10.9
$10 \leq CDD \leq 16$ $O \leq 1$ $D \leq 1$	0.001	1.375	1.979	12.598	6.295	-10.99	1.979
$3 \leq CDD \leq 9$ $O \geq 3$ $D = 2$	0.001	0.389	0.574	0.010	13.474	20.000	0.574
$0 \leq CDD < 3$ $O \leq 2$ $D \leq 2$	1.041	1.304	-2.438	13.281	7.641	10.555	-2.438
$HDD \geq 30$ $O \geq 0$ $D \geq 0$	0.728	1.100	0.407	0.551	9.557	-5.325	0.407
$20 \leq HDD < 30$ $O \geq 0$ $D \geq 0$	0.885	1.115	1.330	1.736	5.021	-15.914	1.330
$10 \leq HDD < 20$ $O \geq 0$ $D \geq 0$	0.368	1.137	0.933	6.257	6.409	5.787	0.933
$0.1 \leq HDD < 10$ $O \geq 0$ $D \geq 0$	0.180	1.143	-1.270	11.732	5.839	-10.59	-1.270

It is very convenient for practical implementation. However, the energy consumption of a residential building depends upon the habits of residents living there, responses to different environmental condition chance, mode of comfort, etc. Therefore, these three equations can be implemented for any building provided that the co-efficient are re-tuned based on the energy consumption pattern and other conditions.

2. Adaptive Neuro Fuzzy 2 Inference System (ANFIS2) Based Prediction System

The adaptive neuro fuzzy inference system (ANFIS) is a hybrid model that combines beneficial features of both neural network and fuzzy systems. It is very useful for non-linear system when the system has uncertainty, or it is very difficult to implement any linear relationship. In this work, a Sugeno-type ANFIS structure is considered that is divided into two parts namely antecedent and conclusion parts. Both parts are connected by fuzzy rules. For the chosen Sugeno type ANFIS system, the fuzzy rules are given by the following equation [30]:

$$If\ (x_1 = A_i)\ and\ (x_2 = B_i)\ then \\ f_i = p_i x_1 + q_i x_2 + r_i \tag{9}$$

where, x_1 and x_2 are the inputs to the ANFIS system that represent temperature and a variable, R respectively, for this work. Fuzzy sets are denoted by A_i and B_i. Therefore, f_i represents the output that is dependent on the fuzzy rules. The parameters (i.e., p_i, q_i, and r_i) are determined during the training process. The second input, R is determined by (10), given below:

$$R = occupant + 1.5 \times d \tag{10}$$

where, values of d for the normal working day, normal weekend and special day are considered as 0, 1, and 2, respectively.

The ANFIS system involves four steps. These are: 1) data generation, 2) rule extraction and membership functions, 3) training and testing, and finally 4) the results. For this work, two input and one output data of 304 days are provided for the training purpose. The input data are temperature and R values and the output is the energy consumption. The input data are trained by the hybrid algorithm that combines the backpropagation of the parameters of the input membership function and regression for the output membership function. In order to tune the input membership function and the fuzzy rule formation, either the number of membership function and the

membership type can be chosen manually, or subtractive clustering can be used. The following parameters, as shown in Table 4, are used for subtractive clustering for determining the number of membership functions, tuning of the membership function and fuzzy rule generation.

In this method, after these four steps mentioned above are completed, the conventional Sugeno type fuzzy system is converted into type 2 fuzzy system where the input membership functions are different from conventional input membership function as shown in Fig. 3 and the output membership functions, which are linear functions considered for this work, remain the same as in conventional fuzzy system method [108]. The parameters of upper membership functions of type 2 fuzzy systems remain the same as the corresponding membership functions of the conventional fuzzy system [109].

Table 4: Subtractive Clustering Parameter

Parameter	Value
Range of Influence	0.18
Squash Factor	1.25
Accept Ratio	0.85
Reject Ratio	0.15

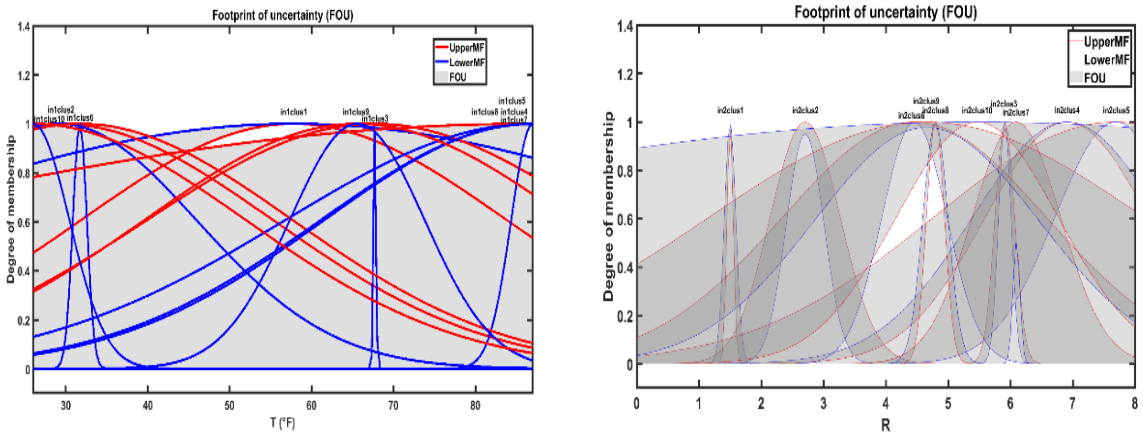

Fig. 4. Input membership functions for ANFIS2 system.

From, Fig. 4, it is evident that type 2 membership function is defined by upper and lower membership functions that are represented by red and blue lines respectively. The area between

the upper and lower membership function is called footprint of uncertainty (FOU) as indicated by ash-colored shaded areas. The input values are fuzzified by calculating the degree of membership, based on the rule antecedent, from both upper and lower membership functions. Then the ranges of strength firing rules are obtained by implementing the fuzzy operator to the fuzzified values of membership functions. In this case, the maximum values of the upper membership function and minimum values of the lower membership function are considered for Sugeno type system. In the aggregation step, the output level of each rule of type 2 fuzzy system remains the same as the conventional system although in the conventional system they are done in the consequent step. In addition, in the aggregation step, the rule output levels are arranged in the ascending order which defines the universe of discourse for type 2 fuzzy set. The upper and lower membership values, for each output level, are chosen based on the maximum and minimum firing range values of the corresponding rule. Finally, the type 2 fuzzy set is reduced to type1 interval fuzzy sets by using the reduction method to get the crisp output for the inference system. The type 1 interval fuzzy set considers a range of values with lower (C_L) and upper (C_R) limit that, are considered as centroids, can be approximated by the following equations [110]:

$$C_L \approx \frac{\sum_{k=1}^{L} x_k \mu_{umf}(x_k) + \sum_{k=L+1}^{N} x_k \mu_{lmf}(x_k)}{\sum_{k=1}^{L} \mu_{umf}(x_k) + \sum_{k=L+1}^{N} \mu_{lmf}(x_k)} \tag{11}$$

$$C_R \approx \frac{\sum_{k=1}^{R} x_k \mu_{umf}(x_k) + \sum_{k=R+1}^{N} x_k \mu_{lmf}(x_k)}{\sum_{k=1}^{R} \mu_{umf}(x_k) + \sum_{k=R+1}^{N} \mu_{lmf}(x_k)} \tag{12}$$

where, N, x_k, μ_{umf}, μ_{lmf} correspond to the number of samples considered over output variable range, kth output sample value, upper and lower membership function respectively. The enhanced iterative algorithm with stop condition (EIASC) is used for this work as it is reported to be the most promising of all methods [111]. Finally, after the reduction steps, the input and output

membership function parameters are tuned and updated by PSO optimizing algorithm based on the inputs (x) and anticipated output that are obtained from smart meter data.

3. *Adaptive Neuro Fuzzy Inference System*

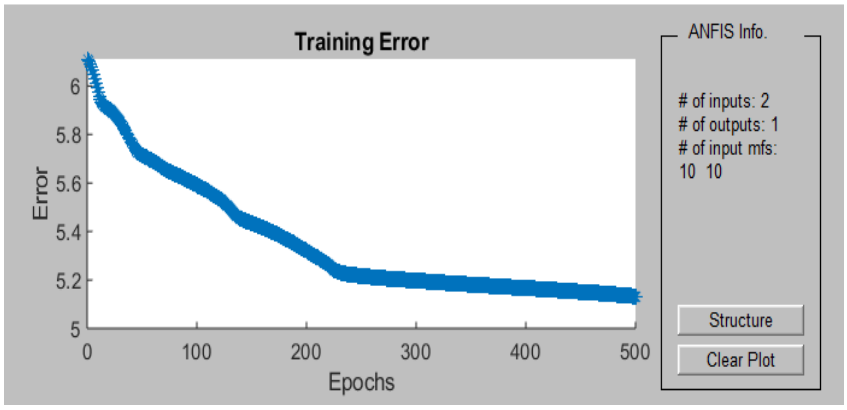

Fig. 5. ANFIS input data training.

For the simple ANFIS system, procedures and equations (9)-(10) are the same and for chosen subtractive clustering parameters, as shown in Table 5, the number of membership functions for both inputs became ten as shown in Fig. 5. The minimum error and the number of epochs are chosen to be 0 and 500, respectively. The minimal RMSE error after training reached 500 epochs is found to be 5.13.

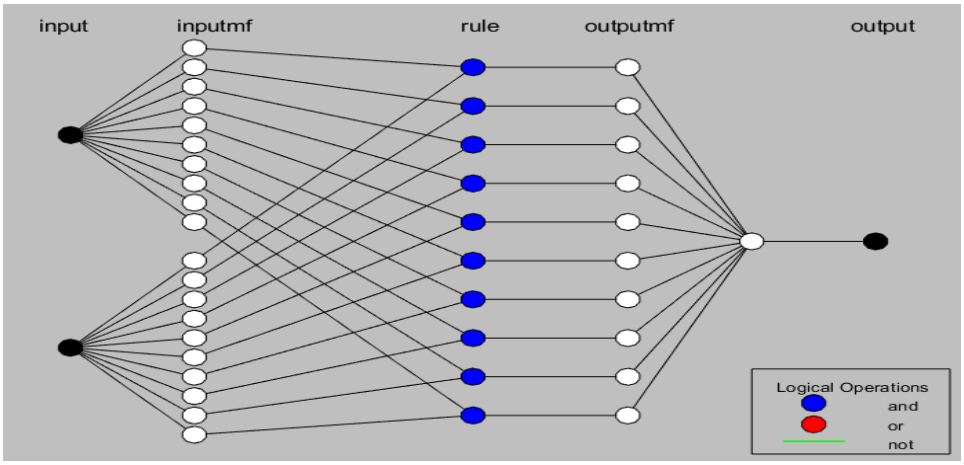

Fig. 6. ANFIS structure.

Table 5: ANFIS Parameter

Parameter	
Number of nodes	65
Number of linear parameters	30
Number of nonlinear parameters	40
Total number of parameters	70
Number of training data pairs	304
Number of checking data pairs	0
Number of fuzzy rules	10

From Fig. 6., it is clear that ten membership functions are used for each input and only ten fuzzy rules are created. The parameters of the ANFIS system are shown in Table 5. The gaussian fuzzy membership functions, that are used after tuning for both inputs, are shown in Fig. 7.

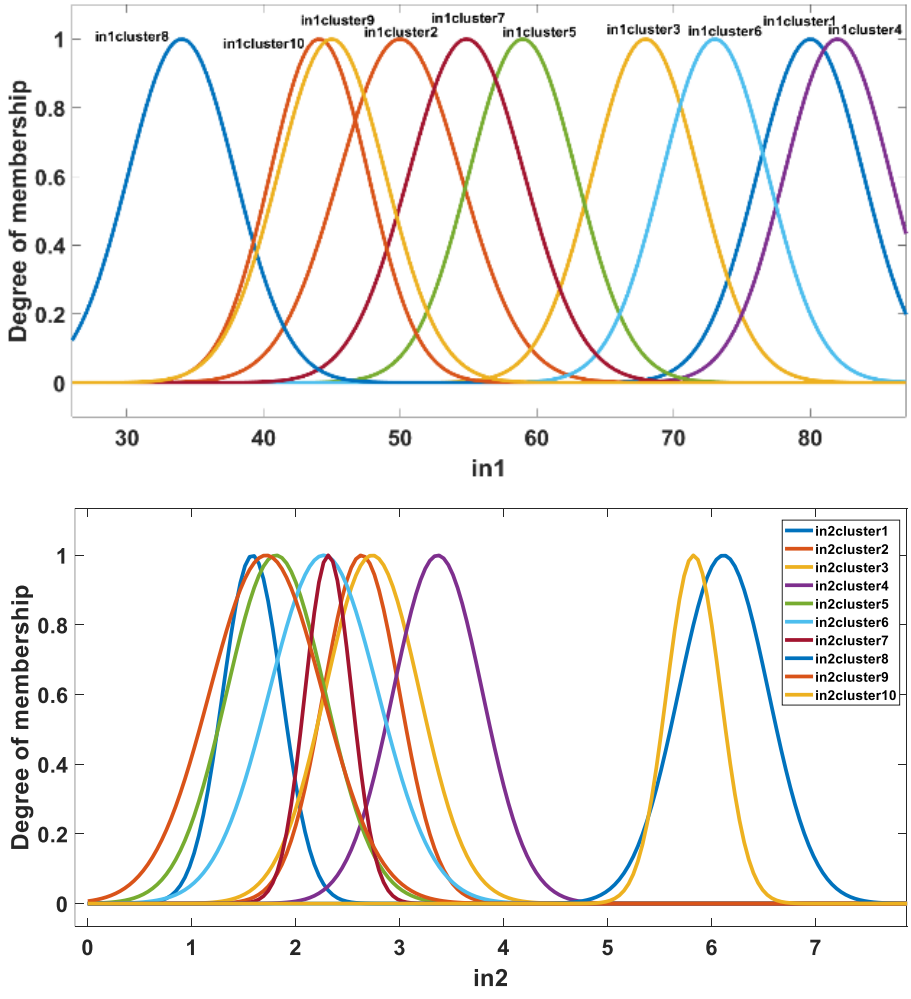

Fig. 7. Input membership function.

4. Fuzzy logic system

The Fuzzy logic is a non-linear system. It operates well based on IF-THEN logic in case of non-linearity or uncertainty present in the system or where mathematical modeling implementation is difficult [47]. The proposed fuzzy system is shown in Fig. 8.

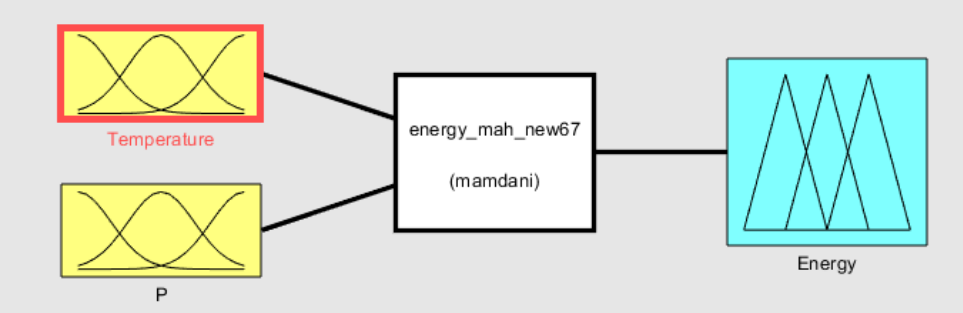

Fig. 8. The architecture of fuzzy system.

In the proposed fuzzy logic system, the temperature and a variable P are used as inputs. The fuzzy system provides the predicted energy consumption as output. The P variable is dependent on occupancy and day type and calculated using (13) given below:

$$P = Occupancy + 1.5 \times d \tag{13}$$

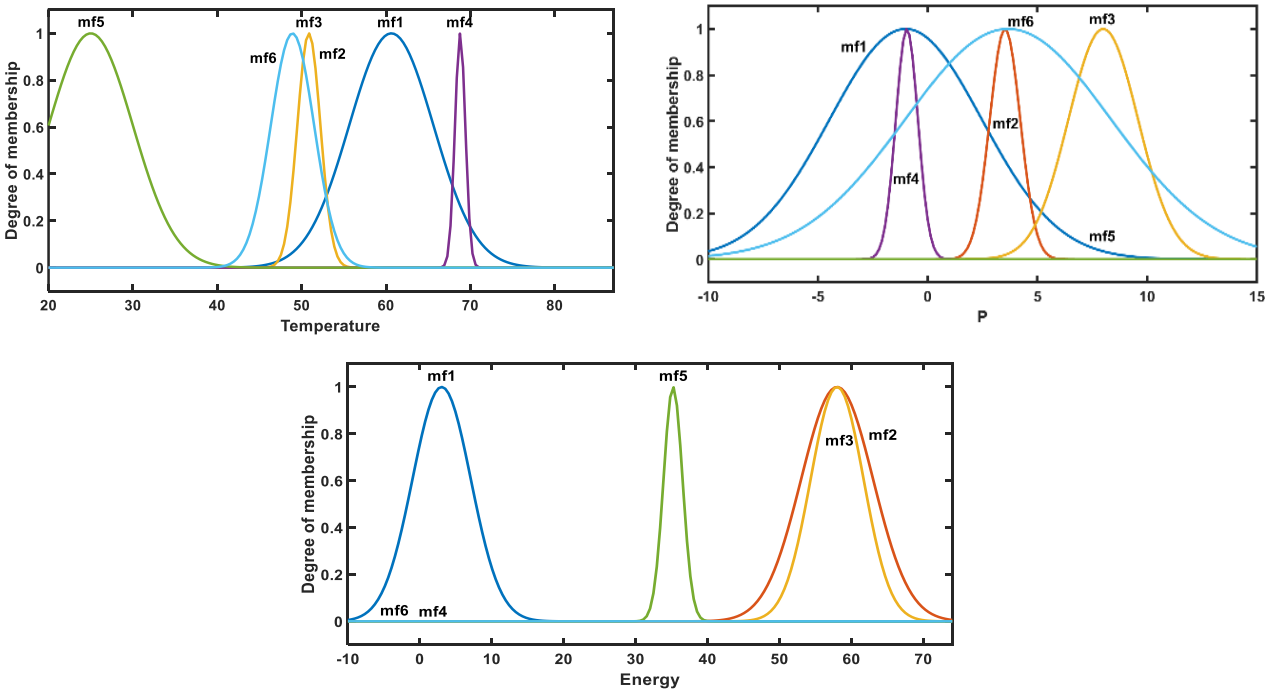

Fig. 9. Inputs and output membership function of the proposed fuzzy system.

The 6 membership functions for each input and output are designated as mf1 to mf6 as shown in Fig. 9. Although several membership functions such as triangular, trapezoidal, bell-shaped, Gaussian, etc., can be used for the fuzzy system, the Gaussian type membership functions, which are tuned by the PSO algorithm, provide the best results for prediction. The Gaussian membership functions, that are used to determine the grade of membership values, can be defined by (14) [47], [112].

$$\mu_{Ai}\,(x) = e^{-\left(\frac{x-c}{\sigma}\right)^2} \tag{14}$$

where μ_{Ai} (x) represents the values for the grade of memberships and i represents the rule number.

Similarly, c and σ represent the mean and deviation, respectively, for the Gaussian membership function. The values c and σ are optimized by the PSO algorithm. Since the proposed fuzzy system operates on the Mamdani method [47], the degree of conformity (W_i) is given by (15) as shown below:

$$\sum W_i = \mu_{Ai}\,(x_1) \times \mu_{Ai}\,(x_2) \tag{15}$$

As both inputs have 6 membership functions, the total number of fuzzy rules would be 36. The fuzzy rules are determined based on achieving the optimum output. In the final step, the output energy consumption crispy values are determined by the center-of-area method as defined by (16)

$$Energy\ consumption = \sum W_i\, k_i \Big/ \sum W_i \tag{16}$$

where k_i represents the value of energy consumption that is expressed as a linguistic variable in the fuzzy rule tables. The fuzzy rule table is shown in Table 6.

Table 6: Fuzzy Rules

		Temperature					
		mf1	mf2	mf3	mf4	mf5	mf6
P	mf1	mf1	mf2	mf1	mf2	mf2	mf1
	mf2	mf5	mf5	mf4	mf2	mf3	mf3
	mf3	mf5	mf4	mf1	mf2	mf3	mf4
	mf4	mf5	mf5	mf4	mf4	mf3	mf4
	mf5	mf4	mf5	mf4	mf5	mf4	mf5
	mf6	mf4	mf5	mf6	mf5	mf5	mf6

B. Conventional Methodologies

1. PSO Based Support Vector Regression (SVR) System

The PSO tuned support vector regression (PSO+SVR) method involves three stages for residential buildings' energy consumption predictions, as shown in Fig. 10. In the first stage, the previous historical data inputs (x_{tr}) and known energy consumptions (y_{tr}) are fed into the SVR training stage which produces the values of β_0, b_0. β_0 has fourteen values which correspond to co-efficients for fourteen input parameters such as temperature, humidity, wind speed, etc. The obtained values of β_0, b_0 by the SVR training system are then considered as the initial values for the PSO stage. In the PSO stage, the predicted inputs (x) and anticipated consumption (y) which can be obtained from a smart meter by a similar day/input approach are inserted. As already mentioned, energy consumption in a residential building depends on the temperature range, other environmental conditions range, occupancy, or even the day type. Therefore, more sets of parameter values are required to be considered based on temperature range to predict energy consumption more accurately. Therefore, four sets of β_{optn}, b_{optn} values are generated by the PSO method based on the temperature range and one of four sets values of β_{optn}, b_{optn} based on the corresponding temperature is used by the SVR equation to predict the energy consumption of the

residential building as shown in Fig. 10. where n=1, 2,…,4.

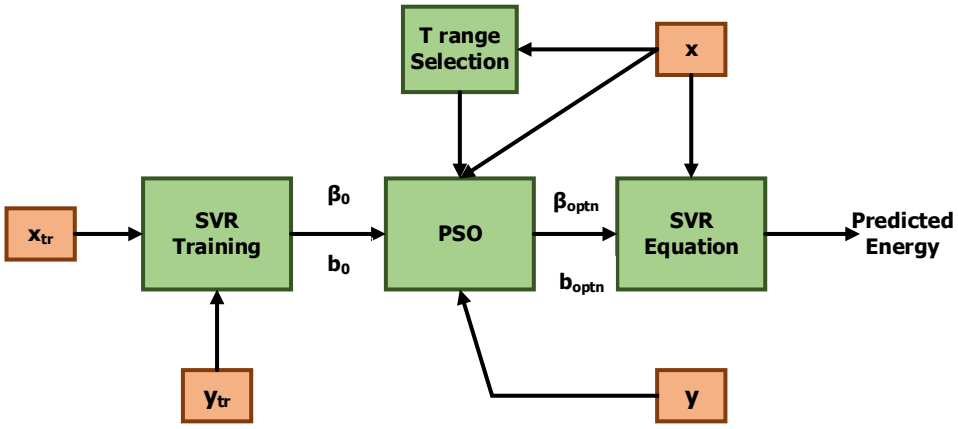

Fig. 10. Block diagram of proposed PSO tuned support vector regression-based prediction system.

The support vector regression, because of its dependence on kernel function, is considered as a nonparametric technique [113]. In MATLAB, epsilon-insensitive support vector regression is available in which the set of training data of both predictor variables (x_{tr}) and observed response values (y_{tr}) are provided with a view to deriving a function f(x) which will deviate from all y within the limit of ε values. Therefore, the equation for the f(x) can be expressed as shown in (17) [113]-[114].

$$f(x) = x'\beta + b \tag{17}$$

where, x is the set of N observation, β and b represent the co-efficients of input and bias, respectively. In order to formulate a convex optimization problem and to ensure that f(x) is as flat as possible, it is required to minimize the objective function which can be represented by the following equation:

$$J(\beta) = \frac{1}{2}\beta'\beta \tag{18}$$

Subject to

$$\forall n: \ |y_n - (x'\beta + b)| \leq \varepsilon$$

where ε is the residue. Since it might not be possible for f(x) to satisfy the constraint in (17) for all values of x, two slack variables ξ_n and ξ_n^* are included with a view to maintaining the constraint shown in (18) for all values of x. Therefore, the objective function presented in (18) can be rewritten as follows:

$$J(\beta) = \frac{1}{2}\beta'\beta + C\sum_{n=1}^{N}(\xi_n + \xi_n^*) \tag{19}$$

Which subjects to:

$$\begin{gathered}\forall n: \ y_n - (x'\beta + b) \leq \varepsilon + \xi_n \\ \forall n: \ (x'\beta + b) - y_n \leq \varepsilon + \xi_n^* \\ \forall n: \xi_n \geq 0 \\ \forall n: \xi_n^* \geq 0\end{gathered}$$

where *C* is known as the box constraint that has the ability to control the penalty when the observation does not fall within the ε margin. It also controls the trades off between the flatness of f(x) and maximum tolerable values beyond ε margin.

The linear ε-insensitive loss function can be expressed as:

$$L_\varepsilon = \begin{cases} 0 & if \ \ |y - f(x)| \leq \ \varepsilon \\ |y - f(x)| \leq \ \varepsilon & otherwise \end{cases}$$

$$L(\alpha) = \frac{1}{2}\sum_{i=1}^{N}\sum_{j=1}^{N}(\alpha_i - \alpha_i^*)\left(\alpha_j - \alpha_j^*\right)G(x_i, x_j) + \varepsilon\sum_{i=1}^{N}(\alpha_i + \alpha_i^*) - \sum_{i=1}^{N} y_i(\alpha_i - \alpha_i^*) \tag{20}$$

The non-linear support vector regression can be achieved by Lagrange dual formulations. Then the objective function becomes as shown in (20). The constraints in (20) are:

$$\sum_{n=1}^{N}(\alpha_n - \alpha_n^*) = 0$$

$$\forall n : 0 \le \alpha_n \le C$$
$$\forall n : 0 \le \alpha_n^* \le C$$

where the linear Kernel function can be expressed as:

$$G(x_i, x_j) = x_i' x_j \tag{21}$$

The objective function shown in (20) can be solved by the quadratic programming techniques. In this work, the sequential minimal optimization method (SMO), which is a very popular approach for SVR problems, is considered. In SMO, a series of two-point optimization are considered and these two points are selected by a selection rule that is governed by second-order information. In SVR, the gradient vector is updated after each iteration by the following equation:

$$(\nabla L)_n = \begin{cases} \sum_{i=1}^{N} (\alpha_i - \alpha_i^*) G(x_i, x_j) + \varepsilon - y_n \,, n \le N \\ -\sum_{i=1}^{N} (\alpha_i - \alpha_i^*) G(x_i, x_j) + \varepsilon + y_n \,, n > N \end{cases} \tag{22}$$

After the training process described in (15)-(20), the values of β_0, b_0 are obtained and then fed in the PSO stage for further optimizations.

2. *Artificial neural network (ANN) Based Prediction System*

In this dissertation, in order to see how effective, the proposed methods are in predicting the loads, its performance has been compared with that of the conventional ANN method as ANN has been a very popular method among the researchers for prediction [115]. The ANN requires learning and predicting stage. In the learning stage, the ANN is provided with input data to learn. The learning stage is normally done offline. Sometimes along with the input, targets are also provided which is known as supervised learning. Finally, the network predicts based on the

learning experience. In this work, the supervised ANN is used for load forecasting. The inputs, network architecture and the training process are described below.

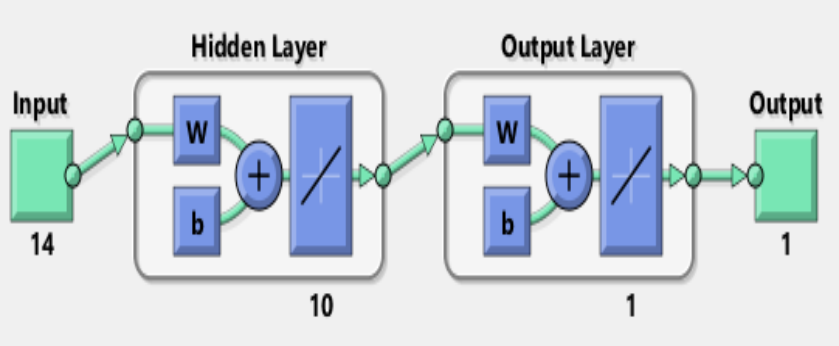

Fig. 11. Architecture of ANN

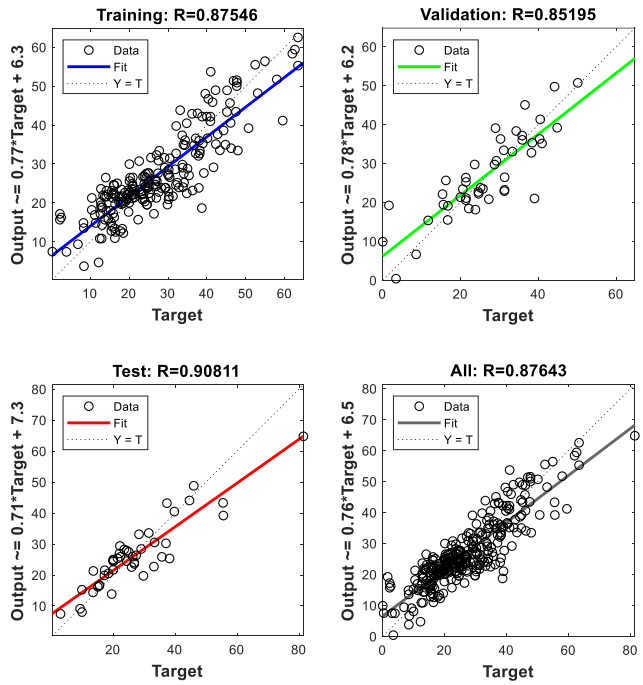

Fig. 12. Regression plot of ANN training.

Although the load consumption of the residential building depends on the indoor and outdoor conditions, the occupancy and day type also have great influences on load consumption that need to be considered. Very few works considered either day type/special days or occupancy or both as input for the neural network in case of building' load prediction [116]-[118]. Moreover, heating degree days (HDD), cooling degree days (CDD) are also influential features for residential

load consumption [119]. Therefore, the special day, day type, occupancy, HDD, CDD along other ten indoor and outdoor factors are considered for the ANN training and prediction in this work. Indoor and outdoor environmental conditions that are considered for this work are temperature, average dew points, relative humidity, specific humidity, indoor humidity, average wind speed, atmospheric pressure, average precipitation, insolation index and solar radiation. The indoor and outdoor data was obtained from [120]-[122]. The occupancy is tabulated daily basis after consulting with the inhabitant. The energy consumption data, which has been used as a target, is obtained from a smart meter connected to Memphis Light, Gas and Water (MLGW) division.

The neural network used for this work is a feed forward back propagation type that has input, hidden layer and output layer as shown in Fig. 11. For the hidden layers, 10 neurons are considered. The transfer functions, for both hidden and output layers, are chosen to be linear. For training purpose, data set of fourteen inputs for 304 days are provided. The data are randomly divided for training and validation process and are trained by Levenberg-Marquardt algorithm as it normally requires less time [123]. Similarly, energy consumption data of 304 days are provided as targets. Moreover, the epoch number is considered to be 1000 for training and the minimum gradient number is 10^{-7}. The regression plot is shown in Fig. 12 in which the values of R, for training, validation and test, are represented. The value of R represents how the outputs are tracking the targets. The value of R closer to 1 represents more accurate tracking. The best value of overall R is found to be 0.87643 after all the trials. For the prediction, after training, another 30 days of data of 14 inputs are provided and based on learning during the training stage, the neural network provides the energy consumption as output.

3. Random Forest Based Load Forecasting

Random forest is an ensemble approach that emphasizes the predictions of all the decision trees that are independent of each other [46]. The sample size is randomly selected and fitted into a regression tree. The process is known as bagging and the selected sample is called bootstrap. This sample is replaced with another random sample each time. The probability of all the observations is assumed to be the same. The bagging algorithm then implements the classification and regression tree (CART) algorithm to obtain a set of regression trees and finally averages the output of all trees based on the following equation:

$$\hat{Y}' = \frac{1}{r}\sum_{i=1}^{r} \hat{h}\,(X', S_n^{\theta_i}) \tag{23}$$

where, $\widehat{\mathbf{Y}}'$ is output estimation based on new input $\mathbf{X}'$ and $\hat{\mathbf{h}}\left(\mathbf{X}', \mathbf{S_n^{\theta_i}}\right)$ is the predicted output of the bootstrap sample of S_n. θ_i represents randomly chosen variable having identical distribution.

For this method, the input variables considered are temperature, occupancy and day type. The energy consumption per day is the output of the prediction system. The unbiased importance of input variables that are measured by the out of bag method and the number of levels are shown in Fig. 13 and Fig. 14 respectively.

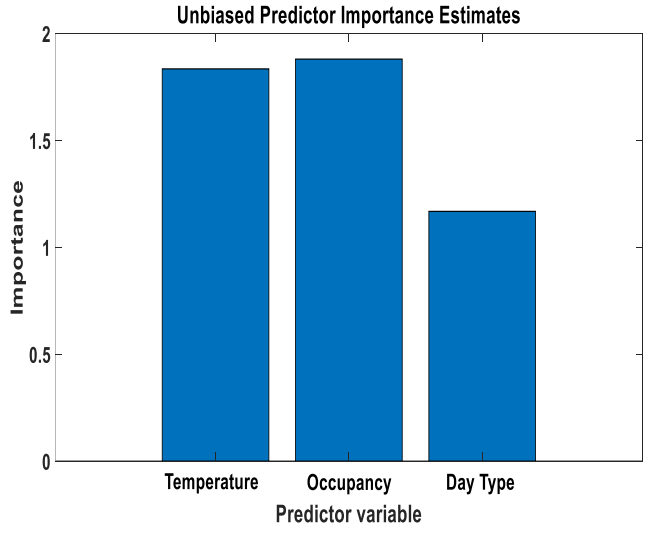

Fig. 13. Random forest predictors' importance.

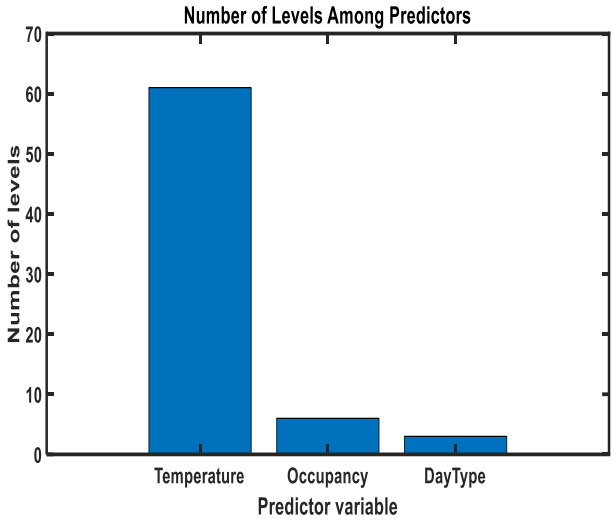

Fig. 14. Random forest predictors' number of levels.

The parameter of this method, optimized by the Bayesian optimization algorithm [124], are summarized in Table 7.

Table 7: Tuned Parameter for Random Forest Based System

Parameter	Value
Maximum Number of Split	55
Min Leaf Size	6
Number of Learning Cycles	494

4. Gradient Boosting Trees Based Load Forecasting

The gradient boosting is an additive model that is characterized by the following equation [125]:

$$F_m(x) = F_{m-1}(x) + h_m(x) \tag{24}$$

where, $F_m(x)$ represents the prediction sum of all m regression trees and $h_m(x)$ is the fixed-sized regression trees. In MATLAB, the least square boosting (LSBoost) is used for regression [126]. At each iteration, the ensemble adds a new tree to the difference between the response observed and the summation of prediction of all trees used before. The LSBoost is efficient in minimizing

the mean-squared error. Like the random forest method, the variables such as temperature, occupancy and day type are considered as inputs for this method. The energy consumption per day is the output of the prediction system. The parameters of this method, that are optimized by the Bayesian optimization algorithm, are summarized in Table 8.

Table 8: Tuned Parameter for LSBoost System

Parameter	Value
Maximum Number of Split	2
Min Leaf Size	1
Number of Learning Cycles	395
Learn Rate	0.043934

5. *LSTM Based Load Forecasting:*

The LSTM is an improved version recurrent neural network (RNN) with added cell state, gates and thus it has the ability to overcome the gradient vanishing problem that the conventional RNN has [51]-[52]. The LSTM structure is presented in Fig. 15 and characterized by the following sets of equations:

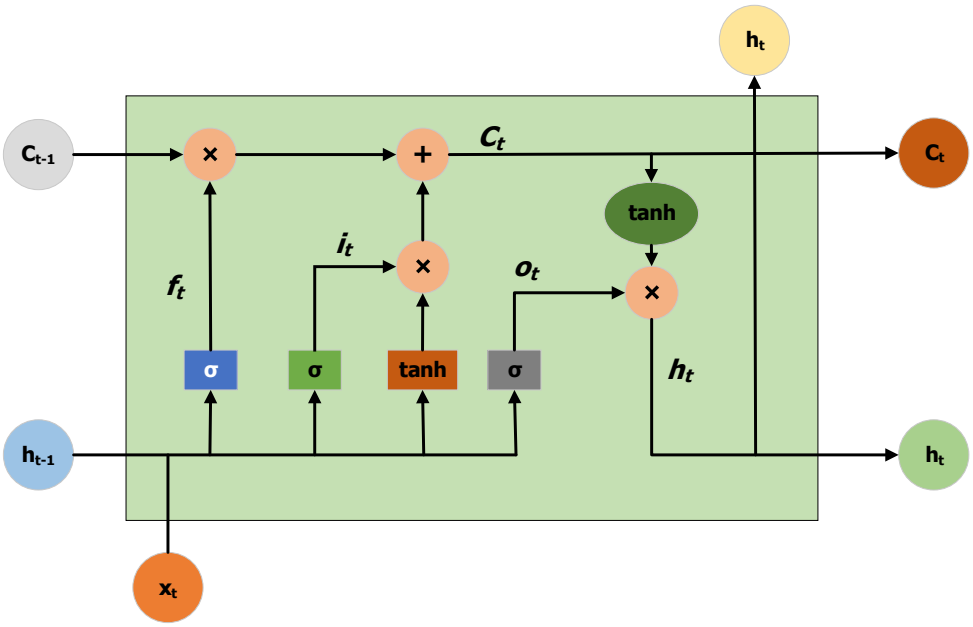

Fig. 15. LSTM structure.

$$f_t = \sigma(W_f \cdot [h_{t-1}, x_t] + b_f) \quad (25)$$

$$i_t = \sigma(W_f \cdot [h_{t-1}, x_t] + b_i) \quad (26)$$

$$o_t = \sigma(W_o \cdot [h_{t-1}, x_t] + b_o) \quad (27)$$

$$\widetilde{C_t} = tanh(W_C \cdot [h_{t-1}, x_t] + b_C) \quad (28)$$

$$C_t = f_t \odot C_{t-1} + i_t \odot \widetilde{C_t} \quad (29)$$

$$h_t = o_t * tanh(C_t) \quad (30)$$

where, f_t represents forget gates that control the amount of previous states to be reflected on the current states. I_t is the input and o_t is the output gates that decide the amount of new information to update the cell state and to give output depending on the cell state. The variable σ keeps the output values between 0 to 1. All the gates are updated based on current input x_t and previous output h_{t-1}. C_t and $\widetilde{\mathbf{C}}_\mathbf{t}$ represent cell state and the value required for calculating cell state, respectively. For the LSTM based load forecasting, the input variables are temperature, occupancy and day type. The training of LSTM approach is shown in Fig. 16. For the LSTM model parameters, the Adam optimization approach is used [52] and the parameters for LSTM are shown in Table 8.

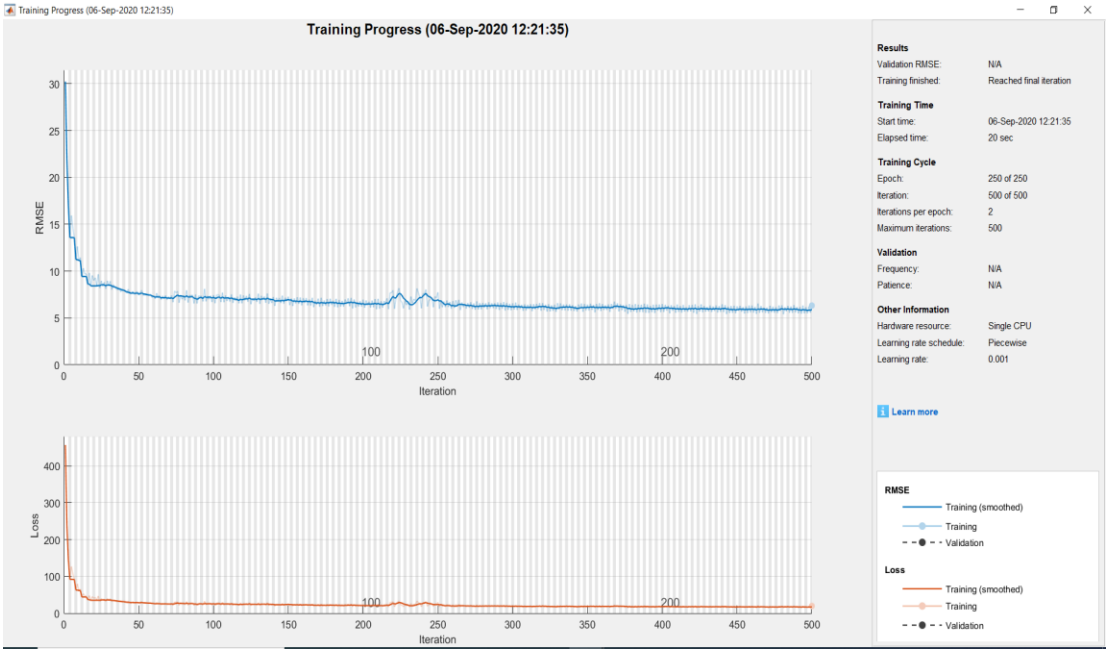

Fig. 16: LSTM model training.

Table 9: Tuned Parameters for LSTM System

Parameter	Value
Number of Hidden Units	500
Fully Connected Layer	150
Dropout Layer	0.1
Maximum Number of Epoch	250
Mini Batch Size	3
Initial Learn Rate	0.005
Learn Rate Drop Period	125
Learn Rate Drop Factor	0.2

C. Performance Analysis for Residential Load Forecasting Methods

1. Simulation Data and Conditions

In this work, the daily total energy demand and the average temperature data of the day are collected from the apartment located at 3571 Midland Avenue, Memphis, TN. The smart energy meter (meter 54BKW988882) data is available in the MLGW web account. Moreover, the number of occupants present at any day and the type of the day information were collected from the resident in the building. A total of 334 days of data (334 sets of data) of the average temperature of the day, the average number of occupants for the day, day type, are collected. Moreover, out of these data, randomly chosen 30 days (30 sets of data) data are used for prediction of total energy consumption per day for comparison purposes and rest 304 days data are used for the ANFIS2, ANFIS, PSO+SVR, artificial neural network, random forest, LSBoost, and LSTM network methods for their training and validation. Similarly, 30 days data of HDD/CDD, Occupancy, day type value (D) were used to get the tuned values of co-efficients for the proposed equation-based systems.

2. Input Parameters of Methods Considered for Simulations

For all the prediction systems, as previously explained, randomly chosen 30 days data were used for prediction and comparison purpose. For the ANFIS2 and ANFIS system, as previously explained, 2 inputs such as the temperature and R values are considered. As for the fuzzy system, temperature and P values are considered as inputs. For the equation-based systems, three inputs (HDD/CDD, occupancy, day type) and for the random forest, LSBoost, LSTM systems, three inputs (temperature, occupancy, day type) are considered. Since for all methods, occupancy and day type are common inputs, these data for 30 predicted days are shown in Fig. 17 and Fig. 18 respectively.

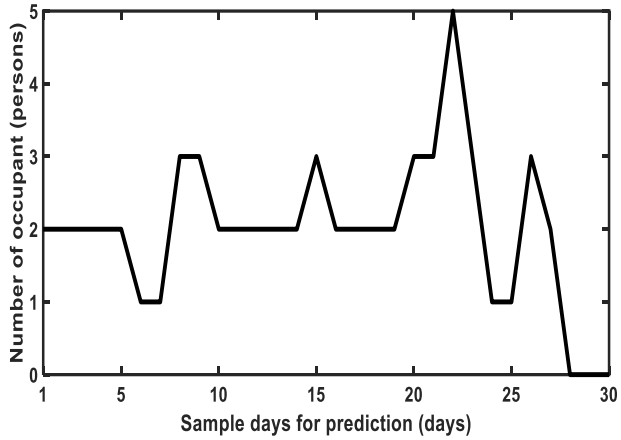

Fig. 17. Occupant data used for all the methods during prediction.

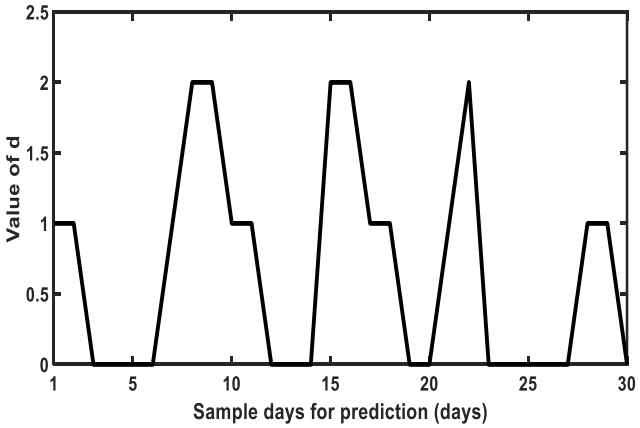

Fig. 18. Day type data used for all the methods during prediction.

3. Performance Analysis

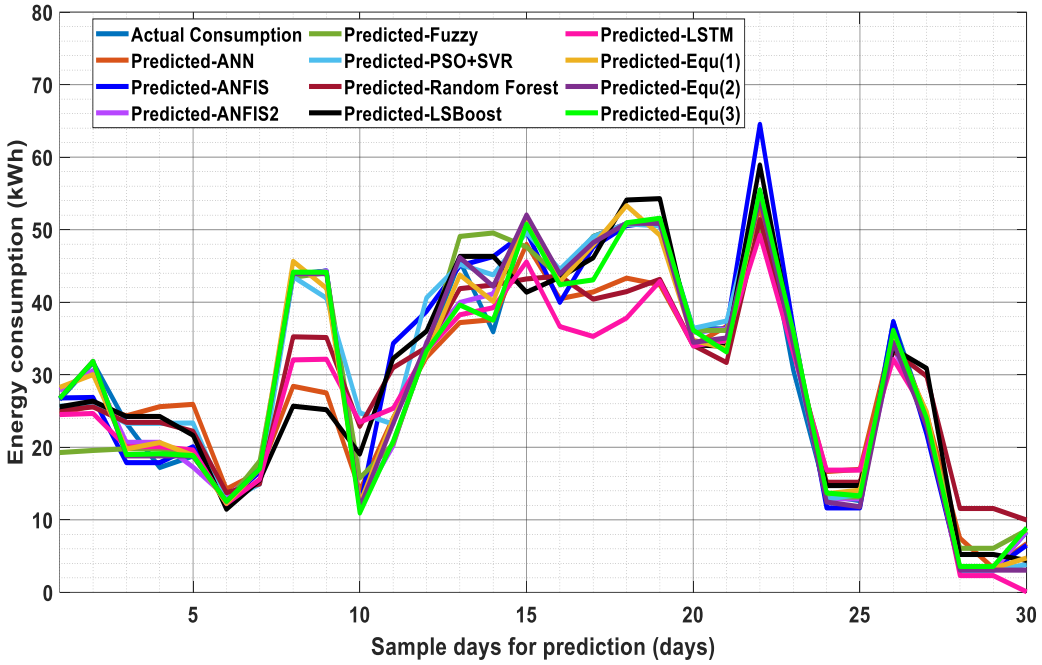

Fig. 19. Comparison of performance all the methods for energy consumption forecasting.

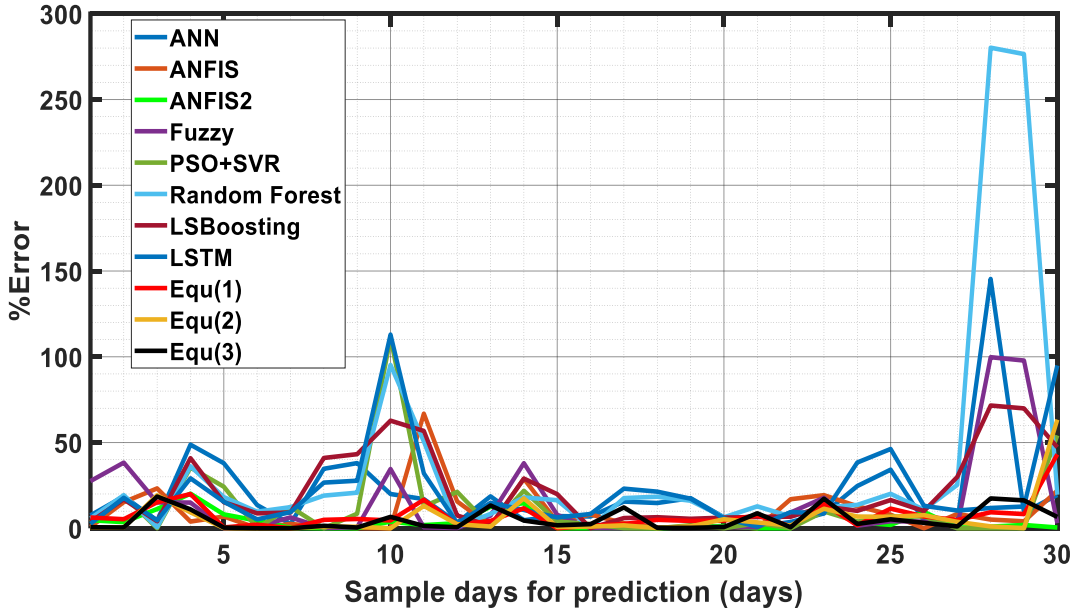

Fig. 20. Comparison of absolute percentage of error of all the methods for energy consumption forecasting.

Fig. 19 represents the comparison of prediction of energy consumptions by the proposed equations, ANFIS, ANFIS2 and fuzzy system with other conventional methods such as artificial neural network, PSO tuned SVR, random forest, LSBoosting, and LSTM based prediction systems, etc. with actual energy consumption data. From the results, it is evident that the proposed ANFIS2 and equation-based prediction systems perform better as compared to all other systems.

Furthermore, the absolute percentage of error (%Err), the absolute average error (A.E), root mean square error (RMSE), and mean average percentage error (MAPE) for the prediction systems have been calculated using (31), (32), (33), and (34), respectively. The absolute percentage error shows the percentage of total consumption prediction error per day and helps determine the maximum error that occurs within the considered time. The absolute average error predicts the average error of prediction from the actual consumption within the considered time periods. Similarly, the RMSE and MAPE show the root mean square error and mean absolute percentage of error over a period. These error methods are very standard for comparison of performance. The lower values of these errors mean the system predicts very close to the actual predictions. Therefore, these errors are used to evaluate the best system performance. And these errors have been used as performance indices in this work.

$$\%Err = \left|\frac{Actual - Predicted}{Actual}\right| \times 100 \tag{31}$$

$$A.E = \frac{1}{N}\sum_{i=1}^{N}|Actual_i - Predicted_i| \tag{32}$$

$$RMSE = \sqrt{\frac{1}{N}\sum_{i=1}^{N}(Actual_i - Predicted_i)^2} \tag{33}$$

$$MAPE = \frac{1}{N}\sum_{i=1}^{N} \%Err_i \quad (34)$$

Where N=30 is used for equations from (31) to (34). The percentage errors of proposed methods and other systems, for predicting energy demands of chosen 30 days, are shown in Fig. 20 which are calculated using (31) for all the 30 days. Moreover, the average, root mean square and mean average percentage errors for all systems are shown in Table 10, Table 11 and Table 12 respectively. From Table 10, it is evident that the absolute average errors of ANFIS2 and equation-based prediction systems are less than those of ANFIS, fuzzy, PSO+SVR, random forest, LS boosting, and LSTM based prediction systems. In this case, the proposed methods, as shown in (1), (2), and (3), perform 66.30%, 75.03% and 75.35% better, respectively, than the random forest system. However, the proposed ANFIS, ANFIS2 and fuzzy system perform 52.02%, 78.27% and 52.49% better respectively as compared to random forest based prediction system as shown in Table 10. In Table 10, for the percentage of improvement calculation, random forest is considered as base system as it has the highest absolute error, absolute mean average percentage error.

Moreover, from Table 11, it is evident that the root mean square errors of ANFIS2 and equation-based prediction systems are also less than those of ANFIS, fuzzy, PSO+SVR, random forest, LS boosting, and LSTM based prediction systems. In this case, the proposed method shown in (1), (2), and (3) perform 64.43%, 65.89% and 64.22% better, respectively, than the random forest system. However, the proposed ANFIS, ANFIS2 and fuzzy system perform 30.63%, 67.38% and 30.92% better respectively as compared to random forest based prediction system as shown in Table 11. In Table 11, for percentage of improvement calculation, random forest is considered as the base system. However, random forest performs 10.57% and 3.17% better as compared to LSBoosting and LSTM method respectively.

Table 10: Absolute Average Error and Standard Deviation of Average Error of all methods

Method		Absolute Average Error (kWh)	% Improvement	Standard Deviation
Proposed	ANFIS	2.44	52.02	3.49
	ANFIS2	1.11	78.27	1.67
	Fuzzy	2.42	52.49	3.48
	Equ (1)	1.72	66.30	1.33
	Equ (2)	1.27	75.03	1.66
	Equ (3)	1.25	75.35	1.80
Conventional	Random Forest	5.09	0.00	3.36
	LSBoosting	4.79	5.95	4.78
	LSTM	4.94	2.96	3.92
	ANN	4.34	14.67	4.13
	PSO+SVR	2.37	53.37	3.10

Table 11: Root Mean Square Error of all methods

Method		Root Mean Square Error (kWh)	% Improvement
Proposed	ANFIS	4.21	30.63
	ANFIS2	1.98	67.38
	Fuzzy	4.19	30.92
	Equ (1)	2.16	64.43
	Equ (2)	2.07	65.89
	Equ (3)	2.17	64.22
Conventional	Random Forest	6.07	0.00
	LSBoosting	6.71	-10.57
	LSTM	6.26	-3.17
	ANN	5.95	2.04
	PSO+SVR	3.86	36.39

In addition, Table 12 indicates that the mean absolute percentage errors of ANFIS2 and equation-based prediction systems are also less than those of ANFIS, fuzzy, PSO+SVR, random forest, LS boosting, and LSTM based prediction systems. In this case, the proposed Equ (1), Equ (2) and Equ (3) perform 78.92%, 83.01% and 85.41% better, respectively, than the random forest system. However, the proposed ANFIS, ANFIS2 and fuzzy system perform 73.78%, 88.45% and

59.49% better respectively as compared to random forest based prediction system as shown in Table 12. In Table 12, for percentage of improvement calculation, the random forest is considered as the base system.

Table 12: Mean Absolute Percentage Error and Standard Deviation of Mean Absolute Percentage Error of all methods

Method		Mean Absolute Percentage Error	% Improvement	Standard Deviation
Proposed	ANFIS	9.33	73.78	13.58
	ANFIS2	4.11	88.45	5.42
	Fuzzy	14.42	59.49	25.73
	Equ (1)	7.50	78.92	8.45
	Equ (2)	6.05	83.01	12.04
	Equ (3)	5.19	85.41	6.13
Conventional	Random Forest	35.60	0.00	68.32
	LSBoosting	22.19	37.66	21.67
	LSTM	21.36	40.00	25.09
	ANN	19.73	44.57	26.82
	PSO+SVR	12.14	65.91	22.50

It is noteworthy to mention that, the ANN and SVM methods are intelligent and the parameters are tuned based on the input data during the training stage. However, these methods require large data sets for training and validation. On the other hand, the proposed methods perform well with small data set and can predict the energy consumption of any range. Moreover, ANN and SVM systems are black-box whereas the proposed systems are interpretable and implementable. For the proposed systems, the input parameter range consideration and parameter tuning are dependent on family, space like city, communities, and thus should be different from each other, although the residential energy consumptions are dependent on the resident. Therefore the range of the input parameters (HDCC, O, D) can be easily defined. In order to show the performance of the proposed methods, the above three tables (Table 1, Table 2 and Table 3) are presented.

D. Conclusion

This work proposes new equations-based methods, based on HDD, CDD, occupancy and week/special days, for residential load forecasting. Two inputs ANFIS, ANFIS2, fuzzy prediction systems are also proposed in this work. The performance of the proposed methods has been compared with that of the artificial neural network, PSO+SVR, random forest, LSBoosting and LSTM approaches. The forecasted energies by all methods are analyzed with actual energy consumption data for validation. The 304 days data are considered during the training of the ANFIS, ANFIS2, artificial neural network, PSO+SVR, random forest, LSBoosting and LSTM systems. Moreover, data of 30 days of the same apartment are used for the energy prediction by all the methods. Based on the obtained simulation responses and performance indices, the following conclusions can be drawn.

- The proposed equations-based methods, ANFIS, ANFIS2, fuzzy systems

are effective in predicting residential loads with less number of inputs.

- The proposed prediction systems require less computation and perform better than the artificial neural network, random forest, LSBoosting, and LSTM systems.
- The proposed ANFIS2 system has the lowest absolute average errors, root mean square errors and mean average percentage errors followed by equation-based methods, fuzzy method, ANFIS method compared to other conventional methods.
- The proposed equation-based systems, ANFIS, ANFIS2, fuzzy systems can easily be implemented in real practice.

IV. LOAD SCHEDULING

Residential buildings consume almost 30%-40% of the total energy production in the world [58]. With the advancement in technology, the consumers' comfort demands have been continuously increasing over the last decade which has been also the reason behind the increase in residential power consumption. The increase in residential power put huge burden on the grid system as it is responsible for delivering power along with ensuring safety, stability and reliability. The installation of renewable energy sources such as solar, wind, etc., in residence, and implementation of demand side management (DSM) can be prominent solutions to this problem. Driven by this fact, the department of energy (DoE) has been encouraging the installation of renewable energy source in the buildings. It has also been offering incentives to encourage consumers to participate in demand response in terms of load scheduling according to the grid demands or electricity price [67]. Load scheduling is an effective tool in maintaining the stability, reliability of smart residential buildings according to the preference of the inhabitants' or grid demands.

This work proposes an efficient load scheduling with a view to confining the cost of energy within the consumers' preference range while considering the realistic grid power cost, levelized cost of renewable sources, battery and incentives. All the operations are optimized by the well-known PSO technique in MATLAB and the performance indices are tabulated.

A. System Description

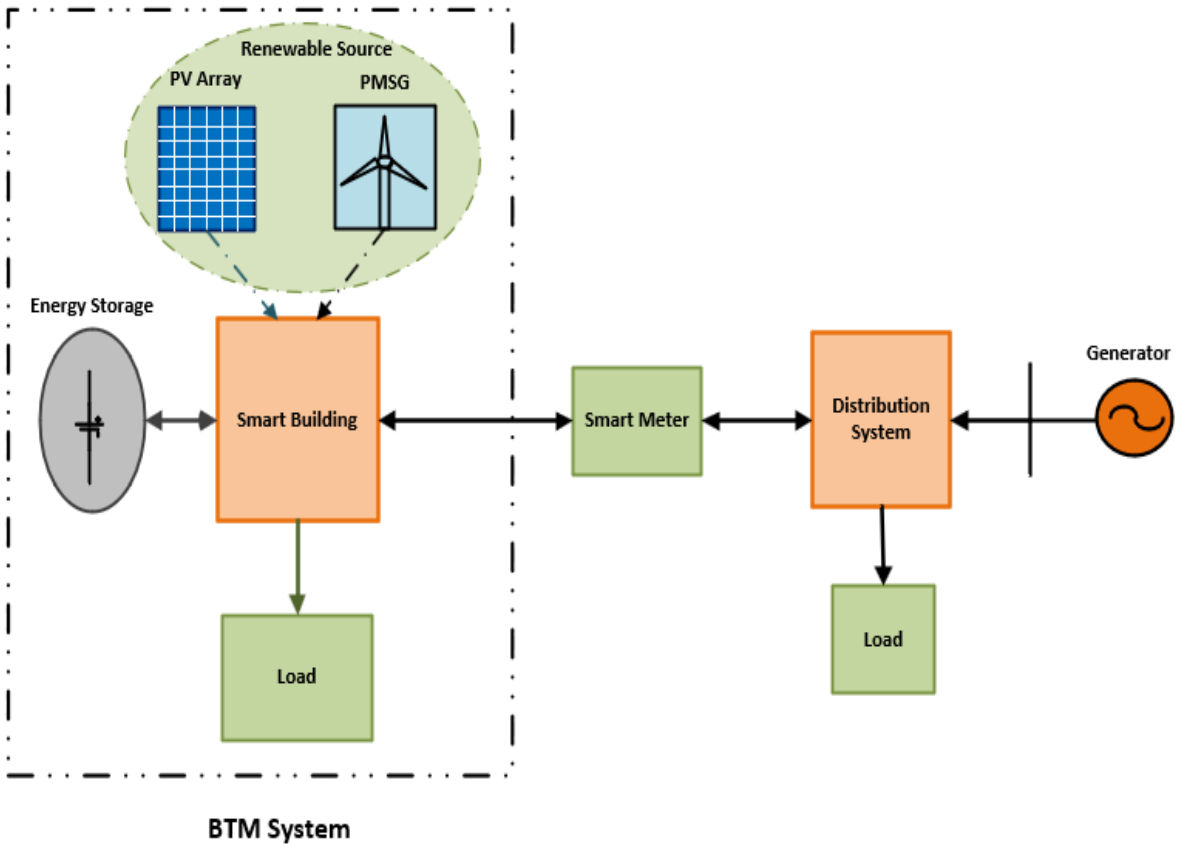

Fig. 21. Component of a smart building connected to smart grid through smart meter.

The smart building is a building with a centralized controller that can access the generation information from the renewable energy sources, charging/discharging condition of the battery energy storage with available of energy to be stored or dispatched. The centralized controller will have control over the operations of all the loads and battery energy storage, and bi-directional communication between the centralized controller and the loads and battery energy storage would be additional features. Moreover, having been connected to the grid through the smart meter, the smart meter will have the electricity price information or even can acknowledge any demand request offered by the grid at any given time. In addition, smart building has future prediction system for energy sources and loads and therefore can be scheduled effectively with available sources or demand preferences of the consumer. The smart building can effectively control the

loads' energy consumption, operations, etc. Fig. 21 shows the renewable energy sources and the battery energy storage considered for this work. The building is considered to be a smart building in this work meaning all the loads, renewable energy sources and battery energy storage are monitored by the centralized controller and the loads, battery energy storage are controlled by it. Moreover, the smart building is also considered to be connected to the grid through a smart meter and the centralized controller controls the bi-directional power flow to and from grids. The residential building in this work is considered to be situated in California, USA. Therefore, climate data such as wind speed, solar irradiance data are considered that are suitable for California [120]. The rating of the PV and wind turbine are selected to be 6.2 kW and 10 kW [127]-[128]. The two-battery energy storage was considered to have rating of 14 kWh each that is practically available [129]-[130]. The distribution company considered for this is PG&E for TOU electricity price, incentive for wind turbine and battery energy storage installation and incentive for the demand response program participation.

B. Calculation of Levelized Cost of Energy Sources and Energy Storage

The levelized cost of energy (LCOE) of any system can be defined as shown below [127]:

$$LCOE = \frac{ICC \times FCR + AOE}{AEP} \tag{35}$$

where, ICC, FCR, AOE, AEP represent the installed capital cost, fixed charge rate (%), annual operating expenses and annual energy production, respectively. The fixed charge rate, FCR, can be defined by the following equation (36) shown below [131]:

$$FCR = \frac{d(1+d)^n}{(1+d)^n - 1} \times \frac{1 - (T \times PV_{dep})}{1 - T} \tag{36}$$

where, d, T, PV_{dep} represent, interest rate (%), effective tax rate and present value of depreciation (%), respectively. These are the two equations that have been used for LCOE calculation to be considered in scheduling.

1. *Localized Cost of PV System*

According to [127], the residential solar system ranges from 3-10 kW. The average solar system rating is 6.2 kW. Therefore, for this work, a 6.2 kW solar system is considered for residential buildings. In [127], the installed cost ($/W) is reported to be 2.70. The federal tax rate 21%, California state tax rate 7%, total lifetime of the solar system is 30 years, 4% interest loan, etc., are considered for this installation cost calculation. The operational and maintenance cost is reported to be 22$/kW-yr [127]. Moreover, a solar panel of 1kW peak dc capacity is reported to produce an average of 1642 kWh annually in California [132]. Therefore, using equation (35), the levelized cost of residential PV system, that is considered for this work, is found to be 0.0681 $/kWh.

2. *LCOE of Wind System*

The wind turbine system, that is considered in this work, has a rating of 10 kW as in [128]. Although a lot of wind turbines are available, for this work, the Excel 10 of Bergey wind power company is considered [133]. The installation cost of this wind turbine requires around $60,000 as found in the manufacturer's website. Considering 30% incentive by the federal government and .90$/W incentive self-generation incentive program by PG&E [134] in California, the initial installation cost becomes 33,000$. Moreover, considering 1.3% interest for 25 years with federal and state tax rates as same as the PV system, the FCR value was found to 0.0654. The maintenance cost is considered to be 40$/yr. Moreover, Excel 10 is capable of producing 13,800 kWh /yr for a

location where the average wind speed is 5 m/s [135]. From the NASA toolbox [120], locations are selected where the average wind speed over the last two years is found to be slightly more than 5 m/s at 100 feet above sea-level. Therefore, the levelized cost of wind energy is found to be 0.1593$/kWh according to (1).

3. LCOE of Battery Energy Storage

The battery energy storage system, as discussed in the system description section, has a rating of 28 kW of which 27 kW is practically available. From the manufacturer's website, the installation cost is found to be around $16,100. Again, considering the 30% incentive from the federal government and 0.25$/Wh incentive by PG&E in California for residential energy storage, the equivalent installation cost reduces to 4270$. Moreover, 2.5% interest is considered for 10 years for which the FCR value is found to be 0.1586. The warranty period for the battery storage is 10 years as mentioned on the manufacturer's website. Therefore, the operation and maintenance cost is considered 0$/yr. Again, considering the daily operation of 35.1 kWh per day, the annual operating energy becomes 12811.5 kWh/yr. Therefore, the levelized cost of battery energy storage for both charging and discharging condition is calculated to be 0.05289 $/kWh.

C. Load Scheduling Methodology

In this work, the main objective function is to keep the cost of energy per hour close to the desired value of the consumers along with load consumption per hour close to the load demand for that hour, reducing power loss of the system to be minimum. Three conditions regarding the power sources are considered. The first condition grid power is considered to be the residential building’s only source of power. In the second condition, grid power and battery energy storage are considered as sources. In the final condition, renewable energy sources such as solar, wind energy

sources, battery energy storage, grid power are considered as energy sources. In the third/final case, in addition to the objective mentioned above, the objective function will ensure the maximum utilization of renewable energy for load while taking minimum power from the grid and giving maximum power to the grid to earn incentive whenever possible. In all conditions, the load scheduling with a view to keeping the objective function minimum is done by the particle swarm optimization (PSO) technique. Therefore, the characteristic equations from (5) to (7) are used for PSO with same procedures and parameters that are mentioned in the previous chapter.

D. Load Scheduling under Normal Conditions

1. Smart Building Operated by Only Grid Power

In this work, six days are considered in some places in California in 2019 for load scheduling. Among them, the first two consecutive days are considered as normal working days and next two consecutive days are considered as weekend. The last two days are considered as special days of which the first one is the normal working day, and another day is the weekend. The load patterns for normal working days are considered as similar to the load demand found in [128].

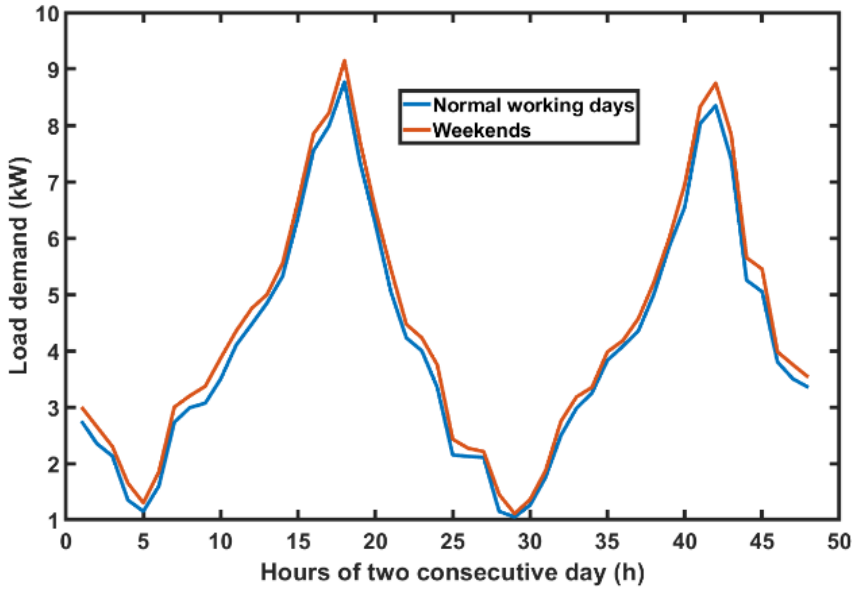

Fig. 22. Load demands of two working days and weekends

The load demand on the weekend is considered higher than the normal working days and the load demand is the highest for the special day as shown in Fig. 22 and Fig. 23, respectively.

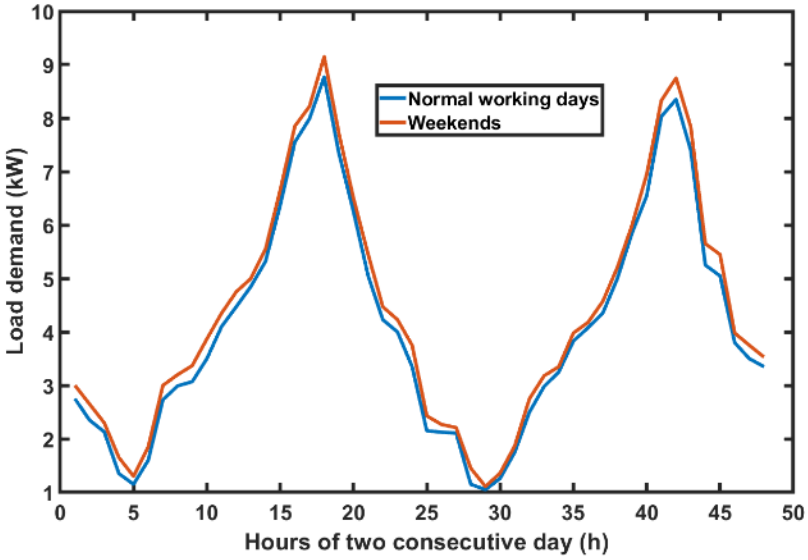

Fig. 23. Load demands of two special days.

At first, it is considered that the residential building is powered only by grid power. As previously discussed, PG&E has been considered for this work as a utility service provider. PG&E has three TOU electricity rates [136]. The first one is the E-TOU option-A considers peak hours from 3-8 p.m. in the summer season for normal working days. E-TOU option-B considers the peak hours to be from 4-9 p.m. for normal working days in summer. E-TOU-C3 considers peak hour to be from 4-9 p.m. every day. Therefore, the TOU rates for the considered normal working days, are shown in Fig. 24. Fig. 25 shows the TOU rates for weekends where option-A and option-B have nonpeak hours rates throughout the days. However, E-TOU-C3 has peak hours rates like the normal working days. TOU rates for two special days are shown in Fig. 26. As special day1 is normal working days, all TOU rates have high rates according to their peak hours. For the second special day, as it is weekend, option-A and option-B have nonpeak hours rates throughout the day and E-TOU-C3 has peak hours rates like the normal working days.

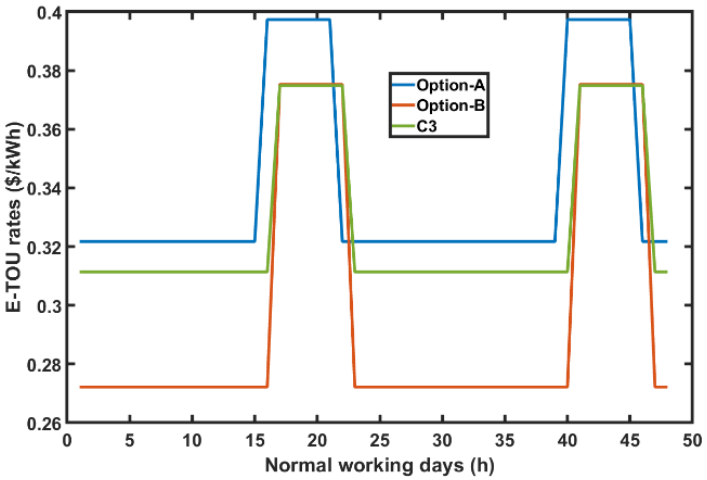

Fig. 24. Three different E-TOU rate option on working days.

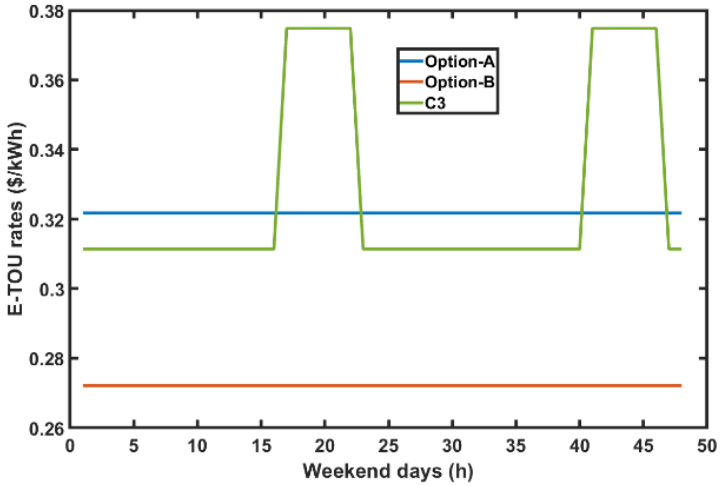

Fig. 25. Three different E-TOU rate option on weekend days.

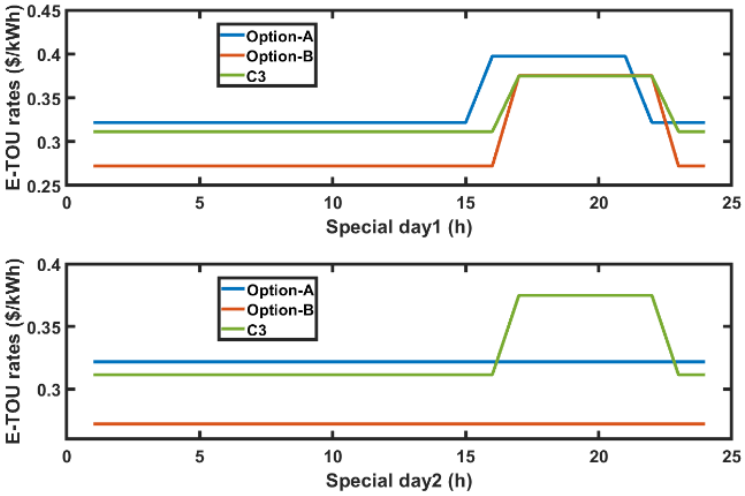

Fig. 26. Three different E-TOU rate option on special days.

Therefore, the average energy cost per hour for E-TOU option-A is calculated to be 0.340645 $/kWh for normal working days. For E-TOU option-B and E-TOU-C3, the average energy costs per hour are determined as 0.297925 $/kWh and 0.32726 $/kWh respectively. Similarly, the average energy cost per hour for E-TOU option-A, E-TOU option-B, E-TOU-C3 are calculated to be 0.32175 $/kWh, 0.27216 $/kWh, 0.32726 $/kWh respectively. Based on these calculations, using E-TOU option-B rates are most economical as it is cheapest among all rates for both normal working days and weekends. Therefore, this rate will be used as electricity rates for the rest of the calculations.

The objective function for the first case can be defined as:

$$f_{obj} = \sqrt{K_1(C_e(h) - C_{g\_actual}(h))^2 + K_2\left(\frac{P_{l\_actual}(h) - P_e(h)}{1000}\right)^2 + \frac{P_{sys_{loss}}(h)}{P_e(h)}} \qquad (37)$$

Where, λ_g, P_g represent the grid electricity rate, consumed grid power respectively. C_g represents the consumer desired cost of consumption per hour. P_l, P_e, P_{sys_loss} represent load demand at any particular hour (h), the actual load consumed at that hour and system power loss respectively. K_1 and K_2 are the contributing factors that determine the consumer's preference of cost saving and load consumption over the desired cost of energy and the load demands. The higher value of K_1 means the difference in the first term should be small to minimize the objective function. The PSO optimization algorithm will try to minimize the above objective function shown in (37) subject to:

$$P_g(h) = P_e(h)$$
$$C_e(h) = \lambda_g(h)P_g(h)$$
$$K_1 + K_2 = 1$$
$$P_l(h) - P_e(h) \geq 0$$
$$P_{sys_{loss}}(h) = 0.01P_e(h) \leq 0.8\ kW$$
$$0 \leq C_e(h) \leq 4C_g(h)$$

The average per day electricity cost of the building is found to be 30$. The purpose of scheduling is to keep the electricity cost around 25$. Therefore, the values of C_g during normal operating hours and peak hours are considered to be $0.8333 and $1.6666, respectively. However, if the energy cost, C_e of one hour is less than C_g, then the difference between the C_g and energy cost can be added with the next hour C_g to utilize more load if required during the off-peak hour. During the peak hour, because of the higher electricity cost, only demanded loads will be considered. However, if the load utilized in any hour, P_e is less the actual load demand, P_l, then the difference between the actual demand and consumed load is added with the demand of next hour during off-peak hour. The above two conditions are expressed in equations (38) and (39), respectively.

$$C_{g\_actual}(h) = \begin{cases} C_g(h) + \left(C_g(h-1) - C_e(h-1)\right) & off-peak \\ C_g(h) & peak \end{cases} \quad (38)$$

$$P_{l\_actual}(h) = \begin{cases} P_l(h) + \left(P_l(h-1) - P_e(h-1)\right) & off-peak \\ P_l(h) & peak \end{cases} \quad (39)$$

where h represents any hour between 1 to 48 for normal working days or weekends but corresponds to 1 to 24 for special days.

In this condition, where only grid power is the only source considered, three cases are considered for normal working days, weekends and special days. In case1, case 2 and case 3, the K_1 values are considered to be 0.5, 0.7 and 0.8 respectively. Therefore, for the first case, both of the first two terms in, the objective function (37), will have equal importance. In order to have the minimum value of the objective function, therefore, in this case, both load costs should be very close to the desired value whereas the load consumption should be closer to the demand values. In the second and third cases, more priority is given to the first term of the objective function,

meaning the cost of loads is required to be close to the desired values to get the objective function minimum.

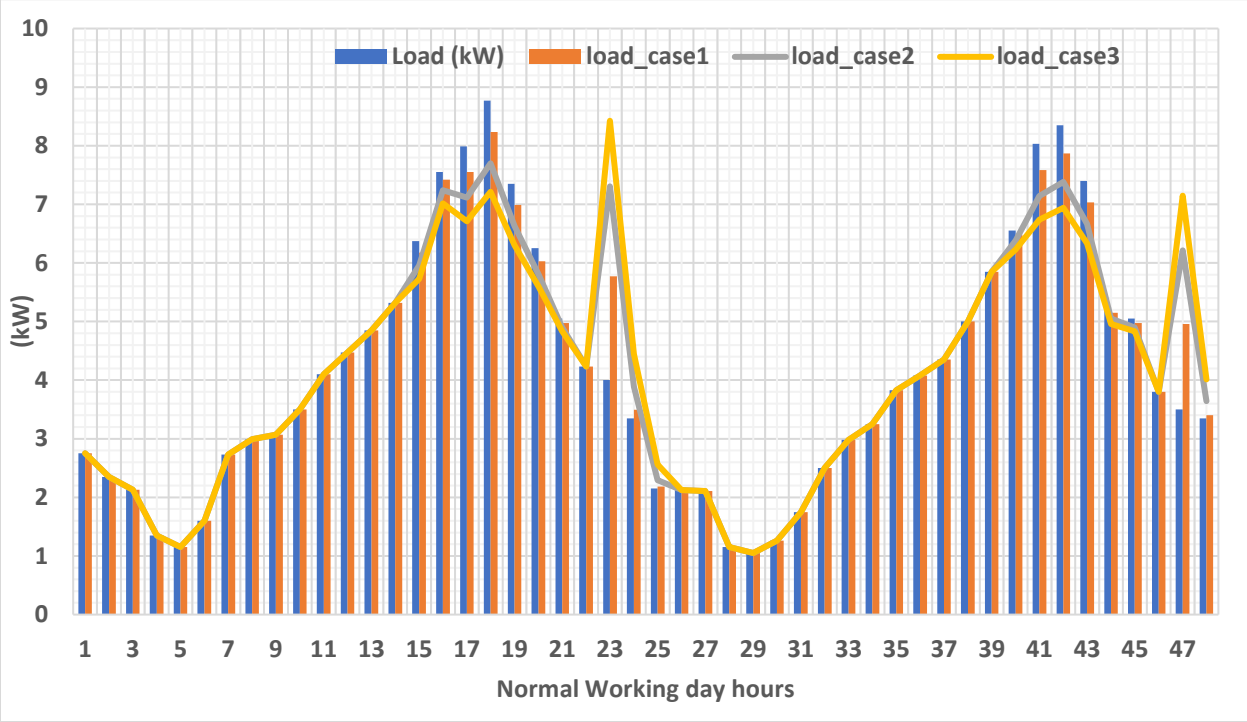

Fig. 27. Load scheduling using grid power for normal working days.

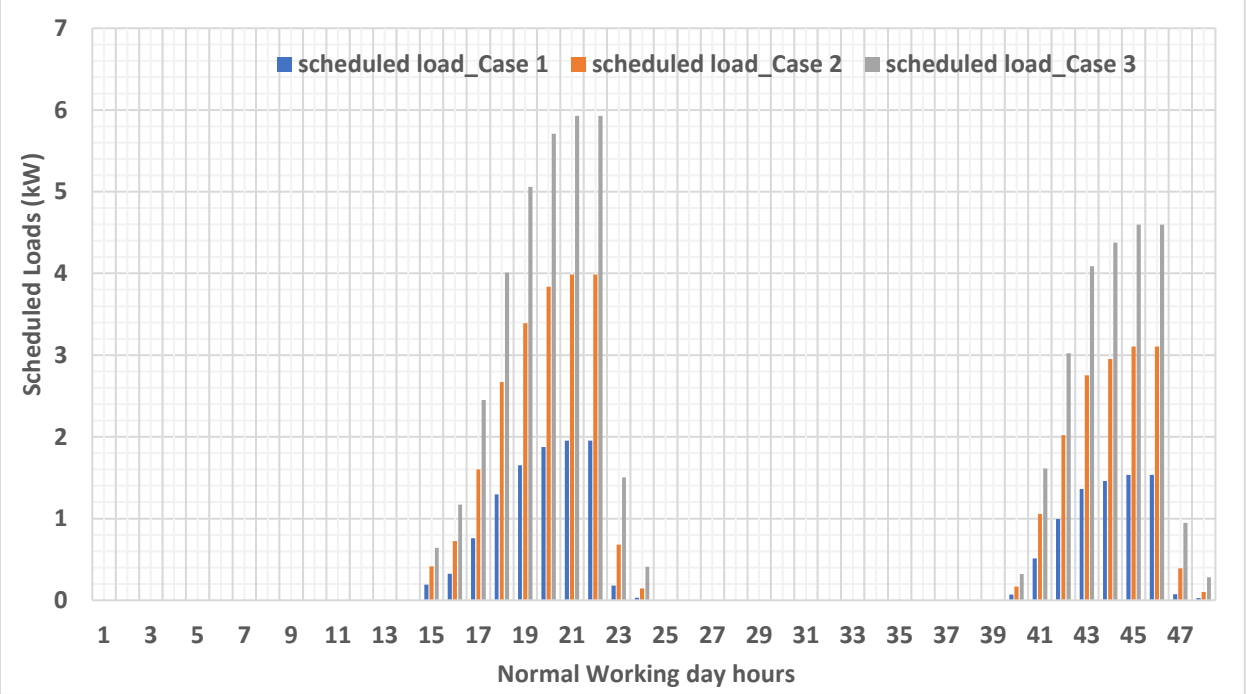

Fig. 28. Scheduled loads for normal working days.

Fig. 27 shows the unscheduled load consumption (demand) and load consumption for the considered three cases. For the first case, the load consumptions are closest to the demand values as mentioned in the previous paragraph. Therefore, the scheduled load values in case 1 will be lesser as compared to case 2 and case 3 as shown in Fig. 28. Moreover, case 2 and case 3 loads' cost have the higher priorities, therefore, loads' values will lesser as compared to case 1 as load demands get higher from 16 to 22 hours and 40 to 46 hours as the electricity rates are higher with higher demands during that time.

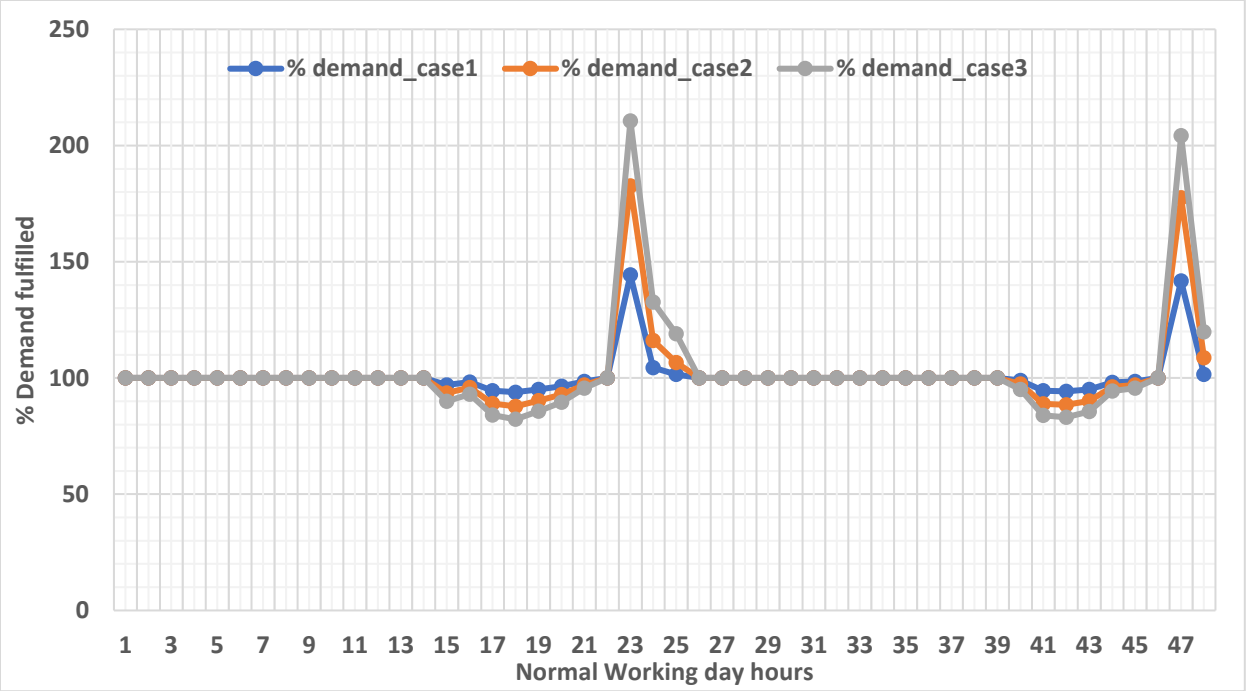

Fig. 29. Percentage of load demand fulfilled per hour for normal working days.

The percentage of demand fulfilled in all three cases per hour is shown in Fig. 29. From the figure, it is evident that from 0 to 14 hours, the demand fulfillment is 100% for all three cases. However, during peak hours demand fulfillment is higher in case 1 as compared to case 2 and case 3.

Fig. 30 represents the load energy cost for the unscheduled (demand) and three considered scheduling cases. The overall energy cost in case 1 is higher followed by case 2 and case 3 respectively.

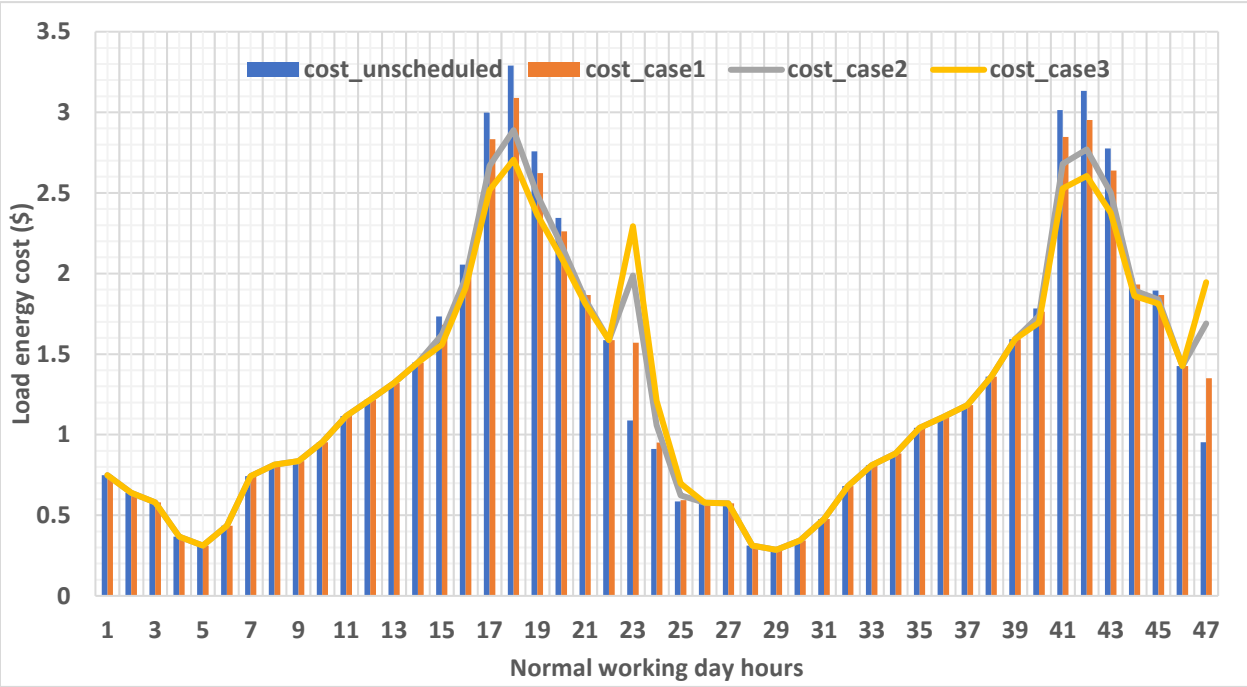

Fig. 30. Cost of load energy per hour for normal working days.

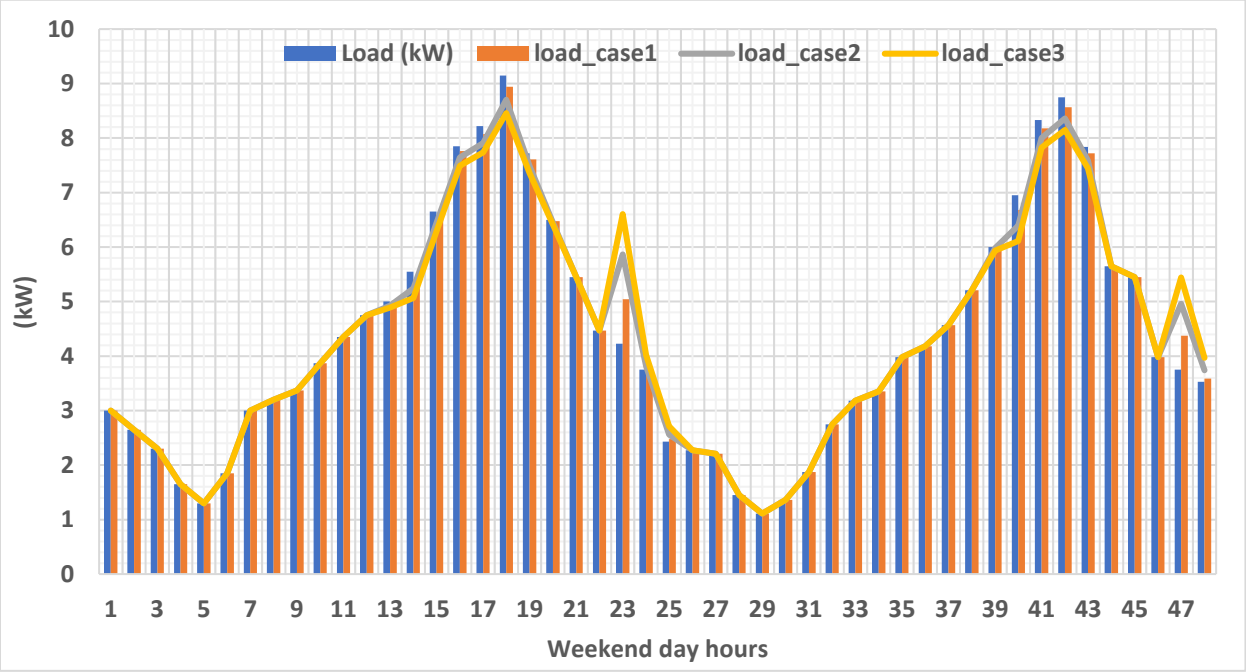

Fig. 31. Load scheduling using grid power for weekend days.

Like normal working days as shown in Fig. 27, Fig. 31 shows the unscheduled load consumption (demand) and load consumption for the considered three cases for the weekend days. Similar to the normal working days, in case 1, the load consumptions are closest to the demand values for weekend days. Therefore, the scheduled load values in case 1 will be lesser as compared to case 2 and case 3 as shown in Fig. 32.

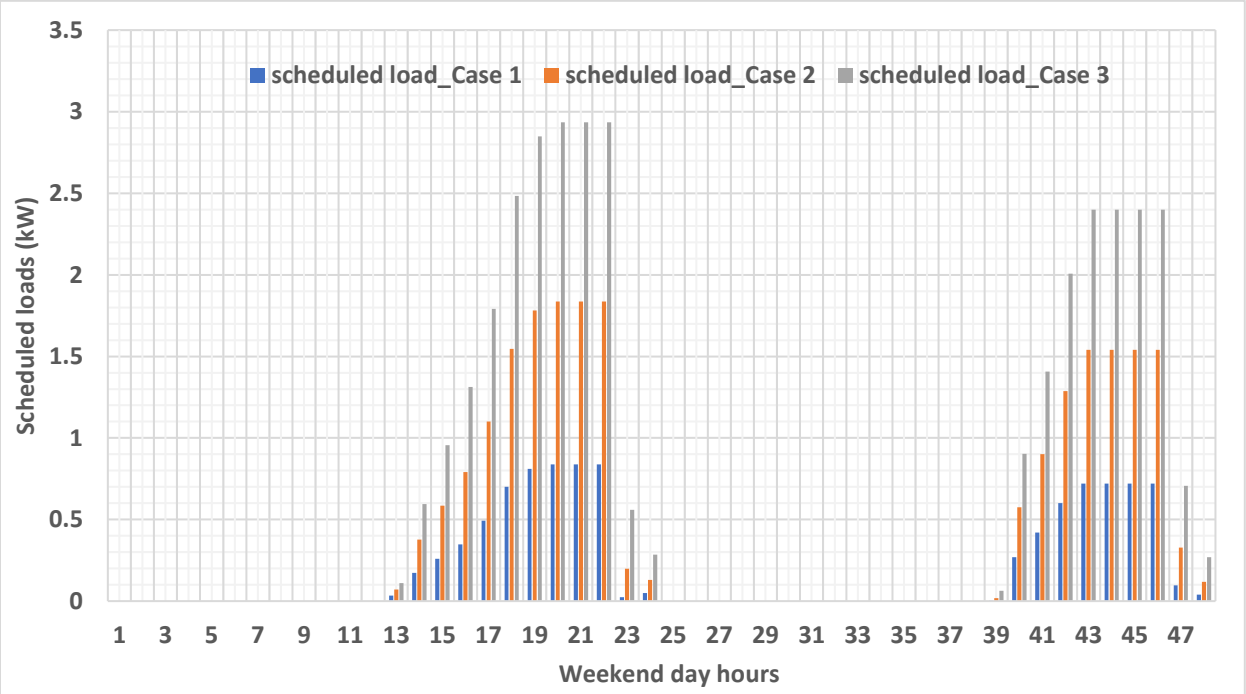

Fig. 32. Scheduled loads for weekend days.

The unscheduled load consumption (demand) and load consumption for the considered three cases on weekend days are shown in Fig. 32. The scheduled load for case 1 is the least followed by case 2 and case 3 respectively.

Fig. 33 indicates the percentage of demand fulfilled in all three cases per hour for the considered weekend days. From the figure, it is evident that, among the three cases, the demand fulfillment is highest for case 1 followed by case 2 and case 3 respectively as the load demands get higher. However, during peak hours demand fulfillment are higher for all cases as compared

to the normal working days as there is no electricity price difference between the peak and off-peak hours.

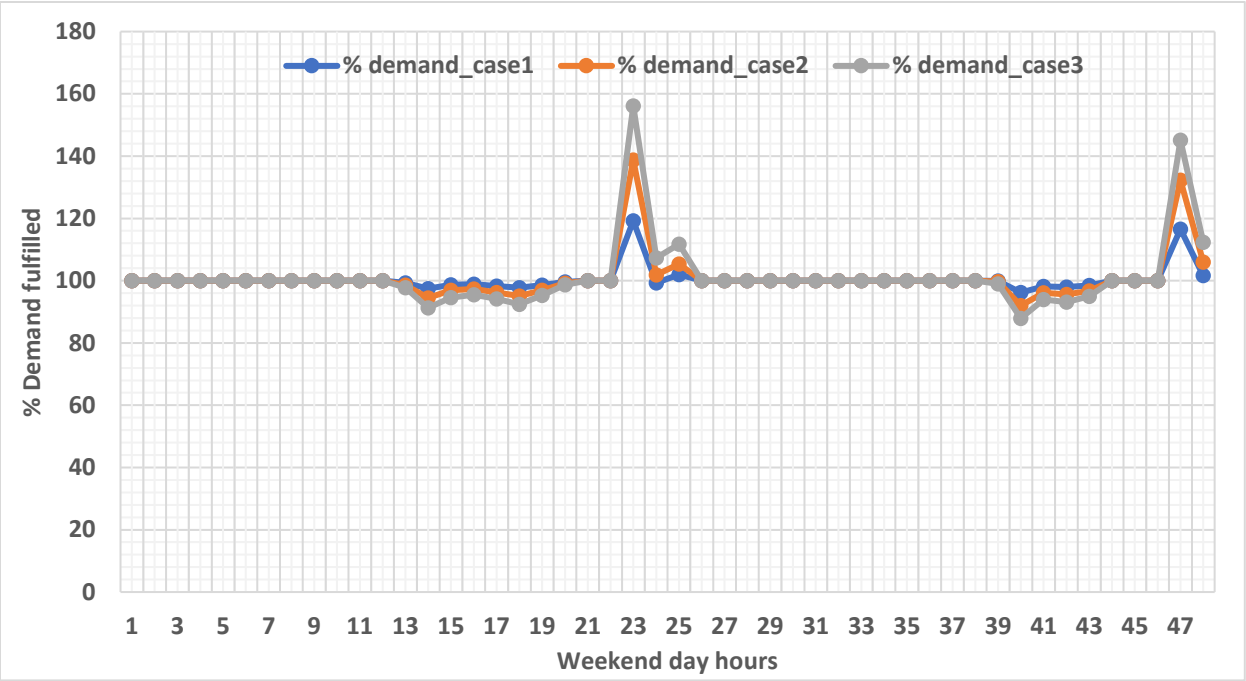

Fig. 33. Percentage of load demand fulfilled per hour for weekend days.

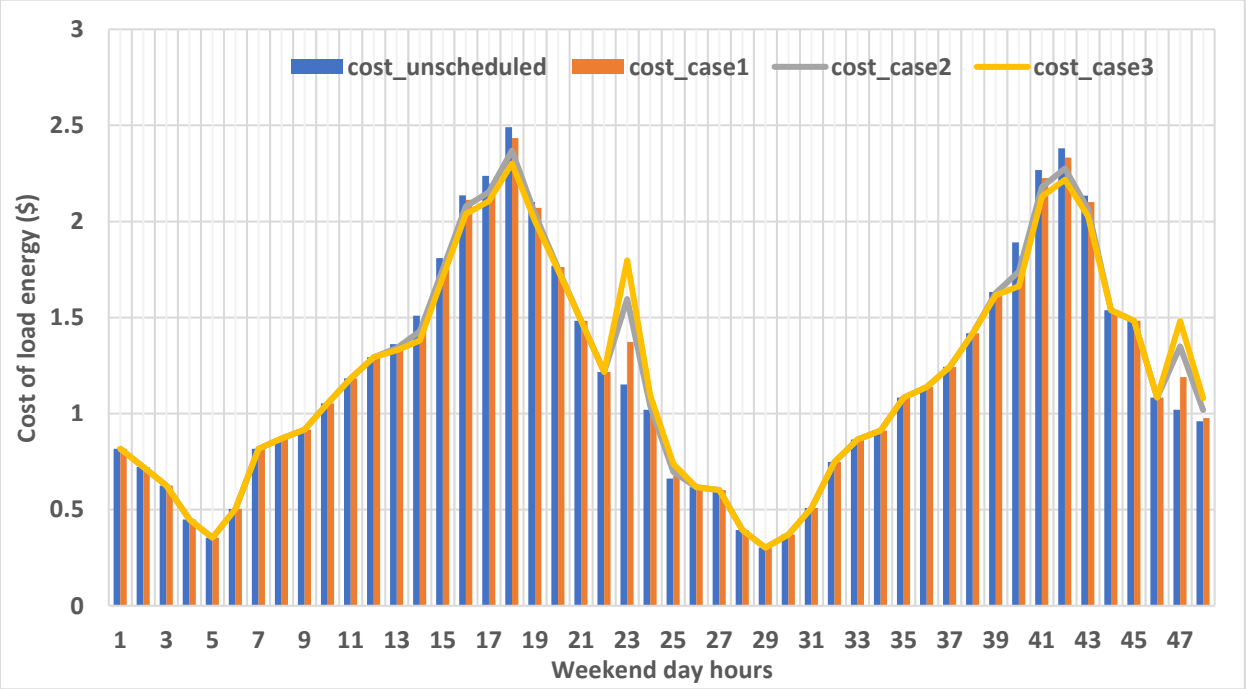

Fig. 34. Cost of load energy per hour for weekend days.

The energy cost, as shown in Fig. 34 for the considered three cases, indicates that the costs are very close to each other as electricity price is the same for all hours in the day.

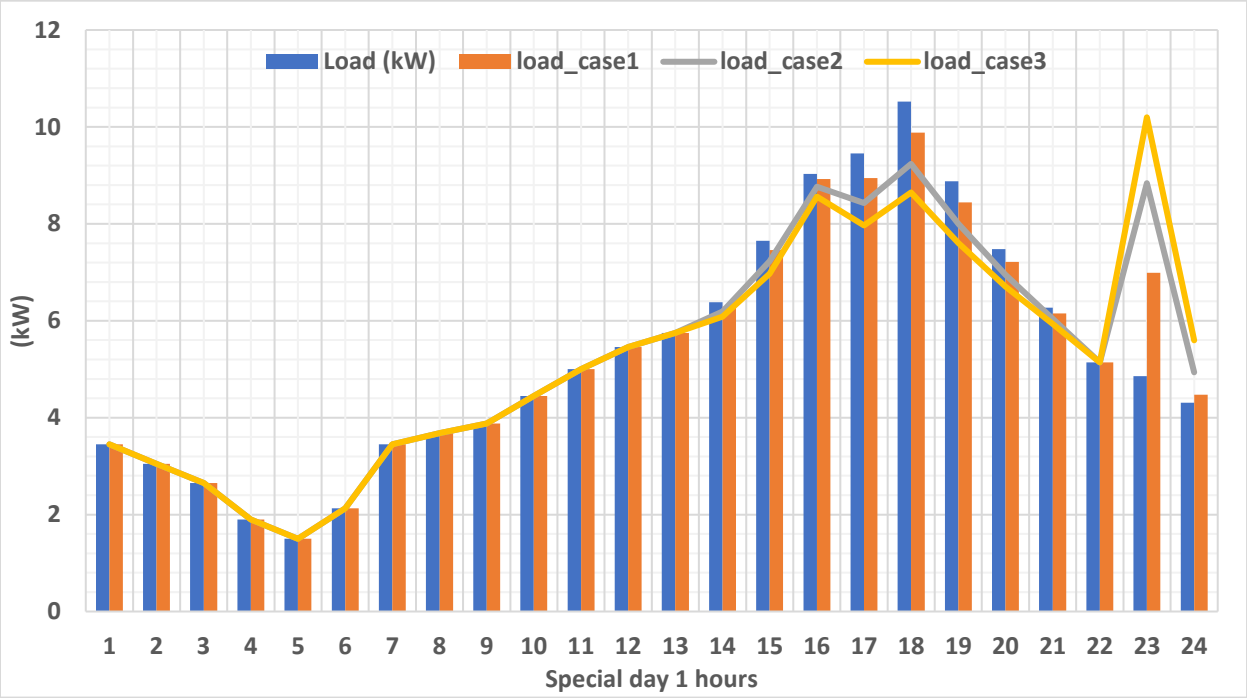

Fig. 35. Load scheduling using grid power for special day1.

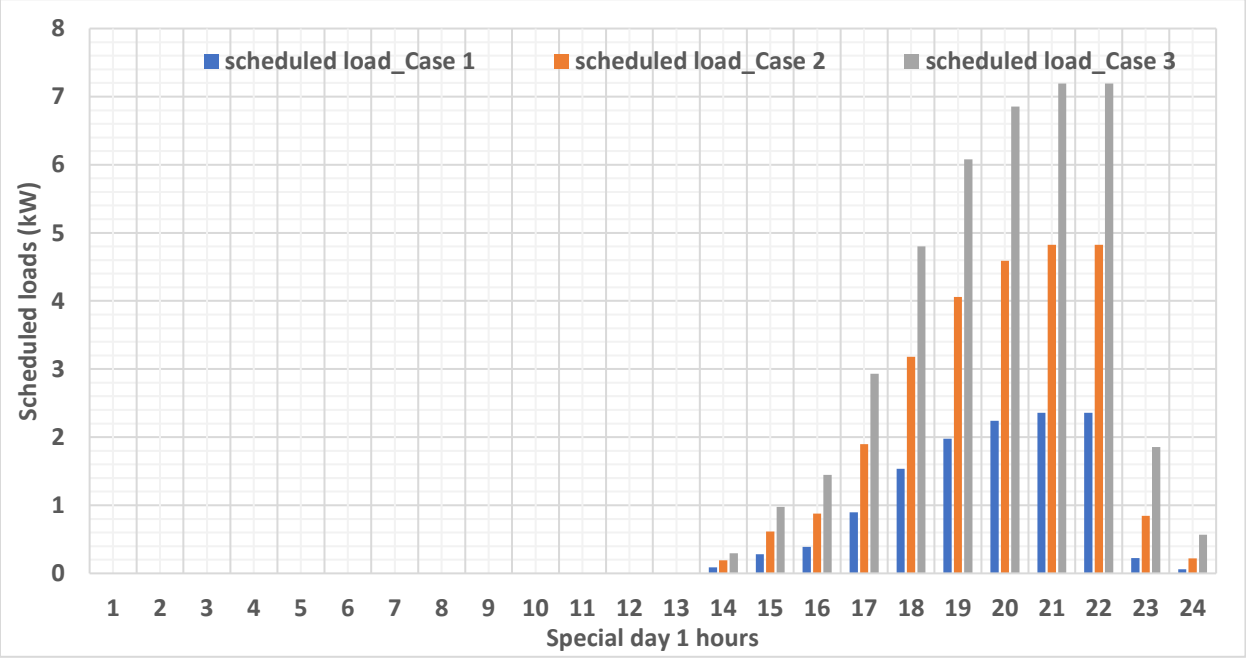

Fig. 36. Scheduled loads for special day1.

The unscheduled loads and load consumption for the considered three cases are shown in Fig. 35 followed by the scheduled loads in Fig. 36. As special day 1 is considered to be a normal

working day, therefore, the performances of the considered three cases are similar to the normal working days cases discussed before. In addition, the desired cost of energy is considered to be 1.00$ and 1.75$ respectively for peak and off-peak hours.

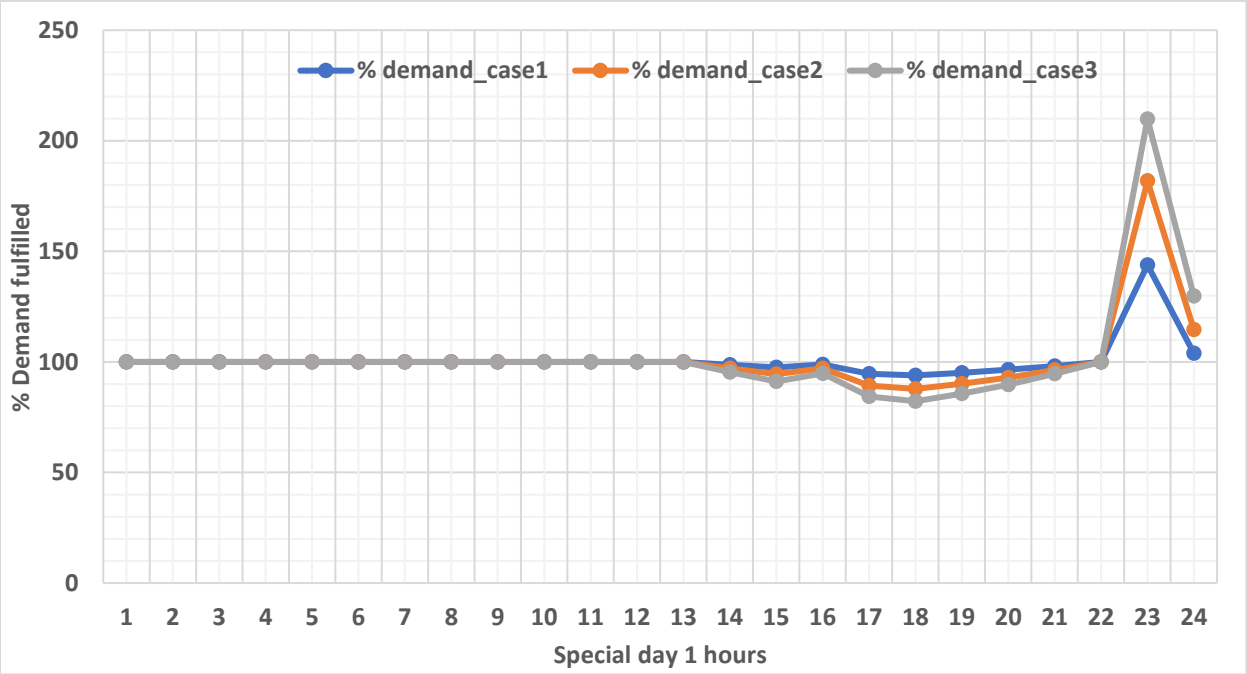

Fig. 37. Percentage of load demand fulfilled per hour for special day 1.

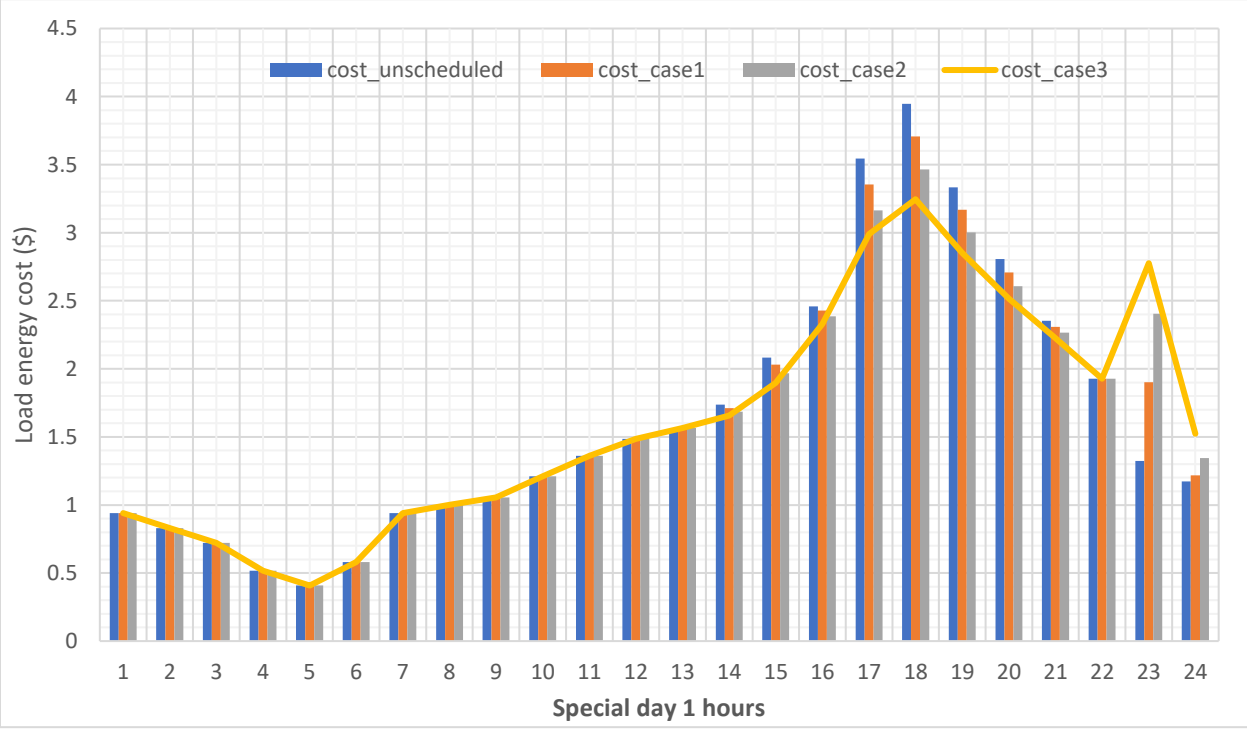

Fig. 38. Cost of load energy per hour for special day 1.

Fig. 37 and Fig. 38 represent the percentage of demand fulfillment and the energy cost for the considered three cases.

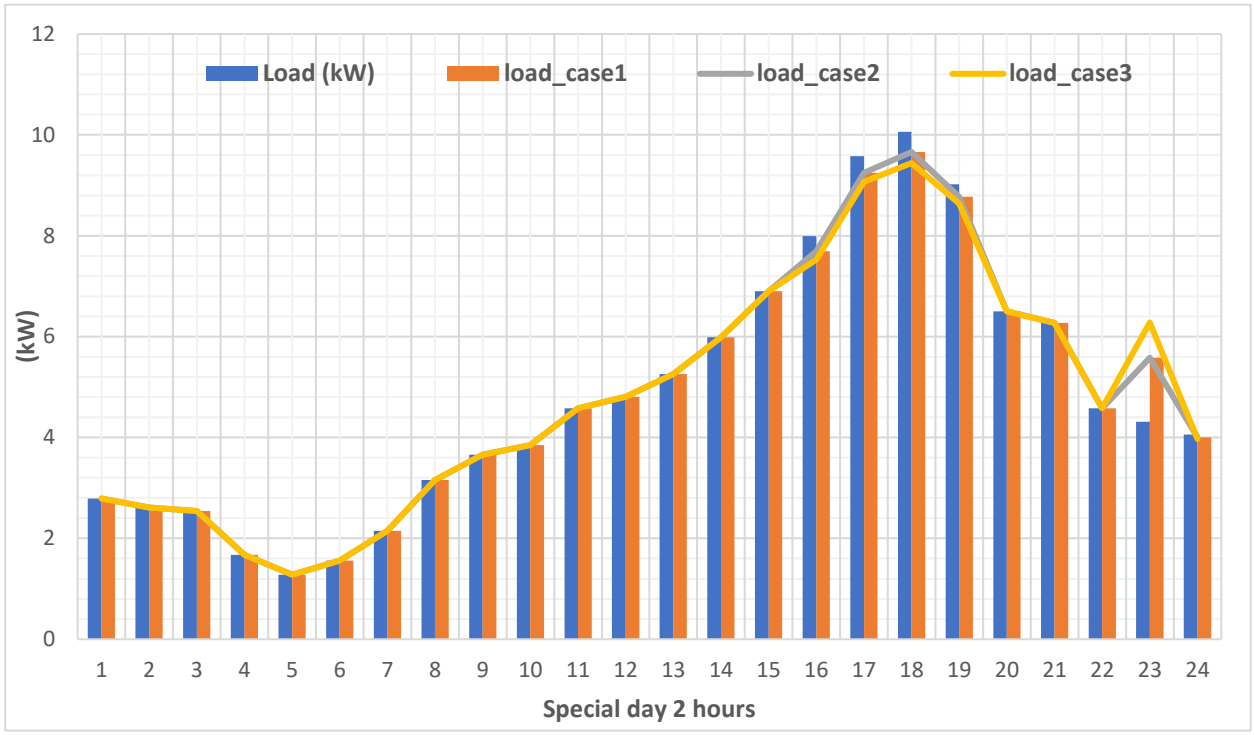

Fig. 39. Load scheduling using grid power for special day2.

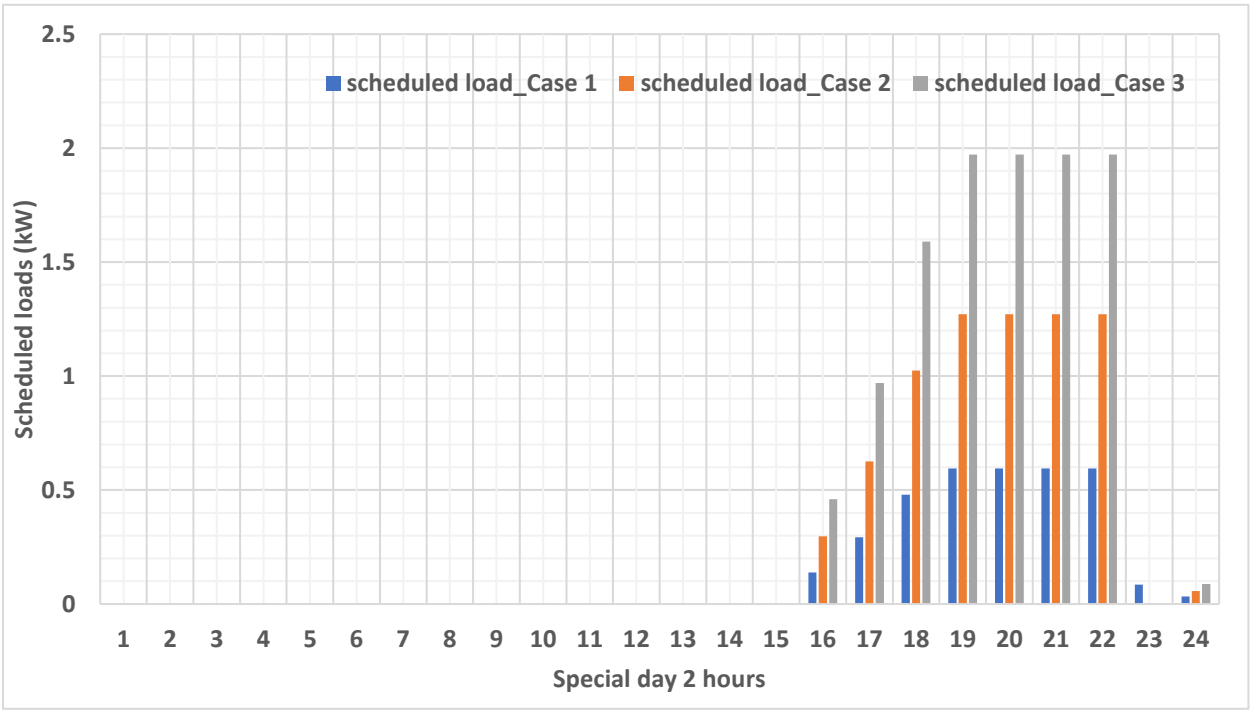

Fig. 40. Scheduled loads for special day2.

Fig. 39 and Fig. 40 represent unscheduled loads and load consumption for the considered three cases followed by the scheduled loads respectively for the special day 2 which is assumed to be a weekend day. Therefore, three cases perform similarly to the weekend cases discussed before. The desired cost of energy is considered to be the same for peak and off-peak hours as considered for special day 1.

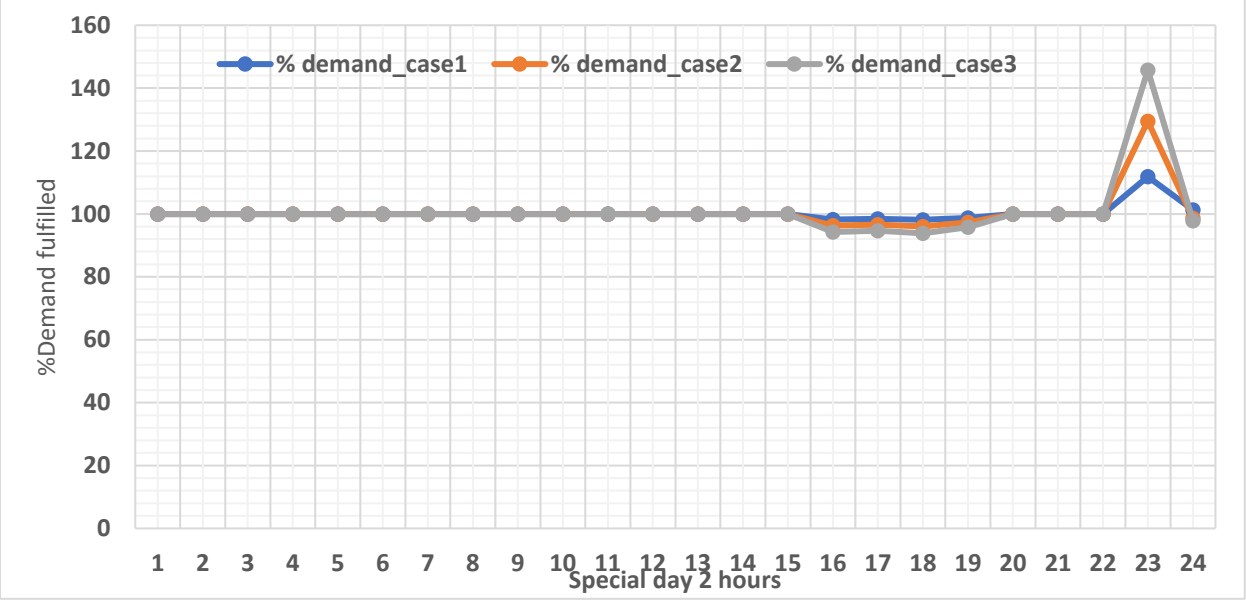

Fig. 41. Percentage of load demand fulfilled per hour for special day 2.

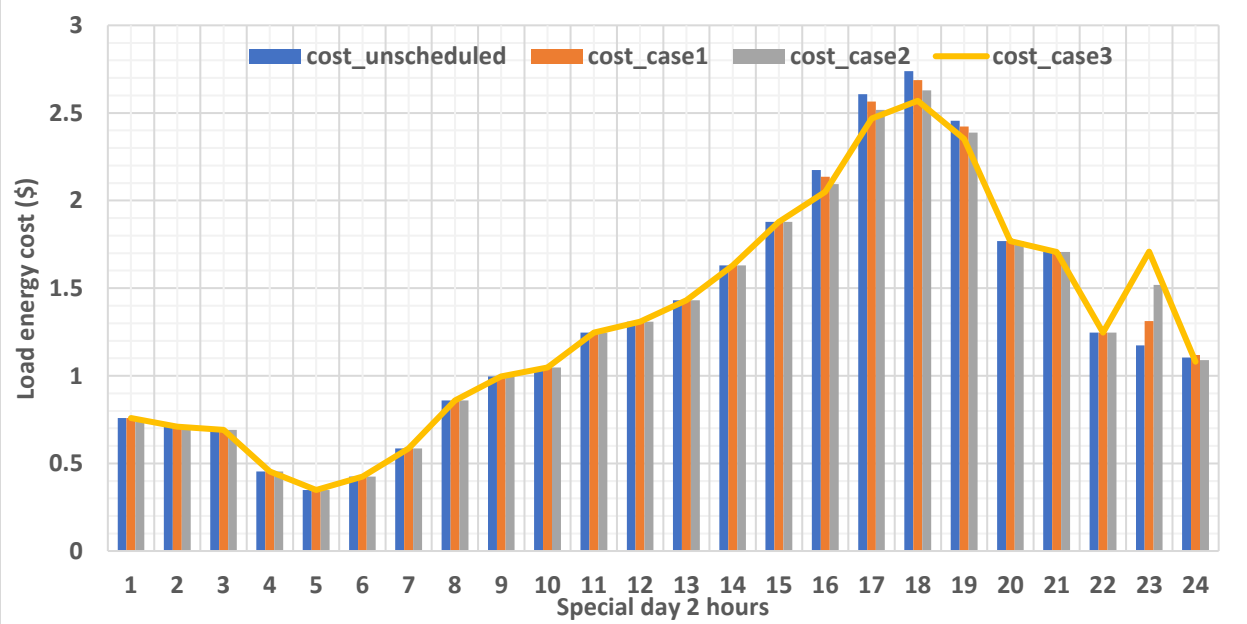

Fig. 42. Cost of load energy per hour for special day 2.

Moreover, the percentage demand fulfillment and the cost of energy for special day 2 are shown in Fig. 41 and Fig. 42 respectively.

Table 13: C_{saving} and $P_{delayed}$ summary for load scheduling using grid power

Day Type	Performance Index	Cases		
		1	2	3
Working days	C_{saving} ($)	-11.548	-11.208	-10.033
	$P_{delayed}$ (kW)	0.0251	0.1002	0.2828
Weekend	C_{saving} ($)	-7.1395	-7.1182	-7.0771
	$P_{delayed}$ (kW)	0.0390	0.1174	0.2684
Special day1	C_{saving} ($)	-9.1517	-8.8334	-8.5522
	$P_{delayed}$ (kW)	0.0594	0.2184	0.5693
Special day2	C_{saving} ($)	-1.3385	-1.3319	-1.3234
	$P_{delayed}$ (kW)	0.0325	0.0568	0.0882

Table 13 summarizes the performance of the proposed three cases for normal working days, weekend and special days in terms of C_{saving} and $P_{delayed}$. The higher value of C_{saving} and lower value of $P_{delayed}$ represent better performance. The negative value of C_{saving} indicates that the overall value of energy saving is negative meaning the cost of the energy is mostly above the desired value. Similarly, the positive value of $P_{delayed}$ indicates the total load scheduled for the next hour after the end of the considered day. Based on the above discussion, it can be concluded that in terms of cost saving case 3 performs better for all days as it has the lowest negative values although the values for the three cases are very close to each other for weekend days and special day 2 as the electricity price remain same for the whole day. In terms of delayed/scheduled load value case 1 performs better for all days. Case 2 performance in terms of cost and scheduling of load are

always in the second position for all days. Therefore, case 2 will be considered for the next discussions.

2. Smart Building Operated by Grid Power and Battery Energy Storage

In this case, the combination of grid power and battery energy storage is used for providing power to the load. The load patterns for all day types are considered the same as shown in Fig. 22 and Fig. 23. As E-TOU rate Option-B performs better in the above case and has low rates for both working days and weekends as compared to the other rates, therefore, this rate is considered as the grid power rate. The two batteries each of 14 kWh is considered in this work, of which 13.5 kWh is available for operations. The constraints for battery charging and discharging power, P_d and the maximum and minimum energy level, B_e are defined below. Moreover, the charging and discharging efficiencies of the battery system is assumed to be 95% and 90%, respectively. The battery energy level, Be and the percentage state of charge (%SOC) can be expressed by the following two equations:

$$B_e(h) = B_e(h-1) + P_d \Delta h \tag{40}$$

$$\%\, SOC(h) = \frac{B_e(h)}{B_{e_{rated}}} \times 100 \tag{41}$$

where, Δh is considered to 1 hour for all cases. The constrains considered for the battery energy storage are:

$$-5kW \leq P_d \leq 5kW$$

$$2.7kWh \leq B_e \leq 24.3kWh$$

Now in this case, for charging of the battery, the off-peak hour should be chosen as it has the lowest TOU rates. In order to provide 1 kW of power for an hour from the grid to a battery,

the cost would be 0.27217 $. The levelized cost for battery energy storage for both charging and discharging condition is found to be 0.05289 $/kWh. Therefore, 0.95 kWh energy would be stored in the battery energy storage considering charging efficiency to be 95%. Therefore, the cost would be 0.32506 $ (0.27217$ + 0.05289$). Now, when energy is provided to the load, out of 0.95 kWh energy, 0.855 kWh is provided with an additional discharging cost of 0.05289$. Therefore, the overall cost of 0.855 kWh becomes 0.37795 $. For providing 1 kWh energy from battery energy storage, this cost would be 0.44204$ which is 1.62 times and 1.17 times higher than off-peak hour and peak-hour electricity cost respectively if this energy is directly provided from the grid to the loads during peak and off-peak hours. Based on this calculation, it can be concluded that battery energy storage, when it is charged by the grid power, is not a good option for regular load scheduling practice even in peak hours as it is more expensive. However, battery energy storage can be kept in this case as a backup option for critical situations such as blackout.

3. *Smart Building Operated by Grid Power, Renewable Energy Sources and Battery Energy Storage*

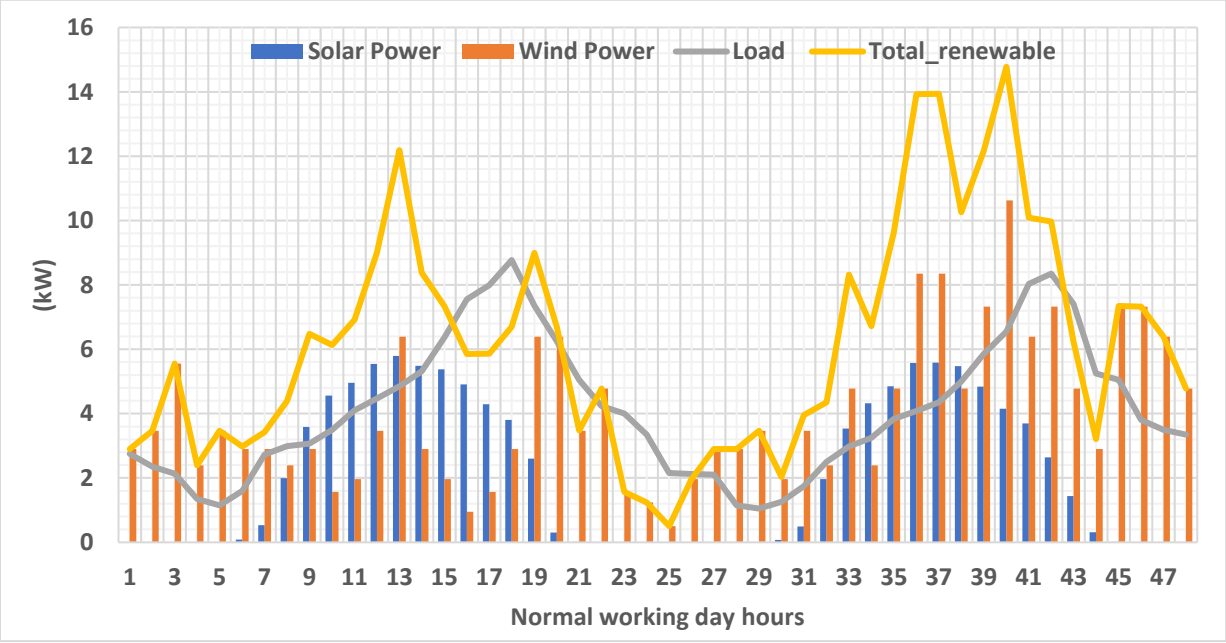

Fig. 43. Renewable source power and load considered for normal working days.

Fig. 43 shows the solar, wind power available for the considered normal working days with the load demands. For scheduling purposes, in addition to the objective function proposed in (37), another objective function is considered as shown in (42).

$$f_{obj} = \sqrt{K_3A^2 + K_4B^2 + K_5C^2 + K_6P_g + \frac{P_{sys_{loss}}(h)}{P_e(h)}} \tag{42}$$

where,

$$A = C_e - C_{g\_actual}(h)$$

$$C_e = \lambda_g(h)P_g(h) + \lambda_s P_s(h) + \lambda_w P_w(h) + \lambda_{batt}|P_{batt}(h)|$$

$$B = \frac{P_{l\_actual}(h) - P_e(h)}{1000}$$

$$C = \frac{P_w(h) + P_s(h) + |P_{batt}(h)| - P_e(h)}{1000}$$

$$P_{sys_{loss}}(h) = 0.01P_e(h) + P_{batt_{loss}}$$

where λ stands for cost of energy and P stands for power. The subscript s, w, batt stand for solar, wind and battery, respectively.

The first term represents the difference between the system cost per hour and the desired cost. The second term corresponds to the difference between the actual load demand and load consumption. The third term is the difference between the available renewable energy, battery energy storage and consumed loads. Therefore, this objective function would be minimum if the system cost would be close to the desired cost, the difference between demand and actual consumption. Moreover, in order to have a minimum value, the consumption should be close to the available renewable sources and battery energy storage while taking less power to the grid (P_g positive) and giving maximum power to the grid (P_g negative) if possible. In addition, the load loss and battery energy loss should be minimum to have a minimum value of the objective function. Therefore, this objective function should satisfy every aspect of the net-zero energy function to

have a minimum value. The constraints considered for this objective function are the same as it has been considered for (37). In addition, the constraints included are:

$$K_3 + K_4 = K_5 + K_6 = 1$$

For the system having renewable sources, battery energy storage and grid power, three cases are considered. In the first case, renewable energy sources are considered without battery energy storage. For optimization, the objective function in (37) is considered with K_1=0.7. In the second case, renewable energy sources without battery energy storage is considered and objective function (42) is used. During the peak and off-peak hours, K_3=0.7, K_5=0.5 values are considered. For the third case, renewable energy sources are considered with battery energy storage. The objective function in (42) is used for optimization, and K_3, K_5 values are considered the same values used in case two. For all cases, the desired cost per hour for off-peak and peak hours are considered to be 1$ and 1.75$, respectively.

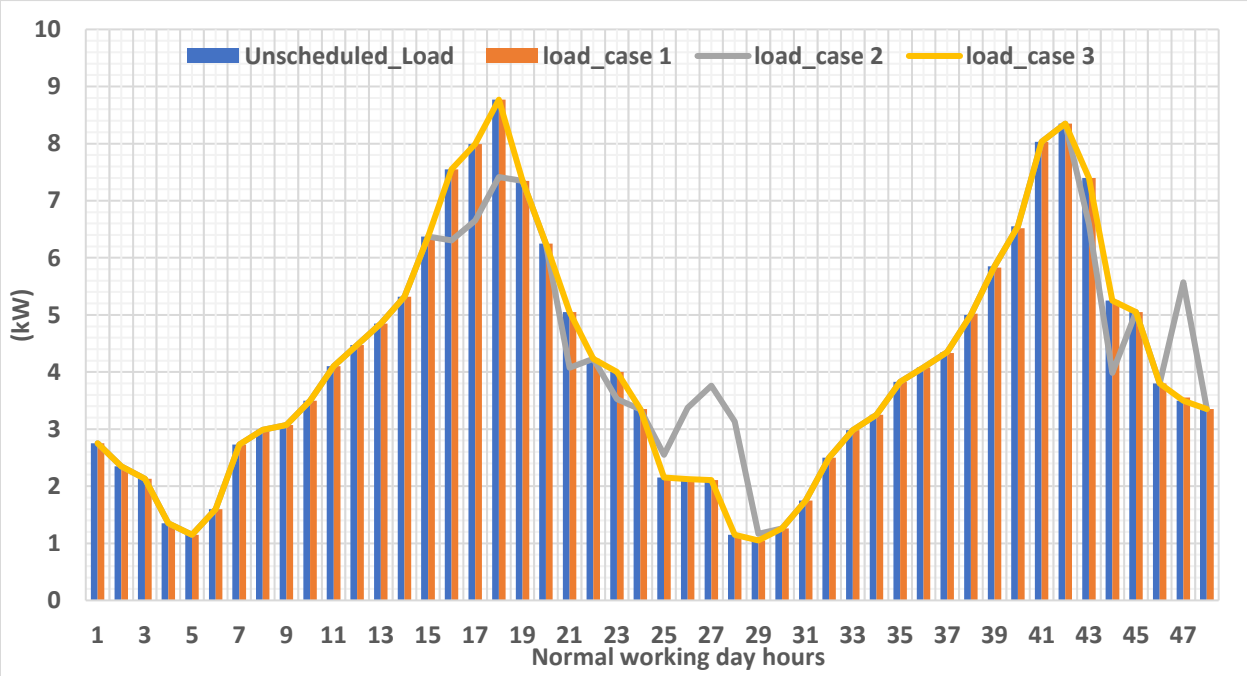

Fig. 44. Load scheduling for different cases for normal working days using renewable sources and with or without battery energy storage.

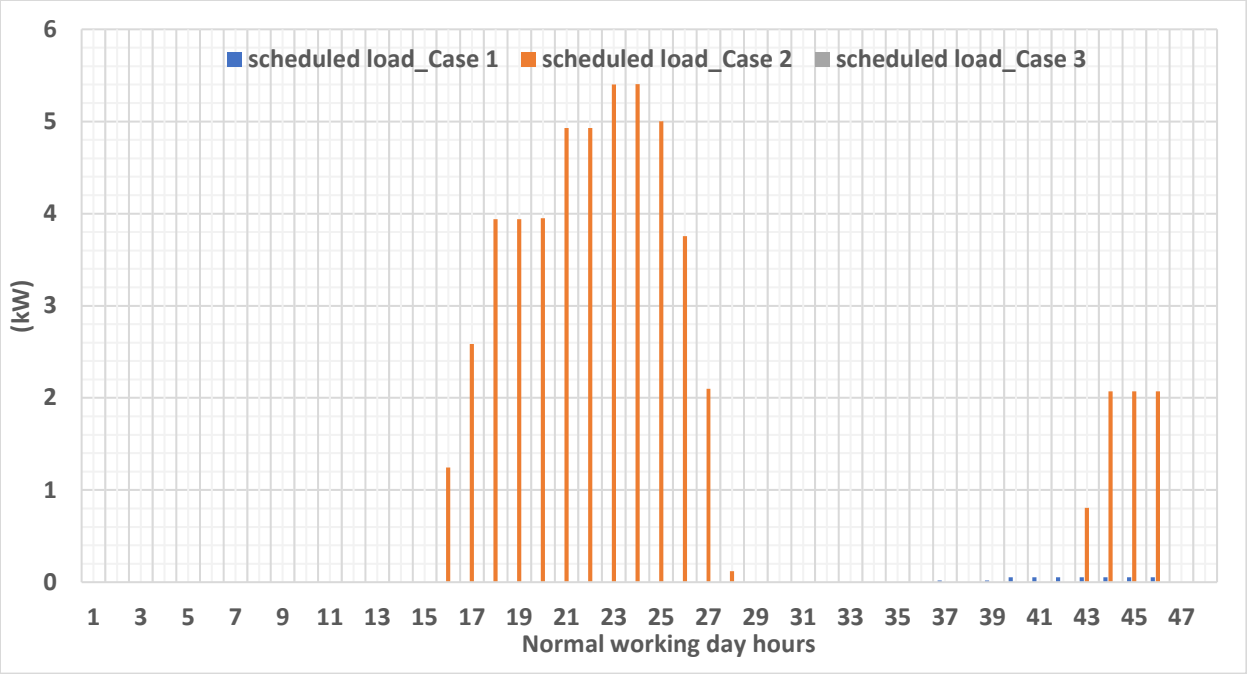

Fig. 45. Scheduled loads for different cases for normal working days using renewable sources and with or without battery energy storage.

Fig. 44 shows the unscheduled (demand) and load consumption for the considered three cases. For case 1, the load consumption is close to the demand as renewable energy sources and grid power are used for load consumption. In case 2, the load scheduling is mainly done with renewable energy available while taking less power from the grid as shown in Fig. 47. Therefore, the scheduled load for case 2 will be higher than case 1 which is evident in Fig. 45. For case 3, the battery energy storage provides any discrepancy between renewable energy and load demand. Therefore, no scheduling is required which is evident in Fig. 45.

The percentage of demand fulfillment for different cases is shown in Fig. 46 for each hour. Moreover, the grid power requirements for all the cases are shown in Fig. 47. In Fig. 47, the unscheduled grid power represents the power that are required from the grid only if all the demands are supplied by the grid only. Case 3 requires the least grid power followed by case 2 and case 1.

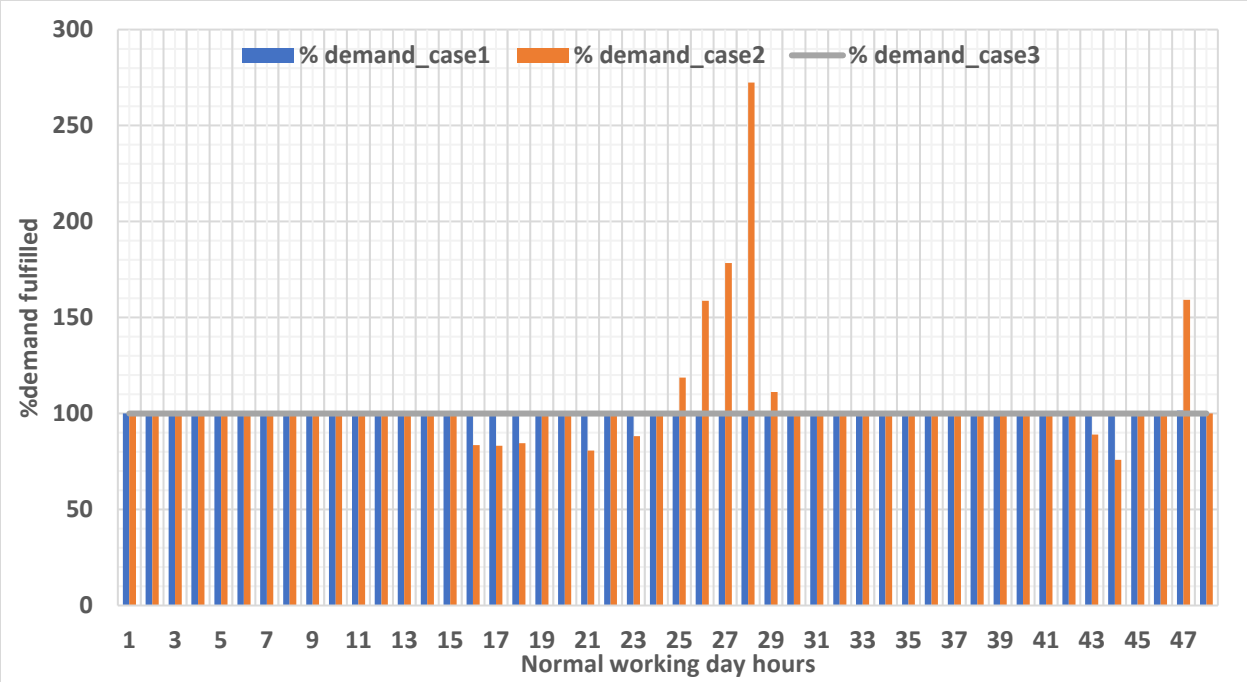

Fig. 46. Percentage of load demand fulfilled for normal working days using renewable sources and with or without battery energy storage.

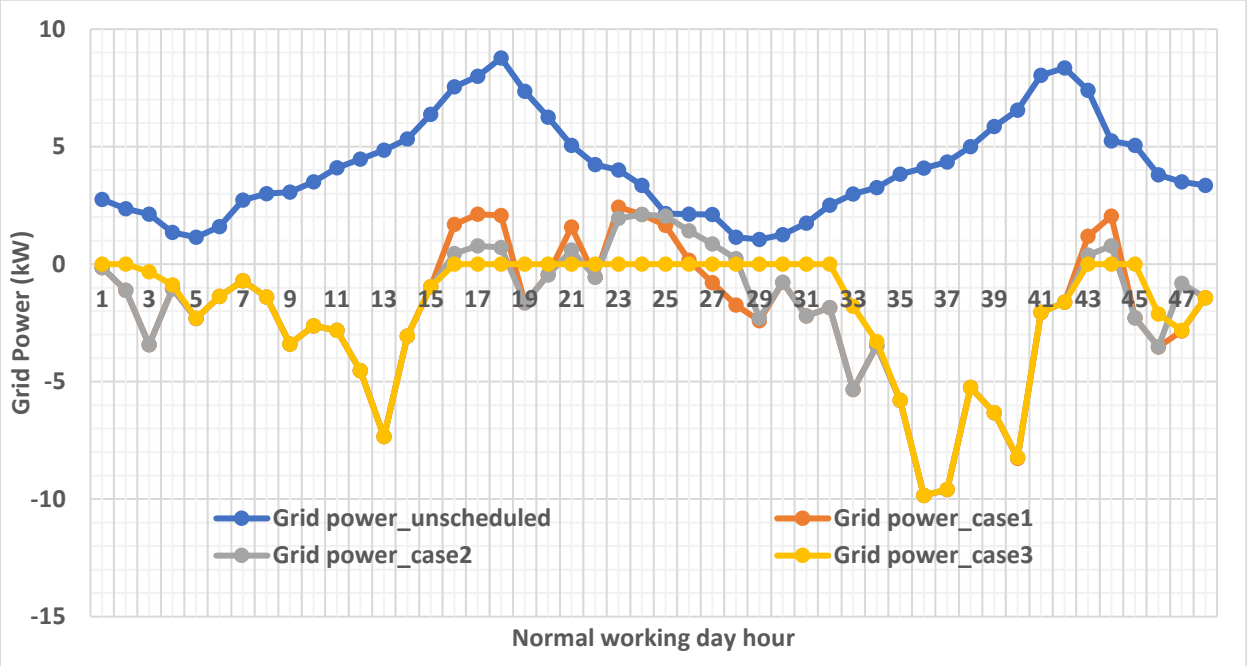

Fig. 47. Grid power required for normal working days using renewable sources and with or without battery energy storage.

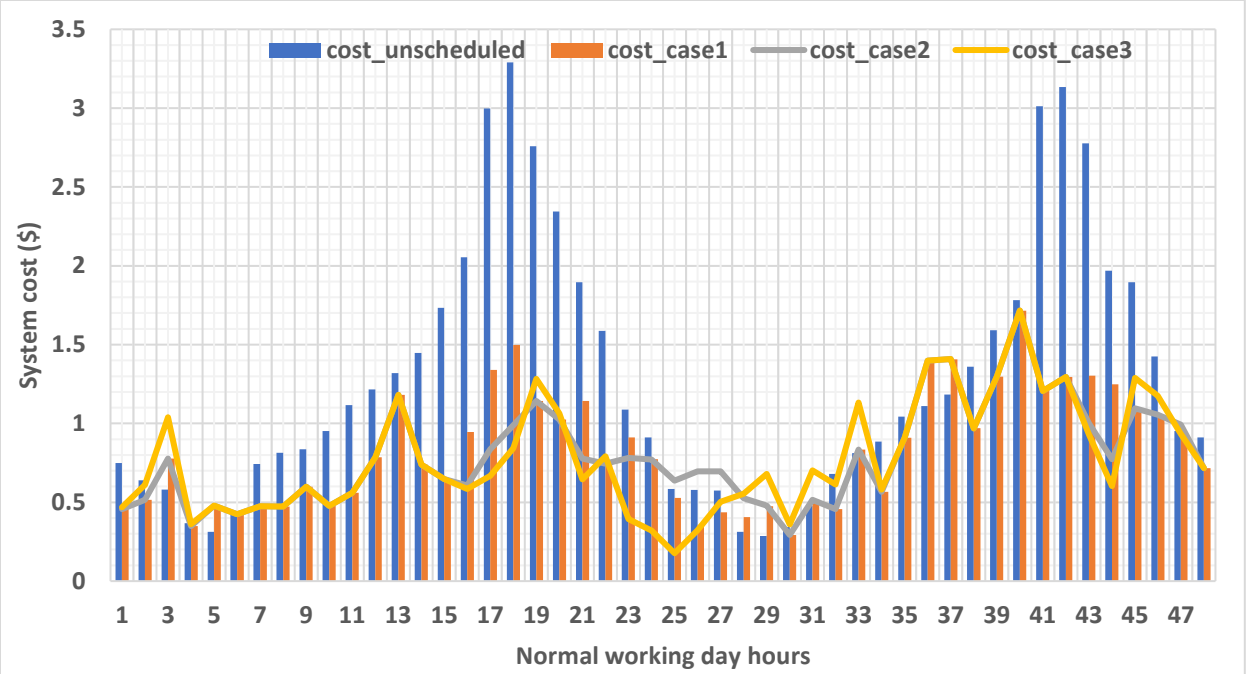

Fig. 48. Cost of system per hour for different cases for normal working days.

Fig. 48 represents the system cost for all three cases for normal working days. The system cost in case 1 is higher as compared to case 2 and case 3 as it utilizes more grid power. The grid power cost is higher than the wind and solar power for both peak and off-peak hours.

The power losses for the considered three cases are shown in Fig. 49. The power loss in case 1 and case 2 is lower than that of case 3 as for the first two cases as the loss is assumed to be 1% of load consumption. However, for case 3, the battery charging and discharging losses are considered which make the system lossier as compared to case 1 and case 2.

The charging and discharging operation for battery energy storage in case 3 is shown in Fig. 50.

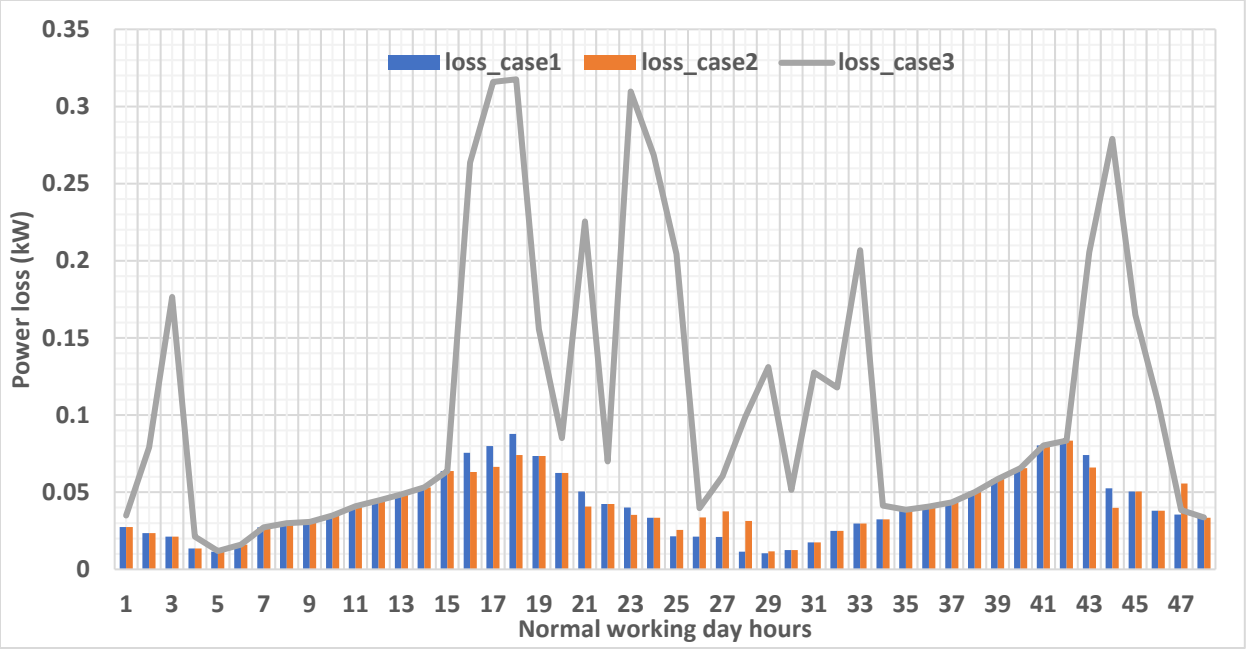

Fig. 49. Power loss per hour for different cases for normal working days.

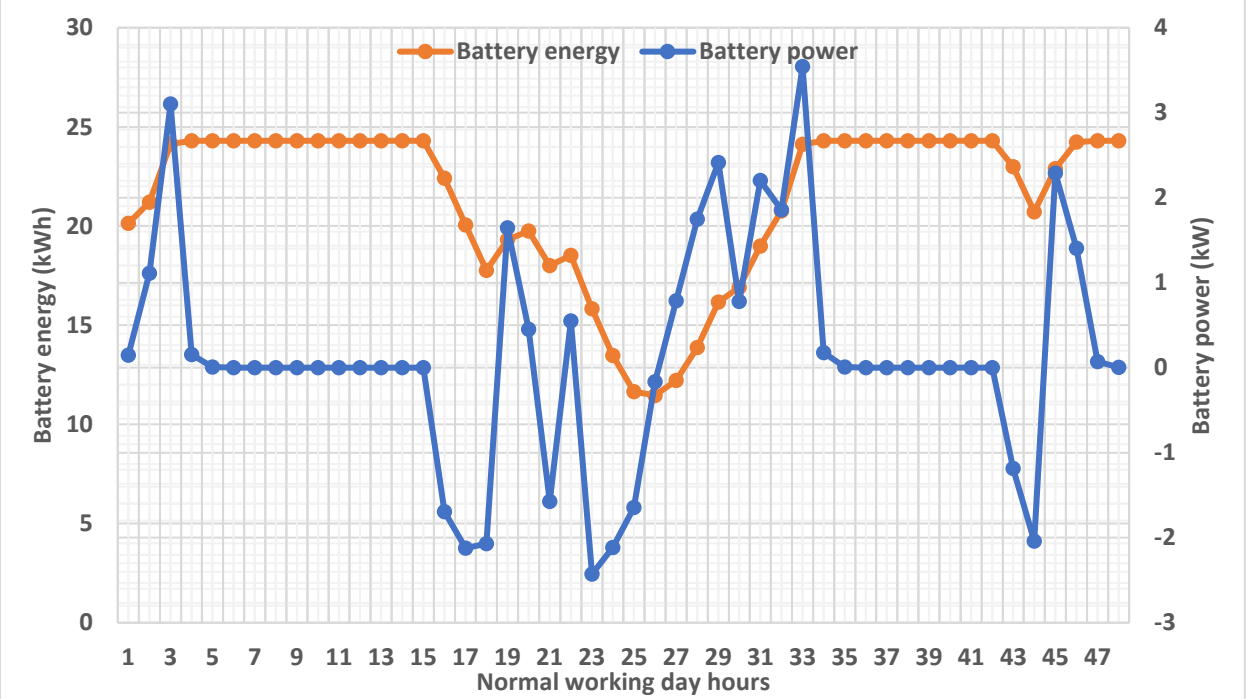

Fig. 50. Battery power and energy for case 3 for normal working days.

Table 14: C_{saving} and $P_{delayed}$ summary for load scheduling for normal working days

Day Type	Performance Index	Cases		
		1	2	3
Working days	C_{saving} ($)	17.1197	18.8466	19.6180
	$P_{delayed}$ (kW)	0.0	0.0	0.0

For all cases, the scheduled load is 0 which indicates that our proposed objective functions perform well for normal working days. In terms of cost saving, case 3 performs better as compared to case 2 and case 1. However, case 3 has the maximum power loss as compared to other cases. Case 2 does not have any battery loss and it performs well as compared to case 1 in terms of cost savings.

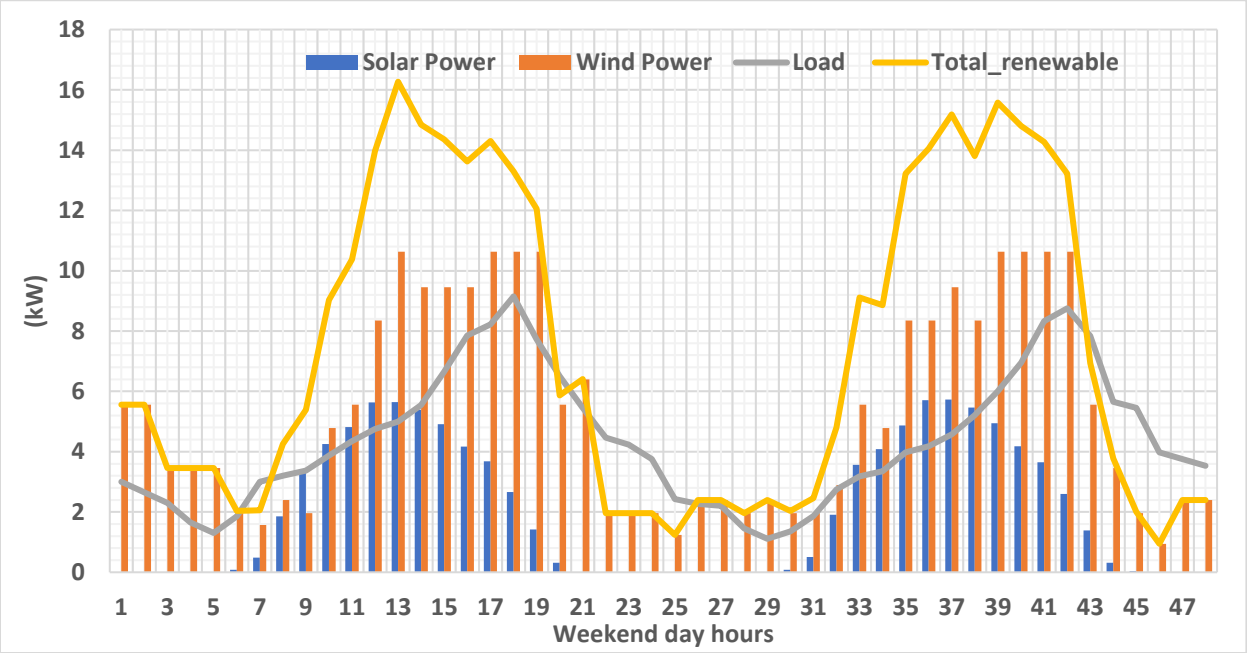

Fig. 51. Renewable source power and load considered for weekend days.

The available renewable energies along with the load demand for the considered weekend days are shown in Fig. 51. Like the normal working days, the same three cases are considered for weekend days.

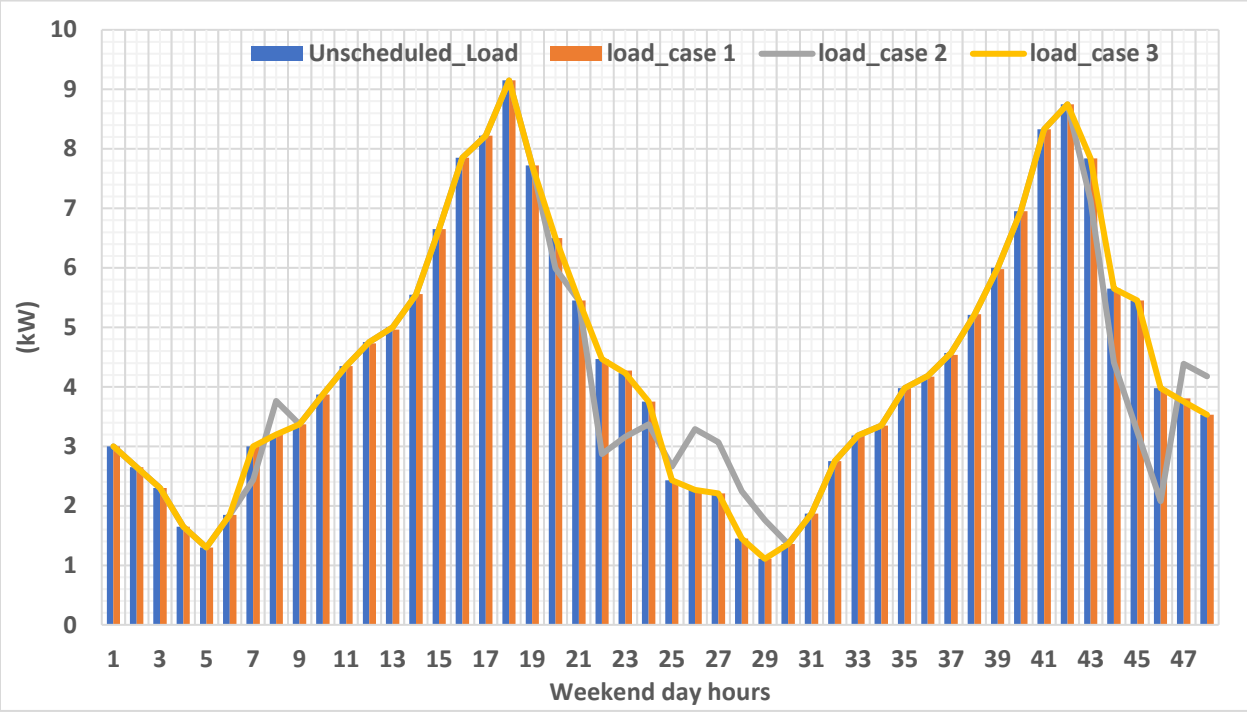

Fig. 52. Load scheduling for different cases for weekend days using renewable sources and with or without battery energy storage.

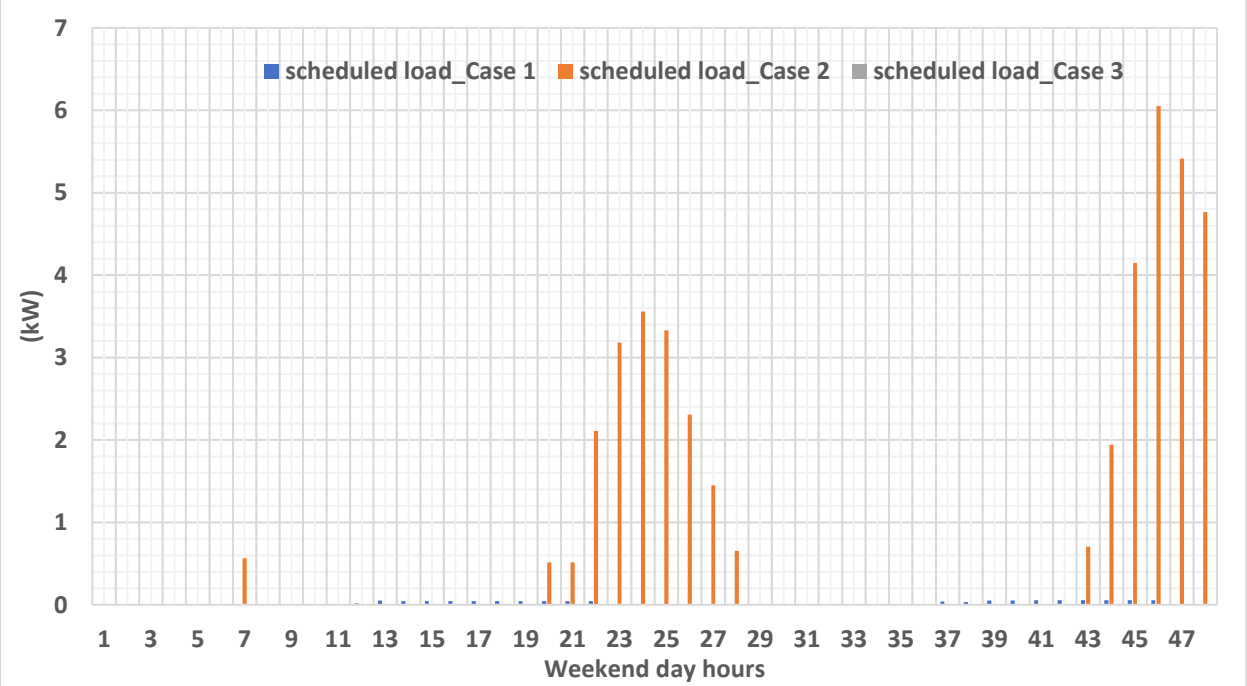

Fig. 53. Scheduled loads for different cases for weekend days using renewable sources and with or without battery energy storage.

The unscheduled load and the load consumption for the considered three cases are shown in Fig. 52 followed by the scheduled loads shown in Fig. 53. From Fig. 53, it is evident that the required load, to be scheduled for later hours, is least for case 3 and highest for case 2 as it tries to cope up the loads with available renewable sources taking minimum power from the grid.

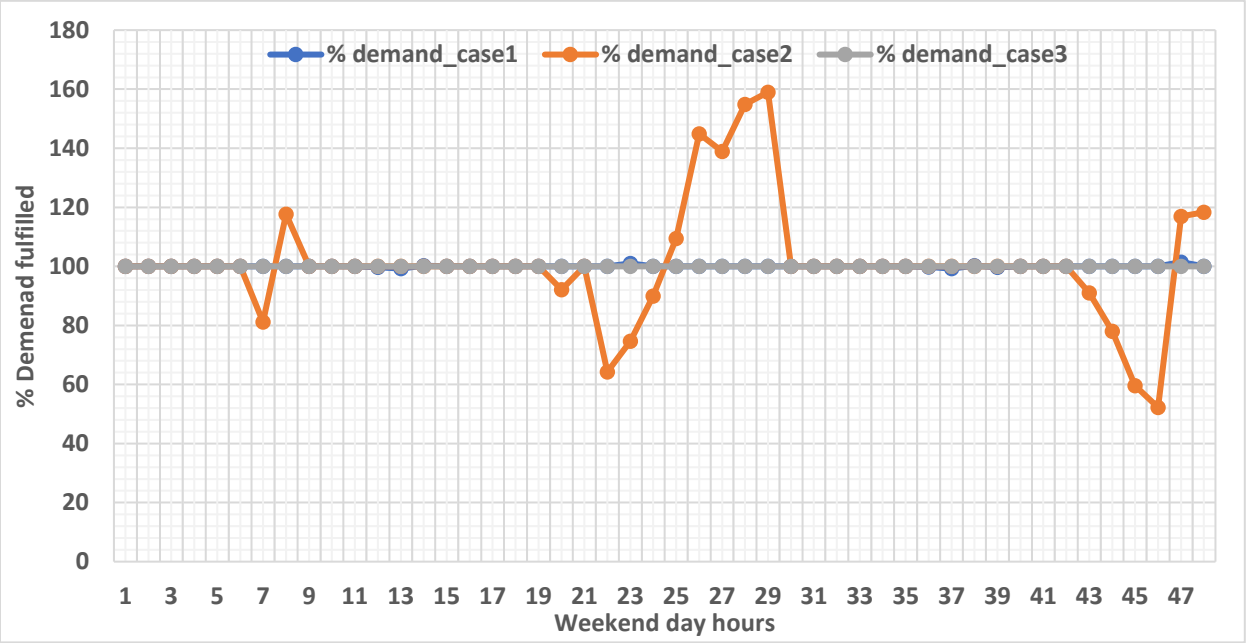

Fig. 54. Percentage of load demand fulfilled for weekend days using renewable sources and with or without battery energy storage.

Fig. 54 represents the performance of the proposed three systems in the fulfillment of load demands. From the figure, it can be concluded that both case 1 and case 3 fulfill the load demand for most of the considered range of hours.

The grid power exchange for the considered three scheduling cases is shown in Fig. 55 which indicates that in case 3 no grid power is taken as the battery energy storage supplies the extra power required in addition to the renewable power available. For case 1, the maximum grid power is taken.

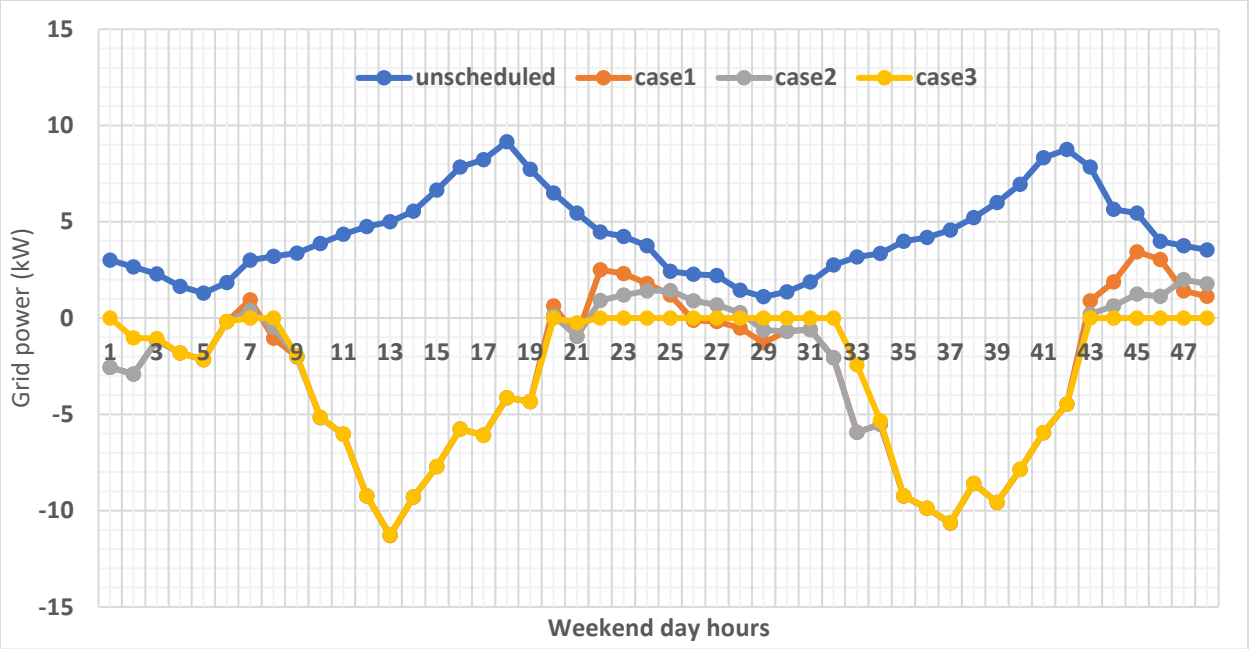

Fig. 55. Grid power required for weekend days using renewable sources and with or without battery energy storage.

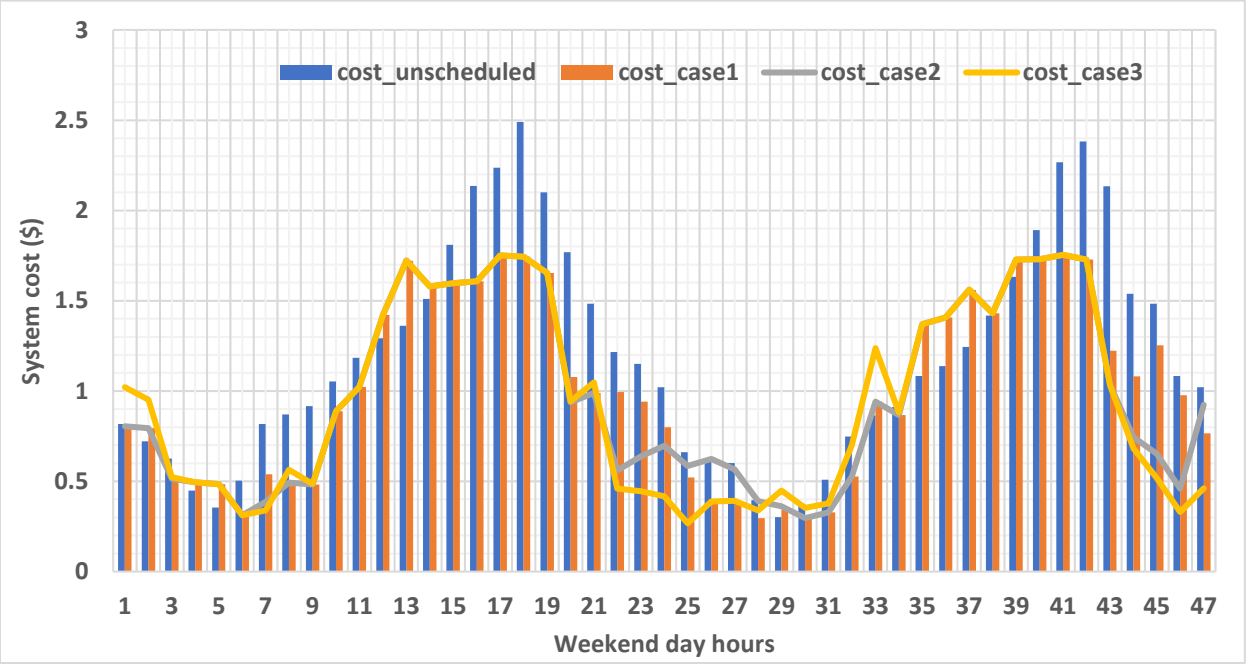

Fig. 56. Cost of system per hour for different cases for weekend days.

Fig. 56 represents the cost of the systems for the considered three cases. The power loss for the proposed three scheduling cases is shown in Fig. 57. Among the three cases, case 3 has the highest power loss as it has both load loss and battery charging and discharging loss.

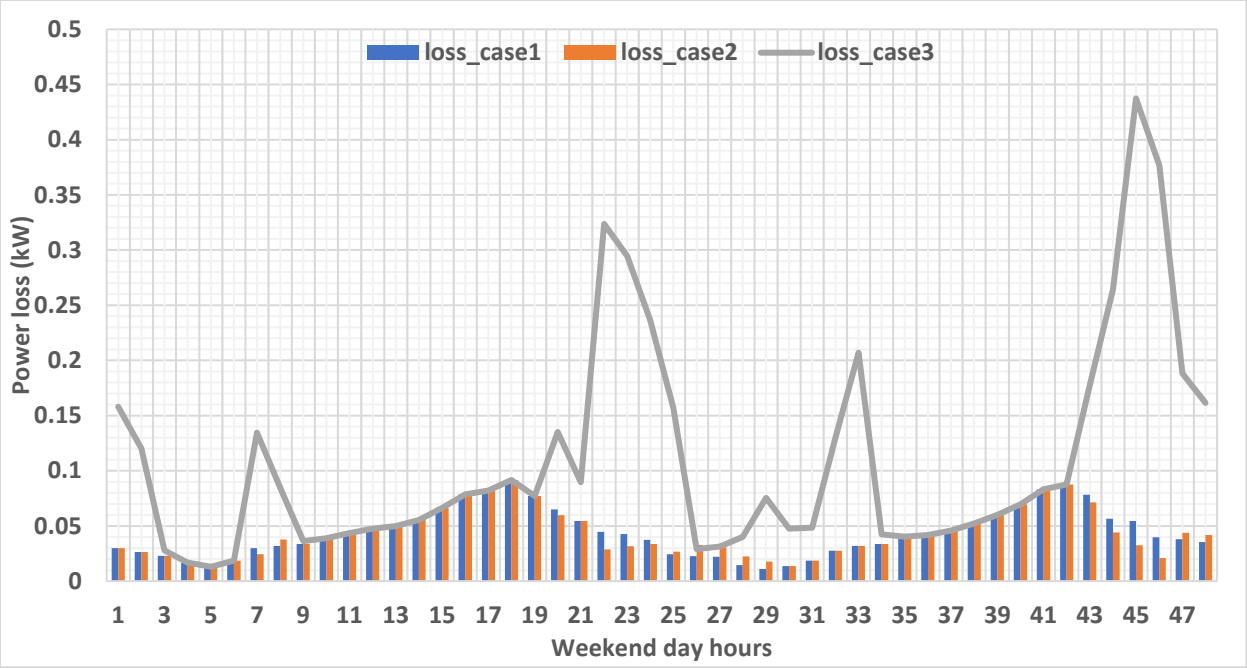

Fig. 57. Power loss per hour for different cases for weekend days.

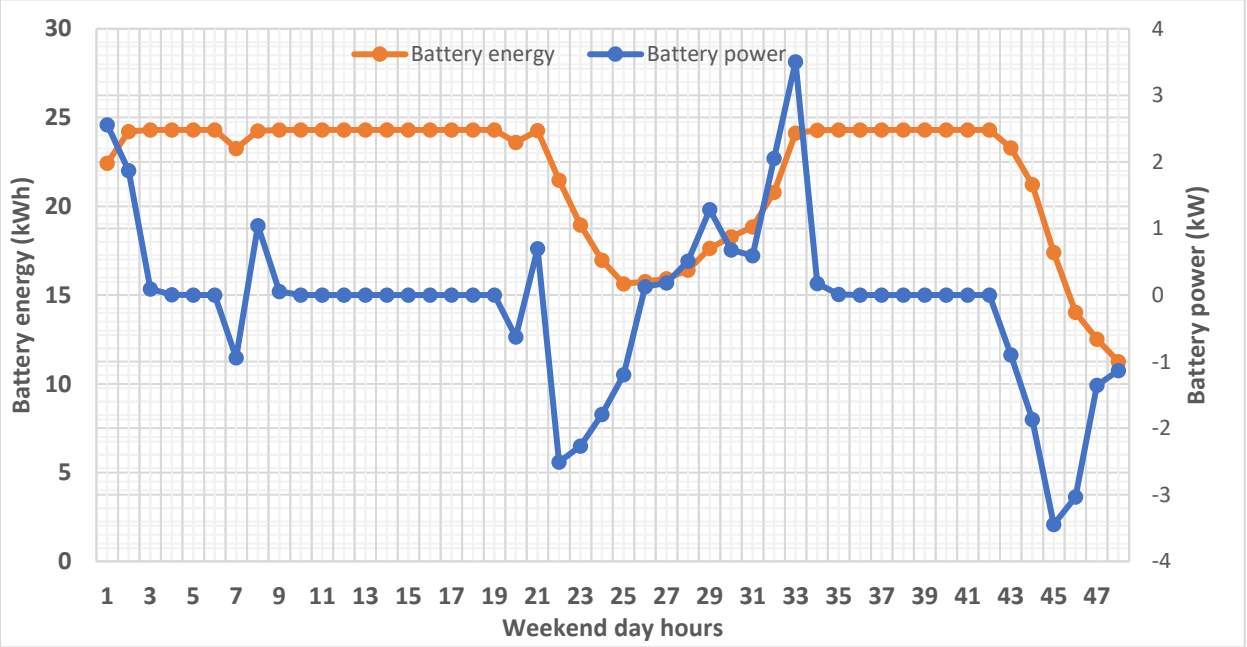

Fig. 58. Battery power and energy for case 3 for weekend days.

The battery operation for case 3 for the weekend days is shown in Fig. 58. The maximum charging and discharging power are kept at 5 kW, and the energy is varied from 2.7 kWh to 24.3 kWh.

Table 15: C_{saving} and $P_{delayed}$ summary for load scheduling for weekend days

Day Type	Performance Index	Cases		
		1	2	3
Weekend days	C_{saving} ($)	9.4887	11.3004	12.6778
	$P_{delayed}$ (kW)	0.0	4.7642	0.0

Table 15 represents the performance of the considered scheduling cases in terms of cost savings and load delayed. In terms of load delayed, case 1 and case 3 perform similarly. However, in terms of cost saving, case 3 performs the best. As for case 2, the delayed loads are 4.7642 kW after the considered periods. However, in terms of cost savings, it performs better than case 1.

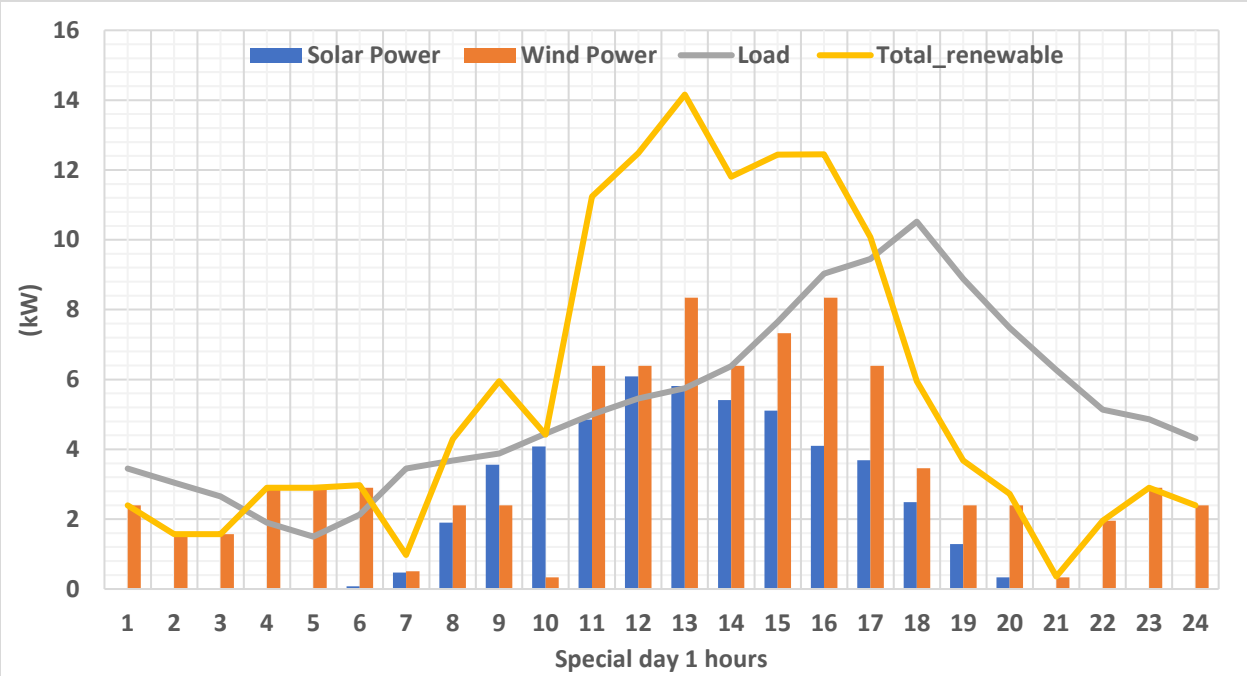

Fig. 59. Renewable source power and load considered for special day 1.

Fig. 59 represents the renewable sources' power and load demand for special day 1 which is assumed to be a normal working day. As for scheduling cases, in addition to the cases considered

for both normal working days and the weekend days, two new cases are considered which are named as case 4 and case 5.

In case 4, all the conditions are considered to be the same as in case 2 except if the demand gets more than or equal to twice of renewable source power, the K_3=0.5 is chosen instead of 0.7. As for case 5, all the conditions are similar to case 3 except the fact that the battery energy storage system only provides power to the load during peak hours and only takes power during peak and off-peak hours whenever the available renewable energy is higher than the load demand.

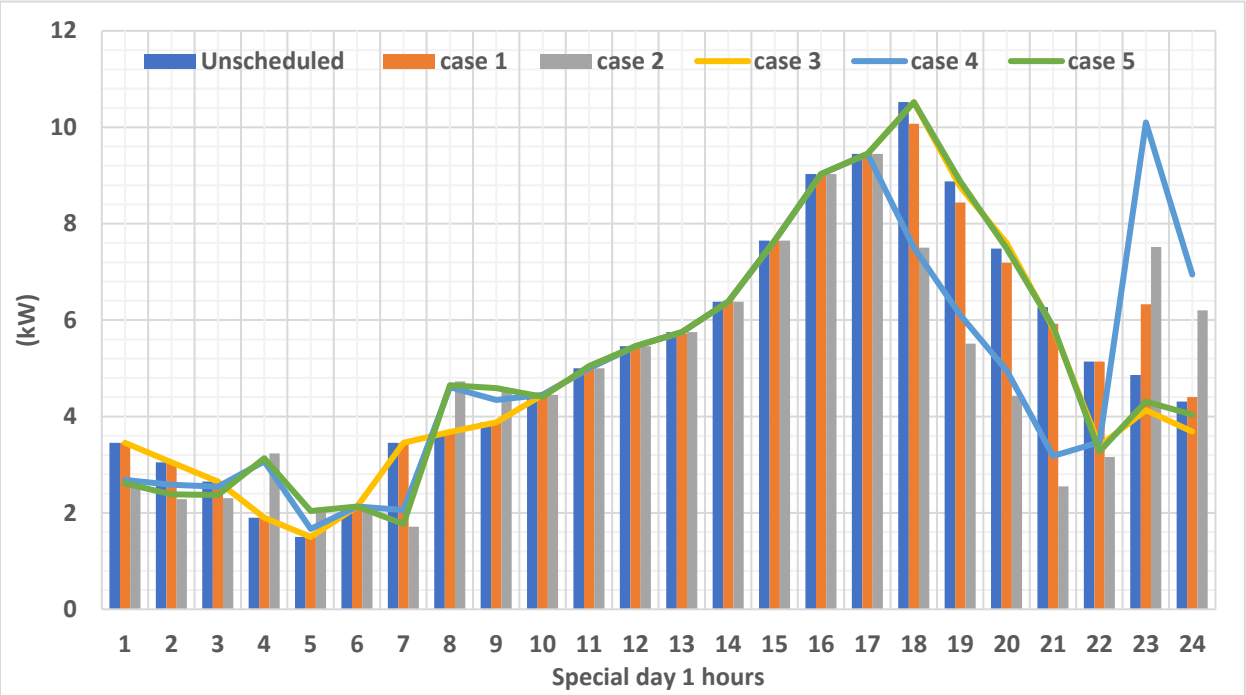

Fig. 60. Load scheduling for different cases for special day 1 using renewable sources and with or without battery energy storage.

Fig. 60 represents the load consumption for considered five scheduling cases for special day 1. The scheduled loads for the proposed five cases are shown in Fig. 60 which indicates that the scheduled loads for case 2 and case 4 are higher as compared to the other cases.

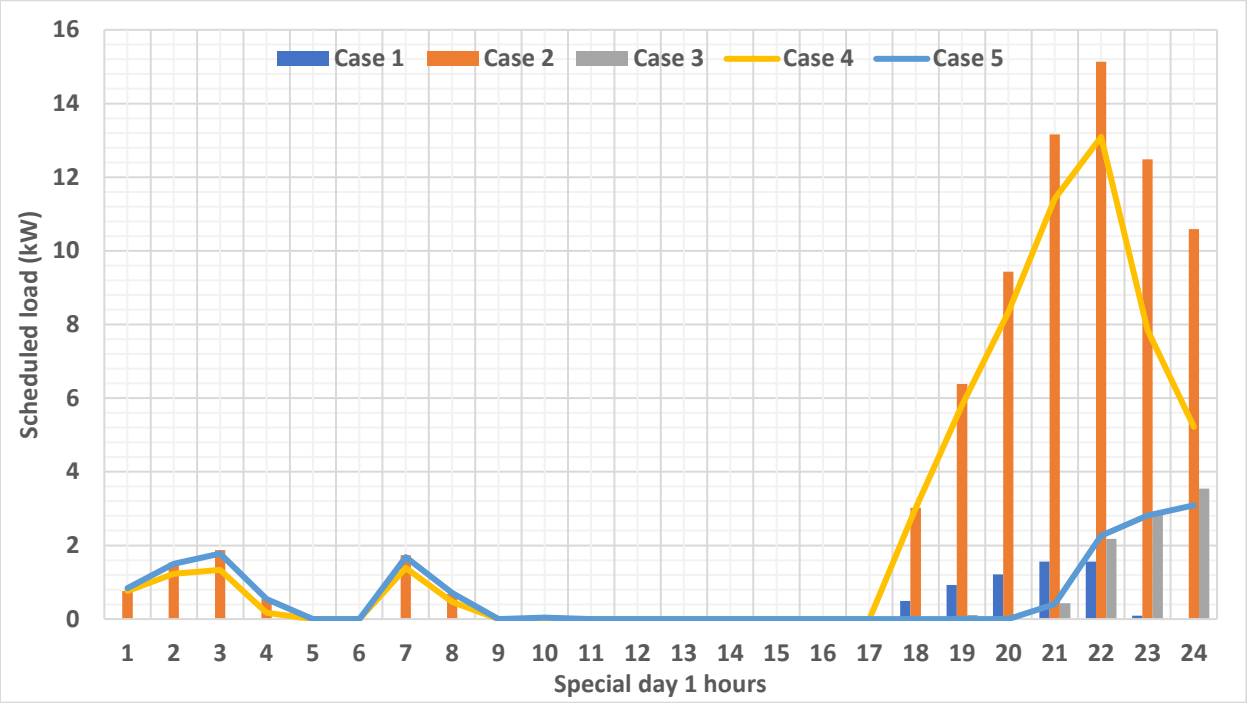

Fig. 61. Scheduled loads for different cases for special day 1 using renewable sources and with or without battery energy storage.

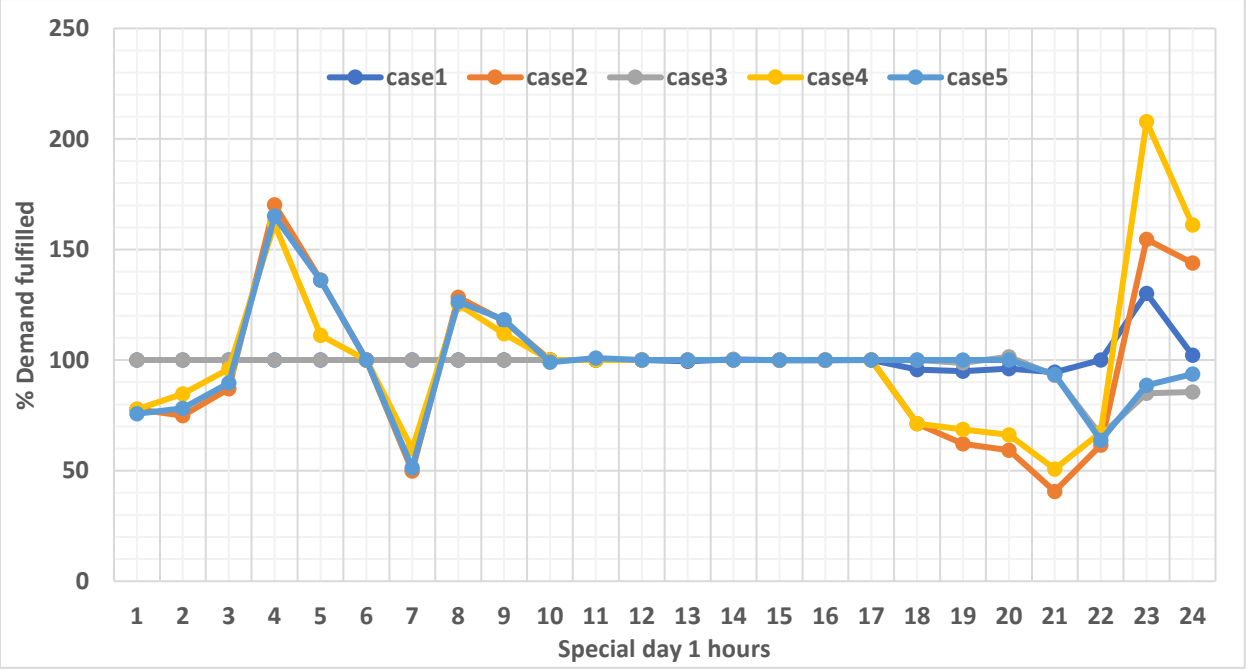

Fig. 62. Percentage of load demand fulfilled for special day 1 using renewable sources and with or without battery energy storage.

Among all proposed scheduling cases, case 3 performs better in meeting load demands most of the time which is evident from Fig. 62. The grid power exchanges for the proposed five cases are shown in Fig. 63. Like other days, grid power required for loads is less for case 3 followed by case 5 as the battery is involved for both cases.

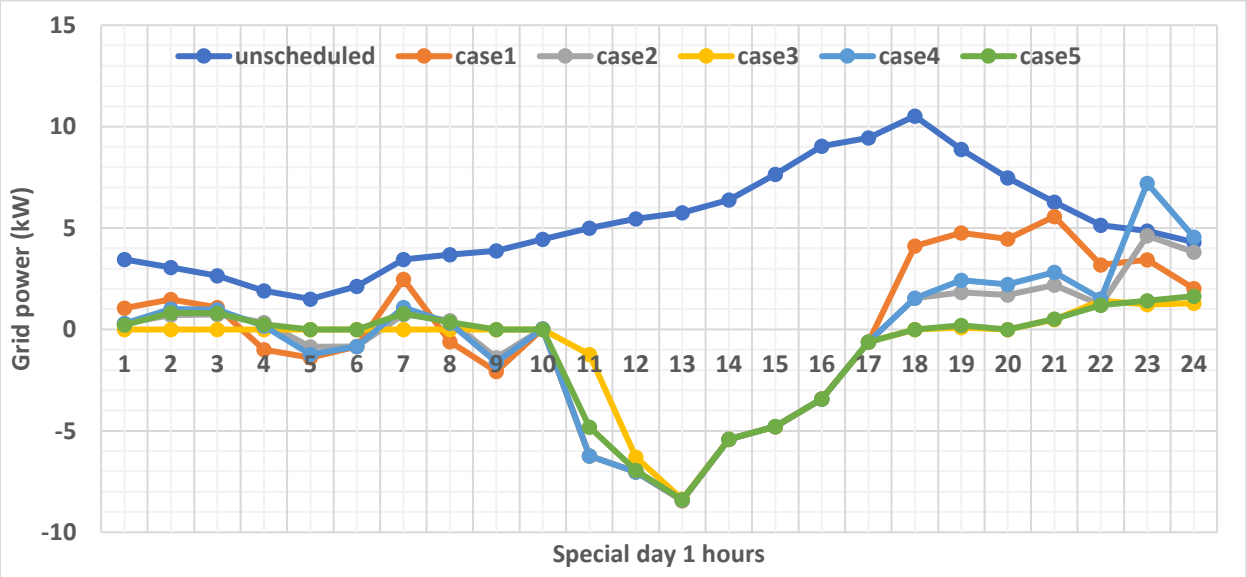

Fig. 63. Grid power required for special day 1 using renewable sources and with or without battery energy storage.

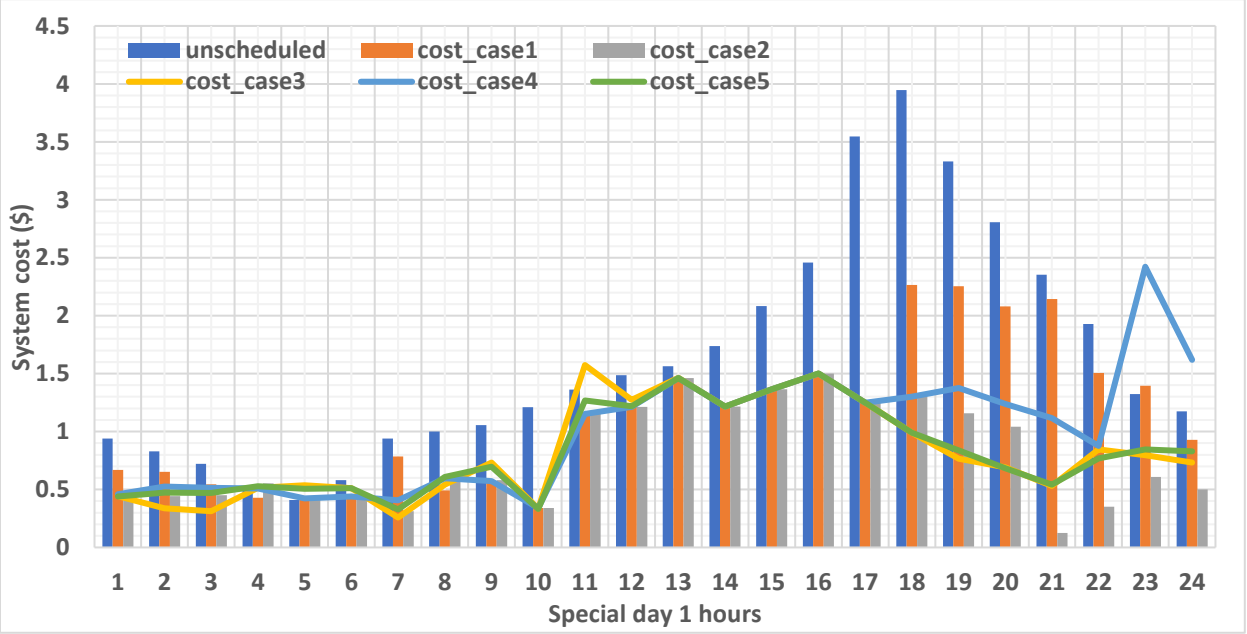

Fig. 64. Cost of system per hour for different cases for special day 1.

The system costs per hour for different scheduling cases are shown in Fig. 64 which demonstrates that the system overall system cost is highest in case 1 among all considered cases.

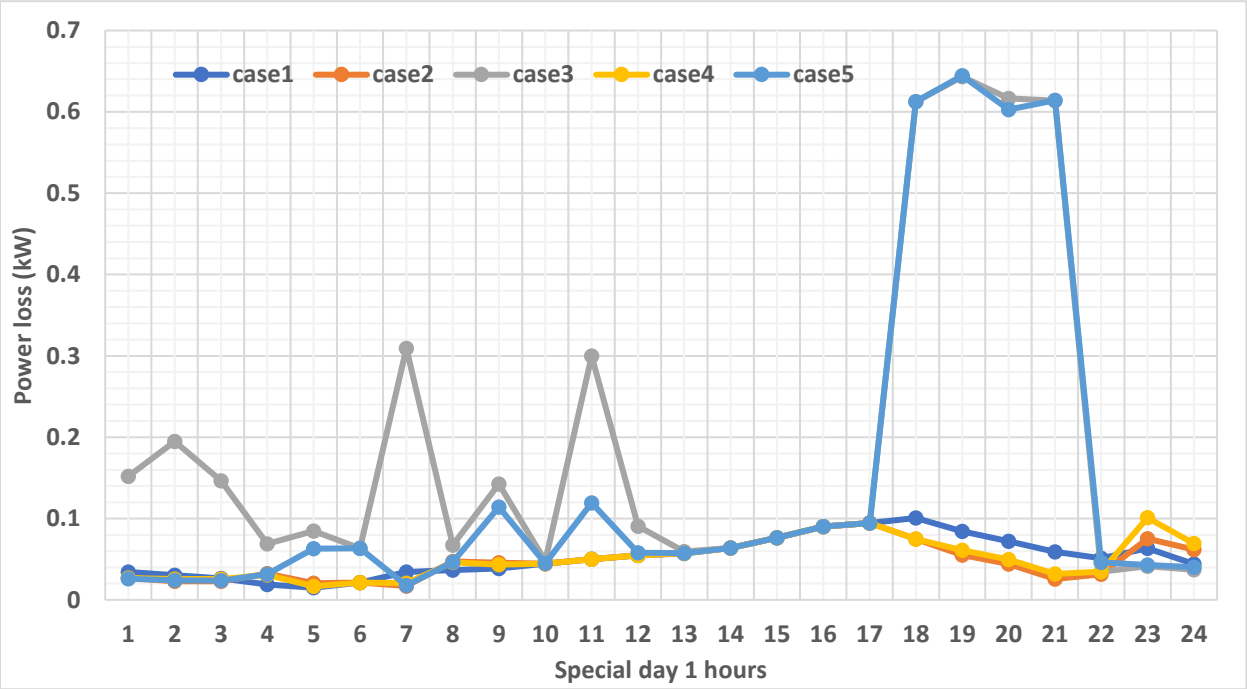

Fig. 65. Power loss per hour for different cases for special day 1.

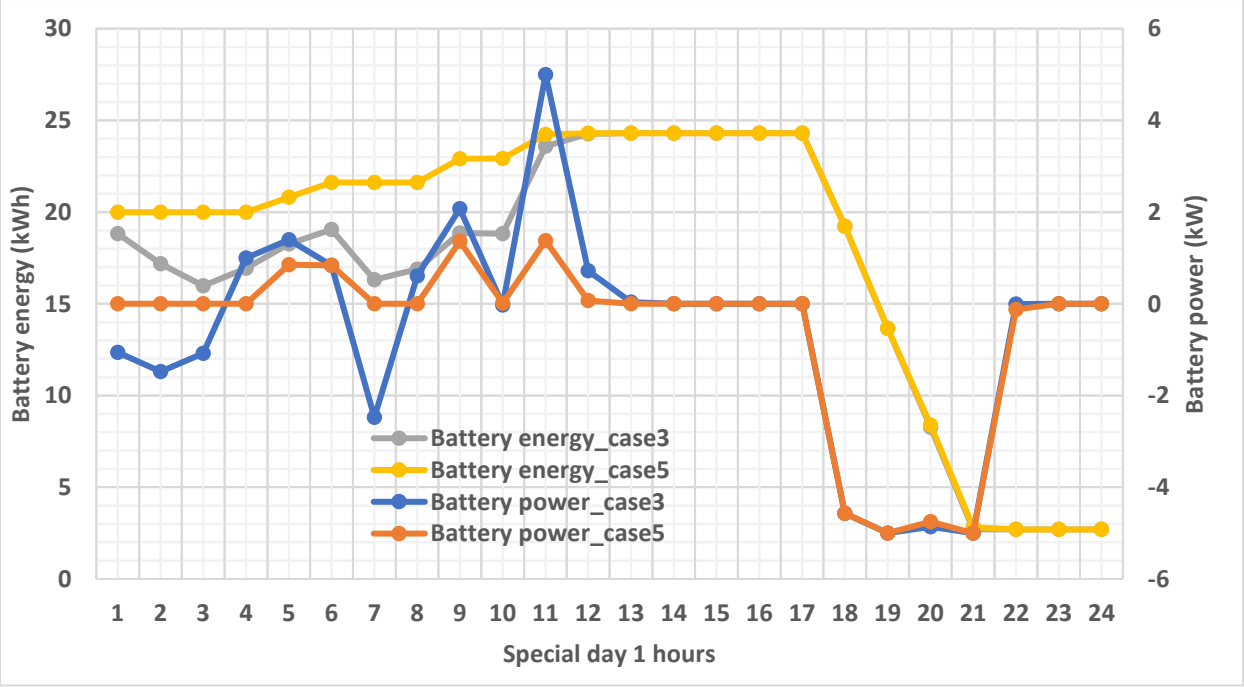

Fig. 66. Battery power and energy for case 3 and case 5 for special day 1.

From Fig. 65, it is evident that the power loss is higher in case 3 and case 5 as the battery is involved in both cases. Moreover, battery operation for case 3 and case 5 are shown in Fig. 66.

Table 16: C_{saving} and $P_{delayed}$ summary for load scheduling for special day 1

Day Type	Performance Index	Cases				
		1	2	3	4	5
Special day 1	C_{saving} ($)	1.4463	9.9979	8.9863	4.6059	8.8372
	$P_{delayed}$ (kW)	0.0	10.5867	3.5388	5.2187	3.0899

Table 16 represents the performance of the proposed five scheduling cases. Except for case 1, all other cases have delayed loads although it has the lowest cost savings. Case 2 has the highest delay with highest cost saving, as it tries to schedule loads based on the available renewable energy. The delayed load problem in case 2 is reduced to a lower value by slight change in the objective function as in case 4. The battery operation in case 3 and case 5 keep the delayed loads' value small and cost saving high.

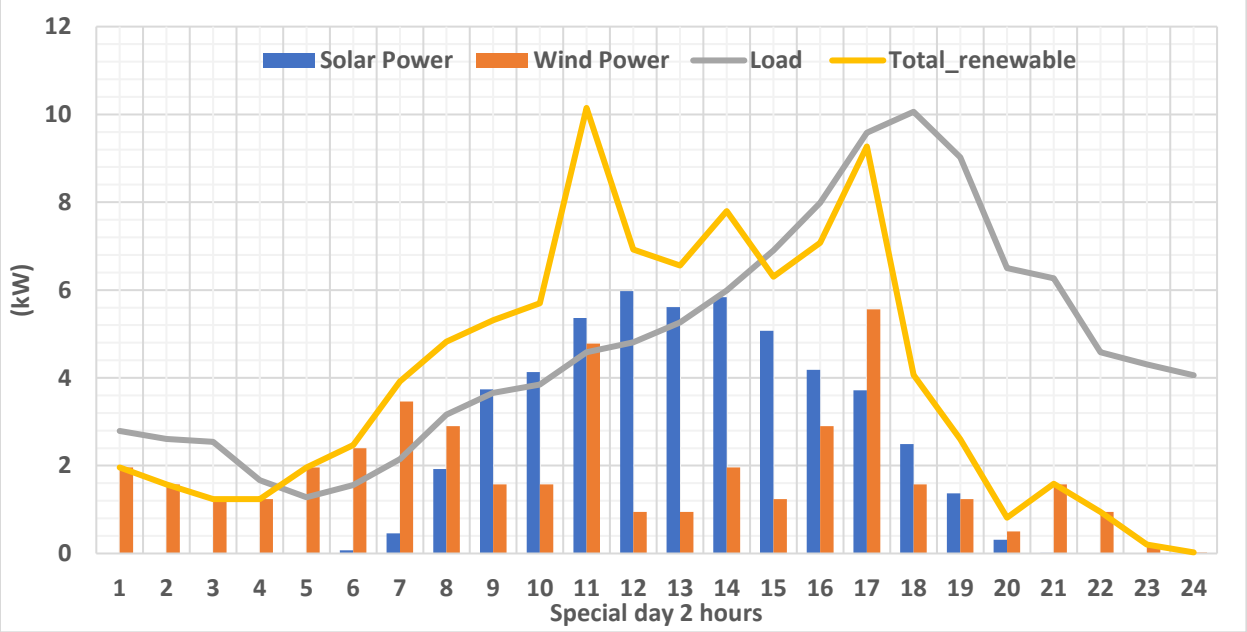

Fig. 67. Renewable source power and load considered for special day 2.

Fig. 67 represents the renewable source power and demand for special day 2 which is assumed to be a weekend day. For scheduling purposes, all the cases that are considered for special day 1 are considered for special day 2 as well.

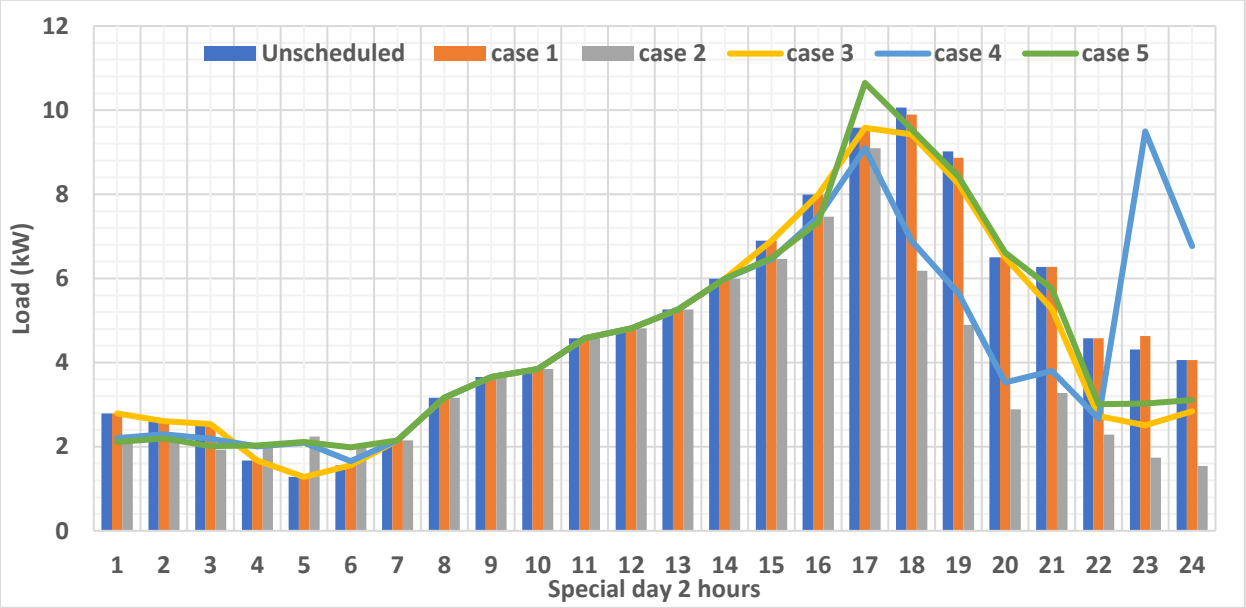

Fig. 68. Load scheduling for different cases for special day 2 using renewable sources and with or without battery energy storage.

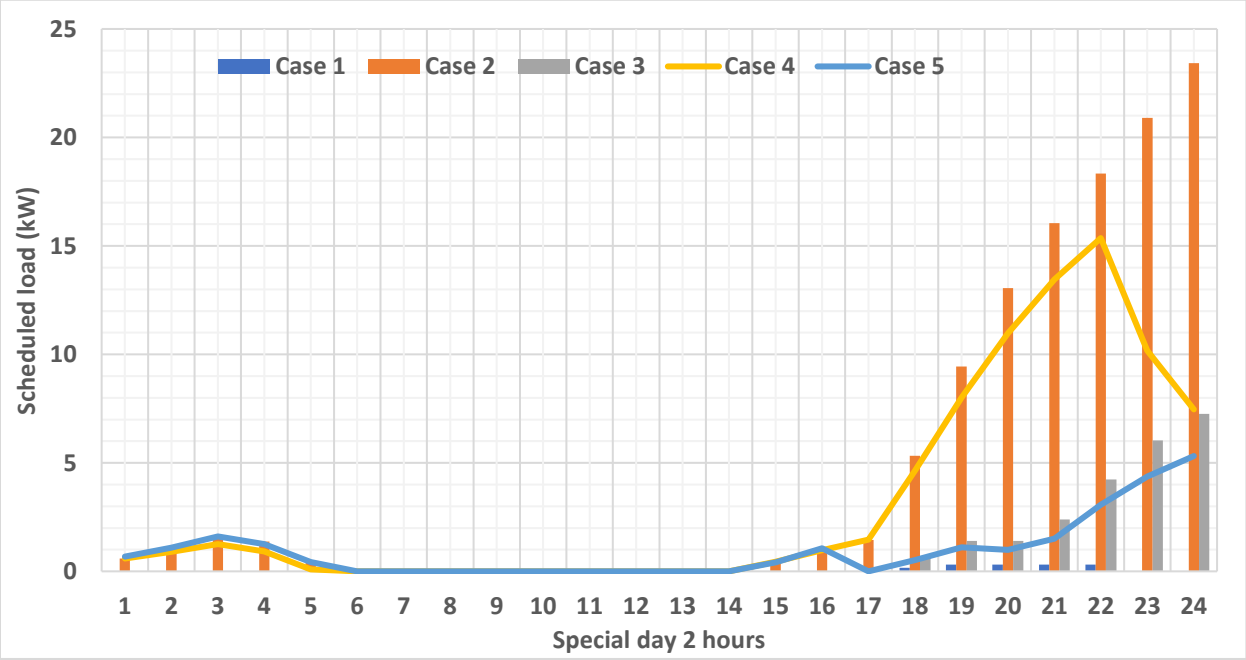

Fig. 69. Scheduled loads for different cases for special day 2 using renewable sources and with or without battery energy storage.

The load consumptions for different cases are shown in Fig. 68. From Fig. 69, it is evident that the scheduled loads are minimum for case 1 followed by 3 and case 5 as compared to the rest of the methods. Case 2 has the maximum scheduled loads among all considered cases.

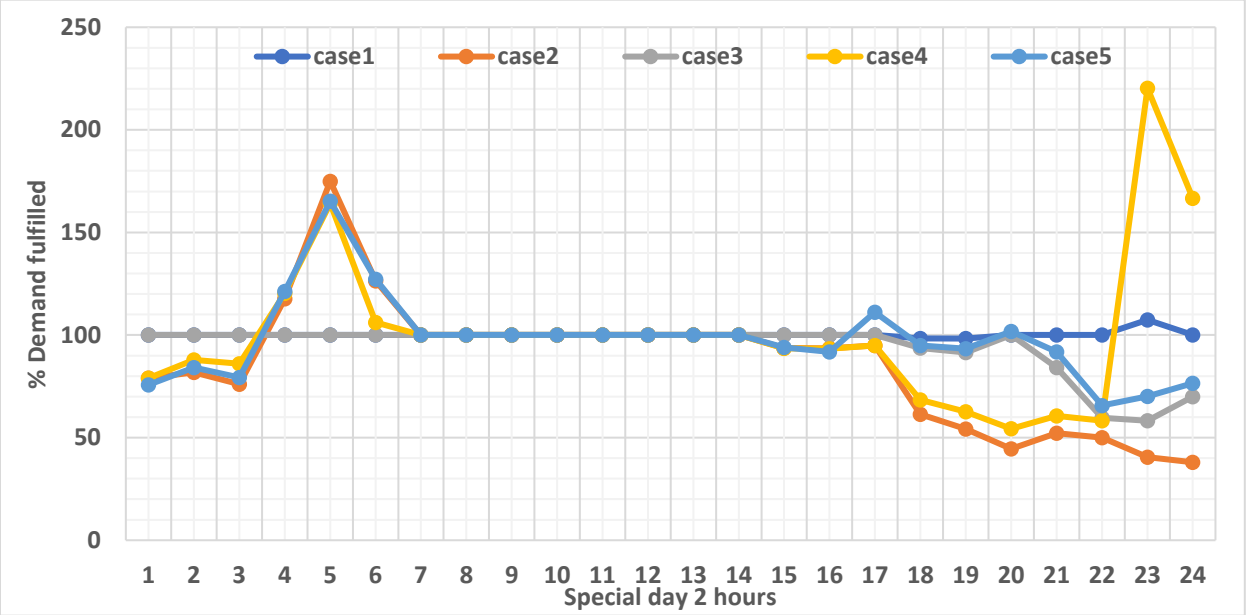

Fig. 70. Percentage of load demand fulfilled for special day 2 using renewable sources and with or without battery energy storage.

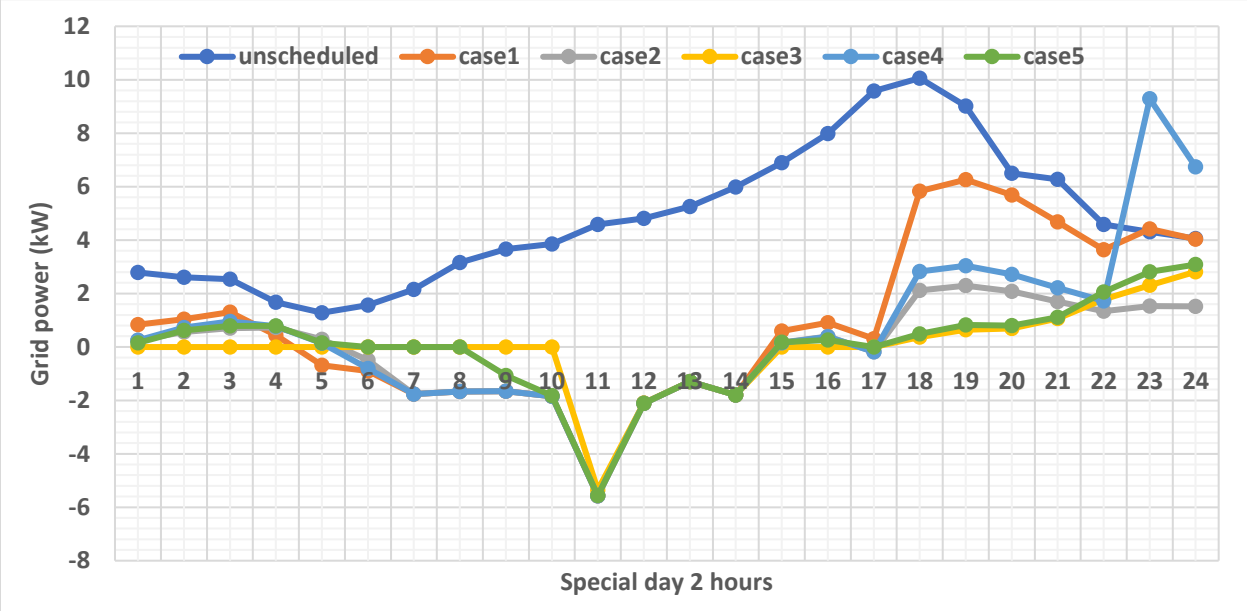

Fig. 71. Grid power required for special day 2 using renewable sources and with or without battery energy storage.

Fig. 70 represents the demand fulfilled per hour by different scheduling cases. Case 1 performs better in fulfilling demands in almost all hours. As for case 2, the percentage of fulfilled demand keeps reducing around the end of the day as renewable energy starts to decrease. From Fig. 71, it is evident that case 3 and case 5 take the least grid power as compared to the other scheduling cases.

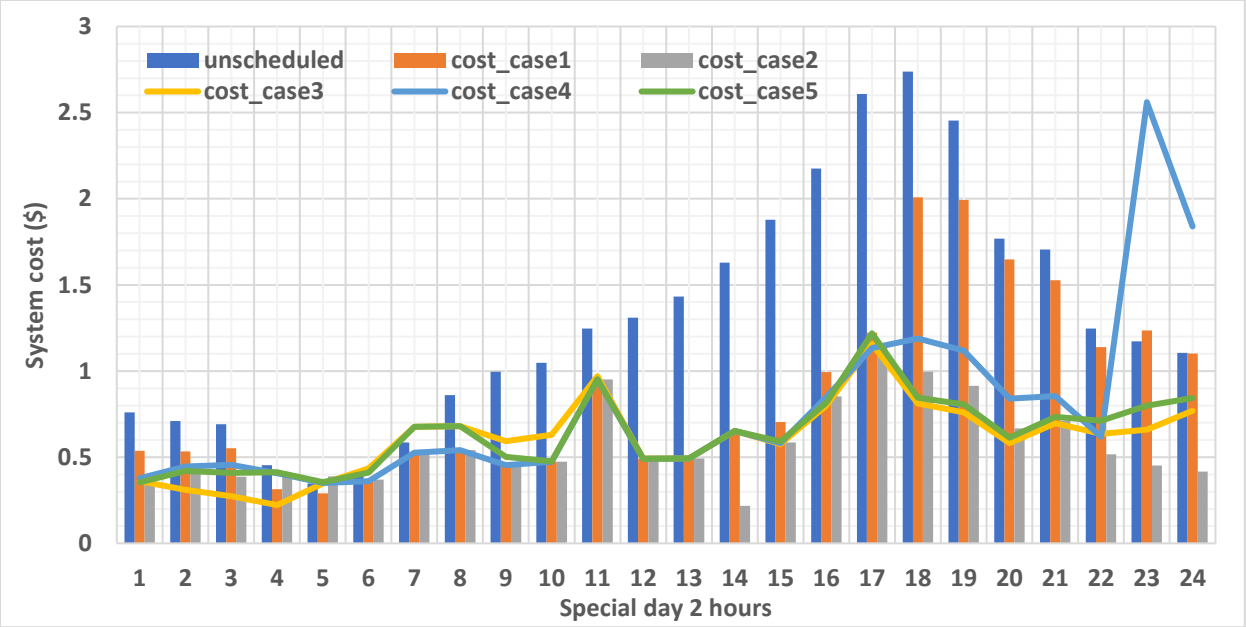

Fig. 72. Cost of system per hour for different cases for special day 2.

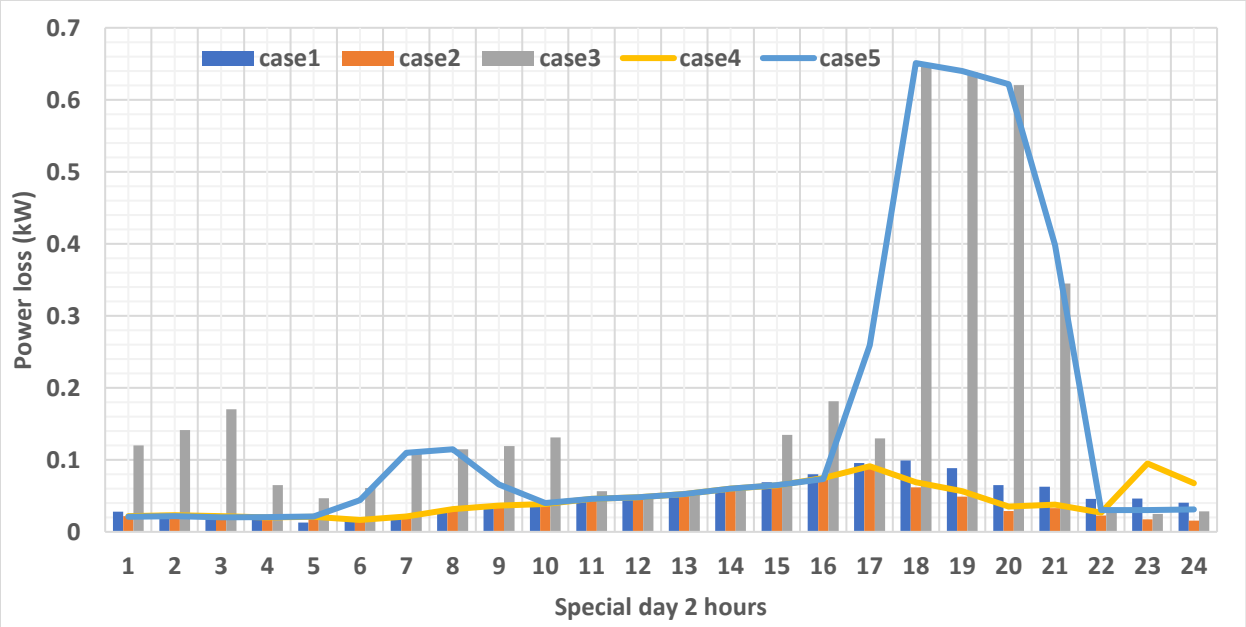

Fig. 73. Power loss per hour for different cases for special day 1.

Fig. 72 indicates that the cost of the system is highest for case 1 as it utilizes grid energy in fulfilling the demands. The system cost in case 2 is the lowest as it tries to utilize only the available renewable power. The power losses for considered different cases are shown in Fig. 73 which indicates that the loss of the system with battery energy storage is higher as compared to other considered cases. The battery operations for case 3 and case 5 are shown in Fig. 74.

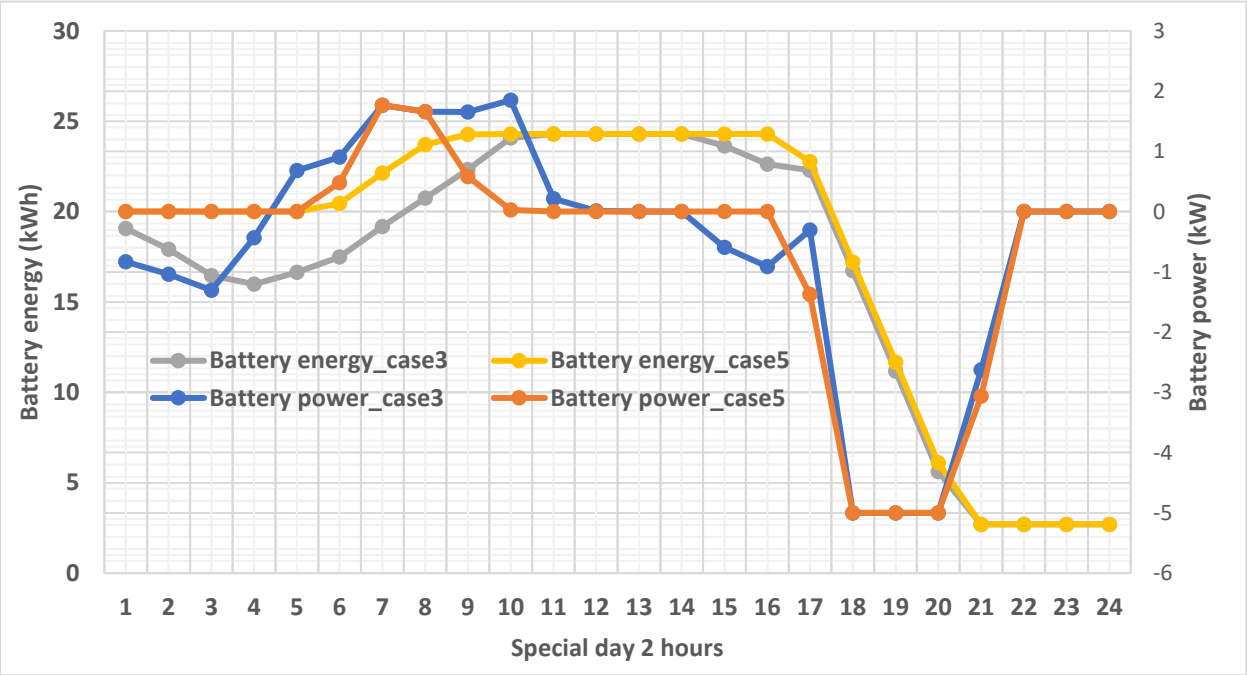

Fig. 74. Battery power and energy for case 3 and case 5 for special day 1.

Table 17: C_{saving} and $P_{delayed}$ summary for load scheduling for special day 2

Day Type	Performance Index	Cases				
		1	2	3	4	5
Special day 2	C_{saving} ($)	7.7576	14.7865	13.9136	9.9343	13.2364
	$P_{delayed}$ (kW)	0.0	23.4232	7.2604	7.4700	5.315

The performance of the considered five cases, in terms of cost saving and load delayed are shown in Table 17. Case 1 utilizes grid power for fulfilling the demand along with renewable energy sources. Therefore, the delayed load in this case is minimum. The cost saving is minimum as well. After case 1, case 3 and case 5 have lower delayed loads as they fulfill the demand with

renewable source and battery energy storage. The cost savings in both cases are higher as compared to case 1. The cost saving in case 2 is the highest with the highest delayed load as well as it fulfills the demand with renewable sources only.

E. Conclusion

In this work, the scheduling of loads in a smart building considered the levelized cost of energy sources and energy storage. Two objective functions are formulated with a view to evaluating their performance under different load demands for different day types and different renewable power availability. Different scheduling strategies are also considered. Based on the analysis, the following conclusion can be made:

- Battery energy storage cannot be a promising option for load scheduling when it is charged by grid power.
- The objective function proposed in (37) is efficient in fulfilling load demand for all considered day types. However, it has the lowest cost saving.
- The objective function proposed in (42) has higher cost saving as compared to the objective function proposed in (37) as it schedules the loads based on the renewable power available.
- The objective function proposed in (42) with the renewable energy sources and the battery energy storage improve the performance as compared to the same objective function with renewable sources without battery energy storage in scheduling loads.

V. SMART LOAD CONTROL

With the technological advancement, loads in smart buildings are becoming smarter and can be controlled, monitored remotely. Previous works have considered the diagnosis and detection of faults in case of the heating, ventilation, and air conditioning (HVAC) system only. But other loads such as water heater, refrigerator, etc., can also have their health issues. It is crucial to have real-time knowledge of the conditions of all the smart loads in residential buildings. Based on this background, this work proposes a new method of real-time health determination and monitoring for all the loads in smart residential buildings. A program has been developed in MATLAB environment that shows the operational and health issues of the loads on the smart television screens or smart mobile phones.

Moreover, this work analyzes the impact of increased residential loads due to the COVID-19 situation on residential transformer losses. The effect of increased consumption and the presence of harmonics in the currents are considered for the hottest winding temperature rise of the transformer, top oil temperature rise, and increased loss of life. Moreover, the operation of the BTM sources such as the PV power, battery energy storage, and electric vehicle during office hours, load scheduling, and scheduling with less utilization of loads having high harmonic distortion are proposed as mitigating solutions to reduce the losses in distribution transformer. The objective here is that the proposed solutions will meet the increased amount of energy consumptions so that loads on distribution transformers decrease and also the percentage loss of life (%LOL) of the residential transformers gets reduced. It is considered that the grid will provide power at houses as usual, however, the proposed solutions will be able to provide the increased amount of energy consumptions during office hours.

For the analysis, six types of energy consumptions data having different types of loads and sources to power the loads, are collected from the smart meters data available in MLGW web accounts of six consumers who live in Memphis city, TN, USA.

A. Real Time Determination and Visualization of Health Conditions of Smart Loads in Residential Buildings

1. List of Considered Smart Loads and Their Health Issues

The smart loads along with their common problems or faults in the smart buildings are discussed in the following subsections:

- *Heating, Ventilation, and Air-conditioning (HVAC) System*

The efficient operation of HVAC system is very crucial for smart buildings, as it consumes most of the energies required for the building. It is also essential for keeping the room temperature within the comfort level of the consumers. Therefore, if the HVAC system is unable to keep the temperature according to the temperature setting, then the thermistor setting should be changed or there might be a problem in the HVAC system. The airflow in the HVAC system should be properly controlled to ensure proper operation. The body temperature of the HVAC unit should be regularly checked. The proper operational data of the coil thermistor, that is used for heating, should always be checked. Moreover, regular maintenance or checking on the filter should be done in order to avoid additional stress on the HVAC system. If the manufacturing warranty period is over, the technician should be consulted.

- *Water Heater*

A water heater provides water with the required temperature for cleaning, washing, bathing and other usages in the buildings. Therefore, keeping the water temperature within the acceptable range is very crucial, as too much hot water can cause scalding hazard or too cold water can cause

uncomfortable feelings to the consumers. Power consumption of the heating element as well as the body temperature of the water heater should be closely monitored. Sometimes sediment in the base causes extra power consumption and unusual noise. The water gathering on the tray of the water heater can be very damaging for the ceiling if it is not monitored regularly. Moreover, after a certain period, regular checking should be done along with the consultancy with the professional if lifetime gets over.

- *Lighting System*

Today's lighting system has become very smart with features such as turning on or off with motion or the outside irradiance variation, the change in the intensity based on the number of occupant or mode selected by the occupant. The excess power consumption based on a specific mode can be harmful, as it may cause fire if the circuit breaker does not function properly. Moreover, proper turning on and off the lights based on outdoor irradiance that is far from home or in a place where the movement of people is rare is crucial and should be monitored.

- *Refrigerator*

Proper functioning of refrigerator is very important for food quality preservation. Therefore, maintaining the inside refrigerator temperature is very crucial. The heart of the refrigerator is a condenser. The condenser may run very frequently because of the dust layer on the condenser, any leak, etc. It may cause excess electricity billing. The temperature of condenser temperature should be regularly checked to avoid any damage to the condenser. The presence of water in the refrigerator may be an indication of refrigerator not cooling properly and should be checked. Moreover, after a certain period, regular checking should be done along with the consultancy with the professional if lifetime gets over.

- *Television*

The usage of television by the inhabitants while staying in the building is expected. Any short circuit of electronic components inside the television may cause issues with resolution, screening, and excess consumption of energy. This also may cause overheating of the television along with the radio interferences produced by electronic, communication devices placed nearby the television. If the manufacturing time is over, the technician should be consulted.

- *Ceiling Fan*

Ceiling fans operate mainly during summertime. The main problem with a ceiling fan is its speeding issue. If for a chosen mode the ceiling fan runs slower, it may have a capacitor or bearing issue. If it suddenly stops after running while the switch is on and taking power from the line, then it may have a stator or capacitor issue. Moreover, if the normal operating temperature exceeds, then it can be harmful to the ceiling fan. Therefore, the temperature should be checked. Moreover, the manufacturing lifetime and regular maintenance time should be monitored carefully.

- *Washing Machines*

Washing machine is a load that is used more frequently. Therefore, proper operation of washing machine is crucial. Both Filling with enough water before washing, and drainage of that water after washing are mandatory. Otherwise, there might be problems in the pressure switch or pump used for drainage. A detector should detect water level for these purposes. Moreover, maintaining temperature while washing in warm or hot mode is essential and should be properly monitored by the thermal sensor. Thermistors that are responsible for heating should be checked. Moreover, if the drum does not rotate while the motor is in motion, there might be a problem in the conveyer belt or bearing. If both drum and motor do not rotate while the motor is taking power from the supply or if it suddenly stops after running for some time, then the problem is in the motor. Motor and drum speeds should be monitored by the speed sensors. Moreover, the manufacturing lifetime and regular maintenance time should be monitored carefully.

- *Dryer*

Dryer is a load that is also used frequently for drying clothes. Therefore, proper operation of dryer is crucial as well. Maintaining temperature while drying for different modes is essential and should be properly monitored by the thermal sensor. The heating element that is responsible for heating should be checked. Filter should be checked regularly to get proper heating for clothes. Moreover, the manufacturing lifetime and regular maintenance time should be monitored carefully.

- *Electric Oven*

The electric oven is operated occasionally in the buildings. However, the inside temperature of the oven should be the same as the temperature setting. If it does not happen, then the temperature setting should be changed. Moreover, if the heating element takes excess power or no power, then that is an indication of a problem with the heating element. If the electric oven stops before the specified time, then there is a problem with the controller. Moreover, regular checking after a certain period should be done along with the consultancy with the professional.

- *Electric Stove*

The electric stove is operated every day in the buildings. However, the temperature of the coil should be the same as the temperature setting for proper cooking. If it does not happen, then there is a problem with the heating coil. Moreover, if the heating element takes excess power or no power, then there is a problem with the heating element. If the electric stove stops before the specified time, there is a problem with the heating element. Moreover, regular checking should be done along with the consultancy with the professional if the lifetime gets over.

- *Dish Washer*

Dishwasher is a load that can be used every day or occasionally. Therefore, proper operation of dishwasher is needed. Both filling with enough water before cleaning and drainage of

that water after cleaning are mandatory. Otherwise, there might be problems in float or pump used for drainage or sensor responsible for it. A detector should detect water level for these purposes. If the dishwasher stops before the specified time, there is a problem with the controller. Moreover, the manufacturing lifetime and regular maintenance time should be monitored carefully.

- *Pool Pump*

A pool pump is also an important load in a smart building. The main function of the pool pump is to circulate water properly to and from the pool. If the flow is not proper, there might be the problem of debris stacked on the plumbing lines or components. If the pump is spinning slower, there might be a voltage issue. If the pump is overheated, then there might be a problem of low or high voltage. If the motor hums or stops after running, there might be a problem with the capacitor or even in the motor. If the pool water temperature is not right, there may be a problem with the temperature sensor, or maybe the heating/cooling pump is not functioning properly.

Based on the above discussion, the important parameters that are pivotal for health condition monitoring of smart loads are summarized in the following Table 18. In this work, all the loads are considered to be smart and electrically powered. Therefore, the parameters, that are mentioned in TABLE 18, are collected through the sensors connected to the loads. Moreover, all the loads can be effectively monitored and controlled by a health monitoring system. The bi-directional information exchanges between the health monitoring system and smart loads are shown in Fig. 75.

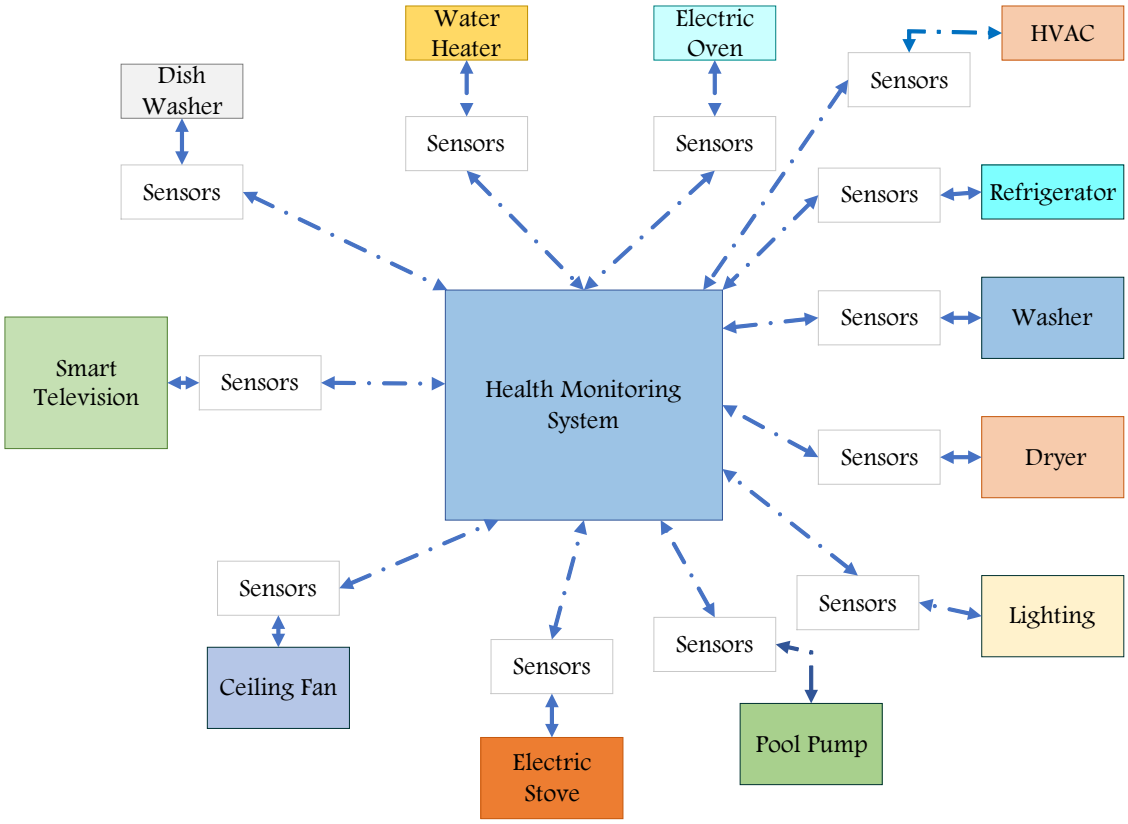

Fig. 75. Smart load connectivity with the health monitoring system.

Table 18: Pivotal Parameters for Smart Loads' Health Monitoring

Smart Loads	Parameters for Health Condition Monitoring
HVAC	Manufacturing lifetime, body temperature, cooling/heating temperature of room and temperature setting, airflow volume, HVAC power consumption, the time elapsed after last maintenance.
Water Heater	Manufacturing lifetime, water in the tray, body temperature, thermostat setting and water temperature, water heater power consumption, the time elapsed after last maintenance.
Lighting	Power consumption, motion sensor signal, outdoor irradiance, lighting intensity.
Refrigerator	Manufacturing lifetime, condenser temperature, inside temperature and temperature setting, condenser running count in a day, power consumption, the time elapsed after last maintenance.
TV	Manufacturing lifetime, body temperature, power consumption, the time elapsed after last maintenance.
Ceiling fan	Manufacturing lifetime, body temperature, speed, power consumption, controller setting, the time elapsed after last maintenance.
Washing Machine	Manufacturing lifetime, speed of drum and motor, water temperature and temperature setting, operational time, the time elapsed after last maintenance, water level detector signal, mode of washing.
Dryer	Manufacturing lifetime, drum and motor speed, heating temperature, power consumption, operational time, the time elapsed after last maintenance, mode of drying.
Electric oven	Manufacturing lifetime, temperature, power consumption, mode of operation, operational time, the time elapsed after last maintenance.
Electric Stove	Manufacturing lifetime, temperature, power consumption, mode of operation, operational time, the time elapsed after last maintenance.
Dish Washer	Manufacturing lifetime, water temperature, water level detector data, power consumption, operational time, the time elapsed after last maintenance.
Pool Pump	Manufacturing lifetime, water flow rate, speed, power consumption, operational time, the time elapsed after last maintenance.

2. *Proposed Methods of Determination of Health Condition of Smart Loads*

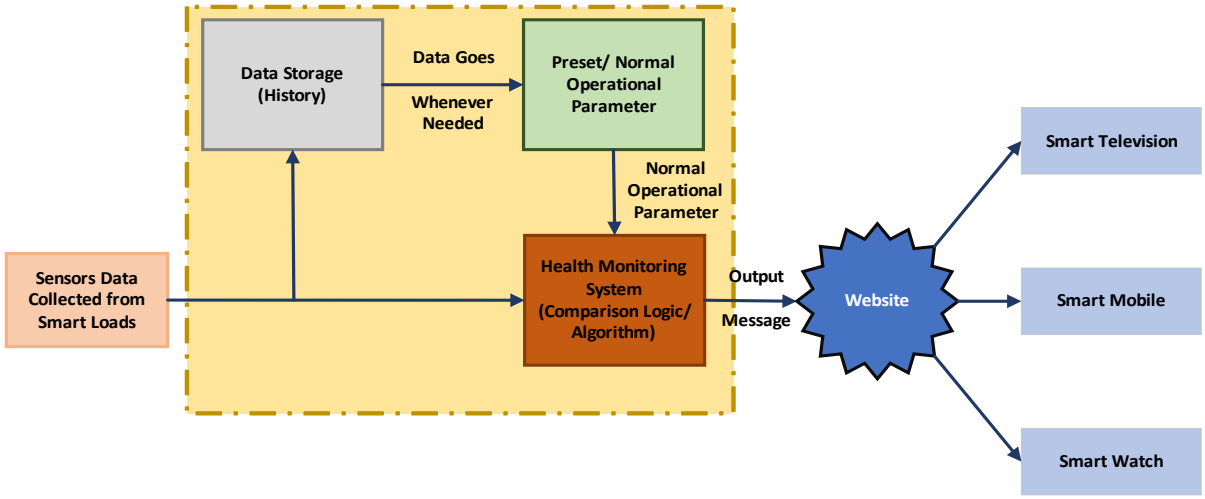

Fig. 76. Block diagram of proposed health monitoring system.

In this work, all the loads are assumed to be smart in nature meaning their operational data can be transmitted to and read by the centralized controller to monitor and control loads. As shown in Fig. 76, real-time data collected from the sensors are sent to the health monitoring system, wherewith the help of the required logic or algorithm, the real data will be compared with the preset data kept at the Preset/Normal Operational Parameter block. The sensor data are continuously stored in the data storage system to keep a record of the history of real-time data. The methods used for monitoring health conditions are discussed in the following subsections.

- *Preset/Normal Operational Parameter System*

As shown in Fig. 76, the preset/operational parameter system, upon asked by the Health Monitoring system, provides the preset parameters of each load to the comparison logic/algorithm system. It is assumed that all the preset data are at their desired and safe levels. When a new house or a building will be built and the proposed health monitoring system will be needed to install there, initially the data, stored at the "Data Storage" block, will be used as the preset data for the "Normal Operational Parameter System' block. Once this block is populated by the required preset

data, no further data will go there. In the future, for any reason if the preset conditions need to be changed, then based on the history of the 'Data Storage' system that will be determined.

- *Health Monitoring System*
- *Health Monitoring of HVAC, Water Heater, and Refrigerator System*

Fig. 77 represents a common flowchart for health monitoring of the HVAC, water heater, and refrigerator systems. The sensor data for the HVAC system includes indoor room temperature, temperature setting data, power consumption, and airflow data. The sensor data for the water heater system includes water temperature, temperature setting data, heating element power consumption, and water level in the tray by water level detector data. For the refrigerator health monitoring, the temperature inside the refrigerator along with refrigerator temperature setting, the temperature of the condenser, power consumption data are received from the sensors.

Moreover, the above systems have maintenance time period counters that count the days that have elapsed after the last maintenance along with the operational time period counter. In addition, the counter counts the number of running cycles of the condenser in a day, door opening in the morning, noon, and evening for the refrigerator system. If the sensor data exceeds the normal operating data obtained from the preset/operational parameter system, there will be an alert message given by the system as that may lead to a fault or other hazards. The counter will pre-alert the user to do maintenance or check the condition after the manufacturing period is over. Therefore, parameters obtained from the sensors and the normal operational parameters obtained from the preset/operational parameter system are summarized in the following Table 19.

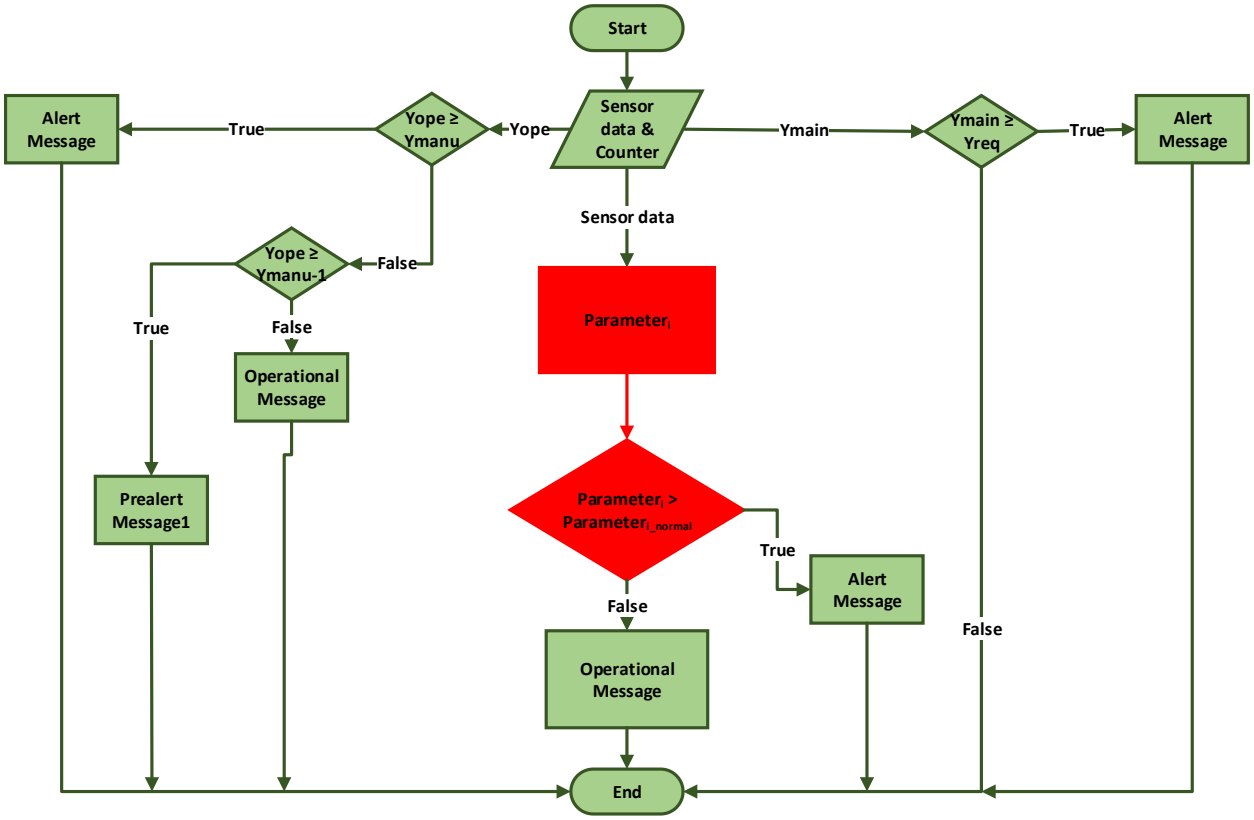

Fig. 77. Common flow chart of HVAC, water heater and refrigerator health monitoring.

Table 19: Parameters of Sensors and Operational Parameter check System

Loads	Parameter$_i$	Parameter$_{i_Normal}$
HVAC	Room temperature, Airflow, Power consumption, body temperature.	Normal airflow, power consumption, body temperature, room temperature setting.
Water Heater	Water temperature, body temperature, water level detector data, power consumption	Water temperature setting, normal body temperature, power consumption, desired water detector signal.
Refrigerator	Inside temperature, condenser temperature, condenser running cycle per day, power consumption	Inside temperature setting, normal condenser temperature, normal running number, power consumption.

- *Health Monitoring of Lighting System*

The sensor data for the lighting system is illuminance that is sent by the illuminance detector. If the illuminance in the room or outdoor illuminance is higher than what is required

based on the presence of people and the light is still on, then an alert message will be sent by the health monitoring system as shown in Fig. 78. Moreover, if the lighting system is taking more power than what is required for the mode selected, then there will be another alert message shown on the system. The preset/operational parameter system will provide the desired illuminance and power consumption data to the health monitoring system based on the outside illuminance, the number of people present in the room and the normal power consumption data based on the mode/ illuminance selected.

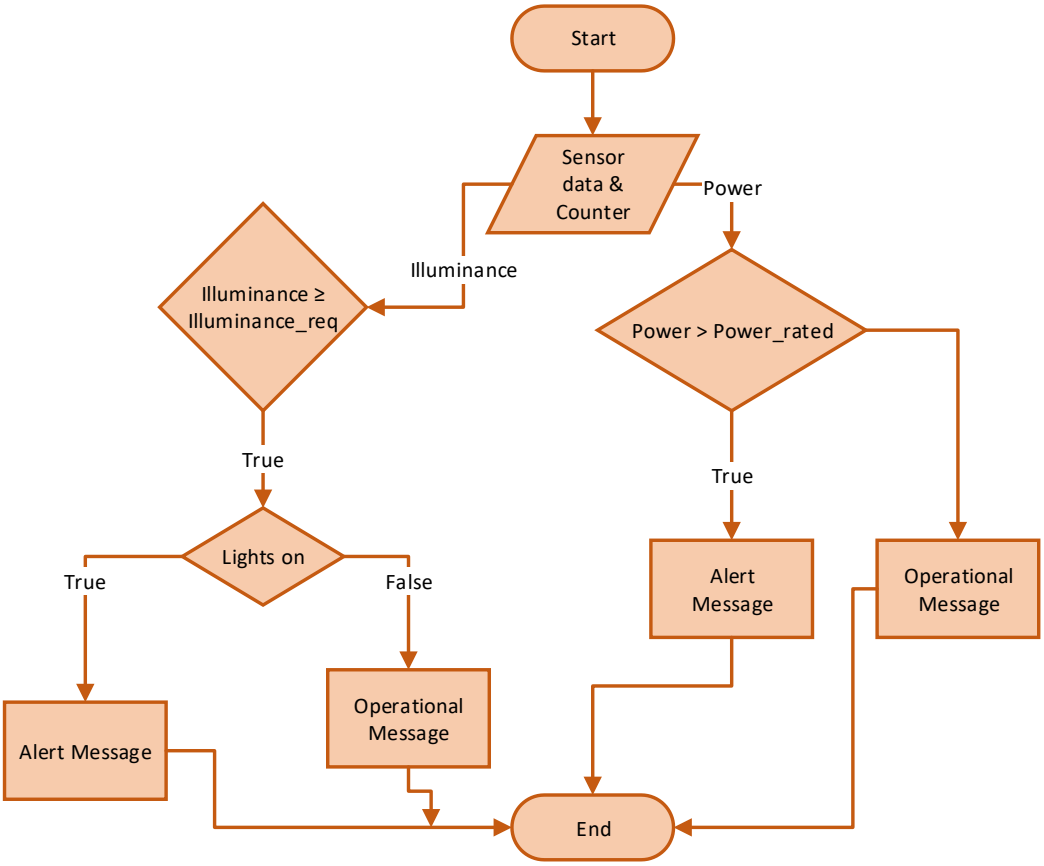

Fig. 78. Flow chart of lighting health monitoring system.

- *Health Monitoring Systems of Television, Ceiling Fan, Washing Machine, Dryer, Electric Oven, Electric Stove, Dish Washer and Pool Pump*

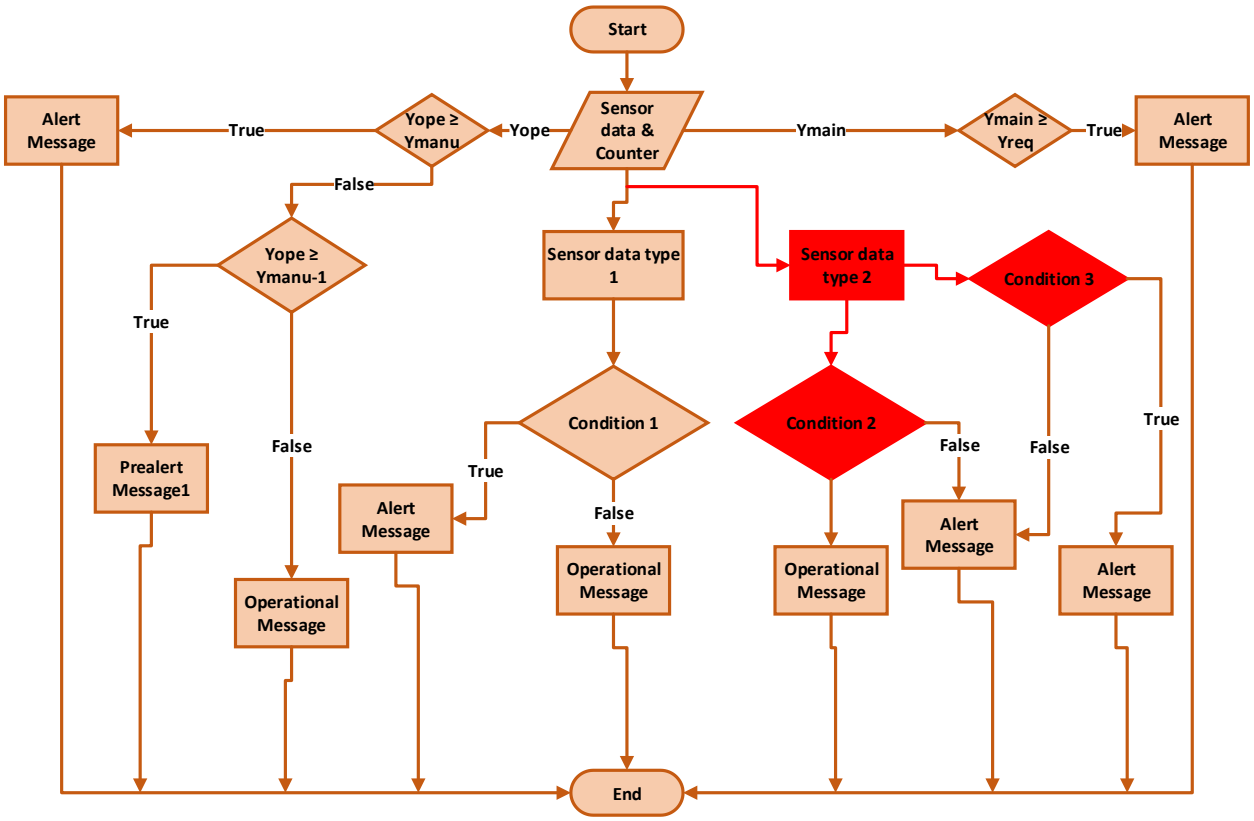

Fig. 79. Common flow chart of television, ceiling fan, washing machine, dryer, electric oven, electric stove, dishwasher and pool pump health monitoring system.

Fig. 79 represents the flowchart of health monitoring systems for the television, ceiling fan, washing machine, dryer, electric oven, electric stove, dishwasher, and pool pump. The functions of the health monitoring system for the television system are to look for overheating conditions and overpower consumption conditions. Therefore, the sensor data includes television body temperature data and energy consumption data. The ceiling fan health monitoring system receives power consumption data, ambient temperature data, rotational speed data as sensors data. The sensor data for the washing machine health monitoring includes water temperature, water level data, power consumption, motor speed, and drum speed data. The dryer health monitoring system receives power consumption data, the dryer inside temperature data, the rotational speed of drum

and motor data as sensors data. The functions of health monitoring system for an electric oven system are to look for required temperature conditions, operating time and overpower consumption conditions. Therefore, the sensor data includes the inside oven temperature data and energy consumption data, operational time data. The electric stove health monitoring system receives power consumption data, temperature (intensity) data, and operational time data. The sensor data for the dishwasher health monitoring system includes water level data, power consumption, and operational time data. The sensor data for the pool pump health monitoring system includes water temperature data, temperature setting, water flow rate data, power consumption, operational time data, and speed data.

For all the loads mentioned above, there will also be counters for counting operational time and maintenance time that represent the time elapsed after the last maintenance. For the television health monitoring system, an alert message will be given if the temperature of the television or the power consumption of the television gets higher than the value obtained from the preset/operational parameter system. Moreover, if the speed of the ceiling fan becomes zero after running for some time while it continues to take power, the health monitoring system will provide the alert message of ceiling fan's condition. Moreover, if the speed of the motor of the dryer becomes zero after running for some time while it continues to take power, the system will provide the alert message for the dryer. In addition, if the motor and drum speed does not match, there will be another alert message for the dryer. In case of electric oven, electric stove, dishwasher, pool pump, if they stop before the time set for them to be on, then there will be another alert message for those systems. All the conditional data (Condition 1, 2, 3) data, as shown in Fig. 79, are provided by the preset/operational parameter system. The sensor data that are used as conditions for the health monitoring system are summarized in Table 20.

Table 20: Parameters of Sensors

Loads	Sensor data type 1 (for condition 1)	Sensor data type 2	
		Condition 2	Condition 3
Television	Body temperature, Power consumption	NA	NA
Ceiling fan	Body temperature	Speed	Power consumption
Washing Machine	Water level detector, Water temperature, On time, Drum speed	Motor speed	Power consumption
Dryer	Heating temperature, On time, Drum speed	Motor speed	Power consumption
Electric oven	Temperature, power consumption	On time	NA
Electric stove	Temperature, power consumption	On time	NA
Dish washer	Water level detector	On time	Power consumption
Pool pump	Water flow rate, water temperature	Pump speed	Power consumption

B. Performance Analysis of Real Time Health Monitoring System

1. Sensors' Data

Fig. 80. Smart residential load simulator for sensor data generation.

For this work, power consumption, temperature, on (operational) time data, obtained from the simulation tool of smart residential tool simulator [137] as shown in Fig. 80, are used as sensors data. The simulator is created by the University of Waterloo, Canada. The other data such as speed data are collected from online resources of appliances manufacturing companies [138] in North America.

2. *Response of the Health Monitoring System by MATLAB*

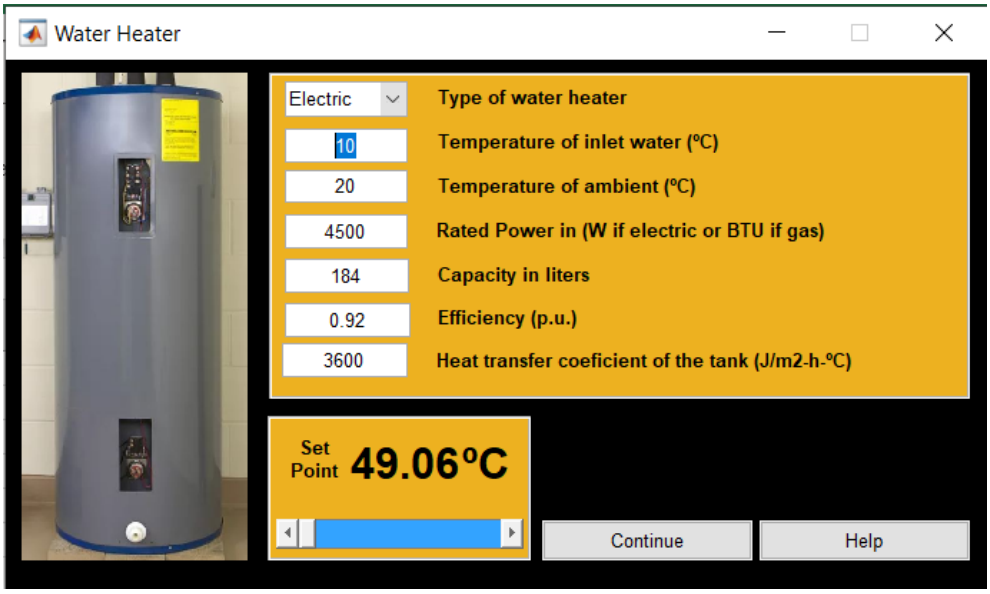

Fig. 81. Water heater considered for health monitoring system.

In this work, as mentioned above, all the data from different sensors of all the loads are collected by the health monitoring system. Also, preset operational parameters are collected from the preset/operational parameter system for health inspection of loads. If the sensor data exceeds the normal operating data, then an alert message will be shown. Otherwise, normal operating conditions will be shown. For example, in the case of the water heater, the water level detector will provide a 10 V signal from the sensor, if it detects water on the water tray. The maximum water heater body temperature can be 76.67 °C (170° F). Water temperature setting is given at 49.06 °C (as 120° F is normally recommended by the Department of energy) as shown in Fig. 81.

The manufacturing lifetime, given by the manufacturer, and maintenance requirement are 8 years and 1 year, respectively.

The rated energy consumption data for the water heater to keep the required water temperature at 49.06 °C would be 0.0472 kWh/Ltr. This information is obtained from the preset/operational parameter system based on the input water temperature (15°C) when the ambient temperature around the water tank is at 20°C. Moreover, based on the ambient temperature data, the expected body maximum temperature data should not exceed 20.3°C which is obtained from the same preset/operational parameter system. In the health monitoring system, now all the sensor data and the counter data are compared with the preset operational data based on the flowchart shown in Fig. 76. For the first instance, consider the data, received by the health monitoring system in the form of a matrix, is [0.1, 20, 49.06, 49.04, 6, 0.5, 0.0471] where the first element of the matrix represents the water level detector data. The rest elements are water heater body temperature data, water temperature setting data, water temperature data, operational life data, last maintenance time duration data, and energy consumption data. Based on the above, the output response of the health monitoring system is shown in Table 21.

Table 21: Water Heater for Normal Operating Condition.

Loads	Health monitoring response example
Water Heater	Water Heater Tray Condition: No water on the Tray. Water Heater Body Temperature: 20° C Water Temperature: 49.04° C Water Heater Operating Life: 6 yr Water Heater Energy Consumption: 0.0471 kWh/Ltr

As shown in Table 21, since all the sensor data fall within the operating data range determined by the preset/operational parameter system and manufacturing data, the system does not provide an alert message. If the sensor data for a given time is represented by the following

matrix [10, 25, 48.89, 50, 6, .5, .0680], then the output looks like the responses as shown in Table 22. Since the water temperature (50 °C) is above the setting (49.06° C, the alert message of water being overheated is given in Table 22. Moreover, because of overheating by the heating element, the power consumption is high (0.0680 kWh/Ltr) than the normal operating condition (0.0472 kWh/Ltr). Therefore, another alert message is given indicating that the power consumption is high.

Table 22: Water Heater for Degraded Operating Condition.

Loads	Health monitoring response example
Water Heater	Water Heater Tray Condition: Alert!!!! Water on the Tray. Water Heater is Overheated. Body Temperature: 25° C Water is Overheated. Water Temperature: 50° C Water Heater Operating Life: 6 yr Alert!!! Energy Consumption High. Water Heater Energy Consumption: 0.0680 kWh/Ltr

Moreover, the health monitoring system responses for all the loads for one instance with some alert messages are represented in the following Table 23.

Table 23: Health Monitoring System Response.

Loads	Health monitoring response example
Water Heater	Water Heater Tray Condition: No water on the Tray. Water Heater Body Temperature: 20° C Water Temperature: 49.04° C Water Heater Operating Life: 6 yr Water Heater Energy Consumption: 0.0471 kWh/Ltr
Refrigerator	Today Refrigerator has started: 40 times Condenser Body temperature: 20° C Refrigerator Energy Consumption: 1.479 kWh Refrigerator Inside Temperature: 5° C Refrigerator Operating Life: 3 yr
Television	Television Body Temperature: 21° C Television Energy Consumption: 0.4 kWh **Alert!!!! Television Manufacturing Lifetime Finished.** **Operational Time: 5.5 yr**
Ceiling Fan	Ceiling Fan Speed: 215 RPM Ceiling Fan Body Temperature: 20.8° C Ceiling Fan Energy Consumption: 0.162 kWh Ceiling Fan Operating Life: 2 yr
Washing Machine	Currently Off. Washing Machine Operating Life: 3 yr
Dryer	Currently Off. Dryer Operating Life: 2.5 yr
Electric Oven	Currently Off. Electric Oven Operating Life: 3 yr
Electric Stove	Electric Stove Coil 1 Intensity: 80 % Electric Stove Energy Consumption: 0.156 kWh Electric Stove Operating Life: 3 yr
Dish Washer	Currently Off.
Lighting System	Lighting Luminance: 1520 lumen Lighting System Energy Consumption: 0.3149 kWh
Pool Pump	Currently Off. Pool Pump Operating Life: 4 yr. **Alert!!! Checking Required. Last Maintenance time: 1.1 yr.**
HVAC	**Alert!!! Airflow is low. Airflow: 8700 BTU** Average Room Temperature: 20° C. Temperature Setting: 20° C. HVAC Body Temperature: 25° C. **Alert!!! Energy Consumption High. Today Energy Consumption: 0.50 kWh.** HVAC Operating Life: 4yr.

3. *Response of the Health Monitoring System shown in the Television or Mobile by Website*

As shown in Fig. 76, the output message determined by the proposed health monitoring system can be visualized or accessed to any smart devices such as a smart television, a smart mobile phone, etc., that has internet connectivity.

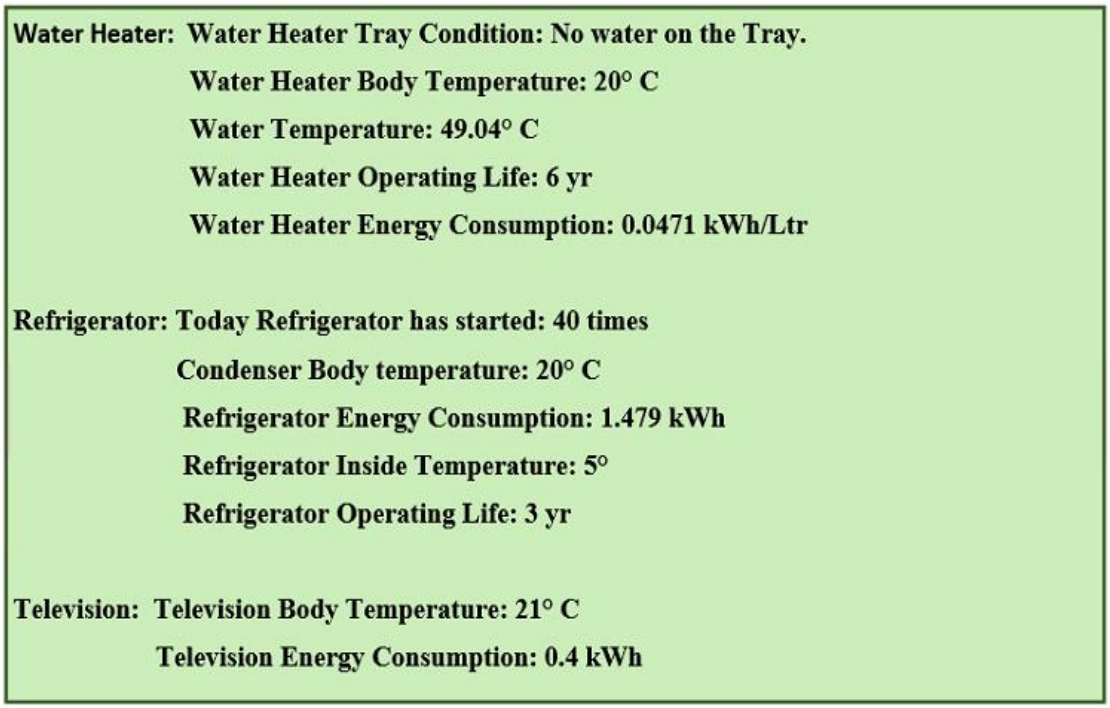

Fig. 82. Display on a smart device.

It is noteworthy that the real-time health monitoring system can be implemented in real practice where sensors from all the loads will update device operating parameters in the cloud through internet of thing (IoT) technology. In the proposed framework, for example, the sensors of the water heater will initially transmit raw data to a cloud server. It should be noted that the sensors should not necessarily have transmission capability over the cloud but each local sensor network should consist of a device that has internet connectivity. From, sensor, analog signals will be converted into digital signals by an analog to digital converter device (analog front end). The

digital signal will be then sent to a microcontroller for buffering and then transmitted to the cloud server through the WIFI module. Since the sensors' data will be continuous and unstructured, therefore, unstructured (No SQL) data storage can be used to store sensors' data. The engine for big data analysis which is known as Spark bigdata analytics will perform periodic analysis on data stored in data storage. The program for operation parameter check and health monitoring system block performance will be available to the consumer end by application programmable interface (API) which are real-time in nature. After that using the API at the consumer end, the health monitoring system information can be observed at any consuming point which can be any Laptop, television., mobile phone or even smartwatch having internet connectivity.

In this work, the output of the MATLAB program is visualized in a demo website which is created by the Visual Studio platform of Microsoft. A demo for the output responses of the water heater, refrigerator, and television is shown in Fig. 82.

C. Analysis of Covid-19 Effect on Residential Loads and Distribution Transformer

This section analyses the effect of pandemic situation on energy consumptions in residential buildings. Moreover, load consumptions data are used to calculate the hottest winding temperature rise, top oil temperature rise and other properties of the distribution transformer. Finally, detailed analysis on how BTM sources and other solutions can reduce the rise in temperature and transformer losses are presented.

1. Effect of COVID-19 on Residential Loads

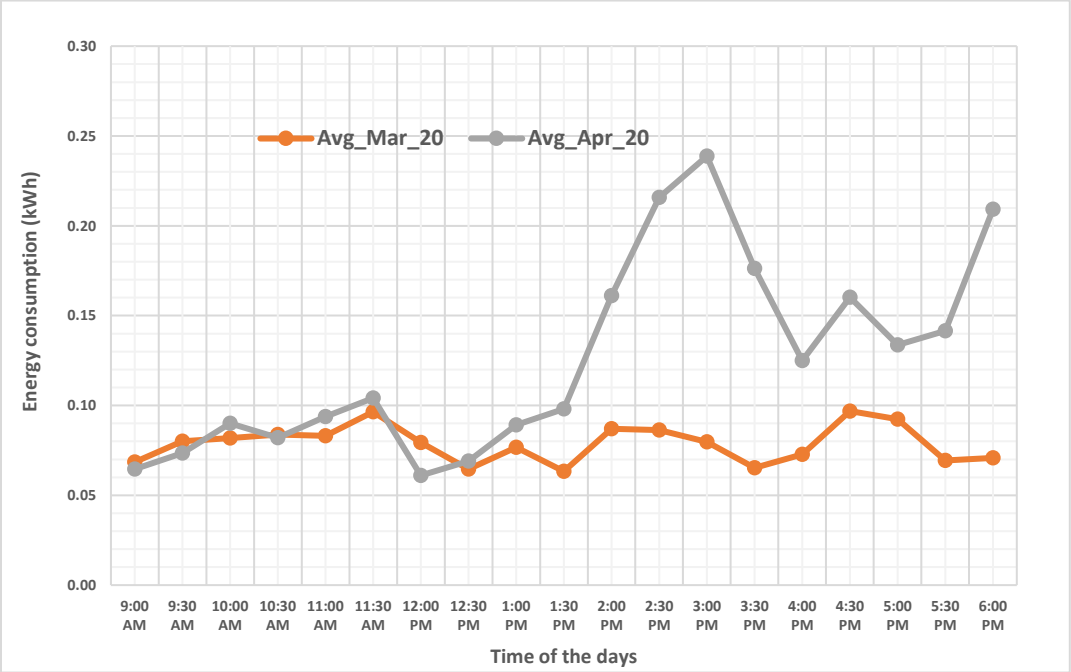

Fig. 83. Energy consumptions in April for consecutive two years of consumer. 1.

Fig. 83 the average load consumptions per half an hour of a house located at Memphis city for the consecutive two months (March and April 2020). The data indicates that a significant amount of load consumption increased during office hours (especially from about noon to 6 pm) due to the lockdown situation in April 2020. In this COVID-19 situation, the load consumption patterns among different classes of people have changed, especially during office hours. In order to demonstrate this situation, six types of consumers have been considered. First, we considered a family (consumer 1) where both husband and wife work and their son studies at a school in Memphis city. The second type of data was collected from a house (consumer 2) where all residents are Ph.D. students who normally work from 10 am to 6 pm in a research lab located at the University of Memphis and during lockdown they stayed at home. The third data was collected from a family having three members (husband, wife and a baby boy). The husband works normally during the office hours and other members stay at home, but during lockdown all stayed at home. The fourth and fifth data were collected from two apartments having three and two PhD students,

respectively, who normally spend their office hours (10 am to 6 pm) in the university labs but during the lockdown situation, they were forced to stay at home. The sixth data was collected from a family having four members (husband, wife and two daughters). The husband works during office hours and the elder daughter goes to school in normal times, but all stayed at home during the lockdown.

The average energy consumptions per half an hour of different months of consecutive two years (2019 and 2020) for consumer 1 are shown in Fig. 84, where the data reflects the fact that the energy consumption of consumer 1 has indeed increased for some parts of the office hours (i.e., for all office hours for April, 9.00 am to 3.30 pm for May, 9.00 am to 12.30 pm and 4.00 pm to 6.00 pm for June, and the entire office hours for July month) as compared to the previous year.

The increase in the energy consumption per half an hour and the percentage of energy consumption increase for March and April 2020, along with the maximum demands (kWh) for both months, have been tabulated in Table 24. The last column of Table 24 represents the percentage of energy consumption increase in April 2020 as compared to that of March 2020. The positive value in the increase column indicates the energy consumption has increased due to the presence of the residents at the house during office hours. Moreover, the current increase data for March and April 2020 have been tabulated in Table 25. The third and fourth columns of Table 25 represent the reactive power in kVar consumption for March and April, respectively, in 2020. The current is calculated from the kWh data shown in Table 24. For example, the energy consumption for half an hour at 9.00 am is 0.069 kWh for March. The supply voltage is considered 120 V for a single-phase system. Now if the kWh value is divided by half an hour and the voltage magnitude, the current magnitude of 1.344 A (assuming 0.85 power factor lagging) can be obtained.

Table 24: Energy Consumption Comparison for Consumer 1

Time	Mar_20 (kWh)	Maximum_ Mar_20 (kWh)	Apr_20 (kWh)	Maximum_ Apr_20 (kWh)	% Increase_ kWh
9:00 AM	0.069	0.150	0.065	0.220	-5.78
9:30 AM	0.080	0.235	0.074	0.145	-8.07
10:00 AM	0.082	0.185	0.090	0.465	9.92
10:30 AM	0.084	0.170	0.082	0.145	-1.99
11:00 AM	0.083	0.170	0.094	0.385	12.78
11:30 AM	0.096	0.670	0.104	0.390	7.99
12:00 PM	0.079	0.275	0.061	0.120	-23.1
12:30 PM	0.065	0.135	0.069	0.330	6.77
1:00 PM	0.077	0.305	0.089	0.350	16.30
1:30 PM	0.063	0.160	0.098	0.305	54.93
2:00 PM	0.087	0.240	0.161	0.600	84.93
2:30 PM	0.086	0.320	0.216	0.695	150.2
3:00 PM	0.080	0.230	0.239	1.035	199.2
3:30 PM	0.065	0.140	0.176	0.725	170.2
4:00 PM	0.073	0.255	0.125	0.575	71.92
4:30 PM	0.097	0.845	0.160	0.950	65.38
5:00 PM	0.092	0.875	0.134	0.625	44.92
5:30 PM	0.069	0.200	0.141	0.460	103.9
6:00 PM	0.071	0.185	0.209	0.610	195.3

Table 25: Current Consumption Comparison for Consumer 1

Time	I_March (A)	I_April (A)	kVar_ March (kVAR)	kVar_ April (kVAR)	% Increase_ Current
9:00 AM	1.344	1.266	0.085	0.080	-5.78
9:30 AM	1.569	1.442	0.099	0.091	-8.07
10:00 AM	1.605	1.765	0.101	0.112	9.92
10:30 AM	1.642	1.609	0.104	0.102	-1.99
11:00 AM	1.630	1.838	0.103	0.116	12.78
11:30 AM	1.891	2.042	0.120	0.129	7.99
12:00 PM	1.556	1.197	0.098	0.076	-23.10
12:30 PM	1.266	1.352	0.080	0.085	6.77
1:00 PM	1.503	1.748	0.095	0.111	16.30
1:30 PM	1.242	1.924	0.079	0.122	54.93
2:00 PM	1.708	3.158	0.108	0.200	84.93
2:30 PM	1.691	4.232	0.107	0.268	150.24
3:00 PM	1.565	4.681	0.099	0.296	199.22
3:30 PM	1.279	3.456	0.081	0.218	170.29
4:00 PM	1.426	2.451	0.090	0.155	71.92
4:30 PM	1.900	3.141	0.120	0.199	65.38
5:00 PM	1.810	2.623	0.114	0.166	44.92
5:30 PM	1.360	2.774	0.086	0.175	103.90
6:00 PM	1.389	4.101	0.088	0.259	195.29

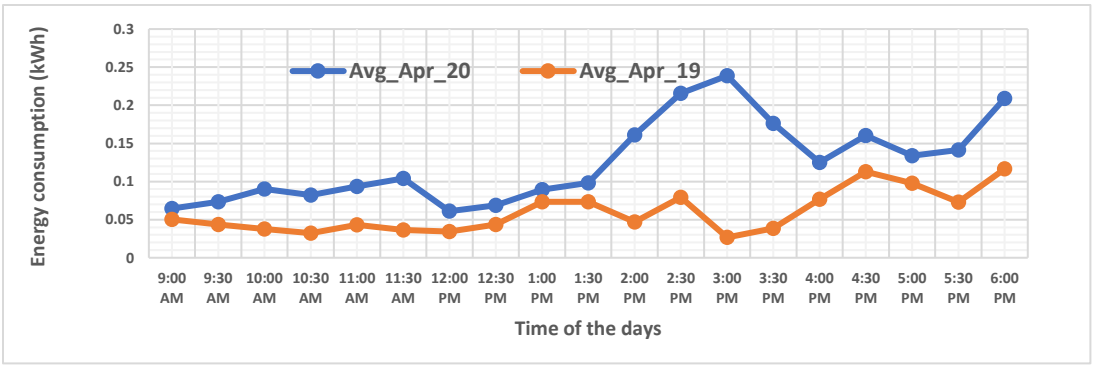

(a)

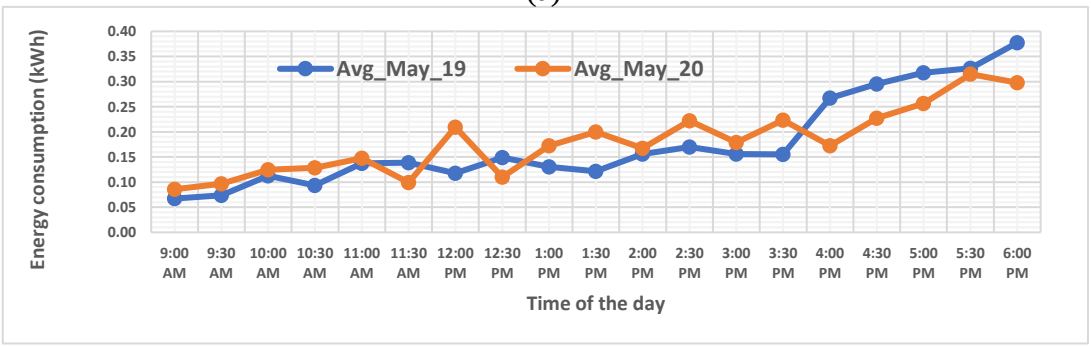

(b)

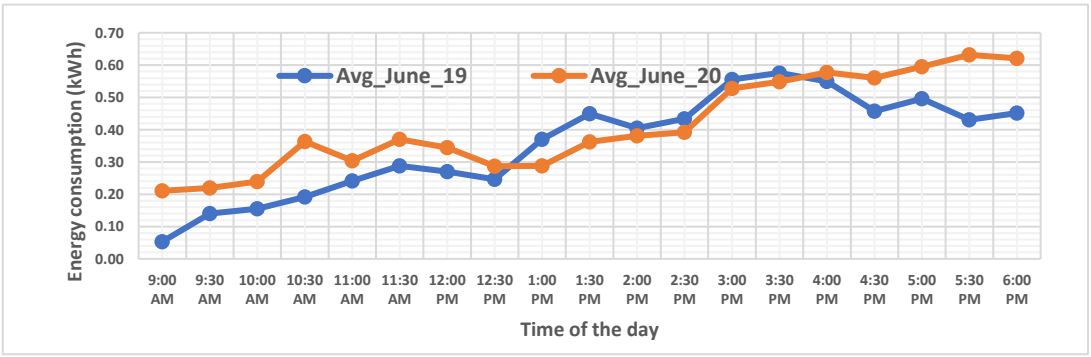

(c)

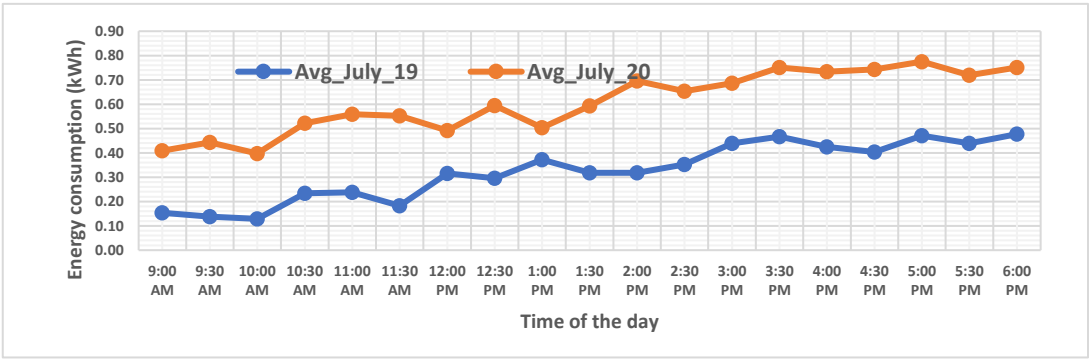

(d)

Fig. 84. Energy consumption of consecutive two years of (a) April (b) May (c) June (d) July months for consumer 1.

For consumer 2, the residents started living in the apartment this year (2020), and therefore no data of the previous year is available. During the COVID-19 situation, their energy consumption has increased from 1.00 pm to 6.00 pm as shown in Fig. 85. Moreover, one of the residents moved to another apartment in the middle of May, therefore, only March and April months are considered for consumer 2. The increase in energy consumption and the percentage of increase in energy consumption have been tabulated in Table 26 for consumer 2 including the maximum demand for both March and April month in 2020. Also, the current consumption comparison is shown in Table 27 along with the reactive power required for both March and April month in 2020. The current is calculated in the same way as already described for consumer 1.

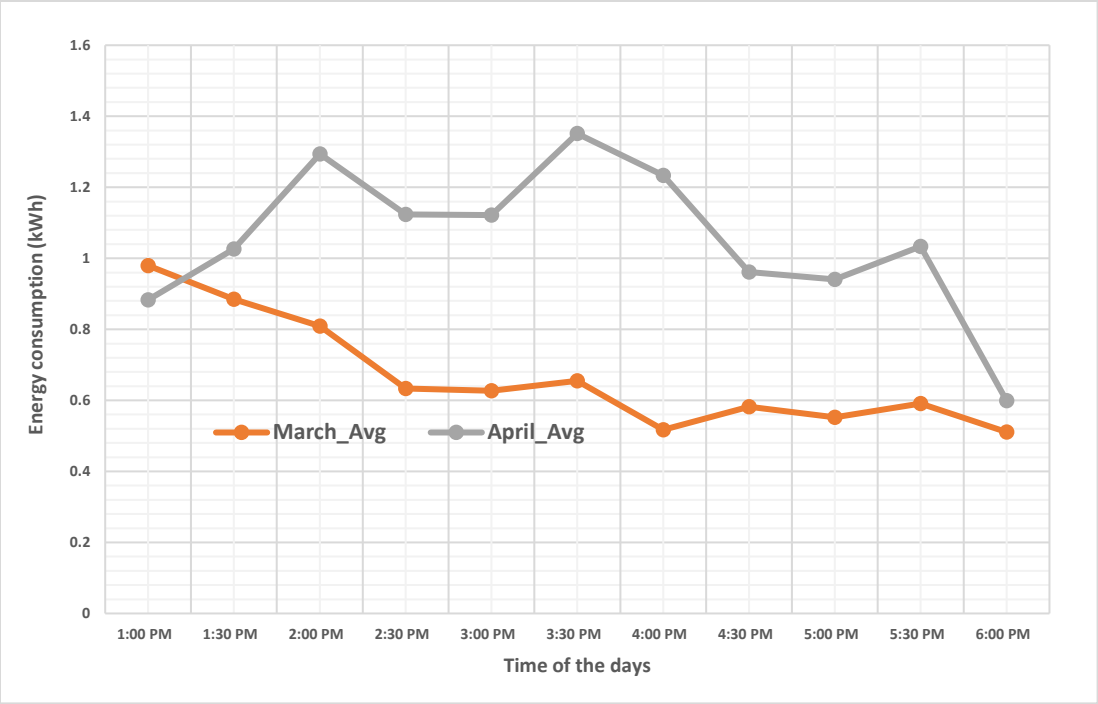

Fig. 85. Energy consumption for consecutive two months in 2020 for consumer 2.

Table 26: Energy consumption comparison for consumer 2

Time	Mar_20 (kWh)	Maximum_ Mar_20 (kWh)	Apr_20 (kWh)	Maximum_ Apr_20 (kWh)	% Increase_ kWh
1:00 PM	0.980	2.920	0.883	2.770	-9.89
1:30 PM	0.885	2.290	1.026	3.480	15.91
2:00 PM	0.809	1.980	1.294	2.365	59.86
2:30 PM	0.634	2.450	1.123	2.440	77.25
3:00 PM	0.628	2.460	1.122	2.960	78.82
3:30 PM	0.655	2.020	1.351	2.625	106.17
4:00 PM	0.517	1.310	1.234	2.510	138.56
4:30 PM	0.582	2.230	0.962	2.690	65.21
5:00 PM	0.553	2.070	0.941	2.025	70.32
5:30 PM	0.591	2.530	1.033	2.170	74.77
6:00 PM	0.511	1.390	0.599	1.540	17.33

Table 27: Current Consumption Comparison for Consumer 2

Time	I_March (A)	I_April (A)	kVar_ March (kVAR)	kVar_ April (kVAR)	% Increase_ Current
1:00 PM	19.208	17.308	1.214	1.094	-9.89
1:30 PM	17.353	20.114	1.097	1.272	15.91
2:00 PM	15.866	25.364	1.003	1.603	59.86
2:30 PM	12.426	22.026	0.786	1.392	77.25
3:00 PM	12.304	22.002	0.778	1.391	78.82
3:30 PM	12.851	26.495	0.812	1.675	106.17
4:00 PM	10.139	24.187	0.641	1.529	138.56
4:30 PM	11.413	18.856	0.721	1.192	65.21
5:00 PM	10.833	18.452	0.685	1.166	70.32
5:30 PM	11.593	20.261	0.733	1.281	74.77
6:00 PM	10.016	11.752	0.633	0.743	17.33

Moreover, the energy consumption pattern of consumer 3 for different months of the consecutive two years are shown in Fig. 86. Fig. 86 indicates that the energy consumption for consumer 3 is higher in 2020 as compared to in 2019 for almost all hours for all months from March to July.

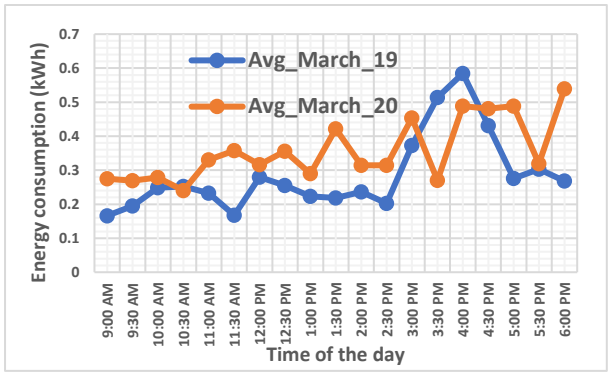

(a)

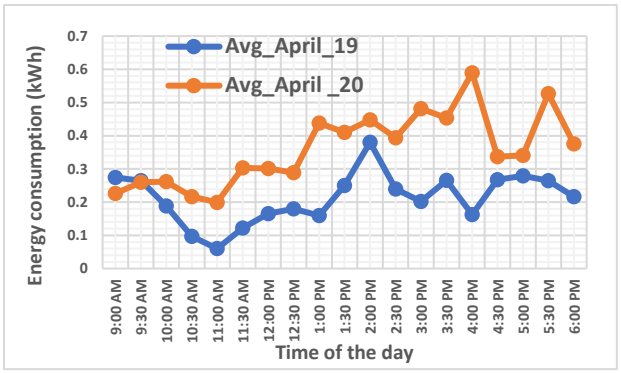

(b)

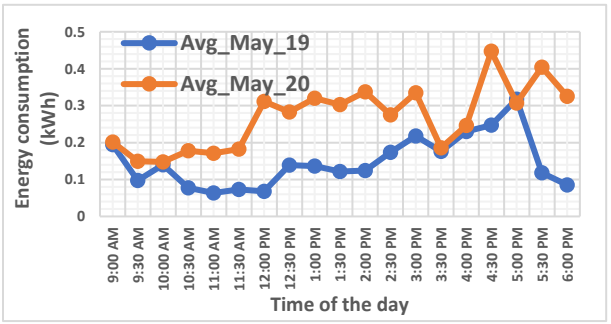

(c)

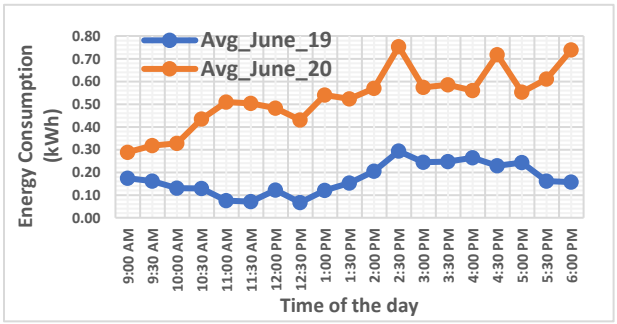

(d)

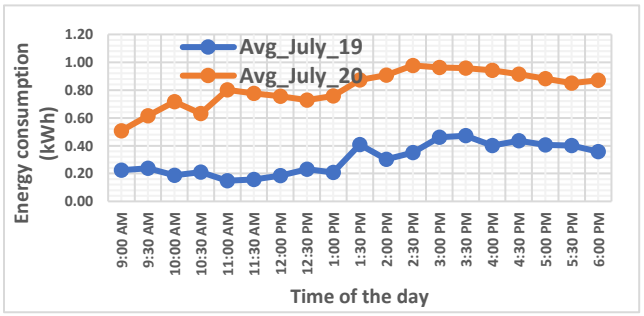

(e)

Fig. 86. Energy consumption of consecutive two years of (a) March (b) April (c) May (d) June (e) July months for consumer 3.

The energy consumption patterns for consumer 4 from March to July months for the consecutive two years are shown in Fig. 87. Like consumer 3, the energy consumption for consumer 4 for all the considered months are higher in 2020 as compared to in 2019.

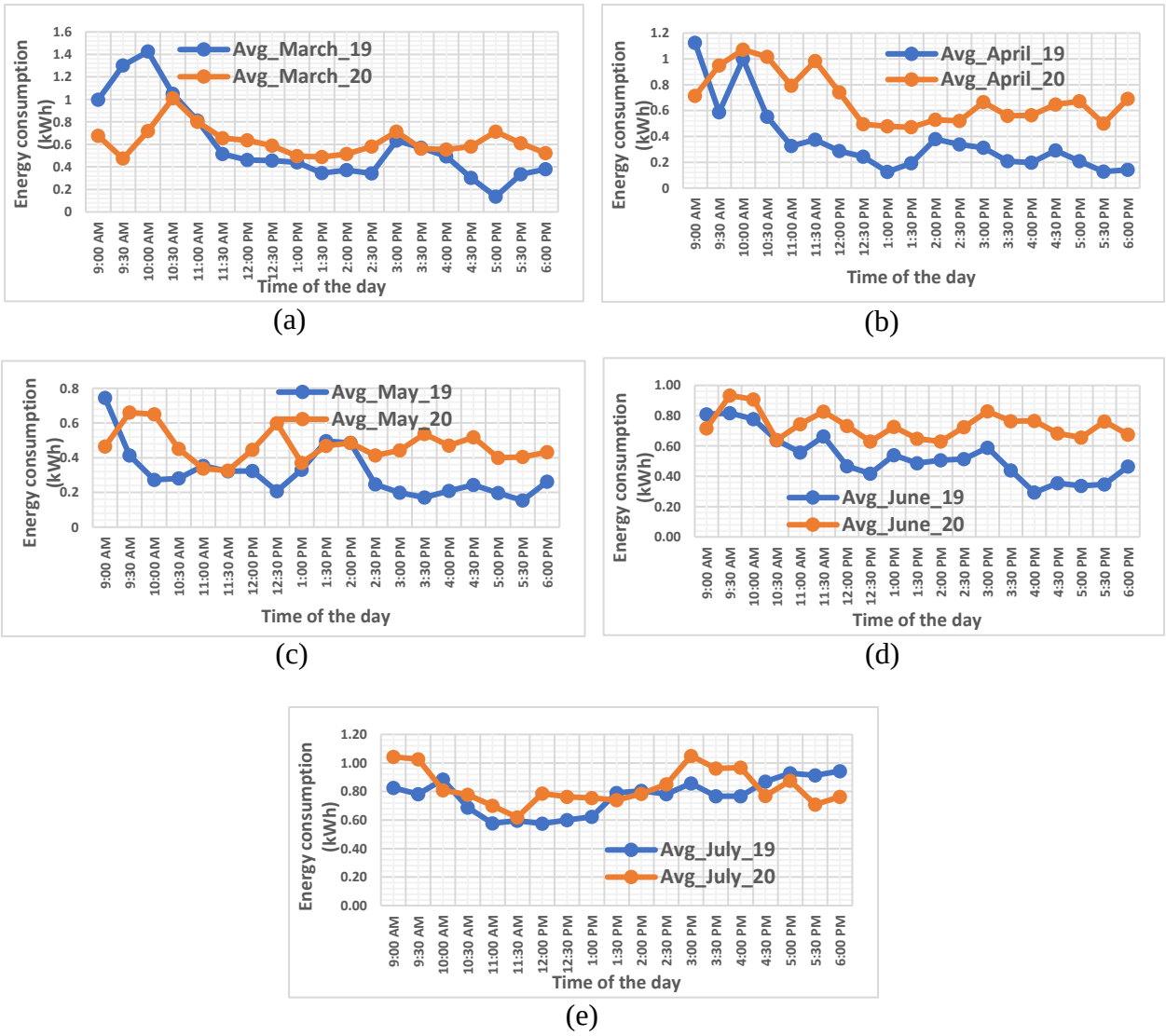

Fig. 87. Energy consumption of consecutive two years of (a) March (b) April (c) May (d) June (e) July months for consumer 4.

For consumer 5, only 2020 energy consumption data are available. Therefore, energy consumptions from March to July in 2020 are shown in Fig. 88. From Fig. 88, it can be said that the energy consumptions in April and May get higher as compared to that of March after 2.00 pm. For June and July, the energy consumptions are always higher as compared to that of March during office hours.

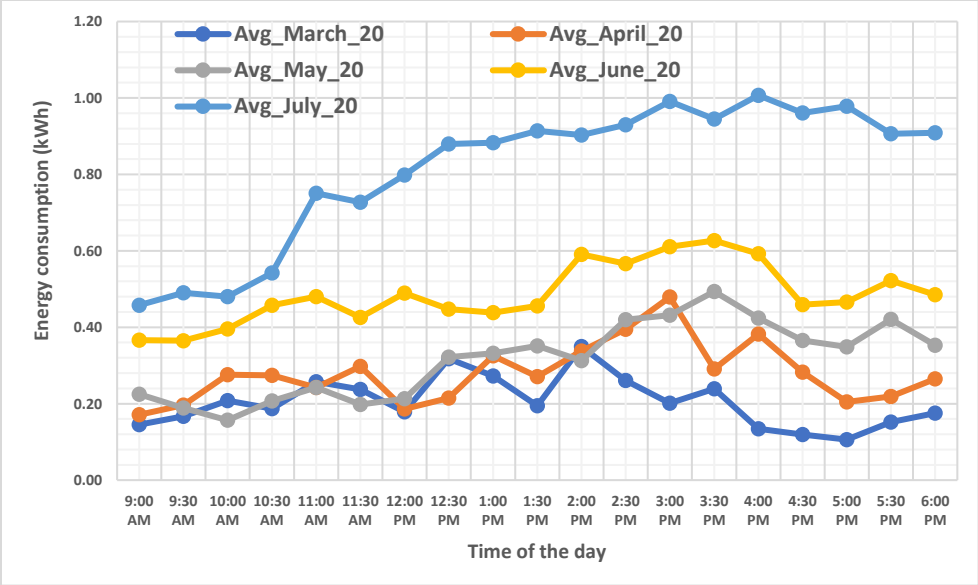

Fig. 88. Energy consumption for consumer 5 in 2020 from March to July months.

The energy consumption comparison for various months of consecutive two years (2019 and 2020) for consumer 6 is shown in Fig. 89. From Fig. 89, it is evident that as father and elder daughter were forced to stay at home, the energy consumptions are higher from 9.00 am to 10.00 am, 12.30 pm to 3.00 pm and 4.00 pm 4.30 pm for April. Similar situations are observed from 12.30 pm to 5.30 pm for the month of June and 12.00 pm to 2.00 pm for the month of July.

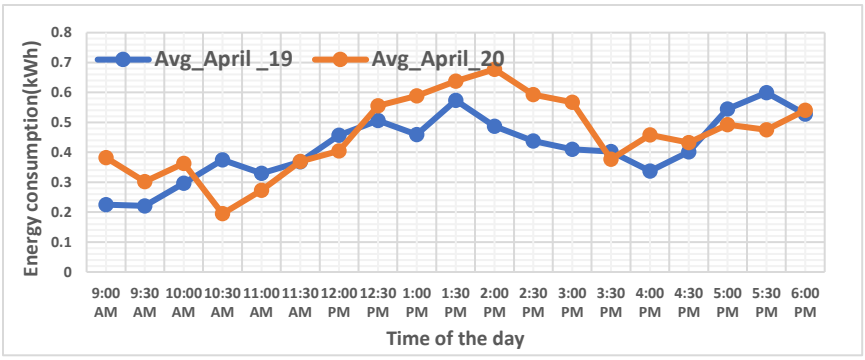

(a)

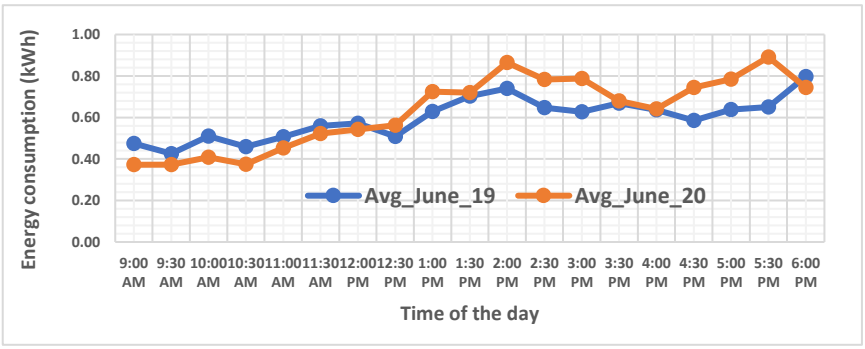

(b)

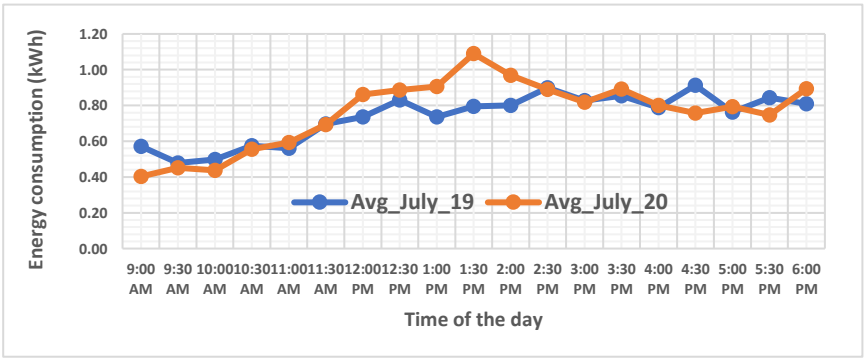

(c)

Fig. 89. Energy consumption of consecutive two years of (a) April (b) June (c) July months for consumer 6.

2. *Formulation of Effect of Residential loads on Local Distribution Transformer without Considering Harmonics*

In this work, two types of conditions are considered. For the first case, no harmonics are considered in the load currents, and for the second case the load currents are considered with different harmonic contents. Based on these two cases, the effect of increased loads on distribution

transformers in terms of hottest spot temperature of the transformer winding, top oil temperature and the percentage loss of life (%LOL) due to insulation aging are analyzed. The total amount of current (per unit) that the transformer needs to provide can be expressed by the following equation:

$$T_{i-pu} = \frac{I_{c,h} \times n \times P}{I_{Trated}} \tag{43}$$

Where, $I_{c,h}$ is the current consumed by one consumer at any given hour h, and n is the number of apartments that are connected to the same residential transformer. P is the factor which defines the likelihood of consumption of other apartments as compared to the currents of the consumer or apartment under consideration. P value of 0.5 represents that the transformer load will be half of the n times higher rather than n times whereas P value 1.5 represents the transformer load to be 1.5n times higher rather than n times to one consumer considered. Moreover, P value of 1 represents that the transformer load will be exactly n times to one consumer considered.

Due to loading, the winding hot-spot temperature (HST) and aging of the transformer need to be calculated. The transformer winding HST, θ_H, can be calculated by using the following equations [139].

$$\theta_H = \theta_A + \Delta\theta_{TO} + \Delta\theta_H \tag{44}$$

where θ_A represents the ambient temperature at any given time. $\Delta\theta_{TO}$ and $\Delta\theta_H$ represent the top oil rise over the ambient temperature and winding hottest spot rise over the top-oil temperature, respectively. The top oil temperature can be represented as:

$$\theta_{TO} = \theta_A + \Delta\theta_{TO} \tag{45}$$

$\Delta\theta_{TO}$ and $\Delta\theta_H$ can be expressed by the following two equations:

$$\Delta\theta_{TO} = \left(\Delta\theta_{TO,U} - \Delta\theta_{TO,I}\right)\left(1 - exp^{-\frac{t}{T_{TO}}}\right) + \Delta\theta_{TO,I} \quad (46)$$

$$\Delta\theta_{H} = \left(\Delta\theta_{H,U} - \Delta\theta_{H,I}\right)\left(1 - exp^{-\frac{t}{T_W}}\right) + \Delta\theta_{H,I} \quad (47)$$

Where, $\Delta\theta_{TO,U}$ and $\Delta\theta_{TO,I}$ represent the ultimate and initial top oil rise, respectively, over ambient temperature, and T_{TO} is the oil time constant. Similarly, $\Delta\theta_{H,U}$ and $\Delta\theta_{H,I}$ represent the ultimate and initial hottest spot rise, respectively, over top oil temperature, and T_W is the winding time constant. Moreover, $\Delta\theta_{TO,U}$ and $\Delta\theta_{H,U}$ can be calculated from the following two equations:

$$\Delta\theta_{TO,U} = \Delta\theta_{TO,R}\left[\frac{K_U^2 R + 1}{R + 1}\right]^n \quad (48)$$

$$\Delta\theta_{H,U} = \Delta\theta_{H,R} K_U^{2m} \quad (49)$$

The aging acceleration factor (F_{AA}) of the thermally upgraded paper can be represented by the following equation:

$$F_{AA} = exp^{\left(\frac{15000}{383} - \frac{15000}{\theta_H + 383}\right)} \quad (50)$$

The equivalent aging factor can be represented as:

$$F_{EQA} = \frac{\sum_{r=1}^{j} F_{AA,r}\Delta t_r}{\sum_{r=1}^{j} \Delta t_r} \quad (51)$$

Where r represents the index number of time interval Δt. The percentage loss of life (%LOL) for operation of t hours can be represented by (52). In this %LOL calculation, the insulation life of transformer is considered to be 180000 hours [140].

$$\%LOL = \frac{F_{EQA} \times t \times 100}{Normal\ insulation\ life} \tag{52}$$

3. Formulation of Effect of Residential loads on Local Distribution Transformer Considering Harmonics

The transformer loss for any load current having harmonics can be defined by the following equation [141]:

$$P_{LL} = \left(\frac{I_L}{I_R}\right)^2 (P_{DC-R} + F_{HL} \times P_{EC-R} + F_{HL-STR} \times P_{OSL-R}) \tag{53}$$

Where, P_{LL}, $P_{DC\text{-}R}$, $P_{EC\text{-}R}$, and $P_{OSL\text{-}R}$ represent load power loss at any load current I_L, rated winding dc loss, rated winding eddy current loss, and other rated stray loss, respectively, and I_R is the rated transformer current. The harmonic loss factor (F_{HL}) and harmonic loss factor for other stray loss ($F_{HL\text{-}STR}$) are defined by the following two equations:

$$F_{HL} = \frac{\sum_{h=1}^{\infty}\left(\frac{I_h}{I_1}\right)^2 h^2}{\sum_{h=1}^{\infty}\left(\frac{I_h}{I_1}\right)^2} = \frac{\sum_{h=1}^{\infty}\left(\frac{I_h}{I_L}\right)^2 h^2}{\sum_{h=1}^{\infty}\left(\frac{I_h}{I_L}\right)^2} \tag{54}$$

$$F_{HL-STR} = \frac{\sum_{h=1}^{\infty}\left(\frac{I_h}{I_1}\right)^2 h^{0.8}}{\sum_{h=1}^{\infty}\left(\frac{I_h}{I_1}\right)^2} = \frac{\sum_{h=1}^{\infty}\left(\frac{I_h}{I_L}\right)^2 h^{0.8}}{\sum_{h=1}^{\infty}\left(\frac{I_h}{I_L}\right)^2} \tag{55}$$

In per-unit, the load power loss can be expressed as the following [141]-[142]:

$$P_{LL}(pu) = \left(I(pu)\right)^2 (1 + F_{HL} \times P_{EC-R}(pu) + F_{HL-STR} \times P_{OSL-R}(pu)) \tag{56}$$

Where, I_R and $P_{DC\text{-}R}$ are taken as the base for current and power loss, respectively. The rated load loss can be expressed by the following equations:

$$P_{LL-R} = (P_{DC-R} + P_{EC-R} + P_{OSL-R}) \quad (57)$$

$$P_{LL-R}(pu) = (1 + P_{EC-R}(pu) + P_{OSL-R}(pu)) \quad (58)$$

$\Delta\theta_{TO,U}$ and $\Delta\theta_{H,U}$ can be calculated by following two equations [141]-[142]:

$$\Delta\theta_{TO,U} = \Delta\theta_{TO,R}\left(\frac{P_{LL} + P_{NL}}{P_{LL-R} + P_{NL}}\right)^{0.8} \quad (59)$$

$$\Delta\theta_{H,U} = \Delta\theta_{H,R}\left(\frac{P_{LL}(pu)}{P_{LL-R}(pu)}\right)^{0.8} \quad (60)$$

The transformer connected to the first consumer, is assumed to have the following loss under rated condition.

Table 28: Transformer loss under rated condition

Transformer Loss	Power (W)
No load loss (P_{NL})	35.71
Rated full load loss (P_{LL-R})	114.29
Rated dc winding loss (P_{DC-R})	97.14
Rated total stray loss (P_{TSL-R})	17.14
Rated winding Eddy current loss (P_{EC-R})	14.57
Rated other stray loss (P_{OSL-R})	2.57
Total loss	150

In order to see the harmonic effect of non-sinusoidal current on distribution transformer, the harmonic loss factor (F_{HL}) and harmonic loss factor for other stray loss (F_{HL-STR}) values are taken from practical transformer data given in [24].

Table 29: Data table for F_{HL} and F_{HL-STR}

F_{HL}	F_{HL-STR}
2.73	1.14
3.11	1.19
6.48	1.38
8.1	1.58

D. Impact Analysis of Covid-19 on Residential Loads, Distribution Transformer

1. Impact of COVID-19 on Residential Energy Consumption

For the consumer 1 house, both electric and gas lines are connected. Therefore, some of the loads are powered by electricity and some are powered by gas. In total, there are 6 apartments for which there is a residential transformer. The transformer's rating is assumed to be 1.5 kVA. Therefore, the rated current of the transformer is 12.5 A. Based on this, the total amount of current (per unit) for different values of P are calculated using (43) for the months of April 2019 and April 2020 and are shown in Table 30 and Table 31, respectively. For this study, the value of P is considered in the range of 0.5 to 1.5.

Table 30: Per Unit Current of Residential Transformer 1 for the Month of April 2019 (Based on Consumer 1)

Time	P											
	.5	.6	.7	.75	.8	.9	1	1.1	1.2	1.3	1.4	1.5
9:00 AM	0.237	0.285	0.332	0.356	0.380	0.427	0.475	0.522	0.569	0.617	0.664	0.712
9:30 AM	0.205	0.246	0.287	0.307	0.328	0.369	0.410	0.451	0.492	0.533	0.574	0.615
10:00 AM	0.178	0.214	0.250	0.268	0.285	0.321	0.357	0.393	0.428	0.464	0.500	0.535
10:30 AM	0.152	0.182	0.213	0.228	0.243	0.274	0.304	0.334	0.365	0.395	0.425	0.456
11:00 AM	0.203	0.244	0.284	0.304	0.325	0.365	0.406	0.446	0.487	0.528	0.568	0.609
11:30 AM	0.171	0.205	0.239	0.256	0.273	0.307	0.341	0.375	0.409	0.444	0.478	0.512
12:00 PM	0.161	0.193	0.225	0.241	0.257	0.289	0.322	0.354	0.386	0.418	0.450	0.482
12:30 PM	0.206	0.247	0.288	0.309	0.329	0.371	0.412	0.453	0.494	0.535	0.576	0.618
1:00 PM	0.346	0.415	0.485	0.519	0.554	0.623	0.692	0.761	0.831	0.900	0.969	1.038
1:30 PM	0.346	0.415	0.485	0.519	0.554	0.623	0.692	0.761	0.831	0.900	0.969	1.038
2:00 PM	0.221	0.265	0.309	0.331	0.353	0.397	0.441	0.485	0.529	0.574	0.618	0.662
2:30 PM	0.374	0.448	0.523	0.560	0.598	0.672	0.747	0.822	0.896	0.971	1.046	1.121
3:00 PM	0.125	0.151	0.176	0.188	0.201	0.226	0.251	0.276	0.301	0.326	0.351	0.376
3:30 PM	0.182	0.219	0.255	0.274	0.292	0.328	0.365	0.401	0.438	0.474	0.511	0.547
4:00 PM	0.362	0.434	0.506	0.543	0.579	0.651	0.724	0.796	0.868	0.941	1.013	1.085
4:30 PM	0.530	0.636	0.743	0.796	0.849	0.955	1.061	1.167	1.273	1.379	1.485	1.591
5:00 PM	0.461	0.553	0.645	0.691	0.737	0.829	0.922	1.014	1.106	1.198	1.290	1.382
5:30 PM	0.343	0.412	0.480	0.515	0.549	0.618	0.686	0.755	0.824	0.892	0.961	1.029
6:00 PM	0.548	0.658	0.767	0.822	0.877	0.986	1.096	1.206	1.315	1.425	1.535	1.644

Table 31: Per Unit Current of Residential Transformer 1 for the Month of April 2020 (Based on Consumer 1)

Time	P											
	.5	.6	.7	.75	.8	.9	1	1.1	1.2	1.3	1.4	1.5
9:00 AM	0.304	0.365	0.425	0.456	0.486	0.547	0.608	0.668	0.729	0.790	0.851	0.912
9:30 AM	0.346	0.415	0.485	0.519	0.554	0.623	0.692	0.761	0.831	0.900	0.969	1.038
10:00 AM	0.424	0.508	0.593	0.635	0.678	0.762	0.847	0.932	1.017	1.101	1.186	1.271
10:30 AM	0.386	0.463	0.541	0.579	0.618	0.695	0.772	0.850	0.927	1.004	1.081	1.158
11:00 AM	0.441	0.529	0.618	0.662	0.706	0.794	0.882	0.970	1.059	1.147	1.235	1.323
11:30 AM	0.490	0.588	0.686	0.735	0.784	0.882	0.980	1.078	1.176	1.274	1.372	1.470
12:00 PM	0.287	0.345	0.402	0.431	0.460	0.517	0.575	0.632	0.689	0.747	0.804	0.862
12:30 PM	0.324	0.389	0.454	0.487	0.519	0.584	0.649	0.714	0.779	0.844	0.909	0.973
1:00 PM	0.420	0.503	0.587	0.629	0.671	0.755	0.839	0.923	1.007	1.091	1.175	1.259
1:30 PM	0.462	0.554	0.646	0.693	0.739	0.831	0.924	1.016	1.108	1.201	1.293	1.385
2:00 PM	0.758	0.910	1.061	1.137	1.213	1.364	1.516	1.667	1.819	1.971	2.122	2.274
2:30 PM	1.016	1.219	1.422	1.524	1.625	1.828	2.031	2.234	2.438	2.641	2.844	3.047
3:00 PM	1.123	1.348	1.573	1.685	1.798	2.022	2.247	2.472	2.696	2.921	3.146	3.370
3:30 PM	0.829	0.995	1.161	1.244	1.327	1.493	1.659	1.825	1.991	2.157	2.322	2.488
4:00 PM	0.588	0.706	0.824	0.882	0.941	1.059	1.176	1.294	1.412	1.529	1.647	1.765
4:30 PM	0.754	0.905	1.055	1.131	1.206	1.357	1.508	1.658	1.809	1.960	2.111	2.262
5:00 PM	0.630	0.755	0.881	0.944	1.007	1.133	1.259	1.385	1.511	1.637	1.763	1.889
5:30 PM	0.666	0.799	0.932	0.999	1.065	1.198	1.332	1.465	1.598	1.731	1.864	1.997
6:00 PM	0.984	1.181	1.378	1.476	1.575	1.772	1.968	2.165	2.362	2.559	2.756	2.953

2. Impact of Residential Energy Consumption Increase on Distribution Transformer

According to IEEE standard C57.91-2011, the top oil temperature and hottest spot temperature should not exceed 120ºC and 200ºC, respectively, to avoid the failure of the transformer [139]. The hottest spot temperature of the transformer for the month of April 2019 and April 2020 for different values of P are shown in Fig. 90 and Fig. 91, respectively. From Fig. 90, it is interesting to notice that the hottest winding temperature for the month of April in 2019 would have exceeded above 200 ºC if the P value became 1.2 or higher. However, the hottest spot temperature for the month of April 2020 as shown in Fig. 91 exceeds 200ºC as the P value increases from 0.6 to upwards, which indicates the COVID-19 effect on the rise of the hottest winding temperature. If this lockdown situation continues, with the increase in ambient temperature in summer, the hottest spot temperature may get even higher.

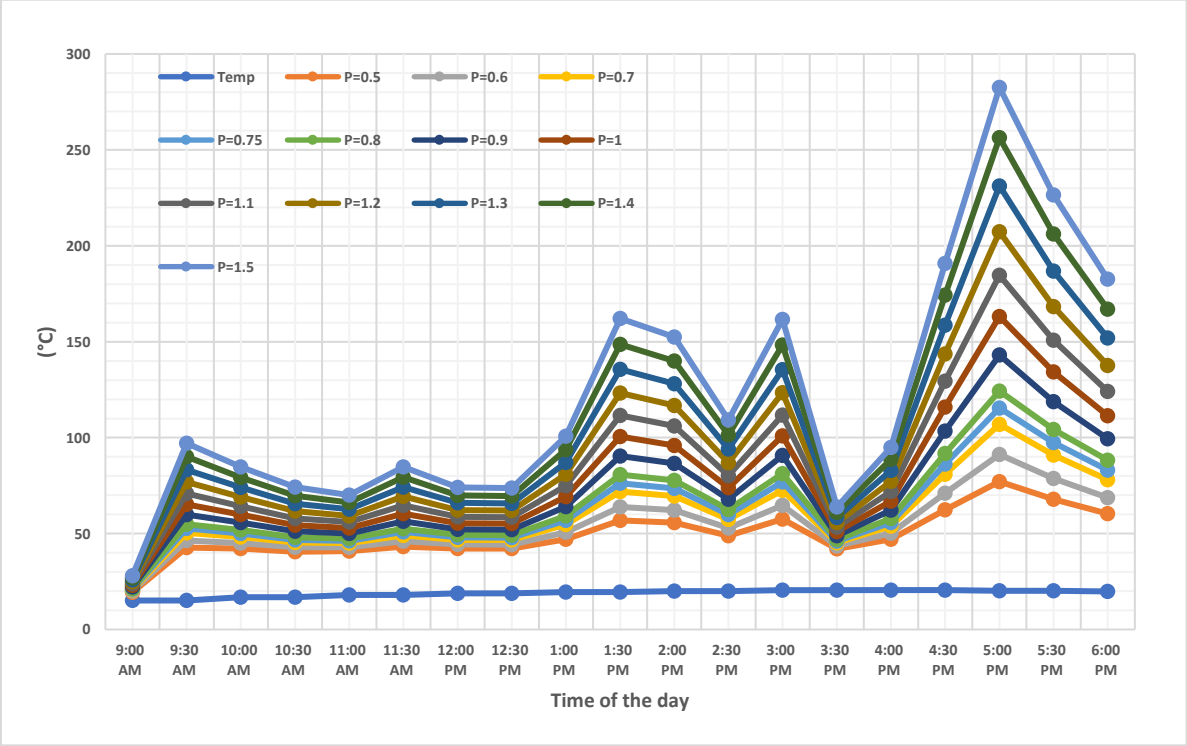

Fig. 90. Hottest spot temperature of winding of transformer 1 for month of April 2019.

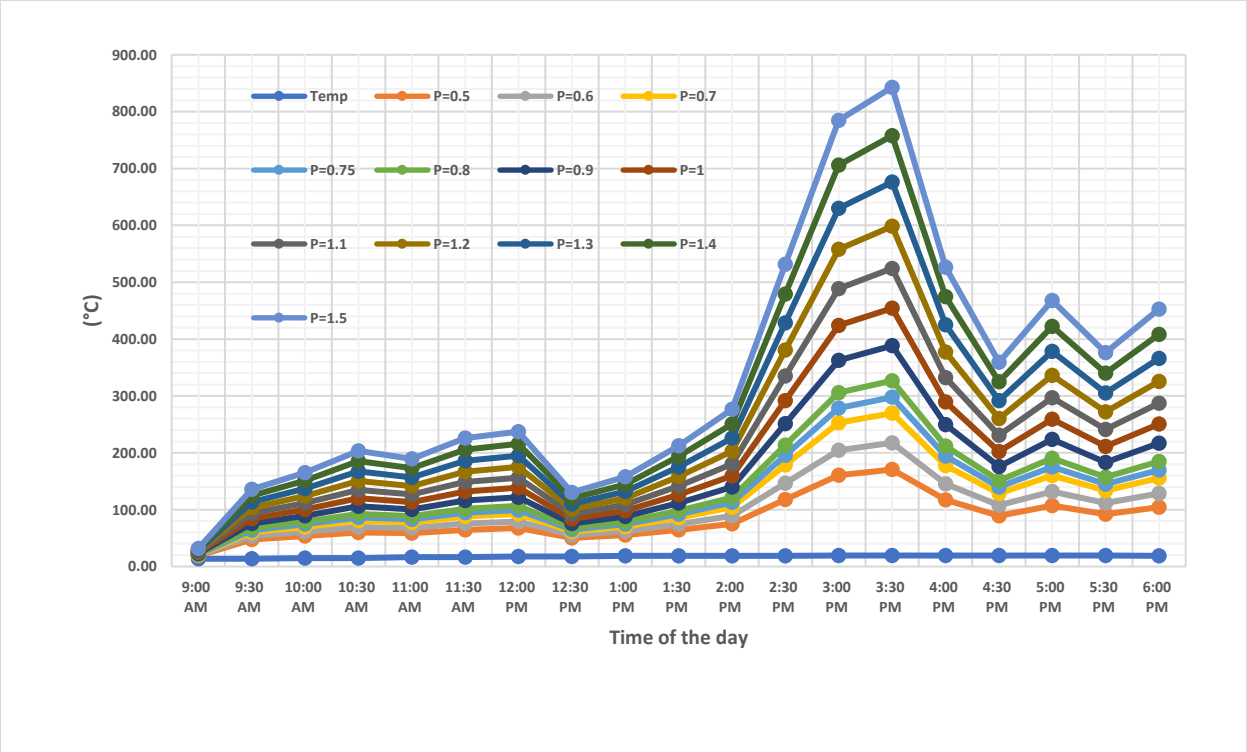

Fig. 91. Hottest spot temperature of winding of transformer 1 for month of April 2020.

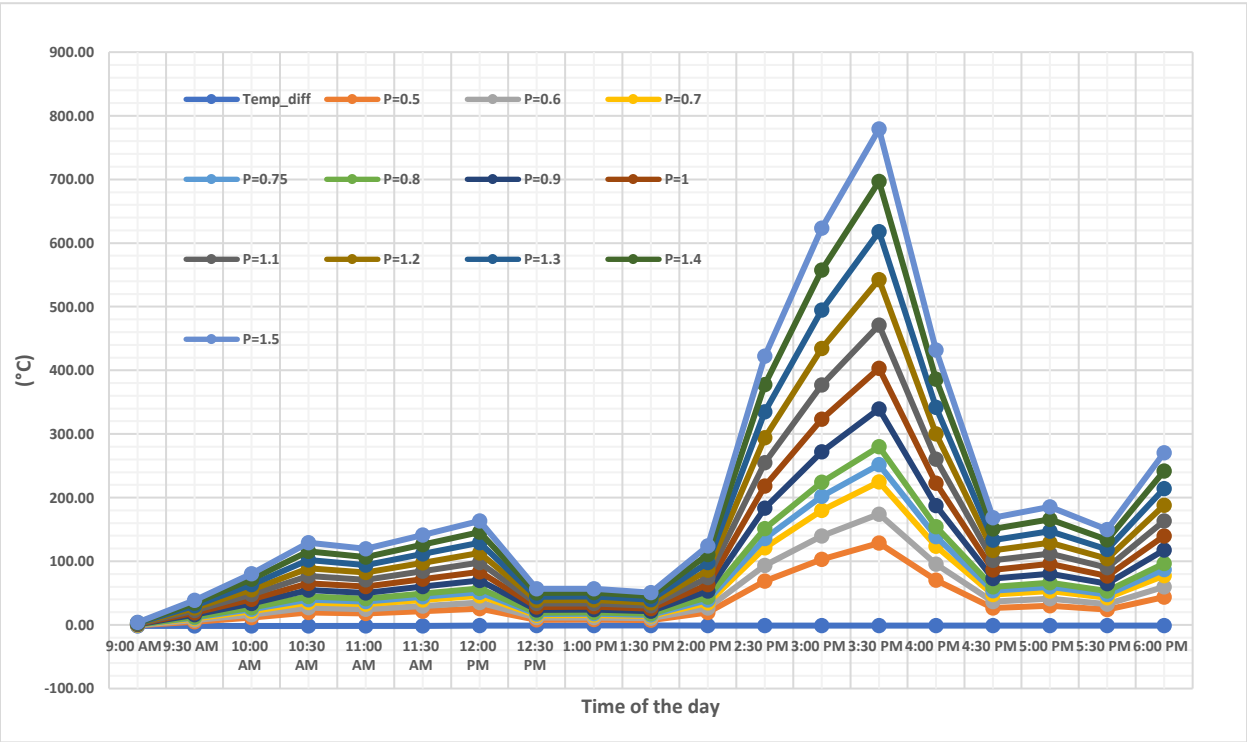

Fig. 92. Increase in hottest spot temperature of transformer 1 winding for month of April 2020 as compared to April 2019.

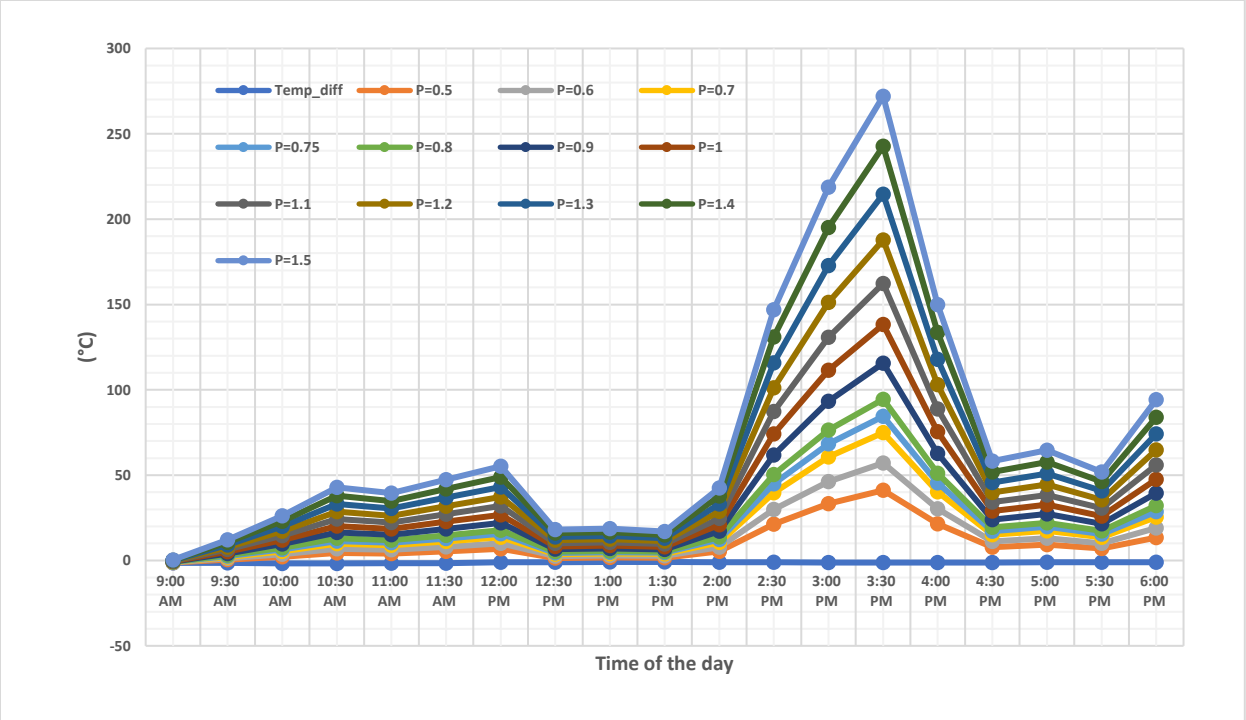

Fig. 93. Increase in top oil temperature of transformer 1 for month of April 2020 as compared to month of April 2019.

Due to the COVID-19 situation the increase in temperature in April 2020 as compared to April 2019 is shown in Fig. 92. The per unit currents data are taken from Table 30 and Table 31 for the month of April of 2019 and 2020, respectively. From Fig. 92, it is evident that the hottest winding temperature of April 2020 is higher than that of April 2019 during office hours especially from 2.30 pm to 4.00 pm. The hottest spot temperature difference exceeds 200ºC as P value increases from 0.7 to upwards in 2020, although the ambient temperature in April 2019 is higher than that of April 2020 as indicated by the negative value of temperature difference in Fig. 92. Moreover, for transformer 1, the top oil temperature difference between the month of April 2020 and April 2019 is shown in Fig. 93. As previously discussed, the top oil temperature should not exceed 120 ºC but the top oil difference exceeds 120 ºC for P values of 0.9 or higher.

Table 32: Per Unit Current of Residential Transformer 1 for the Month of April 2020 (Based on Consumer 1 Maximum Demand)

Time	P											
	.5	.6	.7	.75	.8	.9	1	1.1	1.2	1.3	1.4	1.5
9:00 AM	1.035	1.242	1.449	1.553	1.656	1.864	2.071	2.278	2.485	2.692	2.899	3.106
9:30 AM	0.682	0.819	0.955	1.024	1.092	1.228	1.365	1.501	1.638	1.774	1.911	2.047
10:00 AM	2.188	2.626	3.064	3.282	3.501	3.939	4.376	4.814	5.252	5.689	6.127	6.565
10:30 AM	0.682	0.819	0.955	1.024	1.092	1.228	1.365	1.501	1.638	1.774	1.911	2.047
11:00 AM	1.812	2.174	2.536	2.718	2.899	3.261	3.624	3.986	4.348	4.711	5.073	5.435
11:30 AM	1.835	2.202	2.569	2.753	2.936	3.304	3.671	4.038	4.405	4.772	5.139	5.506
12:00 PM	0.565	0.678	0.791	0.847	0.904	1.016	1.129	1.242	1.355	1.468	1.581	1.694
12:30 PM	1.553	1.864	2.174	2.329	2.485	2.795	3.106	3.416	3.727	4.038	4.348	4.659
1:00 PM	1.647	1.976	2.306	2.471	2.635	2.965	3.294	3.624	3.953	4.282	4.612	4.941
1:30 PM	1.435	1.722	2.009	2.153	2.296	2.584	2.871	3.158	3.445	3.732	4.019	4.306
2:00 PM	2.824	3.388	3.953	4.235	4.518	5.082	5.647	6.212	6.776	7.341	7.906	8.471
2:30 PM	3.271	3.925	4.579	4.906	5.233	5.887	6.541	7.195	7.849	8.504	9.158	9.812
3:00 PM	4.871	5.845	6.819	7.306	7.793	8.767	9.741	10.715	11.689	12.664	13.638	14.612
3:30 PM	3.412	4.094	4.776	5.118	5.459	6.141	6.824	7.506	8.188	8.871	9.553	10.235
4:00 PM	2.706	3.247	3.788	4.059	4.329	4.871	5.412	5.953	6.494	7.035	7.576	8.118
4:30 PM	4.471	5.365	6.259	6.706	7.153	8.047	8.941	9.835	10.729	11.624	12.518	13.412
5:00 PM	2.941	3.529	4.118	4.412	4.706	5.294	5.882	6.471	7.059	7.647	8.235	8.824
5:30 PM	2.165	2.598	3.031	3.247	3.464	3.896	4.329	4.762	5.195	5.628	6.061	6.494
6:00 PM	2.871	3.445	4.019	4.306	4.593	5.167	5.741	6.315	6.889	7.464	8.038	8.612

Table 32 represents the per unit current of transformer 1 based on consumer 1 maximum demands for April 2020 which are tabulated in Table 25. Based on these per unit currents, the hottest winding temperature for transformer 1 is represented in Fig. 94 for different values of P that represents the maximum temperature increase on the transformer windings.

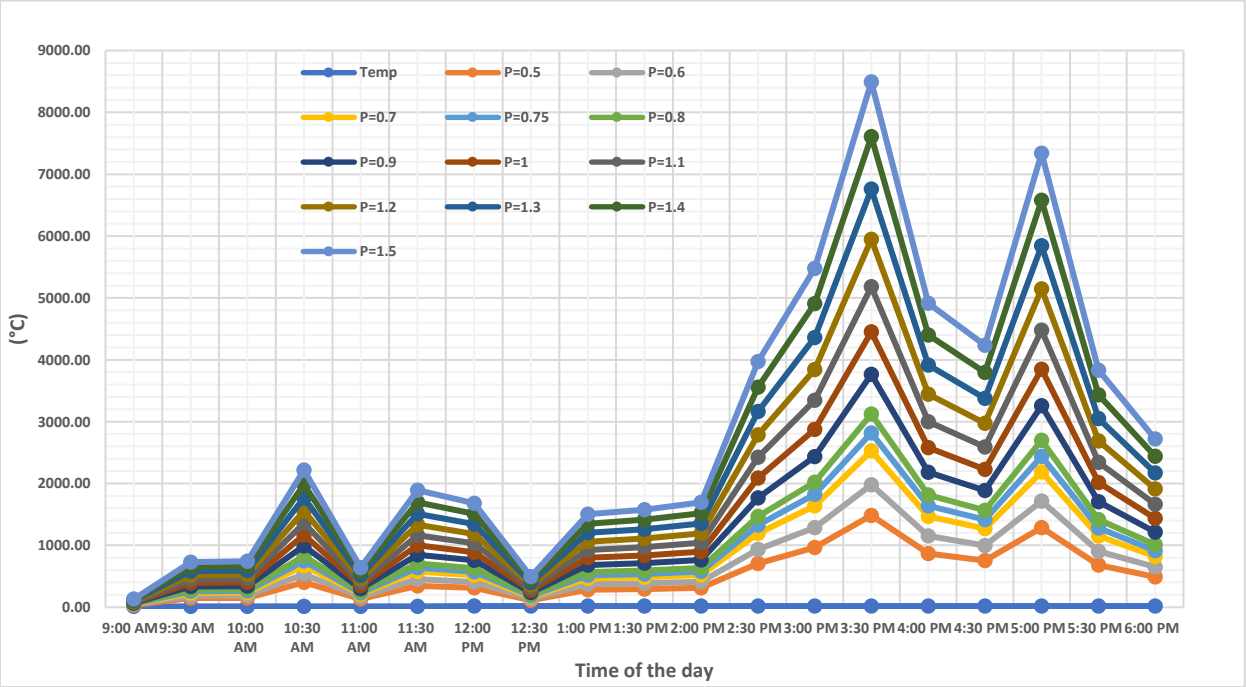

Fig. 94. Hottest spot temperature of winding of transformer 1 for month of April 2020 considering the maximum demand.

From Fig. 94, it is very concerning that the transformer hottest winding transformer becomes very high even for the lowest value of P considered (0.5). The temperature even goes extremely high from 2.00 pm to 6.00 pm. Therefore, consumers should be very careful in energy consumption during that period.

3. *The hottest spot temperature, top oil temperature and percentage loss of life of distribution transformer considering harmonics' presence in load current*

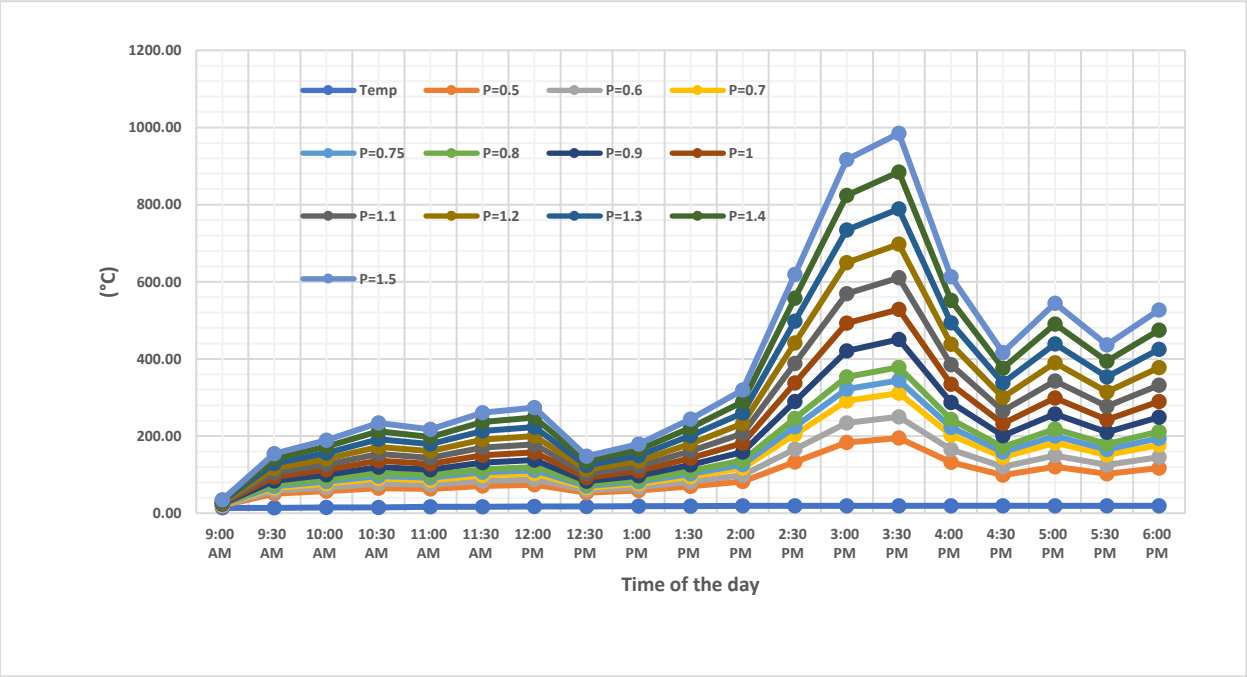

Fig. 95. Hottest spot temperature of Transformer 1winding for month of April 2020 for F_{HL} = 2.73 and $F_{HL\text{-}STR}$ = 1.14.

As discussed in [142], the F_{HL} and $F_{HL\text{-}STR}$ values do not change, as both the harmonic frequency component distribution and frequency component of non-sinusoidal current remain the same. Therefore, F_{HL} and $F_{HL\text{-}STR}$ values are assumed constant as the load current in this work changes considering the harmonic frequency component remains the same and their relative magnitude changes in proportion to the load current. The hottest spot temperatures of transformer 1 for the month of April, considering F_{HL} = 2.73 and $F_{HL\text{-}STR}$ = 1.14, are shown in Fig. 95 which indicate that the hottest spot temperature exceeds 200°C for P=0.5 and above whereas the temperature exceeds 200°C for P=0.6 and above for non-harmonic condition (Fig. 91). Similarly, for higher values of F_{HL} and $F_{HL\text{-}STR}$, the temperature exceeds 200°C for lower values of P.

Table 33 represents the percentage loss of life (%LOL) of transformer 1 for different values of F_{HL} and $F_{HL\text{-}STR}$ for the month of April in 2020 for all values of P. It is evident from Table 32 that, for the month of April the %LOL of transformer gets extremely high. For higher values of F_{HL} and $F_{HL\text{-}STR,}$ lesser values of P keep the transformer %LOL less than 50%. The not applicable (NA) condition in Table 32 indicates that for corresponding P, F_{HL} and $F_{HL\text{-}STR}$, %LOL goes above 50%. The different values of F_{HL} and $F_{HL\text{-}STR}$ considered in this work are taken from [25].

Table 33: %LOL of transformer 1 for different values of FHL and FHL-STR for April 2020

P	%LOL (APRIL)				
	F_{HL} = 1.0 $F_{HL\text{-}STR}$ = 1.0	F_{HL} = 2.73 $F_{HL\text{-}STR}$ = 1.14	F_{HL} = 3.11 $F_{HL\text{-}STR}$ = 1.19	F_{HL} = 6.48 $F_{HL\text{-}STR}$ = 1.38	F_{HL} = 8.1 $F_{HL\text{-}STR}$ = 1.58
0.5	0.021	0.117	0.168	2.52	7.73
0.6	0.517	3.39	5.00	3.6760	NA
0.7	9.62	NA	NA	NA	NA
0.75	37.00	NA	NA	NA	NA
0.8	NA	NA	NA	NA	NA
0.9	NA	NA	NA	NA	NA
1.0	NA	NA	NA	NA	NA
1.1	NA	NA	NA	NA	NA
1.2	NA	NA	NA	NA	NA
1.3	NA	NA	NA	NA	NA
1.4	NA	NA	NA	NA	NA
1.5	NA	NA	NA	NA	NA
1.5	NA	NA	NA	NA	NA

Table 34 represents the transformer loss of life considering the current for maximum demands tabulated in Table 31. It is a matter of concern that, for the chosen values of P, there is no incident found where the transformer loss of life is 50% or lesser. Therefore, higher consumption during the COVID-19 pandemic lockdown period can seriously damage the residential distribution transformer if these energy demands continue for longer times.

Table 34: %LOL of transformer 1 for different values of FHL and FHL-STR for April 2020

P	%LOL (APRIL)				
	F_{HL} = 1.0 F_{HL-STR} = 1.0	F_{HL} = 2.73 F_{HL-STR} = 1.14	F_{HL} = 3.11 F_{HL-STR} = 1.19	F_{HL} = 6.48 F_{HL-STR} = 1.38	F_{HL} = 8.1 F_{HL-STR} = 1.58
0.5	NA	NA	NA	NA	NA
0.6	NA	NA	NA	NA	NA
0.7	NA	NA	NA	NA	NA
0.75	NA	NA	NA	NA	NA
0.8	NA	NA	NA	NA	NA
0.9	NA	NA	NA	NA	NA
1.0	NA	NA	NA	NA	NA
1.1	NA	NA	NA	NA	NA
1.2	NA	NA	NA	NA	NA
1.3	NA	NA	NA	NA	NA
1.4	NA	NA	NA	NA	NA
1.5	NA	NA	NA	NA	NA
1.5	NA	NA	NA	NA	NA

E. Mitigation of Adverse Effects of Increased Energy Consumption on Distribution Transformers

In this work, in order to mitigate the adverse effects of increased energy consumptions at houses on distribution transformers, three types of solutions are proposed. First, the operation of the BTM sources such as the PV power, battery energy storage, and electric vehicle during office hours are considered. It is expected that the BTM sources will meet the increased amount of energy consumptions so that loads on distribution transformers decrease and also the percentage loss of life (%LOL) of the residential transformers gets reduced.

The second solution proposed is to schedule 10% loads from 1.00 pm to 5.00 pm for later hours, as the hottest spot temperature of transformer winding rises high during this time period.

The third solution can be intelligently using loads having less harmonic distortion factor during the scheduling time proposed in the second solution so that the harmonic loss factor

becomes less for current provided by the transformer which will in fact reduce the hottest spot temperature rise of transformer winding and reduce the percentage loss of life.

These three solutions are described in detail below.

1. *Providing Increased Energy Consumption by BTM Sources*

In this case, it is considered that the grid will provide power at houses, as usual, however, the PV system will be able to provide most of the increased amount of energy consumptions during office hours. Moreover, since residents are assumed to be staying at homes, their electric vehicles can be used as a power source during the period from 9 am to 6 pm. Here it is considered that the apartments have a central battery storage of 9 kWh which will be charged by the excess daytime PV power. The electric vehicles will be charged during nighttime only by the battery energy storage. It is assumed that the building has one electric vehicle having battery rating as 4.4 kWh [143] and that can be used from 70% to 90% of the battery capacity.

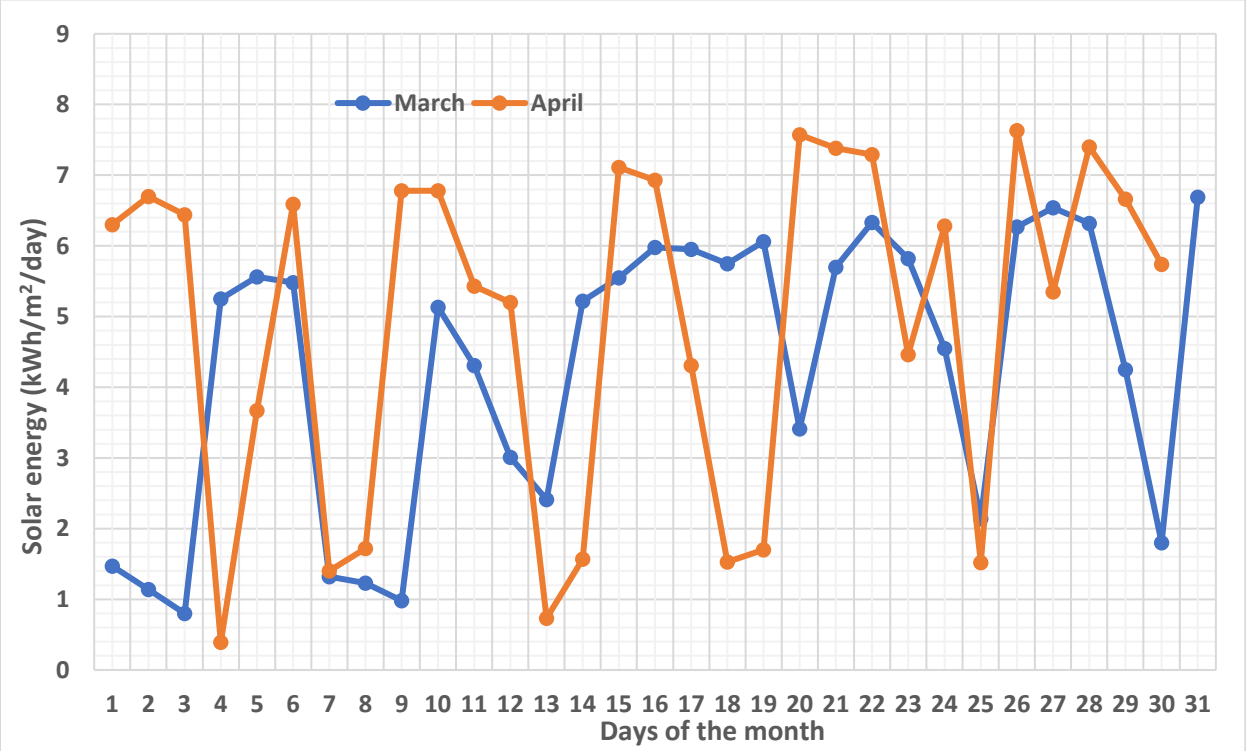

Fig. 96. Total solar energy available per day for March and April 2020.

The available total solar energy for the month of March and April in 2020 are shown in Fig. 96 [120], [144]. From the data in Fig. 96, after calculation, the average solar energy per day appeared to be 4.27 kWh/m^2/day and 4.95 kWh/m^2/day, which means a solar cell having the dimension of 1 m^2 will produce 4.27 kWh/day and 4.95 kWh/day, for the month of March and April, respectively. However, the lengths of days are not equal for the month of March and the office hour is only considered in this work. Hence, it is assumed that during the time from 9 am to 6 pm 80% and 70% of total energy is available, for the month of March and April, respectively. Therefore, for 9 hours, the total available energy will be 3.416 kWh/m^2 and 3.465 kWh/m^2 which give the average solar energy of 0.1897 kWh/m^2 and 0.1925 kWh/m^2 available for every half an hour for the month of March and April, respectively, in 2020.

For consumer 1, the average energy consumption rise in April is 0.0499 kWh for every half an hour (see Table 24). Therefore, in the six apartments that are under transformer 1, will have an average increase in energy consumption of 0.2996 kWh for every half an hour (considering the P value to be 1). The average solar panel of dimension is 5.4 feet by 3.25 feet which is 1.63 m^2. As 0.1925 kWh/m^2 average energy is available for every half an hour for the month of April in 2020, if the solar panel of the above dimension is installed in the building, it will have 0.3138 kWh average of energy for every half an hour available at the sonar panel. Considering 25% efficiency, each panel will produce 0.07845 kWh energy for every half an hour. Therefore, four panels will produce 0.3138 kWh average of energy for each half an hour for the month of April which is slightly higher than the average energy increase (0.2996 kWh). This fact indicates that the proposed PV system can meet the increased energy consumption demand for consumer 1 in April 2020.

2. *Mitigation of Effects of Increased Transformer Temperature and Percentage Loss of Life by BTM Sources*

The transformer per unit current, $T_{iBTM\text{-}pu}$ after considering the BTM sources, is calculated by the following equation:

$$T_{iBTM-pu} = \begin{cases} \dfrac{I_{c,h} \times n \times P - I_{BTM}}{I_{Trated}} \; if \; I_{c,h} \times n \times P > I_{BTM} \\ 0 \qquad if \;\; I_{c,h} \times n \times P < I_{BTM} \end{cases} \tag{61}$$

Where, $I_{c,h}$, n, P and I_{Trated} are the same as in equation (41). I_{BTM} is the current that is provided by the BTM sources during the office hour of the COVID period. It is assumed that the battery energy storage will be charged by the extra current if the first numerator of equation (61) gets lower than I_{BTM} and the transformer neither gives nor receives the extra power from the BTM sources. Moreover, I_{BTM} is calculated from the following equation:

$$I_{BTM} = \frac{E_{BTM} \times 1000}{0.5 \times 120} \tag{62}$$

Where, E_{BTM} is the energy available (0.3630 kWh) for each half an hour by the PV and electric vehicle for transformer 1. Moreover, the E_{BTM} energy available would be 0.5209 kWh for each half-hour for transformer 2.

Furthermore, for the considered case of the proposed PV source and electric vehicle during office hours, the per unit current of the transformer for consumer 1 for different values of P are calculated using (61) and shown in Table 35. It is noticed that the per unit current values are less than the demand on the transformer when all the power is supplied by the transformer (see Table 31). For example, in April 2020, at 9.00 am the $I_{c,h}$ is 1.266 A (Table 25). However, I_{BTM} value is calculated to be 6.05 A using (62) and neglecting the power loss to convert dc currents into ac currents. The first numerator value is 3.798 A (considering P=0.5) which is less than 6.05 A.

Therefore, the current provided by the transformer would be 0 A (Table 35, 9.00 am, P=0.5). However, for the same time and current, the first numerator becomes 7.596 A considering P=1 which is higher than 6.05 A. Therefore, the current provided by the transformer would be 1.546 A. Considering the transformer rated current to be 12.5 A, the per unit current would be 0.124 (Table 35, 9.00 am, P=1).

Table 35: Per Unit Current of Residential Transformer 1 for the Month of April 2020 (Based on Consumer 1)

Time	P											
	.5	.6	.7	.75	.8	.9	1	1.1	1.2	1.3	1.4	1.5
9:00 AM	0.000	0.000	0.000	0.000	0.002	0.063	0.124	0.185	0.245	0.306	0.367	0.428
9:30 AM	0.000	0.000	0.001	0.035	0.070	0.139	0.208	0.277	0.347	0.416	0.485	0.554
10:00 AM	0.000	0.024	0.109	0.151	0.194	0.278	0.363	0.448	0.532	0.617	0.702	0.787
10:30 AM	0.000	0.000	0.057	0.095	0.134	0.211	0.289	0.366	0.443	0.520	0.598	0.675
11:00 AM	0.000	0.045	0.134	0.178	0.222	0.310	0.398	0.487	0.575	0.663	0.751	0.840
11:30 AM	0.006	0.104	0.202	0.251	0.300	0.398	0.496	0.594	0.692	0.791	0.889	0.987
12:00 PM	0.000	0.000	0.000	0.000	0.000	0.033	0.091	0.148	0.205	0.263	0.320	0.378
12:30 PM	0.000	0.000	0.000	0.003	0.035	0.100	0.165	0.230	0.295	0.360	0.425	0.490
1:00 PM	0.000	0.020	0.103	0.145	0.187	0.271	0.355	0.439	0.523	0.607	0.691	0.775
1:30 PM	0.000	0.070	0.162	0.209	0.255	0.347	0.440	0.532	0.624	0.717	0.809	0.901
2:00 PM	0.274	0.425	0.577	0.653	0.729	0.880	1.032	1.183	1.335	1.486	1.638	1.790
2:30 PM	0.532	0.735	0.938	1.040	1.141	1.344	1.547	1.751	1.954	2.157	2.360	2.563
3:00 PM	0.640	0.864	1.089	1.201	1.314	1.538	1.763	1.988	2.212	2.437	2.662	2.887
3:30 PM	0.345	0.511	0.677	0.760	0.843	1.009	1.175	1.341	1.507	1.672	1.838	2.004
4:00 PM	0.104	0.222	0.340	0.398	0.457	0.575	0.692	0.810	0.928	1.045	1.163	1.281
4:30 PM	0.270	0.421	0.571	0.647	0.722	0.873	1.024	1.175	1.325	1.476	1.627	1.778
5:00 PM	0.145	0.271	0.397	0.460	0.523	0.649	0.775	0.901	1.027	1.152	1.278	1.404
5:30 PM	0.182	0.315	0.448	0.515	0.581	0.714	0.847	0.981	1.114	1.247	1.380	1.513
6:00 PM	0.500	0.697	0.894	0.992	1.091	1.288	1.485	1.681	1.878	2.075	2.272	2.469

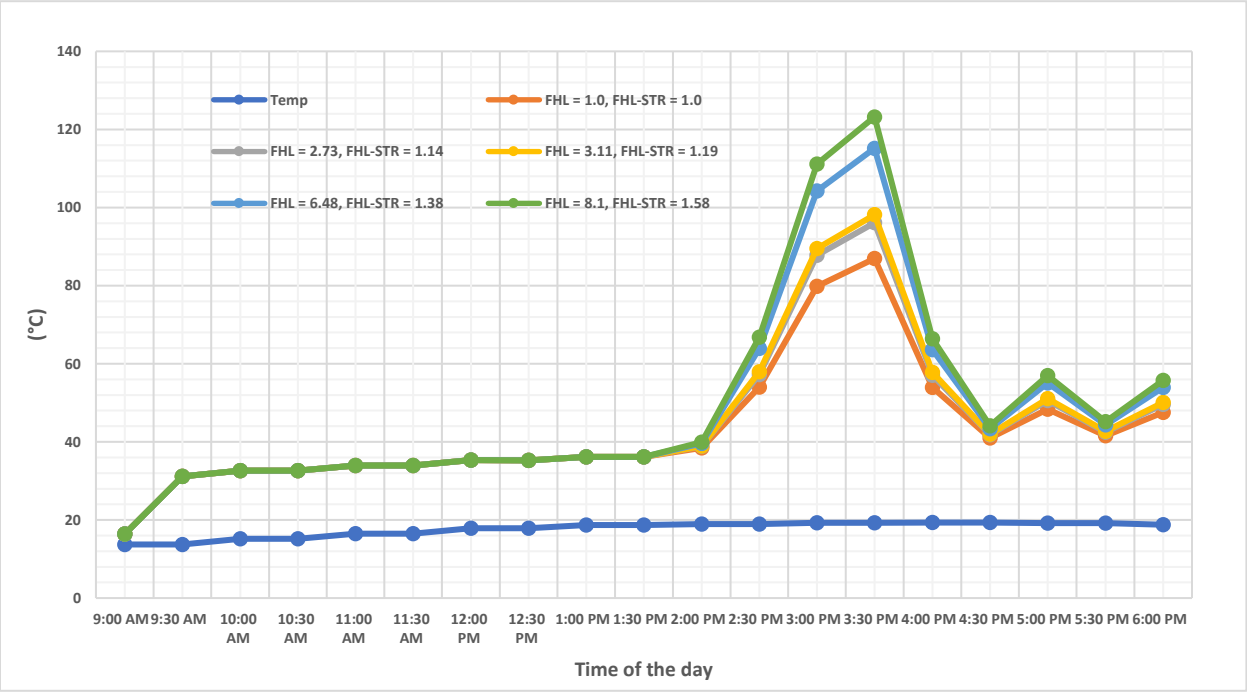

Fig. 97. Hottest spot temperature of transformer 1 winding in April for P=.5 for April 2020.

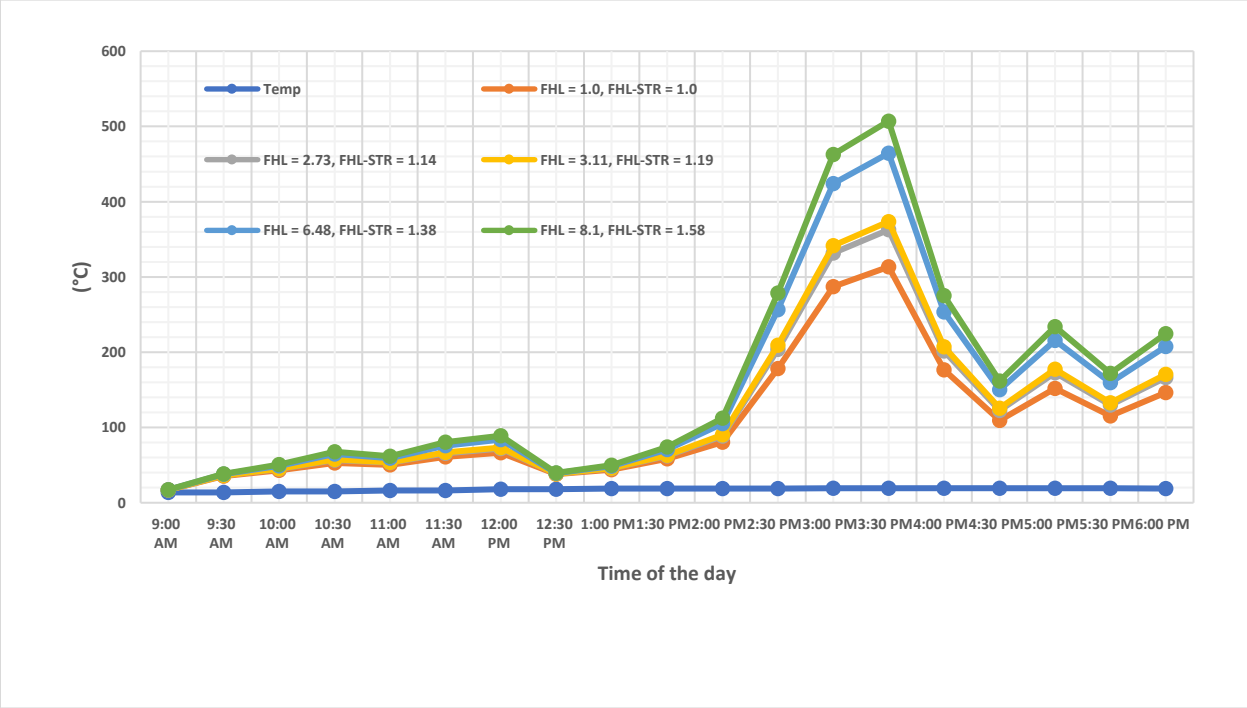

Fig. 98. Hottest spot temperature of transformer 1 winding in April for P=1 for April 2020.

The hottest spot temperatures of the transformer winding for the month of April, for the considered case, are shown in Fig. 97 for P values of 0.5. Due to power provision by PV source,

battery storage and electric vehicle, the hottest winding temperature never crosses 200 °C for case 1 for P=0.5 for all F_{HL} and $F_{HL\text{-}STR}$ values. Moreover, for F_{HL} = 2.73 and $F_{HL\text{-}STR}$ = 1.14, the maximum hottest spot temperature remained under 100 °C where the temperature exceeds above 170 °C for the same F_{HL} and $F_{HL\text{-}STR}$ values as shown in Fig. 95.

Moreover, as shown in Fig. 98, in the case of P=1 the hottest spot temperature of transformer winding exceeds 200 °C for half an hour (3.00-3.30 pm). However, for F_{HL} = 2.73 and $F_{HL\text{-}STR}$ = 1.14, the hottest spot temperature exceeds above 300 °C due to the provision of power by PV, battery storage and hybrid electric vehicle. However, the hottest winding temperature exceeds 500 °C for the same F_{HL} and $F_{HL\text{-}STR}$ values as shown in Fig. 95. The same situation happens for all other F_{HL} and $F_{HL\text{-}STR}$ values which decrease the %LOL of the transformer.

The percentage loss of life, with and without mitigation solution by the BTM sources, is shown in Table 36 for FHL = 2.73 and FHL-STR = 1.14. From Table 35, it is clear that, for the considered case, up to 0.9 value of P can keep transformer loss of life (%LOL) below 50%. For normal operation without considering the proposed BTM solution, the %LOL goes beyond 50% for P=0.6. Therefore, the inclusion of the BTM sources and energy storage certainly increases the operating range of load and decrease the %LOL for the same value of the load.

Table 36: %LOL of Transformer for case 1 for April 2020

P	%LOL (April)	
	Without mitigation solution (F_{HL} = 2.73, $F_{HL\text{-}STR}$ = 1.14)	With proposed mitigation solution (F_{HL} = 2.73, $F_{HL\text{-}STR}$ = 1.14)
0.5	0.117	2.16E-05
0.6	3.39	1.06E-03
0.7	NA	4.60E-02
0.75	NA	2.72E-01
0.8	NA	1.47
0.9	NA	32.6
1.0	NA	7.41
1.1	NA	NA
1.2	NA	NA
1.3	NA	NA
1.4	NA	NA
1.5	NA	NA

3. *Mitigation of Effects of Increased Transformer Temperature and Percentage Loss of Life by Load Scheduling*

As previously described, the lockdown situation increases the energy consumption which in turn increases the hottest spot temperature of transformer winding, top oil temperature especially from 1.00 pm to 4.00 pm. Therefore, if the consumers can shift some of loads of that period for a later time or nighttime, it will decrease the temperature rise in the winding and oil and the percentage loss of transformer's life will be reduced. This shifting of loads can be easily facilitated by shifting all the cooking, washing clothes, dishes, etc., for nighttime or later hours, lowering the temperature setting to a slightly lower value to the consumers' utmost liking.

In this case, only 10% of loads, that are consumed on average from 1.00 pm to 4.00 pm, are assumed to be shifted or scheduled for later hours or nighttime.

The currents for this case are similar to what are tabulated in Table 24 except for the fact that only the average currents shown in Table 24 will be reduced 10% from 1.00 pm to 4.00 pm. This is also true for per unit currents shown in Table 30 for all values of P. Based on this calculation of currents, the hottest spot temperature of transformer winding for P value of 0.5 and 1.0 are shown in Fig. 99 and Fig. 100, respectively for consumer 1.

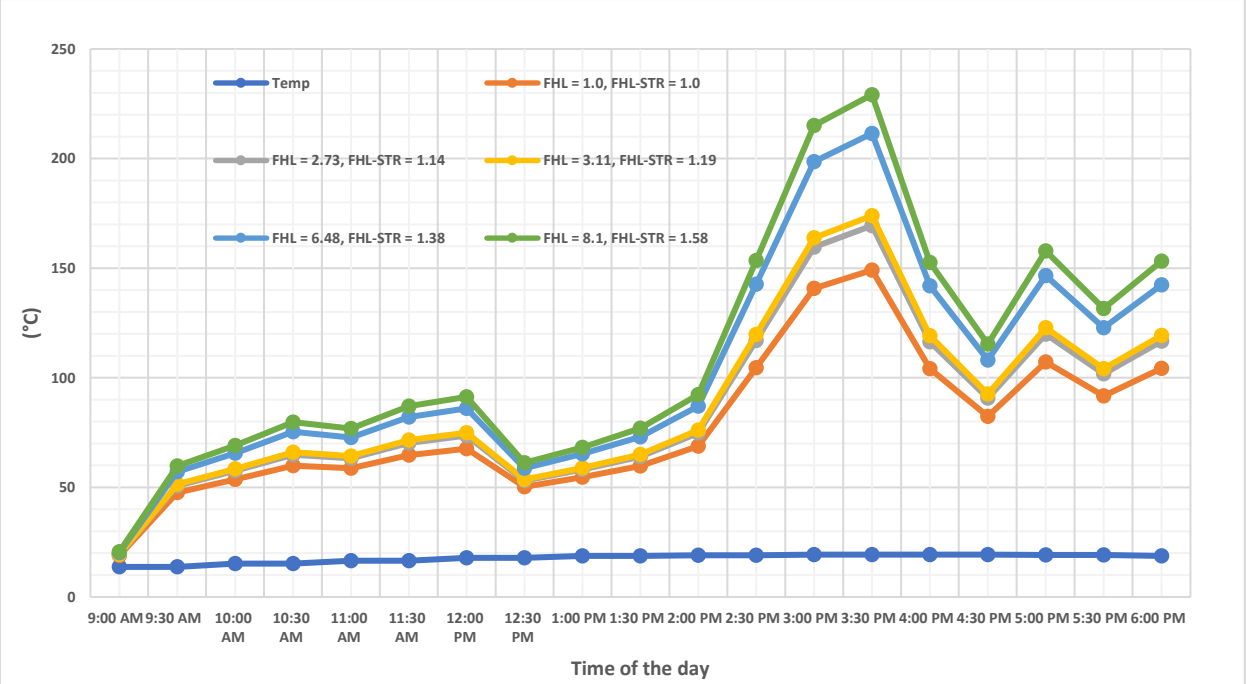

Fig. 99. Hottest spot temperature of transformer 1 winding in April for P=.5 for April 2020.

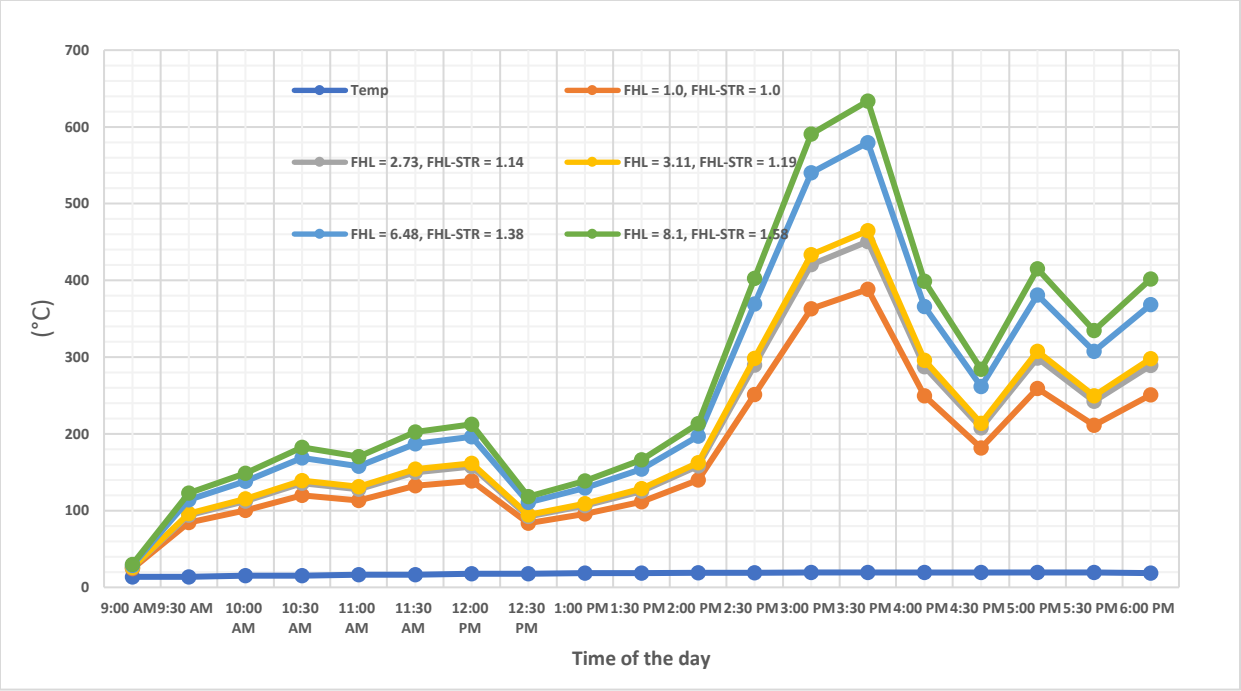

Fig. 100. Hottest spot temperature of transformer 1 winding in April for P=1 for April 2020.

Table 37: %LOL of transformer for case 2 for April 2020

P	%LOL (April)	
	Without mitigation solution (F_{HL} = 2.73, F_{HL-STR} = 1.14)	With proposed mitigation solution (F_{HL} = 2.73, F_{HL-STR} = 1.14)
0.5	0.117	1.94E-02
0.6	3.39	4.73E-01
0.7	NA	8.73
0.75	NA	33.5
0.8	NA	NA
0.9	NA	NA
1.0	NA	NA
1.1	NA	NA
1.2	NA	NA
1.3	NA	NA
1.4	NA	NA
1.5	NA	NA

From Fig. 99 and Fig. 100, it can be concluded that the temperature rise reduction, in this case, will be less than that of the proposed solution (BTM sources) in the previous section, but it

is effective in reducing temperature rise. However, it increases the range of P values for which the percentage loss of life will be less than 50% as shown in Table 37. Moreover, the temperature rise and percentage loss of life can be further reduced if the consumers are willing to schedule more loads for later hours.

4. Mitigation of Effects of Increased Transformer Temperature and Percentage Loss of Life by Load Scheduling and Utilizing Loads Causing Less Harmonic Distortion

There are two types of loads (i.e. ac and dc) that are used in residential buildings. Among them, television, mobile phone, water purifier, microwave oven, washing machine, etc. are dc loads that produce higher harmonic contents in current when taking power from the system [145]. Among the ac loads, fluorescent lamps/tubes, fan with electronic regulator, air conditioner, etc., produce higher harmonics. These harmonic contents can produce excessive heating for the transformer.

Therefore, along with the load scheduling proposed in the previous subsection, the loads can be used in such a way that the loads that produce higher harmonics will be limitedly used from 1.00 pm to 4.00 pm. This will help reduce the harmonic loss factor and harmonic loss factor for the stray losses, and thus the temperature rise and percentage loss of life can be reduced further. In this case, it is assumed that the load scheduling is done in such a way the harmonic loss factor

and harmonic loss factor for the stray losses are decreased by 5% from the considered value for the normal operating conditions.

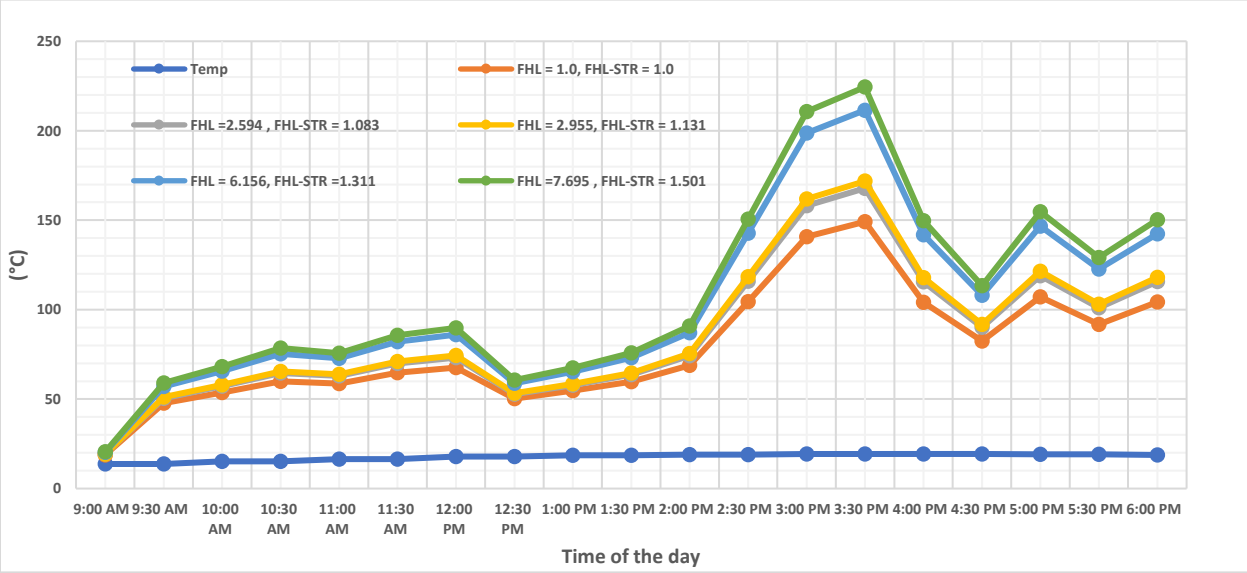

Fig. 101. Hottest spot temperature of transformer 1 winding in April for P=.5 for April 2020.

The new harmonic loss factors and harmonic loss factor for the stray losses, after considering 5% reduction, are shown in Fig. 101 and Fig. 102.

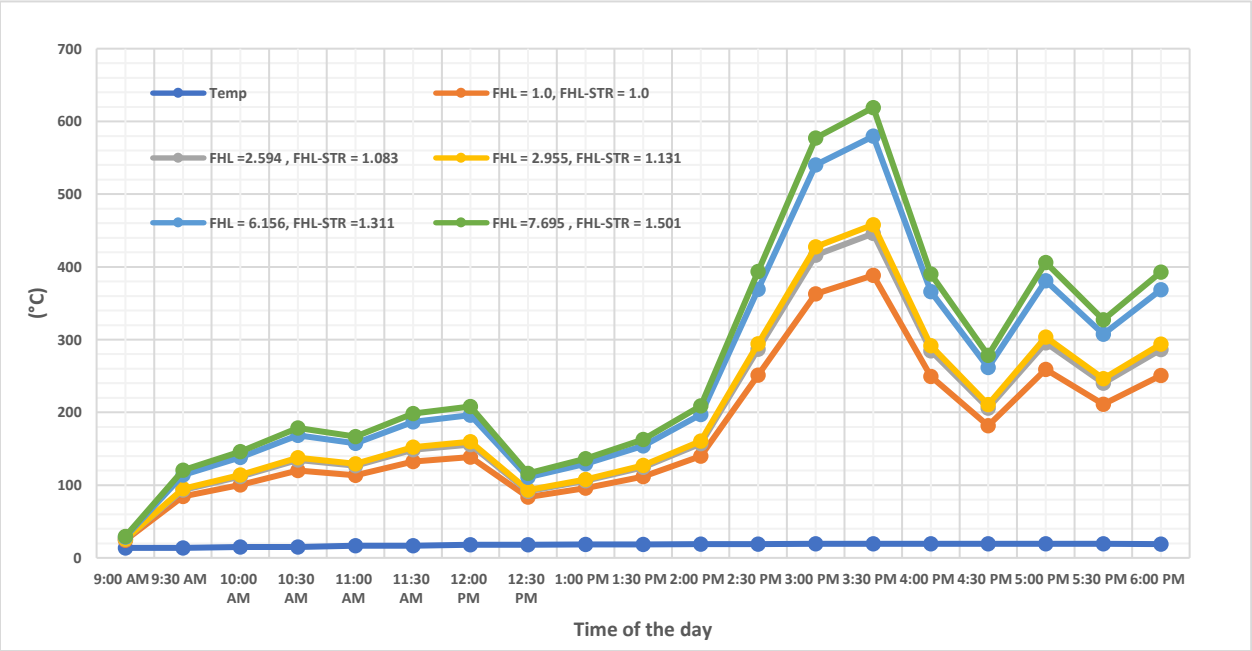

Fig. 102. Hottest spot temperature of transformer 1 winding in April for P=1 for April 2020.

Table 38: %LOL of transformer for case 3 for April 2020

P	%LOL (April)	
	Without mitigation solution (F_{HL} = 2.73, $F_{HL\text{-}STR}$ = 1.14)	With proposed mitigation solution (F_{HL} = 2.594, $F_{HL\text{-}STR}$ = 1.083)
0.5	0.117	1.72E-02
0.6	3.39	4.14E-01
0.7	NA	7.59
0.75	NA	29.1
0.8	NA	NA
0.9	NA	NA
1.0	NA	NA
1.1	NA	NA
1.2	NA	NA
1.3	NA	NA
1.4	NA	NA
1.5	NA	NA

Fig. 101 and Fig. 102 represent the hottest spot temperature of transformer winding for P value of 0.5 and 1.0, respectively. It is evident from these two figures that the temperature reduces further as compared to Fig. 99 and Fig. 100, respectively, due to the considered reduction of harmonic loss factor and harmonic loss factor for other stray losses. From Table 38, it is evident that the percentage loss of life reduces for this case as compared to the case considered in the previous subsection (see Table 36) for all values of P ranging from 0.5 to 0.75.

F. Conclusion

This work proposes a real-time health monitoring system of all loads in smart buildings. It also analyzes all the common problems that can happen for all the smart loads. The proposed health monitoring system can alert the consumers ahead of time about the fault or anomaly behavior that can lead to a probable failure or damage for the smart buildings. A real-time web-based monitoring system for all the loads, that can be easily visualized in smart televisions, mobile phones, smartwatches, etc., are also proposed. Simulation results show the effectiveness and validity of the proposed method. In addition, this health monitoring system can be accessed by the people inside the home or staying outside if internet connectivity is available. Therefore, it is a promising tool that can be implemented easily for future smart homes.

Moreover, this work analyzes the impact of the COVID-19 pandemic situation on residential loads and local distribution transformers. Six types of consumers having different consumption patterns are considered. Based on the analysis, the following conclusions can be made:

1. Due to the lockdown situation, the energy consumptions of consumers have increased during the entire office hour or part of the office hour.
2. The residential transformer gets vulnerable as the value of P gets higher. Also, with a higher harmonic loss factor, the range of P values, for which the transformer can operate safely, decreases.
3. The proposed BTM sources, load scheduling, and load scheduling by using loads that produce lesser harmonics are effective during these lockdown conditions as it increases the range of P values for safe operating

conditions of the residential transformer and reduces the %LOL for all P values.

VI. CONCLUSIONS, CONTRIBUTIONS AND FUTURE WORK

A. Conclusions

In this dissertation, the findings can be summarized as:

- This work proposes new methods for residential short-term load forecasting such as non-linear equation-based prediction systems, new fuzzy and subtractive clustering-based prediction systems. Based on the simulation results, the proposed ANFIS2 system performs the best, followed by the proposed non-linear and linear equation-based system in predicting residential loads as compared to other proposed methods and conventional methods. All the proposed prediction methods that are mentioned above perform better than ANN, random forest, LSBoosting and LSTM methods.
- A new scheduling method is proposed with a view to reducing cost of energy, consumers' discomfort, power quality distortions while ensuring maximum utilization of renewable energy sources and battery energy storage. The simulation results for scheduling show the grid power provided by the smart building meeting the load demands for three types of days. Solar and wind power is also shown for three different day types. The proposed scheduling methods along with renewable energy sources and battery energy storage, not only meet the load demand but also efficient in providing power to the grid.
- A real-time health status monitoring system, for all loads available in the smart buildings, is proposed to facilitate the consumer with real-time health condition checking, pre-alert them in case of possible disaster or faults.

Moreover, the framework is demoed in MATLAB, and the web-based application of this monitoring system is proposed so that it can be accessed from any smart television, mobile devices or smartwatch. The proposed system is efficient in providing alert messages while there is a deviation from the normal operating conditions. Therefore, the proposed system can be an efficient tool in pre-alerting consumers about the advent of a fault or hazard condition for all loads in a smart building.

- The impacts of the COVID-19 pandemic situation on residential loads consumption are analyzed. The transformer's performances in terms of hottest winding temperature, top oil temperature, and percentage loss of life are calculated based on the one group of consumers' load consumption pattern. Finally, realistic solutions, in terms of BTM sources, load scheduling, and using loads having lesser harmonics content while scheduling, are proposed as effective solutions and validated by the simulation results.

B. Future Work

The research presented in this dissertation can be further extended in the future in the following directions:

- In future work, the centralized controller that will be controlling loads based on machine learning algorithms while considering the environmental conditions, renewable energy production, occupants' preferences, etc., will be considered. The smart loads considered could be the HVAC system, refrigerators, washing machines, dryers, lighting systems, hybrid electric vehicles, battery energy

storage, pool heating and cooling machines, etc. For example, the centralized HVAC system will consider the motion sensor to direct the cooling and heating airflow to the occupants. The empty rooms will not get any airflow by closing the ventilator doors. Therefore, the ventilators will be closing and operating based on motion sensors and centralized controller data and the ventilators' motors (small permanent magnet dc motors) will be operated by the signal sent by the centralized controller. The centralized control will have smart meter data of power required for HVAC operation at a specific temperature requirement. Also, considering the occupants' position and the preference of temperature in the room, the centralized controller will send signals accordingly to the ventilators' motors and HVAC system to control temperature and its direction in the room. Permanent synchronous motor can be used as a new motor for HVAC system that is practically available. Moreover, in the building, there might be some normal refrigerators and backup refrigerators whose temperature can be controlled by the centralized controller or it can be remotely controlled by the occupants. The centralized controller will look into any specific temperature or time required for any food, medicine, etc., in the refrigerators. The centralized controller will provide the control signals based on the machine learning algorithms (SVM, ANFIS, neural network-based method, etc.) to control the temperature in the refrigerators. Normally a capacitor start single phase induction is used for refrigerator, but a brushless dc motor or permanent magnet dc motor can be utilized. Similarly, for other loads, new analysis can be done.

- Analysis of probabilistic methods, deep learning methods, a new type of equation-based system for load forecasting that will give much better prediction accuracy as compared to the proposed methods and can be implementable in real practice, can be explored. Moreover, real-time implementation of the proposed system such as equation-based systems would be done for users.
- The inclusion of new objective functions can be considered to make load scheduling more efficient, realistic for application in smart buildings.
- A prediction system for distribution transformer overloading will be another future work based on the consumer presence, environmental conditions, and other factors. This system will show the safe energy consumption limit for consumers under normal or any pandemic conditions.
- The real-time health monitoring system can be implemented in real practice where sensors from all the loads will update device operating parameters in the cloud through the internet of thing (IoT) technology. Using, Spark big data analytics, API can be used to do operation parameter check and health monitoring system block performance. Moreover, unstructured (No SQL) data storage can be used to store sensor data which will be used by the spark analytics for periodic updating.

REFERENCES

[1] L. Wells, B. Rismanchi, and L. Aye, "A review of Net Zero Energy Buildings with reflections on the Australian context," *Energy and Buildings*, 158, 2018, pp. 616-628.

[2] T. M. Lawrence, M. C. Boudreau, L. Helsen, G. Henze, J. Mohammadpour, D. Noonan, D. Patteeuw, S. Pless, and R. T. Watson, "Ten questions concerning integrating smart buildings into the smart grid," *Building and Environment,*108, 2016, pp. 273-283.

[3] I. IHSANE, L. MIEGEVILLE, N. Aït-AHMED and P. GUERIN, "New Evaluation Metrics for Electrical Demand Forecasting: Application to the Residential Sector," *2018 AEIT International Annual Conference*, Bari, 2018, pp. 1-6.

[4] J. Vossen, B. Feron, and A. Monti, "Probabilistic Forecasting of Household Electrical Load Using Artificial Neural Networks," *2018 IEEE International Conference on Probabilistic Methods Applied to Power Systems (PMAPS)*, Boise, ID, 2018, pp. 1-6.

[5] I. S. Bayram and T. S. Ustun, "A survey on behind the meter energy management systems in smart grid," *Renewable and Sustainable Energy Reviews,* vol. 72, pp. 1208-1232, 2017.

[6] L. M. H. do Amaral, A. N. d. Souza, D. S. Gastaldello, T. X. d. S. Palma, A. d. S. Maranho, and J. P. Papa, "Use of virtual load curves for the training of neural networks for residential electricity consumption forecasting applications," *2018 13th IEEE International Conference on Industry Applications (INDUSCON)*, São Paulo, Brazil, 2018, pp. 85-90.

[7] J. Zheng, X. Chen, K. Yu, L. Gan, Y. Wang, and K. Wang, "Short-term Power Load Forecasting of Residential Community Based on GRU Neural Network," *2018 International Conference on Power System Technology (POWERCON)*, Guangzhou, 2018, pp. 4862-4868.

[8] G. Li, D. Wu, J. Hu, Y. Li, M. S. Hossain, and A. Ghoneim, "HELOS: Heterogeneous Load Scheduling for Electric Vehicle-Integrated Microgrids," *IEEE Transactions on Vehicular Technology*, vol. 66, no. 7, pp. 5785-5796, July 2017.

[9] M. A. Nokar, F. Tashtarian, and M. H. Y. Moghaddam, "Residential power consumption forecasting in the smart grid using ANFIS system," *2017 7th International Conference on Computer and Knowledge Engineering (ICCKE)*, Mashhad, 2017, pp. 111-118.

[10] T. Hong and S. Fan, "Probabilistic electric load forecasting: A tutorial review," *International Journal of Forecasting*, vol. 32, *(3),* pp. 914-938, 2016.

[11] M. A. Mat Daut, M. Y. Hassan, H. Abdullah, H. A. Rahman, M. P. Abdullah, and F. Hussin, "Building electrical energy consumption forecasting analysis using conventional and artificial intelligence methods: A review," *Renewable and Sustainable Energy Reviews,* vol. 70, 2017, pp. 1108-1118.

[12] L. Hernandez, C. Baladr´on, J. M. Aguiar, B. Carro, A. J. S. Esguevillas, J. Lloret, and J. Massana , "A Survey on Electric Power Demand Forecasting: Future Trends in Smart Grids, Microgrids and Smart Buildings," *IEEE Communications Surveys & Tutorials*, vol. 16, no. 3, 2014, pp. 1460-1495.

[13] F. Y. Melhem, O. Grunder, Z. Hammoudan and N. Moubayed, "Optimal residential load scheduling model in smart grid environment," *2017 IEEE International Conference on*

Environment and Electrical Engineering and 2017 IEEE Industrial and Commercial Power Systems Europe (EEEIC / I&CPS Europe), Milan, 2017, pp. 1-6.

[14] F. L. Quilumba, W. Lee, H. Huang, D. Y. Wang and R. L. Szabados, "Using Smart Meter Data to Improve the Accuracy of Intraday Load Forecasting Considering Customer Behavior Similarities," *IEEE Transactions on Smart Grid*, vol. 6, no. 2, pp. 911-918, March 2015.

[15] L. Martirano, G. Parise, L. Parise and M. Manganelli, "A Fuzzy-Based Building Automation Control System: Optimizing the Level of Energy Performance and Comfort in an Office Space by Taking Advantage of Building Automation Systems and Solar Energy," *in IEEE Industry Applications Magazine*, vol. 22, no. 2, pp. 10-17, March-April 2016.

[16] L. Martirano, G. Parise, L. Parise and M. Manganelli, "Simulation and sensitivity analysis of a fuzzy-based building automation control system," *2014 IEEE Industry Application Society Annual Meeting*, Vancouver, BC, 2014, pp. 1-7.

[17] P. H. Shaikh, N. B. Mohd Nor, P. Nallagownden and I. Elamvazuthi, "Optimized intelligent control system for indoor thermal comfort and energy management of buildings," *2014 5th International Conference on Intelligent and Advanced Systems (ICIAS)*, Kuala Lumpur, 2014, pp. 1-5.

[18] Y. Raja Vara Prasad, S. Goel, P. Rajalakshmi and U. B. Desai, "Real Time Net Zero Energy Building Energy Manager with Heterogeneous Wireless Ad hoc Network Adaptable To IoT Architectures," *2015 IEEE Region 10 Symposium*, Ahmedabad, 2015, pp. 29-32.

[19] P. Motevakel, B. Ghanbari, H. Nafisi, M. Abedi and H. Hosseinian, "A novel approach for improving voltage profile in low voltage networks with high solar panel penetration level by using flexible loads," *2017 Smart Grid Conference (SGC)*, Tehran, 2017, pp. 1-7.

[20] M. A. Sönmez, M. A. Zehir and M. Bagrıyanık, "Demand response by real-time management of flexible loads using dynamic priorities," *2018 6th International Istanbul Smart Grids and Cities Congress and Fair (ICSG)*, Istanbul, 2018, pp. 155-159.

[21] https://insight.livestories.com/s/v2/covid-19-data-dashboard-%7C-shelby-county-tn/e381a899-7ffe-43fe-b80f-c9e63ebfcef6

[22] H. F. M. Mantilla, A. Pavas and I. C. Durán, "Aging of distribution transformers due to voltage harmonics," *2017 IEEE Workshop on Power Electronics and Power Quality Applications (PEPQA)*, Bogota, 2017, pp. 1-5.

[23] S. Acharya and P. C. Tapre, "Life assessment of transformer using thermal models," *2017 International Conference on Energy, Communication, Data Analytics and Soft Computing (ICECDS)*, Chennai, 2017, pp. 3515-3520.

[24] B. Yildiz, J. I. Bilbao and A. B. Sproul, "A review and analysis of regression and machine learning models on commercial building electricity load forecasting," *Renewable and Sustainable Energy Reviews*, vol. 73, pp. 1104-1122, 2017.

[25] M. Yu, W. Zhou, B. Wang and J. Jin, "The short-term forecasting of wind speed based on EMD and ARMA," *2017 12th IEEE Conference on Industrial Electronics and Applications (ICIEA)*, Siem Reap, 2017, pp. 495-498.

[26] M. K. Bantupalli and S. K. Matam, "Wind Speed forecasting using empirical mode decomposition with ANN and ARIMA models," *2017 14th IEEE India Council International Conference (INDICON)*, Roorkee, 2017, pp. 1-6.

[27] D. Chowdhury, M. Sarkar, M. Z. Haider and T. Alam, "Zone Wise Hourly Load Prediction Using Regression Decision Tree Model," *2018 International Conference on Innovation in Engineering and Technology (ICIET)*, Dhaka, Bangladesh, 2018, pp. 1-6.

[28] Tairen Chen, J. Lehr, O. Lavrova and M. Martinez-Ramonz, "Distribution-level peak load prediction based on Bayesian Additive Regression Trees," *2016 IEEE Power and Energy Society General Meeting (PESGM)*, Boston, MA, 2016, pp. 1-5.

[29] Z. Wang et al, "Random Forest based hourly building energy prediction," *Energy Build.*, vol. 171, pp. 11-25, 2018.

[30] C. Persson et al, "Multi-site solar power forecasting using gradient boosted regression trees," *Solar Energy*, vol. 150, pp. 423-436, 2017.

[31] C. Chen, C. Liang and C. Chu, "Long-term travel time prediction using gradient boosting," *Journal of Intelligent Transportation Systems*, vol. 24, (2), pp. 109-124, 2020.

[32] K. Aurangzeb, "Short Term Power Load Forecasting using Machine Learning Models for energy management in a smart community," *2019 International Conference on Computer and Information Sciences (ICCIS)*, Sakaka, Saudi Arabia, 2019.

[33] A. S. Nair, T. Hossen, M. Campion and P. Ranganathan, "Optimal Operation of Residential Evs using DNN and Clustering based Energy Forecast," *2018 North American Power Symposium (NAPS)*, Fargo, ND, 2018, pp. 1-6

[34] Z. Wang and R. S. Srinivasan, "A review of artificial intelligence based building energy use prediction: Contrasting the capabilities of single and ensemble prediction models," *Renewable and Sustainable Energy Reviews*, vol. 75, pp. 796-808, 2017.

[35] L. Wang, E. W. M. Lee and R. K. K. Yuen, "Novel dynamic forecasting model for building cooling loads combining an artificial neural network and an ensemble approach," *Appl. Energy*, vol. 228, pp. 1740-1753, 2018.

[36] A. Delorme-Costil and J. Bezian, "Forecasting Domestic Hot Water Demand in Residential House Using Artificial Neural Networks," *2017 16th IEEE International Conference on Machine Learning and Applications (ICMLA)*, Cancun, 2017, pp. 467-472.

[37] E. Akarslan and F. O. Hocaoglu, "Electricity demand forecasting of a micro grid using ANN," *2018 9th International Renewable Energy Congress (IREC)*, Hammamet, 2018, pp. 1-5.

[38] Y. Liu, D. Li, H. Pei, K. Liu, Y. Li and L. Yang, "Short-term load prediction method for power distributing method based on back-propagation neural network," *2017 12th IEEE Conference on Industrial Electronics and Applications (ICIEA)*, Siem Reap, 2017, pp. 881-886.

[39] R. Alonso and A. Chávez, "Short term load forecast method using artificial neural network with artificial immune systems," *2017 IEEE URUCON*, Montevideo, 2017, pp. 1-4.

[40] W. Gao et al, "Different states of multi-block based forecast engine for price and load prediction," *International Journal of Electrical Power & Energy Systems*, vol. 104, pp. 423-435, 2019.

[41] N. Ghadimi et al, "Two stage forecast engine with feature selection technique and improved meta-heuristic algorithm for electricity load forecasting," *Energy*, vol. 161, pp. 130-142, 2018.

[42] S. M. M. Alam, M. H. Ali, "A New Fuzzy Logic Based Method for Residential Loads Forecasting," Paper ID: 2020TD0342, accepted for presentation at the *IEEE PES Transmission & Distribution (T&D) Conference & Exposition* to be held at Chicago, IL, USA, on October 12-15, 2020.

[43] H. Khodaei et al, "Fuzzy-based heat and power hub models for cost-emission operation of an industrial consumer using compromise programming," *Appl. Therm. Eng.*, vol. 137, pp. 395-405, 2018.

[44] S. M. M. Alam and M. H. Ali, "A New Subtractive Clustering Based ANFIS System for Residential Load Forecasting," *2020 IEEE Power & Energy Society Innovative Smart Grid Technologies Conference (ISGT)*, Washington, DC, USA, 2020, pp. 1-5.

[45] M. K. Hossain and M. H. Ali, "Transient Stability Augmentation of PV/DFIG/SG-Based Hybrid Power System by Nonlinear Control-Based Variable Resistive FCL," in *IEEE Transactions on Sustainable Energy*, vol. 6, no. 4, pp. 1638-1649, Oct. 2015.

[46] Y. Wang, S. Zhu and C. Li, "Research on multistep time series prediction based on LSTM," *in 2019 3rd International Conference on Electronic Information Technology and Computer Engineering (EITCE)*, 2019, pp-1155-1159.

[47] B. Kwon, R. Park and K. Song, "Short-Term Load Forecasting Based on Deep Neural Networks Using LSTM Layer," *Journal of Electrical Engineering and Technology*,Vol. 15, pp-1501-1509, 2020.

[48] C. Cui, M. He, F. Di, Y. Lu, Y. Dai and F. Lv, "Research on Power Load Forecasting Method Based on LSTM Model," *2020 IEEE 5th Information Technology and Mechatronics Engineering Conference (ITOEC)*, Chongqing, China, 2020, pp. 1657-1660.

[49] O. Abedinia et al, "Optimal offering and bidding strategies of renewable energy based large consumer using a novel hybrid robust-stochastic approach," *J. Clean. Prod.*, vol. 215, pp. 878-889, 2019.

[50] M. Saeedi et al, "Robust optimization based optimal chiller loading under cooling demand uncertainty," *Appl. Therm. Eng.*, vol. 148, pp. 1081-1091, 2019.

[51] H. A. Bagal et al, "Risk-assessment of photovoltaic-wind-battery-grid based large industrial consumer using information gap decision theory," *Solar Energy*, vol. 169, pp. 343-352, 2018.

[52] J. A. Pinzon, P. P. Vergara, L. C. P. da Silva and M. J. Rider, "Optimal Management of Energy Consumption and Comfort for Smart Buildings Operating in a Microgrid," in *IEEE Transactions on Smart Grid*, vol. 10, no. 3, pp. 3236-3247, May 2019.

[53] Z. Yahia and A. Pradhan, "Optimal load scheduling of household appliances considering consumer preferences: An experimental analysis," *Energy*, vol. 163, pp. 15-26, 2018.

[54] A. C. Duman, Ö. Güler, K. Deveci and Ö. Gönül, "Residential load scheduling optimization for demand-side management under time-of-use rate," *2018 6th*

International Istanbul Smart Grids and Cities Congress and Fair (ICSG), pp. 193-196, 2018.

[55] M. Safdar, M. Ahmad, A. Hussain and M. Lehtonen, "Optimized residential load scheduling under user defined constraints in a real-time tariff paradigm," *2016 17th International Scientific Conference on Electric Power Engineering (EPE)*, Prague, pp. 1-6, 2016.

[56] A. Safdarian, M. Fotuhi-Firuzabad and M. Lehtonen, "Optimal Residential Load Management in Smart Grids: A Decentralized Framework," *IEEE Transactions on Smart Grid*, vol. 7(4), pp. 1836-1845, 2016.

[57] Z. Yahia and P. Kholopane, "A binary integer programming model for optimal load scheduling of household appliances with consumer's preferences," *2018 International Conference on the Domestic Use of Energy (DUE)*, Cape Town, 2018, pp. 1-8.

[58] C. C. Chai, "Distributed discrete level energy scheduling for residential load control in smart grids," *TENCON 2017 – 2017 IEEE Region 10 Conference*, Penang, 2017, pp. 1727-1732.

[59] E. Liu and P. Cheng, "Achieving Privacy Protection Using Distributed Load Scheduling: A Randomized Approach," in *IEEE Transactions on Smart Grid*, vol. 8, no. 5, pp. 2460-2473, Sept. 2017.

[60] L. Guo, H. Wu, H. Zhang, T. Xia and S. Mehraeen, "Robust optimization for home-load scheduling under price uncertainty in smart grids," *2015 International Conference on Computing, Networking and Communications (ICNC)*, Garden Grove, CA, 2015, pp. 487-493.

[61] D. Mirabbasi and S. Beydaghi, "Optimal scheduling of smart home appliances considering PHEV and energy storage system," *2015 4th International Conference on Electric Power and Energy Conversion Systems (EPECS)*, Sharjah, 2015, pp. 1-6.

[62] S. L. Arun and M. P. Selvan, "Intelligent Residential Energy Management System for Dynamic Demand Response in Smart Buildings," in *IEEE Systems Journal*, vol. 12, no. 2, pp. 1329-1340, June 2018

[63] H. Wu, A. Pratt and S. Chakraborty, "Stochastic optimal scheduling of residential appliances with renewable energy sources," *2015 IEEE Power & Energy Society General Meeting*, Denver, CO, pp. 1-5, 2015.

[64] T. Li and M. Dong, "Real-Time Residential-Side Joint Energy Storage Management and Load Scheduling With Renewable Integration," *IEEE Transactions on Smart Grid*, vol. 9, no. 1, pp. 283-298, Jan. 2018.

[65] B. Rajasekhar and N. M. Pindoriya, "Multi-stage scheduling for a smart home with solar PV and battery energy storage — A case study," *2015 IEEE Innovative Smart Grid Technologies – Asia (ISGT ASIA)*, pp. 1-6, 2015.

[66] L. Tziovani, P. Kolios, L. Hadjidemetriou and E. Kyriakides, "Energy scheduling in non-residential buildings integrating battery storage and renewable solutions," *2018 IEEE International Energy Conference (ENERGYCON)*, Limassol, 2018, pp. 1-6.

[67] J. Abushnaf and A. Rassau, "An efficient scheme for residential load scheduling integrated with demand side programs and small-scale distributed renewable energy generation and storage," International Transactions on Electrical Energy Systems, vol. 29, (2), pp. e2720, 2019.

[68] I. Worighi et al, "Optimal design of hybrid PV-Battery system in residential buildings: End-user economics, and PV penetration," Applied Sciences, vol. 9, (5), pp. 1022, 2019.
[69] M. Hong, X. Yu, N. Yu and K. A. Loparo, "An Energy Scheduling Algorithm Supporting Power Quality Management in Commercial Building Microgrids," in *IEEE Transactions on Smart Grid*, vol. 7, no. 2, pp. 1044-1056, March 2016.
[70] K. H. Youssef, "Power Quality Constrained Optimal Management of Unbalanced Smart Microgrids During Scheduled Multiple Transitions Between Grid-Connected and Islanded Modes," in *IEEE Transactions on Smart Grid*, vol. 8, no. 1, pp. 457-464, Jan. 2017.
[71] F. Wang *et al*., "Multi-Objective Optimization Model of Source–Load–Storage Synergetic Dispatch for a Building Energy Management System Based on TOU Price Demand Response," in *IEEE Transactions on Industry Applications*, vol. 54, no. 2, pp. 1017-1028, March-April 2018.
[72] B. Rajasekhar, N. Pindoriya, W. Tushar and C. Yuen, "Collaborative Energy Management for a Residential Community: A Non-Cooperative and Evolutionary Approach," in *IEEE Transactions on Emerging Topics in Computational Intelligence*, vol. 3, no. 3, pp. 177-192, June 2019.
[73] K. Li, P. Zhang, G. Li, F. Wang, Z. Mi and H. Chen, "Day-Ahead Optimal Joint Scheduling Model of Electric and Natural Gas Appliances for Home Integrated Energy Management," in *IEEE Access*, vol. 7, pp. 133628-133640, 2019.
[74] F. Luo, G. Ranzi, C. Wan, Z. Xu and Z. Y. Dong, "A Multistage Home Energy Management System With Residential Photovoltaic Penetration," in *IEEE Transactions on Industrial Informatics*, vol. 15, no. 1, pp. 116-126, Jan. 2019.
[75] Chen, Y., Luo, F., Dong, Z. et al., "A day-ahead scheduling framework for thermostatically controlled loads with thermal inertia and thermal comfort model," *J. Mod. Power Syst. Clean Energy*, 7, 568–578, 2019.
[76] Y. Zhao et al, "A review of data mining technologies in building energy systems: Load prediction, pattern identification, fault detection and diagnosis," Energy and Built Environment, vol. 1, (2), pp. 149-164, 2020.
[77] W. Kim and S. Katipamula, "A review of fault detection and diagnostics methods for building systems," Null, vol. 24, (1), pp. 3-21, 2018.
[78] S. Lazarova-Molnar, H. R. Shaker, N. Mohamed and B. N. J⊘rgensen, "Fault detection and diagnosis for smart buildings: State of the art, trends and challenges," *2016 3rd MEC International Conference on Big Data and Smart City (ICBDSC)*, Muscat, 2016, pp. 1-7.
[79] A. Contreras-Valdes et al, "Predictive Data Mining Techniques for Fault Diagnosis of Electric Equipment: A Review," Applied Sciences, vol. 10, (3), pp. 950, 2020.
[80] H. Najeh, M. P. Singh, K. Chabir, S. Ploix and M. Naceur Abdelkrim, "Fault Detection and Diagnosis for Building Systems: New Challenges," *2018 15th International Multi-Conference on Systems, Signals & Devices (SSD)*, Hammamet, 2018, pp. 832-837.
[81] K. Lee, B. Wu and S. Peng, "Deep-learning-based fault detection and diagnosis of air-handling units," Build. Environ., vol. 157, pp. 24-33, 2019.

[82] Y. Yan, P. B. Luh and K. R. Pattipati, "Fault Diagnosis of Components and Sensors in HVAC Air Handling Systems With New Types of Faults," in *IEEE Access*, vol. 6, pp. 21682-21696, 2018.

[83] W. H. Allen, A. Rubaai and R. Chawla, "Fuzzy Neural Network-Based Health Monitoring for HVAC System Variable-Air-Volume Unit," in *IEEE Transactions on Industry Applications*, vol. 52, no. 3, pp. 2513-2524, May-June 2016.

[84] S. Baldi et al, "Real-time monitoring energy efficiency and performance degradation of condensing boilers," Energy Conversion and Management, vol. 136, pp. 329-339, 2017.

[85] B. Jin, D. Li, S. Srinivasan, S. Ng, K. Poolla and A. Sangiovanni-Vincentelli, "Detecting and Diagnosing Incipient Building Faults Using Uncertainty Information from Deep Neural Networks," *2019 IEEE International Conference on Prognostics and Health Management (ICPHM)*, San Francisco, CA, USA, 2019, pp. 1-8.

[86] A. Bhatia, R. Reddy, and V. Garg, "Design of fault detection and diagnostics lab for HVAC system," 2014.

[87] S. Jiang et al, "SVM-DS fusion based soft fault detection and diagnosis in solar water heaters," *Energy Explor. Exploit.*, vol. 37, (3), pp. 1125-1146, 2019.

[88] J. Granderson et al, "Building fault detection data to aid diagnostic algorithm creation and performance testing," *Scientific Data*, vol. 7, (1), pp. 1-14, 2020.

[89] S. Miyata et al, "Fault detection and diagnosis for heat source system using convolutional neural network with imaged faulty behavior data," *Null*, vol. 26, (1), pp. 52-60, 2020.

[90] C. G. Mattera et al, "A method for fault detection and diagnostics in ventilation units using virtual sensors," *Sensors*, vol. 18, (11), pp. 3931, 2018.

[91] N. A. Sulaiman et al, "Fault detection for air conditioning system using machine learning," *IAES International Journal of Artificial Intelligence*, vol. 9, (1), pp. 109, 2020.

[92] R. Zhang et al, "BuildingSherlock: Fault management framework for HVAC systems: Demo abstract," *in Proceedings of the 1st ACM Conference on Embedded Systems for Energy-Efficient Buildings*, 2014.

[93] A. Behravan, A. Mallak, R. Obermaisser, D. H. Basavegowda, C. Weber and M. Fathi, "Fault injection framework for fault diagnosis based on machine learning in heating and demand-controlled ventilation systems," *2017 IEEE 4th International Conference on Knowledge-Based Engineering and Innovation (KBEI)*, Tehran, 2017, pp. 0273-0279.

[94] M. Dey, S. P. Rana and S. Dudley, "A Case Study Based Approach for Remote Fault Detection Using Multi-Level Machine Learning in A Smart Building," *Smart Cities*, vol. 3, (2), pp. 401-419, 2020.

[95] C. Akinci et al, "Fault detection of washing machine with discrete wavelet methods," *Mechanics*, vol. 20, (2), pp. 177-182, 2014.

[96] F. Alfieri et al, "Durability assessment of products: analysis and testing of washing machines, EUR 29487 EN, Publications Office of the European Union, Luxembourg," *Doi: Https://Doi.Org/10*, vol. 2760, pp. 115684, 2018.

[97] P. Tecchio, F. Ardente and F. Mathieux, "Understanding lifetimes and failure modes of defective washing machines and dishwashers," *J. Clean. Prod.*, vol. 215, pp. 1112-1122, 2019.

[98] N. Pandit and R. L. Chakrasali, "Distribution transformer failure in India root causes and remedies," *2017 International Conference on Innovative Mechanisms for Industry Applications (ICIMIA)*, Bangalore, 2017, pp. 106-110.

[99] D. Cai et al., "Analysis of Heavy Load and Overload Distribution Transformer in Regional Power Grid," *2018 2nd IEEE Conference on Energy Internet and Energy System Integration (EI2)*, Beijing, 2018, pp. 1-5.

[100] J. Singh, S. Singh and A. Singh, "Distribution transformer failure modes, effects and criticality analysis (FMECA)," *Eng. Failure Anal.*, vol. 99, pp. 180-191, 2019.

[101] J. Yaghoobi et al, "Impact of high-frequency harmonics (0–9 kHz) generated by grid-connected inverters on distribution transformers," *International Journal of Electrical Power & Energy Systems*, vol. 122, pp. 106177, 2020.

[102] D. Pejovski, K. Najdenkoski and M. Digalovski, "Impact of different harmonic loads on distribution transformers," *Procedia Engineering*, vol. 202, pp. 76-87, 2017.

[103] M. A. Hossain et al, "Energy management of community microgrids considering degradation cost of battery," Journal of Energy Storage, vol. 22, pp. 257-269, 2019.

[104] M. A. Hossain et al, "Modified PSO algorithm for real-time energy management in grid-connected microgrids," Renewable Energy, vol. 136, pp. 746-757, 2019.

[105] Z. Jie and W. Siyuan, "Thermal load forecasting based on PSO-SVR," in 2018 IEEE 4th International Conference on Computer and Communications (ICCC), 2018.

[106] L. Wei and L. Haitian, "Electrical load forecasting using echo state network and optimizing by pso algorithm," in 2017 10th International Conference on Intelligent Computation Technology and Automation (ICICTA), 2017.

[107] Y. Shen et al, "Short-term load forecasting of power system based on similar day method and PSO-DBN," in 2018 2nd IEEE Conference on Energy Internet and Energy System Integration (EI2), 2018.

[108] https://www.mathworks.com/help/fuzzy/type-2-fuzzy-inference-systems.html

[109] https://www.mathworks.com/help/fuzzy/mamfistype2.converttotype2.html

[110] J. M. Mendel, H. Hagras, W.-W. Tan, W.W. Melek, and H. Ying, "Introduction to Type-2 Fuzzy Logic Control," *Wiley and IEEE Press*, Hoboken, NJ., 2014.

[111] D. Wu and M. Nie, "Comparison and practical implementation of type-reduction algorithms for type-2 fuzzy sets and systems," *2011 IEEE International Conference on Fuzzy Systems (FUZZ-IEEE 2011)*, Taipei, 2011, pp. 2131-2138.

[112] Z. Bingül and O. Karahan, "A Fuzzy Logic Controller tuned with PSO for 2 DOF robot trajectory control," *Expert Systems with Applications*, vol. 38(1), pp. 1017-1031, 2011.

[113] https://www.mathworks.com/help/stats/understanding-support-vector-machine-regression.html [online].

[114] G. Ren, S. Wen, Z. Yan, R. Hu, Z. Zeng and Y. Cao, "Power load forecasting based on support vector machine and particle swarm optimization," *2016 12th World Congress on Intelligent Control and Automation (WCICA)*, Guilin, 2016, pp. 2003-2008.

[115] W. Kong, Z. Y. Dong, Y. Jia, D. J. Hill, Y. Xu and Y. Zhang, "Short-Term Residential Load Forecasting Based on LSTM Recurrent Neural Network," in *IEEE Transactions on Smart Grid*, vol. 10, no. 1, pp. 841-851, Jan. 2019.
[116] M. Q. Raza and A. Khosravi, "A review on artificial intelligence based load demand forecasting techniques for smart grid and buildings," *Renewable and Sustainable Energy Reviews*, vol. 50, pp. 1352-1372, 2015.
[117] Q. Meng, M. Mourshed, and S. Wei, "Going Beyond the Mean: Distributional Degree-Day Base Temperatures for Building Energy Analytics Using Change Point Quantile Regression," *IEEE Access*, vol. 6, pp. 39532-39540, 2018.
[118] S. K. Aggarwal and M. Kumar, "ANN based residential demand forecasting using weather and special day information," *2016 7th India International Conference on Power Electronics (IICPE)*, pp. 1-5, 2016.
[119] J. Massana, C. Pous, L. Burgas, J. Melendez, and J. Colomer, "Short-term load forecasting for non-residential buildings contrasting artificial occupancy attributes," *Energy and Buildings*, vol. 130, pp. 519-531, 2016.
[120] https://power.larc.nasa.gov/data-access-viewer/
[121] https://www.wunderground.com/history/daily/us/tn/memphis
[122] https://forecast.weather.gov/MapClick.php?textField1=35.1000&textField2=-90.0000#.XUXykehKhPZ
[123] J. Hao, G. Zhang, Y. Zheng, W. Hu, and K. Yang, "Solution for Selective Harmonic Elimination in Asymmetric Multilevel Inverter Based on Stochastic Configuration Network and Levenberg-Marquardt Algorithm," *IEEE Applied Power Electronics Conference and Exposition (APEC)*, pp. 2855-2858, 2019.
[124] J. Wu et al, "Hyperparameter Optimization for Machine Learning Models Based on Bayesian Optimizationb," *Journal of Electronic Science and Technology*, vol. 17, (1), pp. 26-40, 2019.
[125] S. Touzani, J. Granderson and S. Fernandes, "Gradient boosting machine for modeling the energy consumption of commercial buildings," *Energy Build.*, vol. 158, pp. 1533-1543, 2018.
[126] https://www.mathworks.com/help/stats/ensemble-algorithms.html
[127] R. Fu, D. J. Feldman, R. M. Margolis, "US solar photovoltaic system cost benchmark: Q1 2018," NREL, NREL/TP-6A20-72399, 2018.
[128] A. Ramdas , K. McCabe, P. Das, B. Sigrin, "California Time-of-Use (TOU) Transition: Effects on Distributed Wind and Solar Economic Potential," NREL, 2019.
[129] https://www.tesla.com/powerwall
[130] https://www.tesla.com/sites/default/files/pdfs/powerwall/Powerwall%202_AC_Datasheet_en_northamerica.pdf
[131] https://www.nrel.gov/docs/legosti/old/5173.pdf
[132] https://www.solarreviews.com/blog/how-much-electricity-does-a-solar-panel-produce

[133] https://www.nrel.gov/docs/fy07osti/40744.pdf

[134] https://www.pge.com/en_US/small-medium-business/energy-alternatives/private solar/understand-the-solar-process.page

[135] https://www.selfgenca.com/home/program_metrics/

[136] https://www.pge.com/tariffs/electric.shtml#RESELEC_INCLUTOU

[137] J. M. G. López, E. Pouresmaeil, C. A. Cañizares, K. Bhattacharya, A. Mosaddegh and B. V. Solanki, "Smart Residential Load Simulator for Energy Management in Smart Grids," in *IEEE Transactions on Industrial Electronics*, vol. 66, no. 2, pp. 1443-1452, Feb. 2019

[138] https://products.geappliances.com/MarketingObjectRetrieval/Dispatcher?RequestType=PDF&Name=49-2000254-1.pdf

[139] M. Humayun, M. Z. Degefa, A. Safdarian and M. Lehtonen, "Utilization Improvement of Transformers Using Demand Response," in *IEEE Transactions on Power Delivery*, vol. 30, no. 1, pp. 202-210, Feb. 2015.

[140] M. Dong, A. B. Nassif and B. Li, "A Data-Driven Residential Transformer Overloading Risk Assessment Method," in *IEEE Transactions on Power Delivery*, vol. 34, no. 1, pp. 387-396, Feb. 2019.

[141] E. Cazacu and L. Petrescu, "Derating the three-phase power distribution transformers under nonsinusoidal operating conditions: A case study," *2014 16th International Conference on Harmonics and Quality of Power (ICHQP)*, Bucharest, 2014, pp. 488-492.

[142] IEEE Recommended Practice for Establishing Liquid-Immersed and Dry-Type Power and Distribution Transformer Capability When Supplying Nonsinusoidal Load Currents," in IEEE Std C57.110™-2018 (Revision of IEEE Std C57.110-2008), vol., no., pp.1-68, 31 Oct. 2018.

[143] https://batteryuniversity.com/learn/article/electric_vehicle_ev

[144] https://www.solarenergylocal.com/states/tennessee/memphis/

[145] E. Cherian, G. R. Bindu and P. S. C. Nair, "Pollution impact of residential loads on distribution system and prospects of DC distribution," *Engineering Science and Technology, an International Journal*, vol. 19, no. 4, pp. 1655-1660, 2016.